

BARRIENTOS, RODELL C., Ph.D. Innovative Methods to Advance the Analysis of Intact Glycolipids by Mass Spectrometry. (2019)  
Directed by Dr. Qibin Zhang. 210 pp.

The common etiological feature among the majority, if not all, of human diseases, is the impairment of crucial cellular events stemming from complex reactions at the molecular level. Precise understanding of these processes, such as structure-function relationships between biomolecules, could help guide the design of successful clinical interventions to prevent or halt diseases. Consequently, it is important to measure and characterize biomolecules at the finest possible granularity. Glycolipids, biomolecules comprised of a sugar (glycan) head and a lipid tail, serve as one of the key components of the cell membrane. Aberrant glycolipid metabolism is a hallmark of many pathologies, which accentuates their importance in disease pathogenesis. Despite their vital role, our present understanding of glycolipid biology remains incomplete, partly because of the dearth of technologies available to study them. Mass spectrometry (MS) has inarguably fueled much of our current knowledge on glycolipids. But, contemporary methods using this platform are not powerful enough to either detect low abundant glycolipids or elucidate subtle structural details that could facilitate uncovering of their precise biological functions. Often, the glycan and lipid components are analyzed separately, making correlation between structure and biological function impossible. Recent evidences have showcased that both glycan and lipid moieties dictate the overall function of glycolipids, which underlines the importance of structural analysis at the intact molecule level. In this respect, this dissertation was conceived to address the following aims, 1) To develop innovative MS methodologies to measure and characterize glycolipids in its intact, native form; and 2) To apply the developed methods in reasonably complex biological mixtures. Each method developed here is in-line with the following objectives: 1) to enhance detectability of glycolipids by increasing ionization

efficiency, 2) to facilitate structural analysis, and 3) to improve quantification of glycolipids with potential for high-throughput applications.

Both aims were addressed in four standalone projects that employed both commercially available standard glycolipids and complex biological samples. The first two projects sought to establish a method to determine double bond locations in unsaturated glycolipids. We exploited ozone-induced dissociation MS (OzID-MS), a relatively new fragmentation technique that uses ozone gas inside the collision cell of MS *in lieu* of conventional inert gas. Ozone reacts selectively to carbon-carbon double bonds, as such, the products of the ozonolysis *in situ* could be detected by MS and being used to locate the double bonds. Using complex bovine brain sample, this method revealed low abundant glycolipids, mostly isomers and isobars, that are otherwise non-detectable and non-distinguishable when conventional methods are used. We also discovered that the use of different adducts, such as  $[M+Na]^+$ ,  $[M+Li]^+$ , and  $[M+H]^+$ , could provide distinct OzID-MS patterns. Thus, to rationalize the observed OzID-MS data, theoretical calculations were performed to establish the structures of ionized glycolipids in the gas-phase. The *in silico* generated models were consistent with the experimentally observed fragmentation patterns. Overall, these projects emphasized that innovative approaches like OzID-MS could uncover previously unknown molecular species in a complex sample and the use of different adducts could provide distinct levels of structural detail.

The third project aimed to establish a method that exploits a relatively new approach to quantitation called isobaric labeling, a technique that has been extensively used in proteomics and glycomics fields as a multiplexed analytical tool. It involves the covalent attachment of a molecular tag to an analyte that generates reporter ions when fragmented in MS. The intensities of the reporter ions serve as surrogate measures of their relative concentration in the sample. Because this tag only reacts with a reactive aldehyde or ketone, which is absent in native

glycolipids structures, we first employed a chemoselective oxidation approach to introduce a reactive site in the intact glycolipids, using sialic acid-containing glycolipids called gangliosides as a model. When applied to complex porcine brain total lipids extract, this method not only enabled multiplexed analysis of up to six independent samples and improved sensitivity of gangliosides by two orders, but also provided rich spectra that facilitated the structural analysis of both the sugar head group and lipid backbone.

The fourth project addressed the increasing demand for heavy isotope labeled internal standards, which are currently limited and costly, while improving the detectability, facilitating structural characterization, and enabling multiplexed analysis. In this project, we employed permethylation, a reaction that converts active protons in the molecule to a methyl group using methyl iodide. In this so-called differential isotope labeling approach, using methyl iodide with either light ( $^{12}\text{C}$ ) or heavy ( $^{13}\text{C}$ ) carbon isotopes, two different samples were separately labeled, one of which is a pooled aliquot of individual samples, then mixed and analyzed by LC-MS. The pooled sample, labeled with heavy carbon isotope served as a universal internal standard which was spiked to individual samples at constant amount. Samples were analyzed using reversed-phase liquid chromatography mass spectrometry (RPLC-MS), and the resulting peak areas were used to calculate the  $^{12}\text{C}/^{13}\text{C}$  ratio as a surrogate measure of the relative concentration of analytes in each sample. Using an *in vitro* model of Gaucher's disease, characterized by accumulation of neutral glycolipids, temporal changes in glycolipid profile were measured and each glycolipid was annotated using retention time and MS/MS fragmentation.

INNOVATIVE METHODS TO ADVANCE THE ANALYSIS OF INTACT  
GLYCOLIPIDS BY MASS SPECTROMETRY

by

Rodell C. Barrientos

A Dissertation Submitted to  
the Faculty of The Graduate School at  
The University of North Carolina at Greensboro  
in Partial Fulfillment  
of the Requirements for the Degree  
Doctor of Philosophy

Greensboro  
2019

Approved by

Qibin Zhang, PhD  
Committee Chair

To *nanay*      *at tatay*<sup>†</sup>  
thank you so much for  
raising me the way  
that I am  
today.



## ACKNOWLEDGMENTS

Personally, I would like to thank Drs. Nadja Cech, Nicholas Oberlies, and Norman Chiu for offering their precious time, effort, and expertise as members of my dissertation committee; Dr. Guan-yuan Chen, for training me on proper cell culture techniques and for providing unsolicited advices on my projects; Dr. Liuyi Lao, for training me on flow cytometry; Ngoc Vu, for her assistance in optimizing the conditions for OzID-MS; Dr. Daniel Todd, for his assistance in the mass spectrometry facility; Wendy Helton and Cherie Turner, for their kindness and logistical support; all the faculty and staff of the Department of Chemistry and Biochemistry, and Center for Translational Biomedical Research, my two homes away from home.

Lastly, I would like to express my gratitude to the Zhang research group including the past (Drs. Monica Narvaez-Rivas, Lina Zhang, Chih-wei Liu, Xiaobo He, Hossein Maleki) and current members (Jiangxue Chen and Drs. Tai-Du Lin, Jacob Woo, Sudhir Putty Reddy) for their continuous support both in and out of the lab. Thank you Dr. Qibin Zhang for your advices and guidance all throughout my PhD journey.

This work was partially supported by grants to Dr. Qibin Zhang from the National Institute of General Medical Sciences (Grant No. R21 GM 104678) and the National Institute of Diabetes and Digestive and Kidney Diseases (Grant No. R01 DK114345) of the National Institutes of Health.

## TABLE OF CONTENTS

	Page
LIST OF TABLES .....	vii
LIST OF FIGURES .....	viii
CHAPTER	
I. INTRODUCTION .....	1
Background.....	1
Significance and Innovation .....	2
Methodology .....	3
Conclusion .....	5
II. MODERN METHODS FOR IMPROVED DETERMINATION OF INTACT GLYCOLIPIDS BY MASS SPECTROMETRY.....	7
Introduction.....	7
Overview of GSLs .....	9
Current Challenges in the Analysis of Intact GSLs .....	15
Sample Preparation .....	18
Mass Spectrometry of GSLs .....	24
Direct Infusion MS .....	37
Hyphenated MS Techniques .....	38
Labeling Approaches for Improved MS-Based Quantification of GSLs.....	50
Conclusion and Future Directions .....	56
Acknowledgment .....	57
III. STRUCTURAL ANALYSIS OF UNSATURATED GLYCOSPHINGO- LIPIDS USING SHOTGUN OZONE-INDUCED DISSOCIATION MASS SPECTROMETRY .....	58
Introduction.....	58
Experimental.....	62
Results and Discussion .....	64
Conclusion .....	84
Acknowledgment .....	85
IV. FRAGMENTATION BEHAVIOR AND GAS-PHASE STRUCTURES OF CATIONIZED GLYCOSPHINGOLIPIDS IN OZONE-INDUCED DISSOCIATION MASS SPECTROMETRY .....	86
Introduction.....	86

Experimental Procedures .....	88
Results and Discussion .....	91
Conclusion .....	106
Acknowledgment .....	107
V. ISOBARIC LABELING OF INTACT GANGLIOSIDES TOWARD MULTIPLEXED LC-MS/MS BASED QUANTITATIVE ANALYSIS.....	108
Introduction.....	108
Experimental Procedures .....	111
Results and Discussion .....	114
Conclusion .....	126
Acknowledgment .....	126
VI. DIFFERENTIAL ISOTOPE LABELING BY PERMETHYLATION AND REVERSED-PHASE LC/MS FOR RELATIVE QUANTIFICATION OF INTACT NEUTRAL GLYCOLIPIDS IN MAMMALIAN CELLS.....	127
Introduction.....	127
Experimental Procedures .....	129
Results and Discussion .....	133
Conclusion .....	146
Acknowledgment .....	147
VII. CONCLUDING REMARKS .....	148
REFERENCES .....	150
APPENDIX A. SUPPLEMENTAL TABLES.....	161
APPENDIX B. SUPPLEMENTAL FIGURES .....	169
APPENDIX C. SUPPLEMENTAL CALCULATIONS .....	199
APPENDIX D. COPYRIGHT PERMISSIONS .....	200

## LIST OF TABLES

	Page
Table 1. Core Structures of Mammalian GSLs.....	11
Table 2. Key Biological Functions of the Two Structural Components of GSLs.....	14
Table 3. Assignment of OzID-MS Product Ions Based on Accurate Mass Measurement.....	67
Table 4. Estimated Heat of Formation ( $\Delta H_f^0$ ) and Cation Affinities of Ionized LacCer d18:1/18:1(9Z) Calculated Using MO-G with PM6.....	101

## LIST OF FIGURES

	Page
Figure 1. Representation of Common Glycoconjugates on Mammalian Cell Surface and General Structure of GSLs .....	8
Figure 2. Simplified Biosynthetic Scheme of Mammalian GSLs.....	9
Figure 3. Representative Structures Showing the Structural Diversity of GSLs .....	17
Figure 4. General Workflow for Extraction and Isolation of Specific GSLs.....	20
Figure 5. Strategies to Introduce Reactive Functional Groups in GSLs .....	23
Figure 6. Glycoblotting Technique for Enrichment of GSLs .....	24
Figure 7. Nomenclature of Fragmentation for GSLs .....	29
Figure 8. Fragmentation of Ganglioside GD1 Using Different Techniques .....	33
Figure 9. OzID-MS Spectrum of LacCer d18:1/18:1(9Z) .....	35
Figure 10. Baseline Resolution of Isomeric GD1a and GD1b Gangliosides .....	49
Figure 11. Labelling of GSLs by Isotopic Permethylation .....	51
Figure 12. Labelling of Intact, Monosialoganglioside Using PAEA.....	53
Figure 13. Chemical Structures of Mass Tags Used for Isobaric Labeling of GSLs.....	54
Figure 14. Isobaric Labeling Based Strategy for Multiplexed Quantification of Intact Gangliosides.....	55
Figure 15. High Resolution OzID-MS Spectrum of (a) GalCer d18:1/18:0(2OH), and (b) GlcCer d18:2/16:0(2OH) Standards Obtained in Synapt G2™ HDMS .....	65
Figure 16. Proposed Reaction Pathway for the OzID-MS of the [M+Na] <sup>+</sup> of GalCer d18:1/18:0(2OH) ( <i>m/z</i> 766.5814).....	66
Figure 17. Comparison of OzID-MS Spectra of (a) LacCer d18:1/18:1(9Z) and (b) LacCer d18:1/18:0.....	69

Figure 18. Proposed Reaction Pathway for the OzID-MS of the [M+Na] <sup>+</sup> of GlcCer d18:2/16:0(2OH) ( <i>m/z</i> 736.5330).....	71
Figure 19. OzID-MS of (a) GalCer d18:1/18:1(9Z), (b) GalCer d18:1/24:1(15Z), and (c) Gb4Cer d18:1/24:1(15Z)(2OH).....	78
Figure 20. Application of High Resolution OzID-MS to Major Isomeric Galactocerebroside Species in Bovine Brain.....	80
Figure 21. Application of High Resolution OzID-MS to Major Isomeric and Isobaric Galactocerebroside Species in Bovine Brain.....	83
Figure 22. General Structure of a Glycosphingolipid.....	87
Figure 23. Overview of the Proposed Pathways Leading to the Formation of Ozonolysis Products Observed in the OzID-MS Spectrum.....	92
Figure 24. OzID-MS Spectra of Cationized LacCer d18:1/18:1(9Z) .....	96
Figure 25. Calculated Gas-Phase Structure of Dehydrated LacCer d18:1/18:1(9Z).....	98
Figure 26. Most Stable Conformer of [M+Na] <sup>+</sup> of LacCer d18:1/18:1 Calculated Using MO-G with PM6 .....	102
Figure 27. Most Stable Conformer of [M+Li] <sup>+</sup> of LacCer d18:1/18:1 Calculated Using MO-G with PM6 .....	104
Figure 28. Most Stable Conformer of [M+H] <sup>+</sup> of LacCer d18:1/18:1 Calculated Using MO-G with PM6 .....	106
Figure 29. Representative Structure of a Ganglioside (GM1a d18:1/18:0) (a).....	109
Figure 30. Reactions Involved in the Oxidation and Isobaric Labeling Technique Implemented in this Study .....	110
Figure 31. Full Scan MS Spectrum of Unoxidized (a) and Oxidized (b) Ganglioside GM1a d18:1/18:0 Acquired Using LTQ Orbitrap XL Demonstrating Almost Negligible Side Reactions.....	116
Figure 32. Extracted Ion Chromatograms (EIC) of Individual Ganglioside Standards Oxidized Using 1 mM NaIO <sub>4</sub> Demonstrating its Applicability Across Different Core Structures.....	117

Figure 33. Negative ESI-MS/MS Spectra of Unoxidized (a) and Oxidized (b) Ganglioside GM1a d18:1/18:0 Acquired Using Q Exactive HF. ....	118
Figure 34. EIC of Representative Oxidized Ganglioside GT1b d18:1/18:0 .....	119
Figure 35. Workflow Employed to Demonstrate Feasibility of Multiplexed Experiment Using Porcine Brain Extract (a). ....	125
Figure 36. Schematic of Reaction Workflow Implemented in this Work.....	128
Figure 37. Effect of Reaction Conditions on the Efficiency of Permethylation .....	134
Figure 38. Coelution and Fragmentation Behavior of Permethylated Glycolipid .....	138
Figure 39. Simultaneous Elimination of Dominant Phospholipids During Permethylation .....	139
Figure 40. Evaluation of Quantitative Ability of <sup>12</sup> C and <sup>13</sup> C Permethylation.....	140
Figure 41. Accumulation of Glycolipids in CBE-Treated RAW264.7 Cells.....	145

## CHAPTER I

### INTRODUCTION

#### **Background**

The early 2000s has stamped the beginning of a new era of scientific revolution particularly in the life sciences. The successful culmination of the human genome project not only has shed light to the previously elusive genetic code, but also unlocked new directions for systems biological approaches, *i.e.* transcriptomics, proteomics, metabolomics, lipidomics, and glycomics. These transitions took place alongside the improvements in the field of analytical instrumentation, such as mass spectrometry (MS). This powerful combination of biology and analytical chemistry has enabled scientists to uncover complex molecular pathways that previously were difficult to elucidate. Roughly a decade after the completion of the human genome project, in 2012, scientific leaders convened to come up with a consensus to advance the field of glycoscience by means of establishing consortia and funding mechanisms <sup>1</sup> that ultimately aims to uncover the human glycome <sup>2</sup>.

Glycoscience involves the study of carbohydrates and carbohydrate conjugates (glycoconjugates). An important class of glycoconjugates, glycolipids, also called glycosphingolipids (GSLs) are bioactive molecules comprised of a lipid tail and a glycan (carbohydrate) head<sup>3</sup>. These molecules, together with glycoproteins and other glycoconjugates, form the “glycosynapse” which has been recognized to play vital roles in living systems<sup>4</sup>. GSLs have been associated to a number of different biological processes<sup>5-7</sup> and abnormal metabolism of GSLs has been linked to various human diseases<sup>5,8</sup>. Importantly, both the glycan and lipid

components dictate the biological functions<sup>5-7</sup> of GSLs, as such, determining them at the intact structure level is greatly warranted. This dissertation was conceived to address that premise.

### **Significance and Innovation**

Being amphiphilic molecules with a carbohydrate head and a lipid tail, GSLs are poised to invoke analytical challenges because of two important reasons. First, GSLs are structurally diverse not only in terms of the sugar composition and connectivity, but also in the lipid component. These heterogeneities are difficult to examine using gold standard methods such as NMR or X-ray crystallography because typically, limited quantity of samples is available for measurement. Second, the absence of chromophores in GSLs makes them particularly challenging to detect using conventional optical spectrometric methods. Despite availability of MS instrumentation with improved sensitivity, resolution, and accuracy, GSLs suffer from low ionization efficiency and thus, their detectability is impeded especially in highly complex biological samples. As such, novel strategies are needed to circumvent these barriers to advance the intact analysis of GSLs.

Existing methodologies to analyze GSLs cannot pinpoint the location of carbon-carbon double bonds without disintegrating the native structure. Traditional methods to locate unsaturation involve either chemical or enzymatic processes to separate the glycan from the lipid backbone and then analyzing the lipid component for double bond location using Gas Chromatography-Mass Spectrometry (GC-MS). While helpful, this destructive method suffers from inability to establish the true, intact structure of molecules. Thus, the use of new approaches to locate double bonds while preserving the native structure of the compound is of utmost importance in the field of GSLs research. This dissertation employed an innovative approach called ozone-induced dissociation MS (OzID-MS)<sup>9</sup> for this purpose, which has been previously

used to determine double bond locations in phospholipids but not in the structurally more complexed GSLs<sup>10</sup>.

One of the overarching goals of developing new analytical methods is to improve the coverage of analytes and minimize the costs. In this regard, use of isobaric labeling techniques has gained popularity in proteomics and glycomics, however, it has not been fully utilized in small molecule analysis. This technique relies on the use of a labeling agent called isobaric tag, which can be used to label multiple samples and analyze them as one pooled sample rather than each sample individually. This multiplexed strategy not only increases throughput but also ensures that variability caused by instrument instability is accounted for. Additionally, because multiple samples are analyzed concurrently, the use of isobaric labeling reduces the cost associated with instrument runtime, mobile phases, and column shelf life.

The detectability of GSLs is a major concern in studying these molecules from crude lipid extracts. This largely stems from their low abundance, and low ionization efficiency. Moreover, it is ideal that internal standards in any LC-MS method should have similar response to the target analyte, but limited availability of such comprehensive standards hampers the full utilization of LC-MS in GSLs analysis. To address these concerns, we utilized a differential isotope labeling technique via permethylation. Permethylation is a process where all active protons in a molecule are converted to methyl group using methyl iodide. When different isotopically labeled methyl iodide was employed, two different samples can be labeled, and because their masses have been changed, they can be pooled together and analyzed as one sample.

### **Methodology**

This dissertation developed and applied novel mass spectrometry-based methods for the analysis of GSLs in its native, intact form using three important techniques. The first involves the

use of a unique fragmentation technology, called ozone-induced dissociation (OzID), which was introduced by Blanksby *et al.*<sup>11</sup> in 2008 and has been mainly used for lipids other than GSLs. This technique uses ozone gas inside the collision cell of a mass spectrometer *in lieu* of conventional inert gas. Here, ozone reacts selectively to carbon-carbon double bonds, as such, the products of the ozonolysis *in situ* could be detected by MS and being used to locate the double bonds. While previous works have been performed using unit resolution instruments<sup>10</sup> such as ion trap and triple quadrupoles, in this dissertation, OzID-MS implemented in a high resolution quadrupole-time of flight (Q-TOF)<sup>12</sup> instrument was employed to enable the unambiguous assignment of both precursor and OzID-MS product ions. Of note, since double bond positions cannot be identified using conventional fragmentation techniques alone, this dissertation demonstrated that the use of OzID-MS could reveal the presence of isomeric and isobaric GSLs that differ in the position of unsaturation.

The second method involves the use of isobaric labeling, a relatively new approach to analyze molecules at the MS/MS level. This has been employed extensively in proteomics and glycomics but rarely in lipids<sup>13</sup>. This strategy relies on the use of isobaric tag, which is a reagent that is used to label molecules and can produce unique reporter fragment ions after fragmentation in the MS. One major caveat in using this approach is the absence of reactive functional groups in native structure of GSLs such as aldehyde, ketone, or free amine. As such, prior chemical modification or derivatization is often required. While various derivatization methods are available, most of them are difficult to perform, and with undesirable reactions. As an exception, chemoselective periodate oxidation is a very neat, mild reaction and has been applied to sialic acid-containing molecules like glycans and gangliosides primarily for imaging and metabolic tracing studies<sup>14</sup>. In this dissertation, using MS, we presented the chemoselective oxidation,

isobaric labeling, and MS analysis of intact gangliosides to reveal the structure of the glycan headgroup and the lipid backbone in a single MS/MS spectrum.

Finally, to address the need for universal internal standards for quantification of GSLs, enhance the detectability, and allow the elucidation of the intact structure of GSLs, differential isotope labeling was applied. This approach involves the use of light and heavy isotopes directly incorporated into analytes before mixing them and final analysis by MS. Specifically, in this dissertation, we took advantage of the well-known permethylation reaction to incorporate light and heavy isotopes of carbon into intact GSLs. Permethylation involves the conversion of all active protons, those that are directly connected to nitrogen and oxygen, to methyl groups in the presence of anhydrous alkali hydroxide, with  $^{12}\text{C}$  or  $^{13}\text{C}$ -labeled methyl iodide serving as the methyl donor. Because most of the matrix components, such as phospholipids and glycerides are alkali-labile, majority of them will be depleted, thus effectively reducing the chemical background for GSL analysis. The individual samples are labeled using  $^{12}\text{C}$ -methyl iodide, while a pooled aliquot from each sample is labeled with  $^{13}\text{C}$ -methyl iodide which is then spiked to individual samples making it a universal internal standard. We successfully demonstrated the capability of this method to both identify and quantify the changes in glycolipid profile in mammalian cells.

### **Conclusion**

GSLs are complex and despite their importance, remain relatively underexplored in the realm of lipidomics, as such, this field serves as a rich area of opportunities to establish innovative methods that would facilitate exciting new discoveries. This dissertation developed and demonstrated novel methods for intact analysis of GSLs. These methods enhanced the detectability of GSLs by increasing ionization efficiency, facilitated structural analysis, and improved the quantification with potential for high-throughput applications. These approaches

provide the required technical means to reveal molecular species that were previously hidden and eventually, when applied to real biological questions, could provide novel insights into the exciting biology of these molecules.

CHAPTER II  
MODERN METHODS FOR IMPROVED DETERMINATION OF  
INTACT GLYCOLIPIDS BY MASS SPECTROMETRY

This chapter is intended for submission to the journal *Analytica Chimica Acta* and is presented in that style. Barrientos, R.C. and Zhang, Q. *Anal. Chim. Acta*.

**Introduction**

Glycolipids are complex molecules composed of a carbohydrate head and a lipid tail that are localized on the cell surface and membrane-bound subcellular organelles<sup>3,15,16</sup>.

Glycosphingolipids (GSLs) are the most abundant glycolipids in eukaryotic cells<sup>3</sup>. Since the first discovery of GSLs by Thudichum in 1884<sup>17</sup>, growing number of studies focusing on the structural elucidation and biosynthesis have been performed which partly uncovered the crucial role of GSLs in various cellular processes and diseases<sup>4,6,16</sup>. Currently, GSLs are recognized as potential therapeutic targets and mounting evidences have claimed that the glycan headgroup and the lipid backbone both dictate their biological function<sup>5</sup>. However, thorough understanding of their precise roles remains elusive.

The identification, structural elucidation, and quantification of GSLs using the ‘omics’ approach only emerged recently and new tools are needed to further advance this field<sup>3</sup>. Evidently, the number of publications in this area has increased exponentially in the last decades. Advancements and innovations in mass spectrometry (MS) and chromatography have largely catalyzed this success by facilitating the analysis of GSLs in its intact form<sup>15,18-21</sup>. In Lipid MAPS database, the largest repository of lipids, at least 3,000 molecular species of GSLs are currently

curated, despite this seemingly huge number, it is apparent that some subclasses remain underrepresented, particularly sulfatides and neutral GSLs<sup>23</sup>. This signifies that on-going and future efforts will most likely focus on this relatively young field.

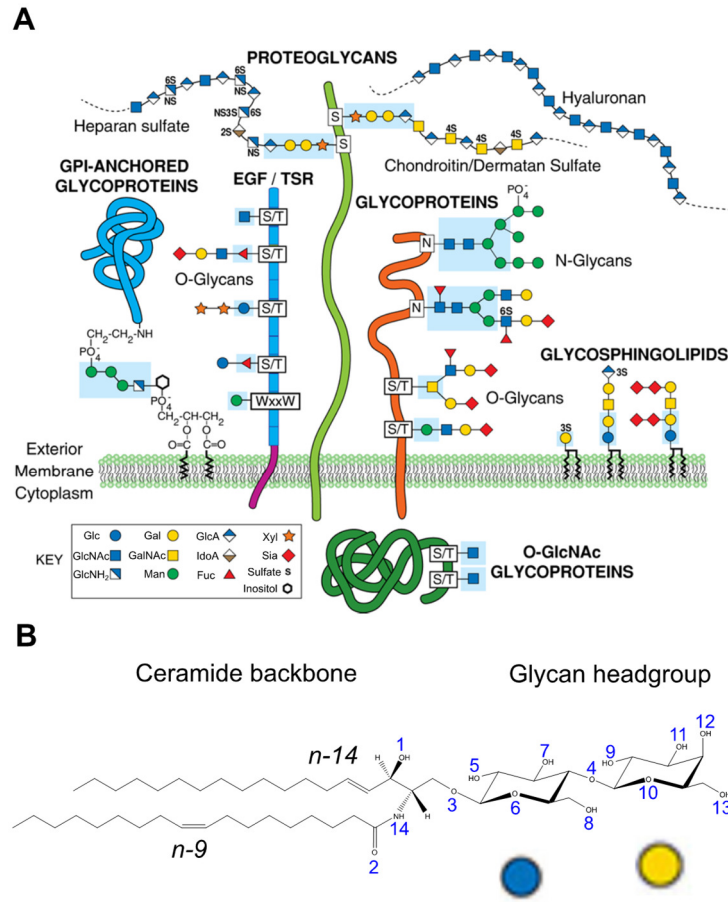


**Figure 1. Representation of Common Glycoconjugates on Mammalian Cell Surface and General Structure of GSLs.** A) Diversity of glycoconjugates on mammalian cell surface. Reprinted with permission from Varki *et al. Essentials of Glycobiology, 3<sup>rd</sup> Ed.*<sup>22</sup> © 2015-2017, Cold Spring Harbor Laboratory Press. B) General structure of GSLs. Shown here is LacCer d18:1 (4E)/18:1(9Z), composed of a ceramide backbone with sphingosine long chain base (d18:1) and oleic acid connected via amide bond. The double bonds are numbered  $x$  in the annotation  $n-x$  from the terminal carbon, the assignment of stereochemistry using E/Z system is likewise shown. The glycan headgroup is consists of glucose (blue circle) and galactose (yellow circle). Key to symbols is also shown.

The objective of this paper is to layout an overview of the field and to summarize the methodologies commonly employed in MS-based analysis of GSLs. The principles, advantages, and limitations of each approach are discussed. Contemporary challenges associated with analysis of intact GSLs that need to be addressed in the future are also emphasized.

## Overview of GSLs

### Structure and biosynthesis

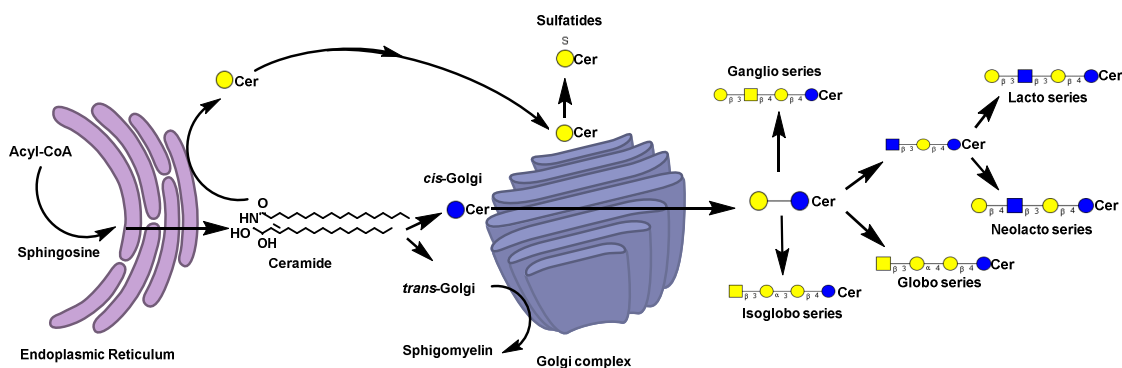


**Figure 2. Simplified Biosynthetic Scheme of Mammalian GSLs.** Ceramide is synthesized from endoplasmic reticulum (ER). The ceramide is galactosylated to form GalCer or exported to *cis*-Golgi to form GlcCer. In the *trans*-Golgi, Cer is used for sphingomyelin synthesis. The GlcCer is used to form LacCer that serves as the precursor of complex GSL core structures.

GSLs are characterized by a hydrophobic anchor (ceramide) and a hydrophilic head containing a glycan chain that is projected toward the extracellular milieu (**Fig. 1**). The ceramide contains an amino alcohol that is linked to a fatty acyl chain through an amide bond. The amino alcohol, also called long chain base (LCB) or sphingoid base is usually consist of 18 carbons with one carbon-carbon double bond at position 4 symbolized as d18:1 where the *d* stands for two hydroxyl groups (one used in glycosidic linkage and the other as free hydroxyl group), 18 for number of carbons and 1 for number of carbon-carbon double bond. Other sphingoid bases such as d16:1 and d20:1 were also observed in mammalian systems though in minor amounts and in

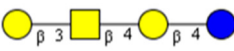
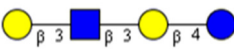
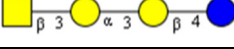
tissue-specific manner as extensively reviewed by Merrill <sup>3</sup>. The absence of fatty acyl chain in the lipid backbone results to *lyso*-GSLs, a known toxic by-product of aberrant GSLs metabolism<sup>24</sup>.

GSLs can be classified as either neutral or acidic based on the glycan component. Neutral species include cerebrosides and globosides while the acidic species include gangliosides and sulfatides. Cerebrosides are composed of a hexose sugar, either glucose (Glc) or galactose (Gal); while the globosides may contain more than one neutral, monosaccharide units. In contrast, gangliosides contain sialic acid that exists as negatively charged species at physiological conditions. Only two different forms of sialic acid exist in humans, namely, N-acetylneuraminic (Neu5Ac) and N-glycolylneuraminic (Neu5Gc) with the latter present only in trace amount <sup>25</sup>. Sulfatides, also called sulfoglycosphingolipids is unique because it contains a sulfate group <sup>26</sup>. The simplest form of sulfatides are sulfated GalCer which are predominantly present in the central and peripheral nervous system, kidney, endometrium and gastrointestinal tract. Sulfation is also found in more complex GSLs. Other variations in the structure include acetylation and lactonization on the glycan part, and hydroxylation and unsaturation on the fatty acyl moieties on the ceramide part. The biological functions of these modifications have been studied extensively and their distribution, both cellular and spatial largely remain unknown.

In contrast to proteins and nucleic acids whose expression can be predicted from the genetic sequence, the biosynthesis of GSLs is non-template driven. It begins from the endoplasmic reticulum (ER) and culminates in the Golgi complex <sup>8,16,27,28</sup>. Depicted in **Fig. 2** is the simplified scheme of the biosynthesis of mammalian GSLs (more details on this topic can be found in recent reviews <sup>3,5,8,28</sup>). First, the ceramide is synthesized in the ER using pre-existing sphingosine and AcylCoA via ceramide synthase. The ceramide could undergo addition of galactose to form galactosylceramide (GalCer) or transported to Golgi complex. In the Golgi complex, it can be used for sphingomyelin (SM) or glucosylceramide (GlcCer) synthesis. Most of

the GSLs in eukaryotes are derived from GlcCer through stepwise addition of monosachharide units with the help of glycosyltransferases. Specifically, in the Golgi, GlcCer further undergoes addition of galactose to form lactosylceramide (LacCer) which serves as precursor for synthesis of complex GSL core structures (**Table 1**). Active glycosyltransferases utilize these core structures to produce a wide array of GSLs in eukaryotic cells which could range up to 10 sugar units or more upon addition of other carbohydrates such as Neu5Ac, L-fucose, or other modifications <sup>3</sup>. On the other hand, the synthesized GalCer in ER is transported to the Golgi complex where it is used for synthesis of sulfatides and GM4 <sup>8</sup>.

**Table 1. Core Structures of Mammalian GSLs.**

Series name	Core structure	CFG symbolic representation	Abbreviation
<b>Ganglio</b>	Gal $\beta$ 3Gal $\beta$ 4Gal $\beta$ 4Glc1-		Gg
<b>Lacto</b>	Gal $\beta$ 3GlcNAc $\beta$ 3Gal $\beta$ 4Glc1-		Lc
<b>Neolacto</b>	Gal $\beta$ 4GlcNAc $\beta$ 3Gal $\beta$ 4Glc1-		nLc
<b>Globo</b>	GalNAc $\beta$ 3Gal $\alpha$ 4Gal $\beta$ 4Glc1-		Gb
<b>Isoglobo</b>	GalNAc $\beta$ 3Gal $\alpha$ 3Gal $\beta$ 4Glc1-		iGb

CFG stands for Consortium for Functional Glycomics. For key to symbols, see Fig. 1.

Recycling of the synthesized GSLs is an important process in cell survival. This begins with internalization of these molecules from the cell surface and enter the endosomal compartments. While some of these are remodeled in the Golgi, majority of internalized GSLs are degraded in the lysosomes through stepwise process involving deglycosylation.

Impairment of these processes result to accumulation of GSLs and are recognized hallmark of lysosomal storage diseases <sup>29</sup>.

Taken together, the complex biosynthetic process illustrates that the type and diversity of GSLs within a specific state depends mainly on the activity of important enzymes required for their synthesis. Because they are downstream products of metabolism, GSLs respond to stimuli more quickly than gene expression does, suggesting that the profile of GSLs could picture the dynamic biological phenotype at a given timepoint.

### **Nomenclature**

The traditional nomenclature of GSLs was originally proposed by Svennerholm for gangliosides <sup>30</sup>. In this two-letter system, the first letter *G* is a notation for gangliosides, while the second is based on the number of sialic acids as one (mono-, *M*), two (di-, *D*), three (tri-, *T*) and four (quadri-, *Q*) and so on. These two letters are followed by a number, denoting their relative sequence during TLC analysis. For example, GM1, GM2 and GM3 are monosialogangliosides eluting in this arrangement on the TLC plate from the origin. Systematic way of naming these biomolecules is based on the joint IUPAC-IUB recommendations for glycolipids in 1997 using the core structure name <sup>31</sup>. Thus, for ganglioside whose composition is GalNAc $\beta$ 1-4(Neu5Ac $\alpha$ 1-3)Gal  $\beta$ 1-4Glc $\beta$ 1-1' connected to a ceramide backbone (named GM2 in Svennerholm system), the IUPAC-IUB symbol for the core structure would be Gg<sub>3</sub>Cer, which corresponds to the ganglioseries possessing the first three monosaccharide units (hence the number 3 in Gg<sub>3</sub>). The complete systematic symbol is II<sup>3</sup>- $\alpha$ -Neu5Ac-Gg<sub>3</sub>Cer which accounts for the Neu5Ac connected to the second monosaccharide unit (Roman numeral II) via  $\alpha$ (1-3) linkage (3 and  $\alpha$ , respectively, in II<sup>3</sup>- $\alpha$ -). Nevertheless, the use of Svennerholm system is acknowledged and still widely accepted.

### **Intact structure and biological significance of GSLs**

GSLs are amphiphatic molecules that form high molecular weight micelles and segregate within the plasma membrane where they form lipid rafts and microdomains along with cholesterol, sphingomyelin and proteins<sup>4</sup>. In these domains, GSLs interact with receptors and modulate signal transduction processes. Owing to their hydrophilic oligosaccharides head, they form cluster of molecules on the cell surface called “glycosynapse” and function as differentiation markers associated with inter- and intra-cellular communication<sup>4</sup>. Some of the known functions of the headgroup and the lipid moiety are summarized in **Table 2**.

The glycan headgroup in the GSLs assumes a vast array of biological functions. For example, it can serve as receptor of viruses and bacteria<sup>5,6</sup>, or as antigen to several autoimmune diseases<sup>32</sup>. The glycan headgroup is also involved in protein-interaction, receptor regulation, adhesion, initiation/modulation of signal transduction, cell recognition and differentiation<sup>4-6</sup> wherein the structure and composition of the glycan moiety play crucial roles. To name a few, a change in glycan structure could significantly alter antigenicity<sup>33</sup> or functions during embryonic development<sup>5,6</sup>. High level of sialylation in GSLs is also crucial in cancer and other diseases. The presence of negatively charged sulfate group in sulfatides show unique physiological role, for example, in kidneys, central nervous system and in cardiovascular processes, as reviewed elsewhere<sup>26</sup>.

The ceramide component serves as an anchor of the glycan to the cell membrane and can modulate the properties of the oligosaccharide moiety<sup>34,35</sup>. For example, in the study of verotoxins, the presence or absence of a carbon-carbon double bond has affected the toxin binding to the Gb3 receptor, with the one containing the double bond shown to have higher affinity than the one without<sup>5,36</sup>. The presence of unsaturation also significantly affects the membrane order and eventually the signal transduction processes. Degree of unsaturation and

length of the fatty acyl chain also affect spermatogenesis and retinal function. In case of hydroxylated fatty acyl chains, the additional -OH group enhances hydrogen bonding and makes lipid rafts more rigid. Taken together, this body of literature emphasizes that not only the glycan, but also the ceramide backbone requires to be thoroughly studied. In cells, the presence of numerous desaturases that introduce double bonds in fatty acyl chains and their diversity in GSLs suggest that location of unsaturation plays an important role in biology and it is necessary to determine the specific location and configuration of these functional groups. Taken together, the determination of the intact structure of GSLs is greatly needed to precisely understand their biological roles.

**Table 2. Key Biological Functions of the Two Structural Components of GSLs.**

<b>Glycan headgroup</b>	<b>Ceramide backbone</b>
<ul style="list-style-type: none"> <li>• Receptor</li> <li>• Antigen</li> <li>• Protein interaction</li> <li>• Receptor regulation</li> <li>• Mediator of cell adhesion</li> <li>• Initiator/modulator of signal transduction</li> <li>• Cell recognition and differentiation</li> </ul>	<ul style="list-style-type: none"> <li>• Hold glycan on plasma membrane</li> <li>• Modulate antigenicity of the glycan moiety</li> <li>• Influence clustering of glycan on membrane surface</li> <li>• Second messenger in signal transduction</li> </ul>

### **GSLs as disease biomarkers and therapeutic targets**

The diverse physiological functions of GSLs are crucial in health and diseases <sup>5,8,16,27</sup>. Cell surface glycan GSLs markers could be altered during pathological conditions, for instance, it was reported that the degree of sialylation can serve as markers of neurological diseases <sup>37</sup>. Generally, in neurological disorders, dysregulation of gangliosides and sulfatides correlate to progression of these pathologies <sup>38</sup>. In lysosomal storage diseases, enzymes necessary for the degradation of GSLs are deficient, absent or weakly active resulting to accumulation of GSLs in

different tissues <sup>27</sup>. In cancer, changes in GSLs composition could distinguish cancer cells from non-cancer cells as well as stem cells and non-stem cancer cells <sup>39</sup>. Likewise, aberrant levels of GSLs have been associated with autoimmune, metabolic and other complex diseases <sup>29,39</sup>. As such, these biomolecules could potentially serve as disease biomarkers.

Recently, GSLs have been considered as potential targets for immunotherapy due to their antigenic properties toward T lymphocytes <sup>40</sup>. For example, invariant natural killer T (iNKT) cells have been widely studied to recognize GSL antigens that are being presented by CD1d molecule analogous to major histocompatibility complex (MHC) class I. Activated iNKT cells could induce the release of cytokines that mediate immune response, making this a promising therapeutic target for cancer <sup>41,42</sup> and infectious disease <sup>40</sup>.

### **Current Challenges in the Analysis of Intact GSLs**

Intact analysis of GSLs is challenging owing to their amphiphilic chemical nature, the co-presence of a plethora of structurally diverse GSLs, their low abundance, and the scarcity of a wide selection of commercially available standards <sup>15</sup>. Because of their chemical nature, GSLs are challenging to extract and isolate in a single step. Specifically, during liquid-liquid partitioning, not all GSLs can be collected in a single solvent phase, thus additional steps are necessary to recover GSLs with bulkier glycan headgroup. For this reason, in contemporary lipidomics that use Folch extraction method <sup>43</sup>, these molecules are often missed during the analysis because only the organic lower phase is recovered. Also, GSLs do not possess any chromophore, hence they are difficult to detect using traditional optical spectrophotometric techniques. Derivatization is often required prior to measurement in UV/Vis or fluorescence. Furthermore, their strong hydrophilic headgroup impedes their ionization in MS as the number of sugars increase. The presence of labile groups such as sialic acid and fucose, also requires careful method

development and selection of appropriate ionization techniques to avoid in-source fragmentation that would otherwise lead to erroneous interpretation of results.

The structural diversity in the glycan and ceramide components is another level of formidable analytical challenge because both glycan and ceramide groups could exist in different isomeric forms (**Fig. 3**). For example, linkage isomers and positional isomers could arise in the glycan part (**Fig. 3a**). Notable examples of linkage isomers are Gb3 and iGb3 which only differ in the attachment of the terminal Gal moiety<sup>44</sup>. Noteworthy, these isomers have distinct, complementary biological function<sup>33</sup>. Positional isomers are more common, such as GD1a/GD1b/GD1c, GM1a/GM1b, GT1a/GT1b, again, these are known to exist in mammalian system with distinct biological functions<sup>45</sup>. The stereochemical configuration is another source of structural variation in the glycan moiety as exemplified by epimers Glc and Gal. In terms of the ceramide backbone, some level of structural diversity includes the presence of hydroxyl group and one or more degrees of unsaturation. The presence of either hydroxyl and carbon-carbon double bonds could arise to isomeric and isobaric species (**Fig. 3b**), for example, GalCer<sub>d</sub>18:1(*n*-14)/23:1(*n*-9)(OH), GalCer<sub>d</sub>18:1(*n*-14)/23:1(*n*-7)(OH), and GalCer<sub>d</sub>18:1/24:0, all of which have a nominal mass of 811 Da. In gangliosides, the major concern is the differentiation of sialic acid variants as Neu5Ac and Nue5Gc which only differ in terms of one hydroxyl group, as well as the different possible connectivity whether  $\alpha$ 2-3 or  $\alpha$ 2-6 (**Fig. 3c**). Although these have been addressed in recent methods<sup>46-51</sup>, the capability for practical utilization of these strategies remains largely unexplored.

The naturally low abundance of GSLs in biological samples is another major analytical challenge. For instance, the dynamic range of lipid concentrations in human plasma and serum spans up to six orders of magnitude, thus profiling of GSLs in this type of sample is difficult because of the co-presence of more abundant species, mainly phospholipids<sup>52</sup>. The latter are

known to cause ion suppression effects in MS<sup>53</sup>. As such, it is necessary to apply pre-concentration and enrichment of these biomolecules prior to MS analysis. Without any fractionation of the total lipid extracts, the currently used techniques based on MS and other instruments could not accurately detect low abundant GSLs.

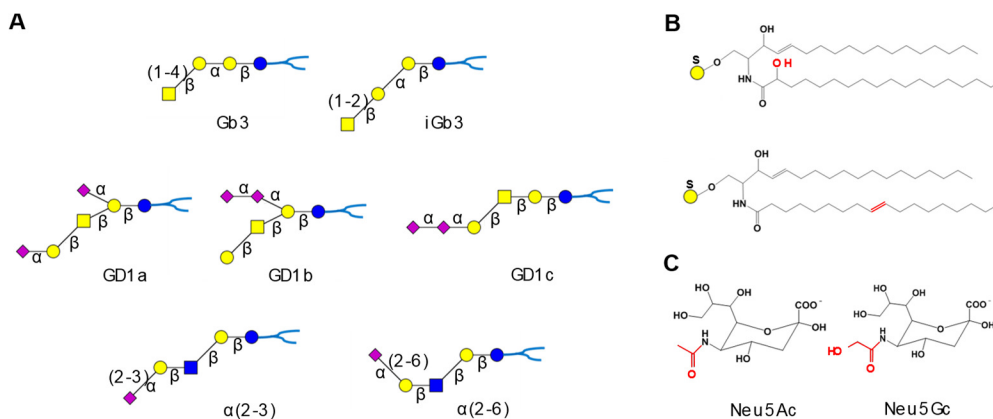


**Figure 3. Representative Structures Showing the Structural Diversity of GSLs.** (A) Isomeric forms of GSL glycan moiety. (B) structural variation and possible source of isomeric forms for the ceramide moiety in terms of the location of unsaturation. (C) Structural variation of sialic acids in mammalian system.

Importantly, commercially available standards for GSLs are limited to only few GSLs such as gangliosides GM1, GM2, GM3, GD1a, GD1b, GD2, GT1, GQ1b which are derived from natural sources, commonly bovine or porcine brain, and a few neutral GSLs such as cerebrosides and globosides containing up to four sugar units. Isotopically labelled standards for quantitative studies, although available, are only limited to few GSLs classes and mostly are deuterated. The use of <sup>13</sup>C-labeled standards would be a better option for LC-MS based analysis using reversed-phase column because it ensures the coelution of the internal standards and the target analytes. Furthermore, to date, there is lack of commercially available standards for *O*-acetylated, lactonized, and sulfated complex GSLs that could facilitate studies on these rare molecules.

## **Sample Preparation**

### **Type of samples**

In principle, due to its ubiquitous nature in the body, any tissue, organ or biological fluid can be used for determination of GSLs<sup>16</sup>. Body tissues obtained from a biopsy procedure or from *post-mortem* samples are currently the most widely used for immunohistochemical staining<sup>54</sup> which easily identifies the distribution of GSLs. In clinical setting, this is important for patients suffering from lysosomal storage diseases where the GSLs accumulates in tissues and body fluids. Among organs and tissues, brain, kidney, and liver are commonly used samples for analysis.

Brain tissue<sup>25,49,55-62</sup>, commonly from rat is the frequently used model for demonstrating analytical methods for gangliosides and sulfatides owing to their abundance in the central nervous system<sup>25,63,64</sup>. Lung<sup>65</sup>, heart<sup>66</sup>, intestines<sup>67-69</sup>, kidneys<sup>54,70,71</sup>, retina<sup>72</sup>, ovarian cells<sup>73 74</sup> and breast cancer stem cells<sup>75-78</sup> have likewise been used to analyze GSLs and interesting information have been found concerning the distribution of these molecules in these samples. Recently, human fetal tissue was subjected to gangliosides analysis and data have revealed the relationship of glycan composition during developmental stages<sup>79,80</sup>. Cerebrospinal fluids<sup>81</sup> have been also used in studies of neurological disorders such as multiple sclerosis and Alzheimer's disease<sup>82,83</sup>  
84.

Other than tissues and organs, probably the most commonly used samples for biomarker studies are blood and urine because of two palpable reasons. First, they could be obtained quite easily in a less invasive way. Second, during pathologic states some of the GSLs could be shed-off from the surface of diseased tissues or cells and therefore are detectable in the blood<sup>85</sup>. Moreover, urine could reflect the pathologic condition of specific organs such as kidneys<sup>86</sup>. In

addition, dried blood spots can also be used, especially in newborn screening set-up<sup>87</sup>. These biological samples have been widely used in GSLs analysis.

### **General sample preparation workflow**

Highly abundant simple lipids and biopolymers like proteins and nucleic acids co-exist with GSLs. In MS-based work, these unwanted molecules cause ion suppression effects, as such, their removal is greatly warranted<sup>88</sup>. Briefly, tissues or cells are homogenized, in case of biological fluids, no homogenization is necessary, but removal of suspended particles is needed (**Fig. 4**). Sample amounts vary depending on the availability of materials and the goal of the study, but commonly, 1.0 to 500 mg of tissue, at least 10<sup>6</sup> counts for cells and 1.0 to 100  $\mu$ L for biological fluids are often used. Total lipids are extracted using monophasic CHCl<sub>3</sub>/CH<sub>3</sub>OH, typically in a ratio of 2:1 using the Folch's method<sup>43</sup>, 1:2 in the case of Bligh and Dyer method<sup>89</sup>, or 1-butanol/CH<sub>3</sub>OH (3:1)<sup>90</sup>. In either case, the CH<sub>3</sub>OH disrupts the interactions between lipids and biopolymers thus effectively dissolving the lipids in the organic layer. Alternatively, the lower phase of the two-layer isopropanol: hexane: H<sub>2</sub>O (55:25:20, v/v) solvent system could be used before and after CHCl<sub>3</sub>/CH<sub>3</sub>OH (1:1, v/v) extractions to further increase the recovery of complex GSLs<sup>91</sup>. The crude extract thus obtained is dried and partitioned with water. The resulting CHCl<sub>3</sub> lower phase contains phospholipids, cholesterol and the more hydrophobic GSLs, *i.e.* cerebroside and sulfatides. The upper phase contains complex neutral GSLs and gangliosides while proteins and other debris retain in the interface.

Cerebroside and sulfatides can be recovered from the lower layer via optional peracetylation, followed by silicic acid column chromatography and subsequent deacetylation (**Fig. 5b**)<sup>92,93</sup>. Thorough removal of impurities was found to be more efficient when acetylation/deacetylation steps are performed. However, these should be avoided when the sample is suspected to contain *O*-acetyl groups because these are removed during this step<sup>92</sup>

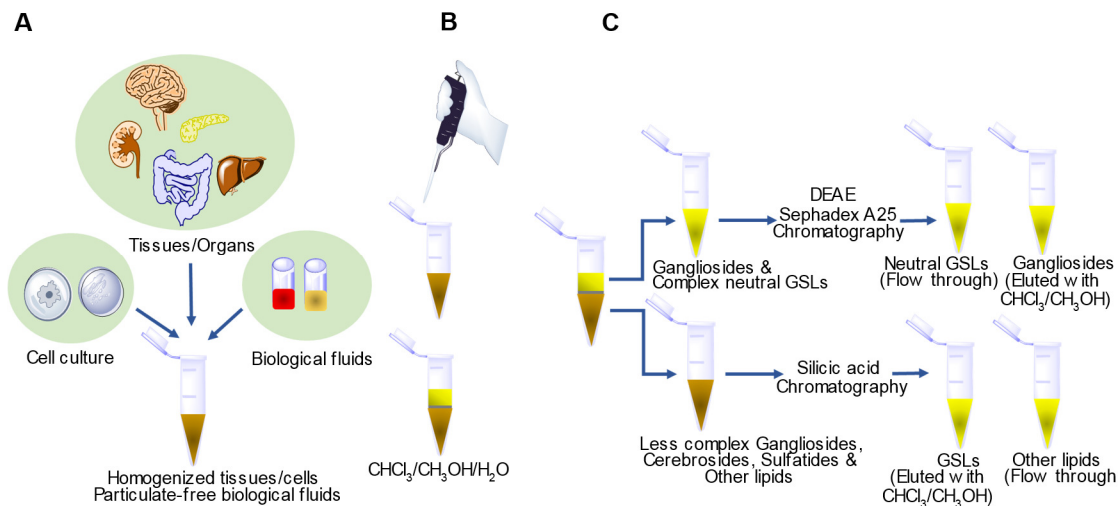


**Figure 4. General Workflow for Extraction and Isolation of Specific GSLs.** (A) The tissue, cell culture or biological fluids are homogenized with chloroform/methanol, which is further partitioned by adding water. (B) The top aqueous layer contains mostly complex hydrophilic lipids such as gangliosides and complex neutral GSL while most lipids including cerebroside and sulfatides are in the lower layer. Further purification uses DEAE cellulose chromatography to recover neutral and acidic GSL. Silicic acid chromatography is used to separate most lipids from GSL.

In silicic acid column chromatography, phospholipids are retained on the column while acetylated GSLs can be eluted with  $\text{CHCl}_3/\text{CH}_3\text{OH}$  gradient. Further separation of sulfatides from cerebroside and gangliosides from neutral GSLs can be done using weak anion exchange column, diethylaminoethane (DEAE)-Sephadex A25. The resulting GSLs fractions are purified by C18, C8 solid phase extraction (SPE) or dialysis using a membrane with 3,000 Da molecular weight cutoff<sup>93</sup>.

There are also available methods for selective extraction of specific subclass of GSLs. The method of Svennerholm and Fredman<sup>94</sup> is used for extraction and isolation of gangliosides. In contrast to Folch's extraction<sup>43</sup>, this method uses higher proportion of polar solvents such as methanol and water throughout the process which increases extraction efficiency owing to the higher solubility of complex gangliosides in aqueous solvents. Methods involving non-ionic

detergent called hexaethyleneglycol mono-n-tetradecyl ether <sup>95</sup> and monophasic extraction <sup>88</sup> have been described. Selective extraction of sulfatides can be accomplished using the method developed by Svennerholm and Thorin <sup>96</sup> and the CHCl<sub>3</sub>-free based method by Hara and Radin <sup>97</sup>. For dried blood samples, extraction of sulfatides was found to be optimum using extraction with methanol or isopropanol with prior water incubation <sup>98</sup>.

Alternatively, preparative thin layer chromatography (TLC) can be used for the isolation of specific classes of GSLs <sup>99,100</sup>. This is done by developing the TLC plate in an appropriate solvent system, followed by detection using reversible stains such as primuline, and then scraping the spots of interest prior to extraction using CHCl<sub>3</sub>/CH<sub>3</sub>OH.

Solid phase extraction (SPE) using aminopropyl and silica gel cartridges can also be used for fractionation of crude lipid extracts. Aminopropyl SPE cartridge has been used for specific isolation of cerebrosides and globosides eluted using the acetone – methanol (9:1.35 v/v) solvent system <sup>101</sup>. However, this approach could not separate sulfatides from sphingosine-1-phosphate and ceramide-1-phosphate. Recently, silica gel SPE column has been applied for fractionation of lipids, particularly effective for sulfatides from the total lipids extract obtained by the Folch's method <sup>102</sup>. The use of titanium dioxide (TiO<sub>2</sub>) has recently been shown as an effective technique for separation of GSLs <sup>103</sup>. For MS methods capable of selected reaction monitoring and precursor ion scans, the organic layers from Folch's method can be utilized directly for sulfatides analysis in the targeted mode <sup>63,82</sup>.

### **Novel enrichment strategies**

Novel enrichment strategies described below require reactive sites to be present in the molecule, often in the form of an aldehyde, ketone, or free amine. Unfortunately, these functional groups are naturally non-existent in the intact, native structure of GSLs. In this respect, some level of chemical modifications is needed such that novel enrichment strategies discussed here

can be used for very low abundant analytes starting from complex biological mixtures. These chemical modifications can be accomplished in various ways (**Fig. 5**). For example, to introduce an aldehyde in the lipid backbone, solution-phase ozonolysis can be used that cleaves the carbon-carbon double bond on the sphingosine backbone <sup>104</sup>. Enzymes such as endoglycoceramidase (EGCase) <sup>85,105,106</sup> or sphingolipid ceramide *N*-deacylase (SCDase) <sup>107,108</sup> can also be used to introduce reactive functional groups. EGCase cleaves the glycosidic bond between the ceramide and the glycan moiety, thus releasing the oligosaccharide with free reducing end that is known to be in equilibrium with its aldehyde form. When using serum, EGCase digestion could be directly applied even without prior extraction. The use of SCDase cleaves the amide bond releasing the fatty acyl chain.

More recently, the group of Cummings has developed a method to release total glycans (both from glycoproteins and GSLs) in biological samples using a very cheap reagent, sodium hypochlorite (NaOCl) in a method they called oxidative release of natural glycans (ORNG) <sup>109</sup>. Using this approach, the ceramide backbone of GSLs is converted to nitrile which could be reduced to amino form and subsequently used for other chemistries. Another way to introduce a reactive site is through chemoselective oxidation of the trihydroxy functional group in Neu5Ac via mild oxidation reaction using sodium metaperiodate (NaIO<sub>4</sub>) <sup>14</sup>.

Sample preparation involving glycoblotting technique has been recently developed for enrichment of GSLs. This involves immobilization of glycans on a functionalized surface or beads (**Fig. 6**). Originally used for glycans released from glycoproteins <sup>110</sup>, it was demonstrated to be equally applicable to GSLs <sup>85,111</sup>. Here, an aldehyde group are made available using an appropriate glycan release strategy. These aldehydes undergo reductive amination with amino groups on the beads, typically hydrazide.

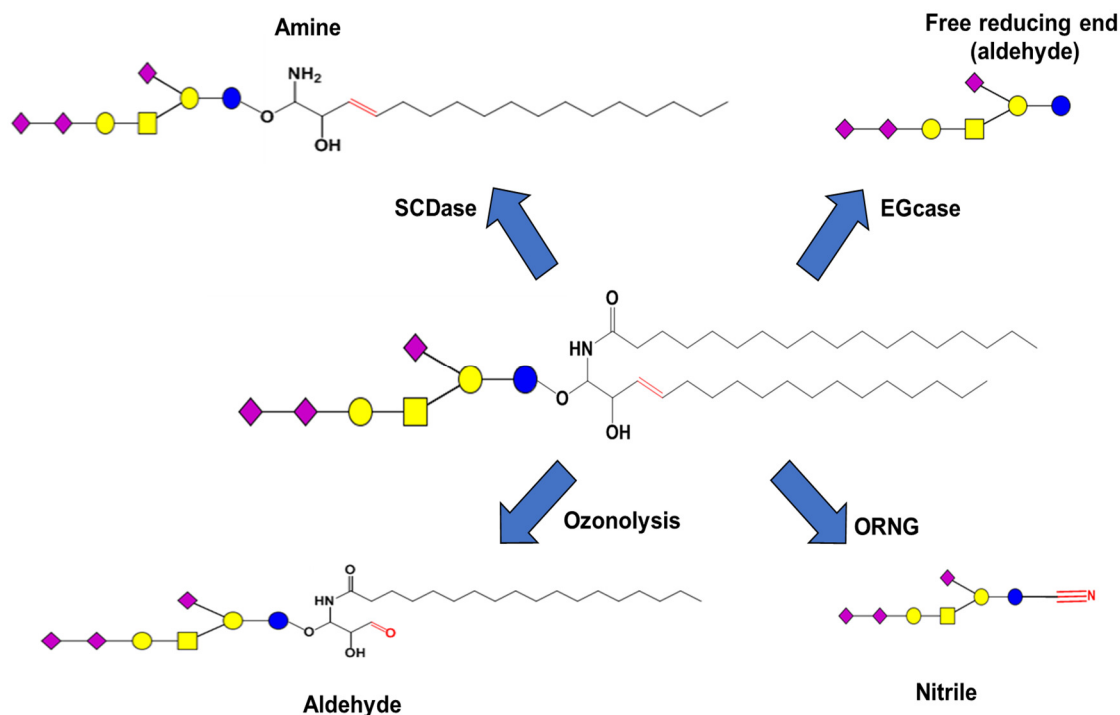


**Figure 5. Strategies to Introduce Reactive Functional Groups in GSLs.** Sphingoid N-deacylase (SCDase) is used to remove the fatty acyl chain leaving behind the sphingosine backbone. Endoglycoceraminiidase (EGCcase) is used to totally remove the lipid part leaving the reducing end of the glycan intact. Ozonolysis cleave the C=C on the sphingosine but could also cleave other C=C bonds if present. Oxidative release of natural glycols (ORNG) uses bleach (NaOCl) converting the rest of the lipid into a nitrile group which could be further reduced to form a primary amine group and used for other chemistries.

Excess hydrazide groups are blocked by esterification. The glycans are recovered by transamination reaction and collected as an aqueous solution. This technique was shown to improve sensitivity in MS analysis<sup>104</sup>. Another approach is to immobilize the GSLs on polyvinylidene difluoride (PVDF) membrane followed by EGCcase treatment<sup>105</sup>.

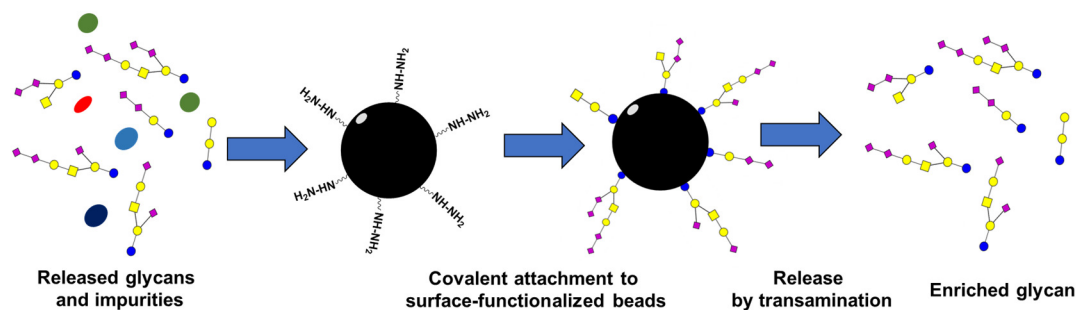


**Figure 6. Glycoblotting Technique for Enrichment of GSLs.** Released glycans with free reducing end or aldehyde could be used to attach the glycan on a functionalized surface, for example, hydrazide. Enriched glycans are released by transamination.

The use of hydrophobic PVDF facilitates immobilization of GSLs through interaction between the surface and the ceramide backbone, thus, effectively exposing the glycan to EGCase action. This technique was successfully applied to ovarian cancer cells and tissues.

### Mass Spectrometry of GSLs

The capability of MS to provide both qualitative and quantitative information in addition to its suitability for high throughput workflows makes it the most widely used tool to analyze GSLs. Moreover, the high sensitivity and dynamic range of modern instruments enable the detection of minute amount of GSLs down to attomole levels. As such, the use of MS in glycoconjugate analysis has been the subject of extensive reviews<sup>18,21,112-114</sup>. In this review, we will focus on application of mass spectrometry to analysis of GSLs.

### **Ion generation**

Neutral molecules are ionized as positive or negative ions prior to MS analysis. Positive ionization mode is commonly applied to neutral GSLs while negative ionization mode is used for analysis of acidic species such as gangliosides and sulfatides because of the facile conversion of these species as negative ions.

Ionization techniques are broadly classified as hard and soft, depending on the extent at which the molecular ion is fragmented at source. Hard ion sources include electron impact (EI), fast atom bombardment (FAB) and liquid secondary ion (LSI). The high energy transferred from the neutral or charged particles to the analyte results to fragmentation of the molecular ion. FAB and LSI were popular in the 1980s until early 2000s. Indeed, most of our current knowledge on GSLs stemmed from seminal studies using FAB and LSI <sup>115</sup>, but they have been widely replaced by soft ionization methods <sup>115</sup>. On the other hand, EI coupled with a gas chromatograph (GC) has been used since 1960's especially when rapid and effective permethylation was developed and is still being used today.

Soft ionization techniques include chemical ionization (CI), electrospray ionization (ESI), matrix assisted laser desorption/ionization (MALDI), atmospheric pressure chemical ionization (APCI), atmospheric pressure photoionization (APPI) and ambient ionization techniques. Although the use of APCI <sup>116</sup> and APPI <sup>117</sup> for GSLs has been reported, only MALDI and ESI are routinely applied for measurement of GSLs, and thus the focus of this review.

### **ESI-MS**

ESI is the most common ionization technique in modern MS instrumentation that comes standard with most commercial instruments. This ionization method essentially involves three important processes namely, nebulization, ionization, and desolvation <sup>118</sup>. Briefly, samples in solution form are electrosprayed through a metal capillary that is applied with high voltage typically 1.5 to 3.5 kV to form a dispersion of fine droplets in the gas phase. The high amount of charge applied during electrospray affords the formation of ionized species. To further aid the nebulization process, more volatile solvents are used to dissolve the sample such as methanol and acetonitrile. Use of sheath gas, typically nitrogen (N<sub>2</sub>) also helps in the nebulization process.

Formation of adducts in ESI have been studied extensively and many mechanisms have been proposed<sup>118,119</sup>.

Using ESI, GSLs can be ionized in different adduct forms such as  $[M+\text{metal}]^+$ ,  $[M+H]^+$ ,  $[M+NH_4]^+$  in positive mode or  $[M-H]^-$ ,  $[M+HCOOH-H]^-$  and  $[M+\text{halide}]^-$  in negative mode, whose cations and anions largely depend on the solvent composition and additives used to dissolve the sample. The most common is  $[M+Na]^+$  because of the ubiquitous nature of and the high affinity of glycosylated molecules to sodium ion. This is particularly true for MS instruments that use sodium formate as calibrants and when no lengthy flushing of the ESI source is made prior to infusing of samples. For LC-MS based methods where additives such as acetic acid or formic acid is used, sodium ions are overwhelmed by the more abundant protons which induce the formation of  $[M+H]^+$  ions. The use of different adducts could affect the downstream MS analysis process, and thus depending on analytical purpose, choice of adduct is extremely important. In most cases, neutral GSLs are analyzed as  $[M+H]^+$ ,  $[M+Na]^+$  or  $[M+Li]^+$  while acidic GSLs are analyzed as  $[M-H]^-$  ions. Gangliosides that contain more than one sialic acids are often observed as multiply charged species in the form of  $[M-H]^{2-}$  and  $[M-H]^{3-120}$ .

## **MALDI-MS**

In MALDI, the sample is co-crystallized with a UV-absorbing matrix on a metallic plate followed by laser irradiation<sup>121</sup>. Common matrices used for GSLs include 2,5-Dihydroxybenzoic acid (DHB), 1,5-Diaminonaphthalene, 4-hydrazinobenzoic acid and 6-aza-2-thiothymine<sup>122</sup>. MALDI can be operated in positive and negative ionization modes that provide high abundant  $[M+Na]^+$  and  $[M-H]^-$  adducts, respectively. In gangliosides analysis, negative mode was found to be more sensitive and provides richer fragmentation<sup>122</sup>.

MALDI was first applied to GSLs by Costello and co-workers, and a comprehensive review on the application of MALDI in glycoconjugate analysis has been extensively reviewed

by Harvey <sup>122-125</sup>. In contrast to ESI, this technique allows ionization of even higher mass glycans, and is tolerant to contaminants such as salts. Here, the sample is mixed with a suitable matrix, commonly 2,5-Dihydrobenzoic acid (DHB) and then irradiated by a laser source. The choice of matrix is important because it affects the ionization as well as possible post-source decay fragmentation of GSLs, especially gangliosides that contain labile sialic acid moieties. The use of ultraviolet (UV) lasers imparts higher energy during ionization process resulting to dissociation of labile groups such as sialic acid. Recent MALDI techniques have utilized infrared (IR) lasers instead of UV as well as introduction of collisional cooling strategies to circumvent this issue <sup>126,127</sup>.

Like other ionization techniques, inherent challenges in MALDI of GSLs include decreasing ionization efficiency with increasing glycan lengths. Another caveat is the post-source decay which results to prominent decarboxylation reactions and loss of sialic acid moiety, especially for gangliosides. To circumvent these issues, gangliosides are typically derivatized using permethylation <sup>128</sup> to increase the stability of Neu5Ac while improving their overall hydrophobicity, and thus, volatility and ionization efficiency.

Another limitation of MALDI-MS is its susceptibility to background noise due to matrix clusters that preclude the detection of low molecular weight GSLs <sup>129</sup>. Newer methods, although do not need a MALDI matrix, have not been utilized for GSLs <sup>125</sup>. Also, due to the absence of prior separation techniques, this method could not distinguish isomers and is prone to ion suppression effects especially in biological samples. Recently, MALDI has been coupled to ion mobility spectrometry to allow resolution of isomers but this has not been applied to GSLs <sup>130</sup>.

The non-uniformity of spotting samples on MALDI plate could result to variability in ion signal intensities. To address this, the group of Peter-Katalinic introduced the coupling of normal phase nano-HPLC with MALDI using an automated robotic spotter to enable the analysis of

complex mixtures of acidic and neutral GSLs<sup>131</sup>. Briefly, the samples are separated in the normal phase nano-HPLC and the eluting compounds are precisely collected on the MALDI plates with co-crystallization of the matrix. Although this method was found to have better uniformity of spotting, it still suffers from tedious method development and practicability for most laboratories.

The use of MALDI-MS for quantitation of GSLs has remained a challenging task, until recently when quantitative MALDI-TOF MS/MS was used to profile human serum GSLs following endoglycanase digestion with glycoblotting sample preparation<sup>85</sup>. A total of 42 distinct GSLs were detected in human serum at a concentration of 12.1 to 21.4  $\mu\text{M}$ , this is lower than those of N-linked glycans in serum which has a range of 700 to 850  $\mu\text{M}$ <sup>85</sup>.

Currently, MALDI-MS is gaining popularity as an imaging tool (also called MALDI imaging mass spectrometry or MALDI-IMS), providing both molecular and spatial distributions of analytes in a sample. This has been utilized for imaging of GSLs in tissues<sup>55,132 133 134 135 136 137</sup>. Comprehensive review<sup>138</sup> has been made on this topic and will not be elaborated here.

### **Mass analyzers**

The ions generated at source are subjected to mass analysis where they are resolved based on  $m/z$  ratio. Several mass analyzers have been developed that include low resolution and high-resolution instruments. Low resolution instruments such as ion trap (IT) and single or triple quadrupoles (QqQ) are often used for targeted analysis while high-resolution such as time-of-flight (TOF), orbitrap, or Fourier Transform ion cyclotron resonance (FTICR)-based instruments are used for untargeted analysis to identify unknowns. The use of analyzer with high resolution accurate mass (HR/AM) measurement capabilities affords not only to distinguish isobaric species which are otherwise non-distinguishable in low resolution instruments but also to enable assignment of elemental compositions<sup>139</sup>. Typically, mass errors of up to 10 ppm for orbitrap, FTICR, and Q-TOF based instruments are achievable. In principle, any mass analyzer can be

used for GSLs studies, however, hybrid instruments has become increasing more prominent in ‘lipidomics’ approaches due to their tandem MS capability.

The multi-stage fragmentation in ion trap makes it a good choice for MS<sup>n</sup> fragmentation and top-down sequencing of GSLs<sup>18,44</sup>. One limitation, however is the low mass cut-off in this instrument which in the case of sulfatides, the diagnostic ion *m/z* 97 is lost. This could be circumvented using the pulsed Q dissociation (PQD)<sup>140</sup> technique that enables the fragmentation and trapping of the resulting low-molecular weight fragments.

### MS/MS fragmentation of GSLs

MS/MS fragmentation involves breaking down a mass-selected precursor ion using collisional activation, ion-molecule reaction, electron-induced activation, or photo-induced activation. The resulting fragment ions are named systematically and are used for reconstructing proposed structures of unknown glycolipid molecules.

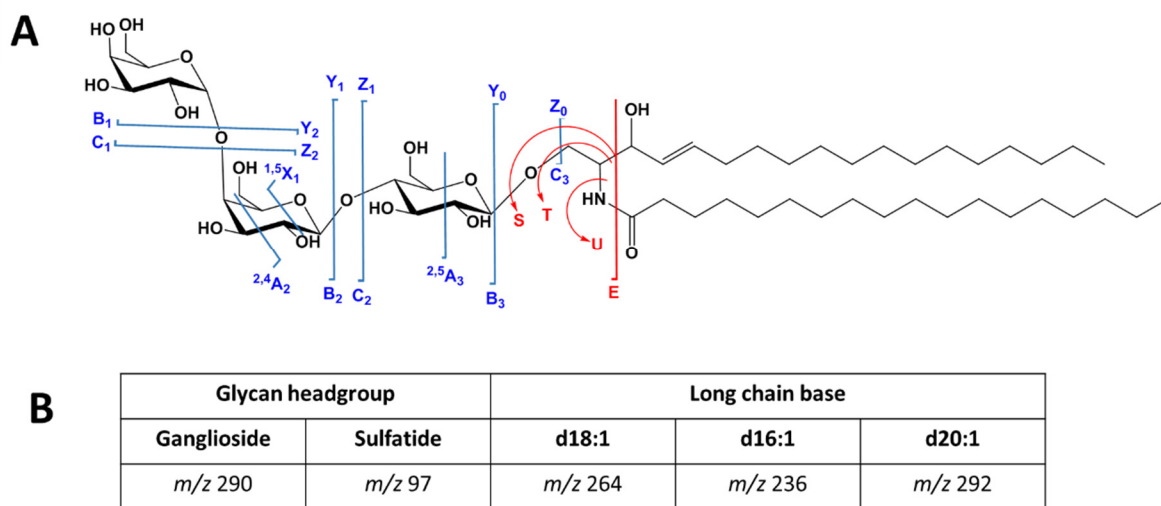


**Figure 7. Nomenclature of Fragmentation for GSLs.** Only the common fragments observed involving ceramide backbone (in red) are shown (A). The diagnostic fragments in MS/MS spectra are shown in (B).

## **Nomenclature of GSL fragments**

The widely accepted nomenclature for GSLs fragmentation is that of Domon and Costello <sup>141</sup>, later modified by Ann and Adams <sup>142</sup>. In this scheme (**Fig. 7**), *A*, *B*, and *C* fragments contain the reducing end of the glycan while *X*, *Y* and *Z* denote the fragments containing the non-reducing end. The *B*, *C*, *Y* and *Z* correspond to glycosidic bond cleavages that allow determination of carbohydrate sequence while *A* and *X* are cross-ring cleavages that allow identification of linkage positions. The superscripts in cross-ring cleavages denote which bond is fragmented, for example, <sup>1,5</sup>*X* ion is formed by cleavage of the bonds between C1-C2 and C5-O.

## **Ion activation**

The structure of GSLs can be established from its fragmentation pattern generated using tandem MS experiments (MS/MS) <sup>18</sup>. Here, the precursor ion is selected and subsequently fragmented through ion activation. Ion activation method simply put, is classified into four– low energy, higher energy, electron aided and photoinduced fragmentation. Low energy fragmentation provides glycan sequence due to the cleavage of glycosidic bonds while electron aided and photoinduced fragmentation provide linkage and branching information due to abundance of cross-ring fragments and difference in the mechanism at which fragmentation is induced.

## **Collisional activation**

In collisional activation, ions are accelerated toward and collide with, an inert gas (*e.g.* Helium, Argon, Nitrogen). The high internal energy brought by collision results to fragmentation of the ions. The most labile bonds are quickly cleaved, and the stability of the resulting ions is reflected by its relative abundance in the spectrum.

Collisional activation comes in two main flavors, collision-induced dissociation (CID) and higher energy collisional dissociation (HCD). CID fragmentation of neutral and acidic GSLs

has been studied extensively as reviewed by Levery <sup>18</sup>. Using CID, abundant fragments corresponding to glycosidic bond cleavages (*B/Y* ions) predominate the spectra, while HCD favors the formation of ceramide fragments, facilitating differentiation of GSLs molecular species <sup>143-145</sup>.

Collisional activation methods yield both the glycan and lipid structural details. The B and C type fragments are often used to elucidate glycan headgroup sequence. Incremental mass differences of 162 Da and 204 Da which result from these types of fragments indicate loss of a hexose and N-acetylhexosamine moiety, respectively. The presence of sialic acid can be confirmed from the presence of *m/z* 290 in the MS/MS spectrum in the negative mode, while sulfate is identified from the presence of *m/z* 97. Importantly, the lipid backbone composition is established by the presence of diagnostic ions *m/z* 264, *m/z* 236, and *m/z* 292 that correspond to d18:1, d16:1, and d20:1 <sup>146</sup>. Using accurate mass measurement of precursor ion mass along with these fragments, the putative structure can be established.

One major limitation of MS<sup>2</sup> is its inability to differentiate isomeric species with very subtle structural differences even with upfront chromatographic separation. In this case, multiple stage collisional activation can also be performed to further elucidate glycan linkage differentiation of GSLs. For example, previous works have demonstrated the differentiation of globo- and isoglobo- GSLs in cell extracts by means of MS<sup>5</sup> experiments <sup>44</sup>. To differentiate anomeric  $\alpha$  and  $\beta$  hexosyl ceramides, CID fragmentation of [M+Na]<sup>+</sup> adduct could be performed as demonstrated previously <sup>51</sup>.

### **Electron-aided activation**

Electron-aided fragmentation involves electron transfer from a donor to precursor ion of interest, converting it to a radical ion that undergoes subsequent fragmentation (thorough discussion is provided in a recent review <sup>147</sup>). This strategy has been implemented in various

ways, the most common are, electron capture dissociation (ECD), electron detachment dissociation (EDD), and electron transfer dissociation (ETD). In ECD, multiply charged positive ions pass through a beam of low energy electrons. In this process, electron capture occurs which results to formation of unstable radical cations that subsequently undergo fragmentation. EDD operates by the same principle as ECD, but instead of using positive ions, negative multiply charged species are used. Both approaches have been implemented mainly in FTICR instruments but attempts have been made to incorporate these fragmentation techniques in common MS platforms such as orbitrap systems which would allow greater access to scientific community <sup>148</sup>.

ETD is somewhat different to ECD and EDD because instead of electrons, multiply charged positive ions react with a radical anion generated *in situ* <sup>147</sup>. This was originally introduced for use in peptide sequencing <sup>149</sup> but was shown to work equally well for oligosaccharides. In this process, positive ions of multiple charge states react with a radical anion generated *in situ*, *e.g.* fluoroanthene. This reaction produces odd and even electron fragments and species with reduced charge state. Application of electron-aided activation to GSLs has been demonstrated and showed that extensive fragmentation provides identities of the ceramide backbone as well as acetylation in the sugar moiety <sup>150</sup>. It was concluded that EDD is a relatively inefficient method for GSLs while ECD provides extensive fragmentation that could aid in structural elucidation. To our knowledge, ETD has not been applied to GSLs, probably because most of these molecules seldom form multiply charged positive ions, a prerequisite for using this technique.

### **Ultraviolet photodissociation**

Photoinduced activation takes advantage of energetic photons as energy source to activate chemical bonds leading to fragmentation. In ultraviolet photodissociation (UVPD), as the name suggests, uses UV to irradiate precursor ions in a collision cell <sup>152</sup>. Typical wavelengths



Despite the promise of this emerging technology in glycolipids analysis, one of its major limitation is the lack of available software that could aid annotation of the resulting UVPD spectrum, owing to the variety of fragments generated by the process.

### **Radical directed dissociation**

Radical directed dissociation (RDD) involves the generation of radical ions after photodissociation. In contrast to UVPD, RDD typically use chromophores with labile bonds as precursor of a radical, e.g. carbon-iodine bonds. This approach was used by Pham and Julian to differentiate the glycosphingolipid epimers, GlcCer and GalCer by forming non-covalent complex with a radical precursor<sup>47</sup>. Briefly, *lyso*-GSLs were prepared and complexed with 4-iodobenzoyl 18-crown-6 (IB18C6). The free amino group in the *lyso*- species served as an anchor for the complexation with IB18C6 reagent. Following photodissociation with 266 nm UV laser, a radical ion was formed which was used for subsequent CID experiments. For intact analysis of GSLs, instead of IB18C6, derivatization with iodophenylboronic acid (IPBA) was used. This compound reacts with adjacent diols, particularly at C3 and C4 positions. This approach yields differential reactivity of Gal and Glc epimers which could be used to distinguish them.

### **Ozone-induced dissociation**

Ozone induced dissociation (OzID) is relatively new fragmentation technique originally based on the olefin and ozone (O<sub>3</sub>) reaction chemistry<sup>10</sup>. Historically, this approach was used to elucidate double bond locations in bottom up lipids analysis using traditional gas chromatography analysis. In 2008, Blanksby's group have implemented this methodology in MS by replacing collision gas with O<sub>3</sub> and O<sub>2</sub> mixture<sup>11</sup>. In this reaction, O<sub>3</sub> forms ozonide through a cycloaddition reaction, this metastable product spontaneously decays to the more stable Criegee and aldehyde product ions. The difference between the mass of precursor ions and the OzID product ions is diagnostic of the location of double bonds.

Recently, our group implemented OzID in a high-resolution instrument with enhanced ozonolysis efficiency<sup>12</sup>. We used this platform to study unsaturated glycosphingolipids analysis, for example, LacCer d18:1(4E)/18:1(9Z) (**Fig. 9**). Subjecting the  $[M+Na]^+$  adduct of this molecule, two pairs of OzID products (Criegee and aldehyde) corresponding to each double bond were observed<sup>9</sup>. The mass difference between OzID products and the precursor ion can be used to pinpoint the location of the double bonds from the terminal carbon<sup>10</sup>.

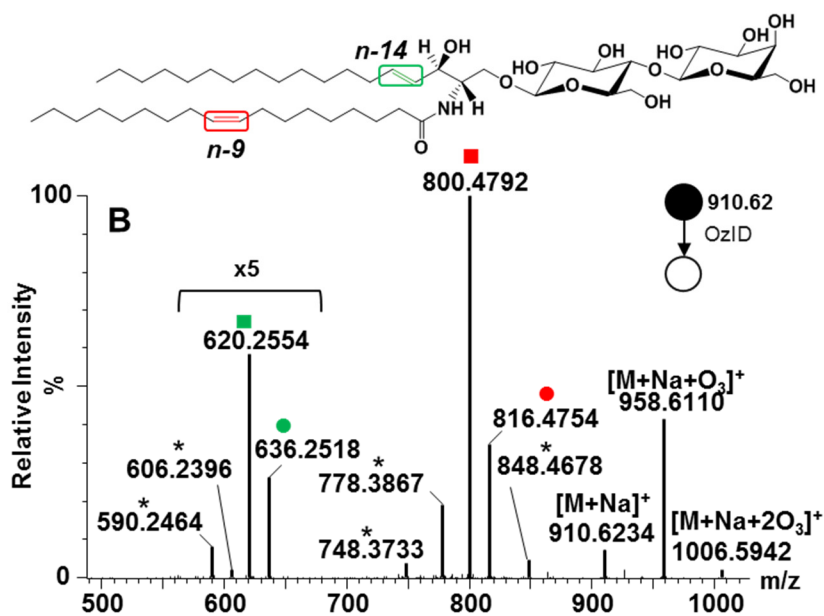


**Figure 9. OzID-MS Spectrum of LacCer d18:1/18:1(9Z).** Gas-phase ozonolysis selectively cleaves carbon-carbon double bonds producing Criegee and aldehyde ions. The neutral losses are used to locate double bond locations. Criegee and aldehyde product ions are depicted as (●) and (■), respectively. Open square (□) and circle (○) indicate ions generated through elimination of  $H_2C=O$  from the aldehyde ion and Criegee ion, respectively. Asterisk (\*) indicates ions generated through secondary oxidation from  $[M+Na+O_3]^+$ . Colors represent different double bond locations. Reprinted with permission from Barrientos R.C., *et al. J. Am. Soc. Mass Spectrom.*, **28**, 2330-2343 (2017)<sup>9</sup> © American Society for Mass Spectrometry.

This approach allowed the discrimination of isobaric and isomeric species in porcine brain galactocerebrosides mixture which are otherwise non-distinguishable by CID alone<sup>9</sup>. The

differential reactivity of the long chain base double bond and the fatty acyl double bond is very useful to easily pinpoint which chain contains the double bond.

### **MS/MS scan modes**

Different MS/MS scan modes can be used to identify and quantify low abundant GSLs, namely, precursor ion scan (PIS), multiple reaction monitoring (MRM), and parallel reaction monitoring (PRM). In PIS, all ions generated from the source are fragmented and precursor ions that produce specific product ions are identified. PIS has been shown to be useful in ganglioside analysis where all ions are scanned for the presence of fragment ion with  $m/z$  290<sup>154</sup>.

In MRM, specific precursor-product ion  $m/z$  pairs are pre-set and only these ions are detected. Briefly, fragmentation of target analytes is first studied to identify potentially discriminating fragment ions. Once these unique ions are identified, the collision energy settings are optimized and the precursor ion – fragment ion pairs are used for detection. This has been helpful in detecting and distinguishing isomeric GSLs as demonstrated by Ikeda *et al*<sup>120,155</sup>. Also, MRM was used to determine Gb3 in plasma and urine of Fabry disease patients by monitoring the loss of  $m/z$  162 in a QqQ instrument<sup>156</sup>. Characteristic product ions are shown in **Fig. 7b**. Sulfatides, yields  $m/z$  97 upon fragmentation while gangliosides provide  $m/z$  290 due to sulfate and Neu5Ac, respectively. Specific ganglioside subclasses can also generate unique fragments useful for MRM-based methods<sup>157</sup>. Thus, GSLs that differ only on the ceramide backbone can be distinguished using specific fragments. Differentiation of the LCB can be done by identifying unique fragments, for instance,  $m/z$  264 is attributed to d18:1 sphingosine backbone (**Fig. 7b**).

In orbitrap-based instruments, PRM can be used for qualitative and quantitative analysis. Unlike MRM that uses only predefined MS/MS transitions, PRM provides all generated ions during MS/MS. This has been demonstrated for deep profiling of sphingolipids<sup>144</sup>, and also used for quantitative analysis of gangliosides after isobaric labeling<sup>145</sup>.

Taken together, MS has inarguably advanced the field of GSLs due to its versatility, sensitivity, and ability to provide structural information, especially for unknown compounds. It can be used either in stand-alone (direct infusion MS) or coupled with front end separation (hyphenated MS). Their application to GSL analysis will be described below.

### **Direct Infusion MS**

Direct infusion MS (DIMS) is probably the simplest and most straightforward approach for profiling of GSLs. Also called shotgun approach, here, the sample is dissolved in appropriate solvent and infused using a syringe pump to an ionization source, but chip-based technologies in the absence of imbedded chromatographic stationary phases, also fall under this category.

Chip-based devices are based on the Lab-on-Chip concept that is geared towards miniaturizing laboratory processes <sup>158</sup>. Due to the suitability for biomolecule analysis, these devices are typically coupled to ESI and has been the subject of recent reviews <sup>159,160</sup>. Currently, there are two existing platforms, namely, out-of-plane chipESI and in-plane chipESI <sup>159</sup>. The former is composed of 100 or 400 nanospray nozzles, made from monolithic silicon substrate and forms the spray perpendicular to the plate. The latter is typically made from glass or polymeric materials etched with microfluidic channels whose tip generates electrospray. Recently, the incorporation of HPLC on a chip has also been realized and applied in diverse areas. The out-of-plane chipESI and the chip-HPLC have been commercially available from Advion Biosciences and Agilent Technologies, respectively <sup>159</sup>. Generally, chip-based techniques offer the following advantages <sup>159</sup>: 1) the nano-flow is well suitable for enhanced ionization efficiency with ESI; 2) good quality MS and MS/MS spectra could be obtained with minimal amount of sample; 3) suitability for automation and high throughput applications; 4) preservation of labile groups such as fucose and sialic acid; 5) favored generation of multiply-charged species; and 6) enhanced reproducibility.

The development of micro- and nanofluidics has enabled unambiguous characterization of biomolecules such as proteins, glycoproteins, lipids and single cells. However, only a limited number of papers has employed this technology specifically for GSLs<sup>160-162</sup>. Fully automated chip-nanoESI has been applied to gangliosides of human cerebellar tissue using minimal amount of sample (15 pmol/uL) affording 46 glycoforms in a Q-TOF MS platform<sup>163</sup>. This was subsequently used to a variety of samples for gangliosides determination, *e.g.* human brain hemangioma, brain metastasis of lung adenocarcinoma, human angioblastic meningioma, caudate nucleus, adrenal neuroblastoma and more recently to lysosomal storage diseases such as Fabry and Schindler diseases<sup>160</sup>. In all these studies, the chip-nanoESI was coupled with a Q-TOF MS instrument.

DIMS and chip-ESI have been applied to diverse types of samples as extensively reviewed by Levery<sup>18</sup> and Zamfir<sup>160</sup>, respectively. Both approaches are facile, rapid and require minimal sample amounts, but neither of these can distinguish isomeric species. Although epimers such as GalCer and GlcCer could be distinguished by intensity difference of  $m/z$  179 and  $m/z$  89 ions<sup>164</sup>, fragmentation using tandem MS instruments often results to a mixture of fragment ions coming from different isomers making automated assignments difficult if not impossible. Furthermore, this method is prone to ion suppression effects, especially when GSLs is present with cell membrane impurities such as phospholipids and cholesterol.

### **Hyphenated MS Techniques**

To overcome the intrinsic disadvantages of shotgun approach in its inability to resolve isomeric species and possible ion suppression effects, front end separation techniques are coupled to MS. The following sections describe these so-called hyphenated MS techniques and their wide-use applications for determination of GSLs.

## Nano LC-MS

Nano-ESI provides better sensitivity to oligosaccharides compared to conventional microbore ESI owing to the very low flowrate and decreased droplet size. Thus, an appropriate separation technique prior to nano-ESI is necessary, such as nano-LC.

A few online nano-LC methods have been developed for neutral GSLs and gangliosides profiling. Coupling of nano-LC and ESI QTOF-MS for neutral GSLs analysis was first reported by Kirsch and colleagues in 2008<sup>165</sup>. In this method, it was possible to separate a complex mixture of neutral GSLs derived from human erythrocytes at low femtomole (200 fmol) detection using only 2 pmol of sample on-column. Separation was achieved using a nanoscale TSK-Gel Amide 80 column. One of the advantages of this technique is the use of intact, underivatized GSLs which provides both the glycan and ceramide information.

The same group demonstrated the resolution of sialic acid linkage isomers and successfully identified other distinct components using the same approach<sup>48</sup>. The  $\alpha$ 2-6 isomer was observed to elute later than the  $\alpha$ 2-3 isomer indicating that sialic acid linkage could result to a difference in the way they interact with stationary phase. Unsaturated ceramide moieties from 0 to 3 degrees of unsaturation were observed, however, the exact location of the double bond positions was not identified. This approach was also used to distinguish Neu5Ac and Neu5Gc present in GM1b derived from murine YAC-1 lymphoma cells. In this chromatographic separation, the Neu5Ac isomer elutes first followed by Neu5Gc isomer. Also, <sup>0,2</sup>A fragments of  $m/z$  220 and  $m/z$  236, for Neu5Ac and Neu5Gc, respectively, have been considered diagnostic ions in the MS/MS spectra.

Using nano-LC-FTICR MS, the group of Marshall<sup>139</sup> showed that high mass accuracy allows unambiguous assignment of unknown GSLs especially when used with an

innovative Kendrick mass defect data analysis technique. It was successfully demonstrated to identify sulfated GSLs in glioblastoma tumor cells<sup>139</sup>.

Recently, fluorescence detector (FLD) and QIT-TOF MS were coupled with nano-LC in one method. Demonstrated by Daikoku and colleagues, this complementary detection allowed the monitoring of enzymatic transformation of labelled GSLs<sup>166</sup>. Using this set-up, the analyte was detectable down to ultratrace level (29 amol). Ohtake and co-workers also employed fluorescently labelled substrates to observe the cellular dynamics of GSLs transformation and to elucidate the structure of downstream enzymatic products using an FLD detection first, followed by offline nano-LC ESI Q-TOF MS<sup>167</sup>. This was applied to study the fate of LacCer in African green monkey kidney fibroblast (COS-7) cells<sup>167</sup>.

Using nano-LC ESI Q-Orbitrap MS, various isoforms of Gb3 and *lyso*-Gb3 were identified in Fabry disease mouse model and in actual human plasma samples<sup>168,169</sup>. With an LOD of 0.01 nM, these methods demonstrated superior sensitivity over HPLC and UHPLC-MS/MS methods, which have LOD of 2 to 10 nM and 0.05 nM, respectively. The use of HRMS, also facilitated the determination of 18 related analogs of *lyso*-Gb3 together with two new potential biomarkers, *lyso*-Gb3 (-12) and *lyso*-Gb3 (+14), which were reported in these studies for the first time.

Taken together, nano-LC coupled to ESI-MS/MS has facilitated the detection of low-abundant analytes in a complex mixture allowing the differentiation of linkage isomers such as  $\alpha$ 2-3 and  $\alpha$ 2-6 sialic acid, as well as Neu5Gc and Neu5Ac isoforms. When additionally coupled with fluorescence detection, labelled GSLs incorporated into cells can be visualized and structurally identified. Furthermore, when an ultra-high mass resolution instrument such as FTICR is used, accurate molecular formula assignment is possible.

## UHPLC-MS

Because they are amphiphilic, GSLs can be analyzed using different chromatographic modes namely, reversed phase liquid chromatography (RPLC), normal phase liquid chromatography (NPLC), and hydrophilic interaction liquid chromatography (HILIC). In RPLC, the GSLs are separated based on the hydrophobic interactions between the stationary phase and ceramide moiety of GSLs. Commonly, C8, C18 and C30 phases are employed although C5 has been shown to be enough for separating simpler gangliosides such as GD3 and GM3 with similar ceramide compositions. In NPLC, GSLs are separated based on the hydrophilic interaction of the glycan moiety and the stationary phase, commonly silica and amino based columns. HILIC separates based on glycan moiety and in contrast to NPLC, it can be easily coupled with MS due to similar solvent properties to RPLC.

Ultrahigh performance liquid chromatography (UHPLC, or UPLC) is currently the predominant method of choice for qualitative and quantitative analysis. In UHPLC, smaller particles are used as column packing materials. Compared to conventional HPLC that uses about 5 to 10  $\mu\text{m}$  particle diameter, UHPLC uses only less than 3  $\mu\text{m}$ . Owing to the recent advances in column particle technology, small particles down to 1.7  $\mu\text{m}$  are now commercially available which facilitates UHPLC-MS/MS based methods to offer superior resolution and faster chromatographic separations. The use of smaller particle sizes results to decreased Eddy diffusion, mass transfer and thus, theoretical plate height. Using UHPLC-MS/MS, the group of Mechref has recently developed a method for the determination of gangliosides in human plasma within 7.5 minutes which expands over four orders of magnitude using only 10  $\mu\text{L}$  of the sample<sup>170</sup>. Another UHPLC-MS/MS method for human plasma gangliosides was developed with an elution time of 9.0 min and a total run time of 20.0 min including column clean-up and re-equilibration<sup>171</sup>.

Typical columns used for UHPLC-MS/MS methods in RPLC mode include C18 and C30, while silica and NH<sub>2</sub> columns are used in HILIC mode<sup>172</sup>. Porous graphitic carbon (PGC) has been used to resolve isomeric GSLs<sup>117</sup>. More recently, the resolution of GlcCer and GalCer using ZIC-HILIC UHPLC-MS/MS<sup>46</sup> was developed and applied to brain and skin. Within 12.0 min gradient, these epimeric GSLs were completely separated. The ZIC stationary phase retains a thick hydration layer that generates strong hydrophilic interactions with the analytes such as glycopeptides and carbohydrates thus allowing the separation of configurational isomers. In contrast to NPLC-based GalCer and GlcCer separation, ZIC-HILIC does not employ highly non-polar mobile phase. HILIC-QTOF MS was recently showed to provide high number of identification of gangliosides and sulfatides from various biological matrices<sup>172</sup>.

While few studies exploited low resolution MS such as ion trap and triple quadrupole, several UHPLC-MS/MS methods have utilized HRMS such as Q-TOF and orbitrap mass analyzer<sup>173,143,170,174,175</sup>. Using ion trap instruments, both quantification and structural elucidation through multi-stage MS<sup>n</sup> (n>2) experiments could be performed as demonstrated for neutral GSLs<sup>18</sup>. However, the method is not well suited for high-throughput applications because both ion isolation and activation happen in the same mass analyzer, eventually downgrading its duty cycle and precludes the detection of low abundant analytes in complex mixtures. The use of UHPLC-MS/MS in a triple quadrupole instrument has shown great results in profiling GSLs using precursor ion scan modes and MRM. It was used to profile gangliosides in mouse retina<sup>143</sup>, and sulfatides in the kidney<sup>71</sup>. On the other hand, the main advantage of UHPLC-HRMS is the added capability to identify molecular formula by measuring an accurate mass down to <5 ppm<sup>139</sup>. The use of HRMS in a recent study, facilitated the differentiation of isobaric gangliosides both based on the fatty acyl chain and the sphingosine backbone using high mass accuracy

measurements<sup>143</sup>. Furthermore, the use of combined CID and HCD capability in the LTQ Orbitrap XL has facilitated the confirmation of ceramide assignments.

Quantitative methods with enhanced sensitivity based on UHPLC-MS/MS have been developed. For example, using HILIC mode, gangliosides were extracted and analyzed from blood serum of patients with different esophagus diseases and rat brain and showed to have a detection range (on-column) of 10 to 50 pg<sup>170</sup>, and 0.08 to 0.84 ng<sup>174</sup>, respectively<sup>63</sup>. Quantification of sulfatides in lipid rafts of the central nervous system using RPLC mode had an LOD of 2 to 5 nM<sup>63</sup>. Quantification of sulfatides using UHPLC coupled with Q-TOF MS in RPLC mode was developed and applied to mouse brain samples and showed a detection limit of 3.29 ng/mL and 10.7 ng/mL for ESI negative and positive modes, respectively<sup>176</sup>. HILIC-MS/MS-based multiplexed method for analysis of GlcCer and GalCer had an LOD of 0.4 to 1.1 nmol/g brain tissue as applied to Parkinson's disease (PD)<sup>49</sup>. HILIC-MS/MS has also been used very recently to resolve intact, diastereomeric GSLs including  $\beta$ -GalCer,  $\alpha$ -GalCer, and  $\beta$ -GlcCer,  $\alpha$ -GlcCer<sup>177</sup>.

In summary, the methods described here show that both nano-LC and UHPLC when coupled with MS can provide the needed sensitivity and resolution to determine complex GSLs.

## **CE-MS**

Capillary electrophoresis (CE) is a technique that separates analytes based on size, charge and shape that typically operate in nanoflow range, typically 20-100 nL/min<sup>178</sup>. This approach has been widely used in glycomics<sup>179</sup>. In contrast to LC, this method offers superior peak capacity and a promising tool for resolving isomers. CE based methods for GSLs typically use optical detection such as UV and FLD. For example, CE with laser induced FLD method was applied in single cell metabolic cytometry<sup>180-182</sup>. This promising method afforded detection limits of 1 zmol BODIPY-labelled LacCer and 500 ymol tetramethylrhodamine-labeled GM1 (GM1-

TMR). Although these methods can be used for quantitative purposes and isomeric distinction, their use is limited to only when commercially available standards are present. Hence, coupling with MS detector would take advantage of the capability of CE for GSLs profiling.

To effectively use a CE-MS platform, the buffers used should be volatile and the flow should provide spray stability when used with ESI source <sup>179</sup>. One of the most challenging part of CE-MS based method for GSLs is the selection of appropriate buffer system. The use of other buffer compositions for gangliosides analysis compatible with MS was reported, yet the resolution is still inferior compared with CE-UV based method which uses borate buffers that are known to be detrimental for MS work. In fact, there was even a need to alter the hardware component of the instrument to achieve comparable resolution <sup>173</sup>. To provide enough flow rate and match the  $\mu\text{L}/\text{min}$  flow rate of ESI, a sheath liquid is typically used, which ranges from 0.2 to 0.4  $\text{nL}/\text{min}$  <sup>179</sup>. One concern of using make-up flow is dilution of analytes resulting to poor sensitivity.

The CE-MS approach has been applied widely in carbohydrates analysis, notably for glycans released from glycoproteins as well as glycosaminoglycans but only a few papers have applied this method for glycosphingolipids analysis <sup>179,183 184</sup>. The first report coupling CE with ESI-MS for gangliosides was made by Her and co-workers <sup>185</sup>. Offline CE-ESI-QTOF MS was also reported by the group of Peter-Katalinic for gangliosides <sup>186</sup>. More recently, a sheath-less interface using a CE-ESI-QIT-TOF MS was applied to pyridylaminated (PA) neutral GSLs <sup>187</sup>. A 20,000x increase in sensitivity was observed when a sheath-less interface was used resulting to a detection limit of 25  $\text{amol}/\mu\text{L}$  in mixtures.

## **TLC-MS**

Thin layer chromatography (TLC) uses silica gel 60 as typical stationary phase coated on aluminum, plastic or glass plates. The separated components of the sample are detected in

different ways, depending on the objectives of the study, namely, 1) chemical staining; 2) overlay technique; 3) indirect MS; and 4) direct MS. These have been widely applied in GSLs studies and specific review on this field has been made by Muthing and colleagues<sup>188</sup>. Because of its recency, only direct TLC-MS will be covered here.

In the direct TLC-MS method, the GSLs on the TLC plate is ionized *in situ*. MALDI is commonly used for this purpose because the adsorbed analytes could be easily desorbed and ionized. Direct TLC-MALDI was introduced by Fuch and co-workers in 2007<sup>189</sup> and was demonstrated to profile GSL compositions of C2C12 myoblasts using an ImagePrep method<sup>190</sup>. Briefly, samples are spotted on a HPTLC plate, developed using an appropriate solvent system and sprayed with DHB matrix in an ImagePrep instrument prior to being analyzed by MALDI-TOF/TOF MS. TLC-MALDI technique has been used to profile sphingoid and GSLs composition of muscle, brain and serum to develop a library for pre-clinical investigations<sup>190</sup>. This paper also demonstrated the need for alkali hydrolysis to deplete ion suppression causing neutral lipids such as phospholipids prior to MALDI-MS analysis.

Another direct MS technique was demonstrated by the group of Costello<sup>191</sup>. In this study, the spots on the TLC plate are extracted by depositing liquid droplet on the surface followed by direct introduction of the extract to a nano-ESI MS interface. These robotic interfaces are commercially available and do not require laborious set-ups to couple TLC with an MS instrument. It was successfully applied to gangliosides and sulfatides in bovine brain as well as other lipid species. One advantage of this TLC-ESI-MS compared to TLC-MALDI-MS is the absence of in-source decay of sialic acid owing to the softer nature of ESI. In this respect, Desorption Electrospray Ionization (DESI) has been used to measure sphingolipids, HexCer and LacCer in human retina<sup>192</sup>.

In most of these direct TLC-MS methods, the GSLs from crude lipid extracts are applied directly on the plate. One of the challenges in using crude lipid extracts in TLC is the co-elution with neutral lipids that cause ion suppression. In a recent study, this was overcome using phospholipase C digestion prior to TLC application. Without the digestion, Gb4Cer was undetectable using IR-MALDI-o-TOF MS, but the signal was observed when phospholipase C digestion was carried out <sup>191</sup>. Similarly, alkali hydrolysis was deemed necessary for the detection of low abundant Gb3Cer, Gb4Cer, HexCer and CerP in muscle tissue analyzed using HPTLC-MALDI-MS <sup>191</sup>.

With the on-going development in direct TLC-MS approaches, it is expected that this will further advance the emerging field of glycosphingolipidomics. However, the use of TLC faces a few limitations. For example, in using TLC-overlay-MS triad, only previously immunostained analyte molecules are targeted, and consequently the heterogeneity of the complete GSLs mixture is only partially identified. Also, thorough separation of isomers is another concern, specifically, in the study of GSLs in neuroblastoma cells by Kaneko and colleagues <sup>191</sup>, HPTLC failed to detect acetylated GSLs but they were otherwise detected using LC-MS.

### **Chip-based LC-MS**

The use of automated chip-nanoESI has revealed a wide diversity of GSLs<sup>48,160-163</sup> in previous works but failed to discriminate isomeric species without prior separation step. To address this, the group of Lebrilla has applied chipHPLC to resolve gangliosides and sulfatides in human milk gangliosides <sup>154</sup>. This technique incorporates a reversed-phase stationary phase on microchip channels that acts as another dimension of separation. Coupled with a Q-TOF MS, it facilitated the determination of 17 gangliosides and 13 sulfatide species fully characterized by MS/MS. The same approach was recently applied to cultured Caco-2 cells where a diverse array of GSLs was detected and elucidated <sup>193</sup>.

Owing to the increasing popularity of chip-based devices and its commercial availability, these tools are expected to facilitate the development of improved methods for GSLs. Although currently, most of the published papers are proofs-of-concept, their practical use especially in industrial and clinical fields is envisaged.

### **Ion mobility-MS**

Ion mobility spectrometry (IMS) is a gas phase separation technique based on size, charge, and shape under applied electric field and buffer gas. Due to the high structural complexity of glycoconjugates, IMS has become an emerging tool for carbohydrates studies and has been the subject of recent reviews<sup>194,195</sup>. One important parameter that can be obtained from IMS is the collision cross section (CCS), a parameter that represents the effective area of the analyte ion that interacts with a buffer gas, thus, a measure of ion conformation in the gas phase. CCS is independent of instrument type and experimental measurement conditions, as such, it could be useful as another dimension for compound identification. Recently, based on this concept, IMS database for glycans and glycoproteins were developed called GlycoMob<sup>196</sup>. For complex mixture analysis, IMS has been shown to increase sensitivity by decreasing chemical background noise which allows the determination of even low abundant species in a complex sample<sup>79</sup>.

Several platforms are currently available for IMS, such as drift tube IMS (DTIMS), traveling wave IMS (TWIMS), and high-field asymmetric wave form IMS (FAIMS), and serpentine multi-pass structures for lossless ion manipulations (SLIMS)<sup>197</sup>. Except SLIMS, all these platforms are commercially available and suitable for coupling to most MS instruments. The simplest form, DTIMS involves application of uniform weak electric field in a series of stacked electrodes containing buffer gas, typically helium or nitrogen. Due to the uniform field strength, CCS measurements could be directly obtained. TWIMS, on the other hand, uses

alternating radiofrequency (rf) potentials on adjacent stacked electrodes and a uniform direct current potential (DC) allowing the generation of ‘traveling wave’ which carries the ions based on their mobility.

In contrast to DTIMS, CCS can be measured only when suitable calibration is carried out. FAIMS, also called differential mobility spectrometry (DMS) uses a non-uniform and high electric field strength to effectively “filtering” ions prior to entering MS. This cannot be used to measure CCS values. Typically, this DMS is useful for targeted analysis where only a specific ion of interest can enter MS for mass analysis. SLIMS operates on similar principle as TWIMS, the major difference is that in the former it employs stacked ring ion guides. Thorough discussion of each of these techniques is provided in recent reviews <sup>195,197</sup>.

Only few papers have been published exploiting IMS for GSLs, to our knowledge, the first demonstration to gangliosides was reported in 2011 by Jackson and colleagues <sup>199</sup>. Using MALDI-IMS-TOF-MS, gangliosides were ionized in positive mode as cesium adducts. The drift time was showed to vary according to the number of Neu5Ac residues. However, this technique failed to resolve GD1a and GD1b isomers. More recently, Sarbu and co-workers applied TWIMS for the first time in human fetal brain gangliosides using Q-TOF MS <sup>79</sup>. In this study, at least 143 distinct gangliosides species were found that differ on both the glycan and ceramide moieties, three times higher than the number previously reported. It was also demonstrated that using IMS, gangliosides were resolved based on the glycan length as well as the degree of sialylation, thus facilitating the determination of these species.

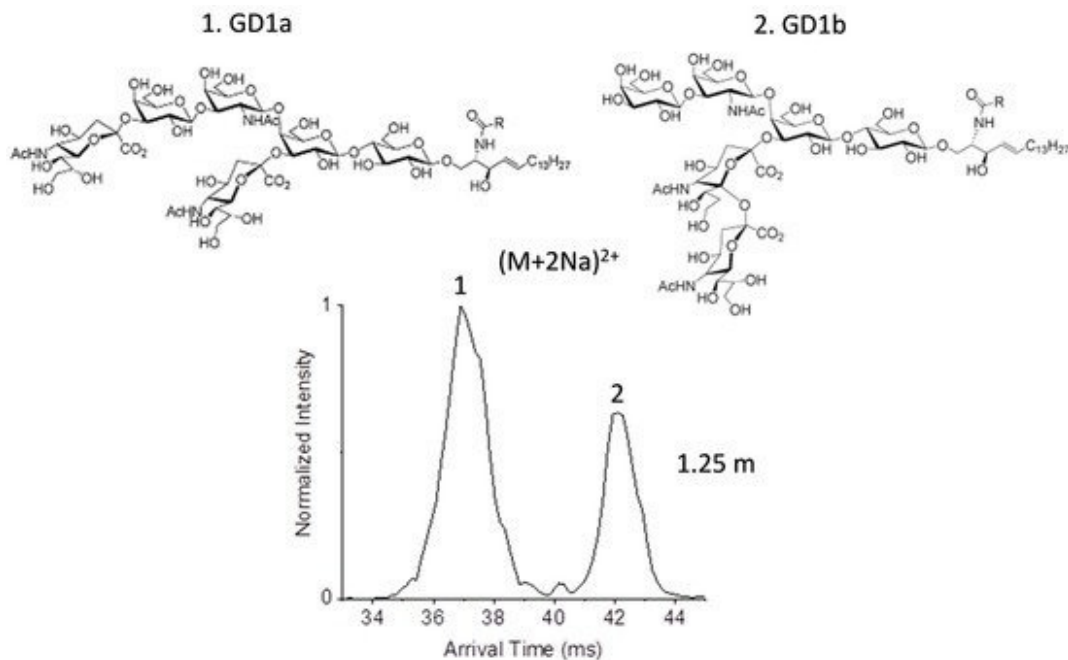


**Figure 10. Baseline Resolution of Isomeric GD1a and GD1b Gangliosides.** Samples were analyzed as  $[M+2Na]^{2+}$  adduct using a serpentine multi-pass SLIM-IMS. Reprinted from Wojcik *et al. Int. J. Mol. Sci.*, **18**, 183 (2017)<sup>198</sup> © The Authors.

Furthermore, IMS has reduced the chemical background noise where the contaminants fall on a different trend line in the driftscope. Wojcik and colleagues also demonstrated SLIMS for the high-resolution separation of isomeric GSLs<sup>198</sup>. In their work, glycosylsphingosine epimers containing Glc and Gal with similar lipid backbone were separated when analyzed in the form of  $[M+H-H_2O]^+$  ions but not  $[M+Na]^+$ . On the other hand, gangliosides GD1a and GD1b, ionized as  $[M+2Na]^{2+}$  were baseline-resolved (**Fig. 10**). In a more recent work using DMS coupled with LC-MS in HILIC mode, GlcCer and GalCer species from human plasma and cerebrospinal fluids were effectively resolved as  $[M+H]^+$  adducts<sup>200</sup>. Very recently, The McLean group has developed the ion mobility conformational lipid atlas which includes some GSLs and showed distinguishing features of these relatively bulky molecules<sup>201</sup>.

In summary, IMS coupled to MS is an emerging tool for analysis of GSLs that enable isomeric differentiation and analytical background noise reduction. Although currently not in place, measurement and availability of CCS values for GSLs could serve as a complementary feature for unambiguous determination of these molecules.

### **Labeling Approaches for Improved MS-Based Quantification of GSLs**

One of the challenges in detecting GSLs is their low abundance compared to other lipids, and their low ionization efficiency, especially with increasing number of sugars in the headgroup, thus, derivatization is often needed. In this section, we focused on the most common derivatization strategies that have been used to improve quantification of GSLs using MS.

#### **Permethylation**

Permethylation involves the conversion of active protons in the form of -OH and -NH in the molecule using methyl iodide in the presence of sodium hydroxide and dimethylsulfoxide (DMSO) as previously proposed by Ciucanu and Kerek<sup>202</sup> and Gunnarsson<sup>203</sup> (**Fig. 11**). This process enhances the volatility of the molecules and thus, improved sensitivity. It has been extensively used to analyze released glycans from glycoproteins mainly for qualitative analysis<sup>204,205</sup> although few previous works have attempted to use permethylation for quantitative purposes using direct infusion MS or MALDI<sup>13,206,207</sup>.

Quantitative use of permethylation involves incorporation of heavy isotopes such as <sup>13</sup>C or <sup>2</sup>H atoms using heavy isotope-labeled methyl iodide<sup>206,207</sup>. Here, different samples are labeled with either light isotopes or heavy isotopes and pooling them together, so called differential isotope labeling technique. The pooled mixture is then measured as a single sample for MS analysis where the ratio of intensities serves as surrogate measure of analyte concentrations in the sample.

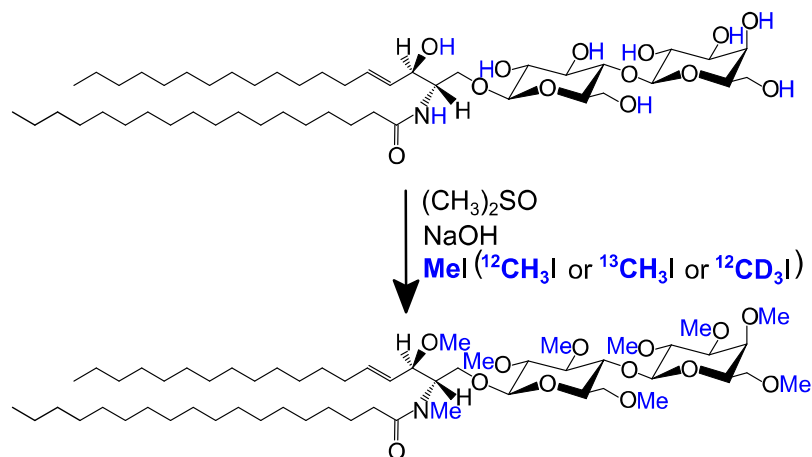


**Figure 11. Labelling of GSLs by Isotopic Permethylation.** Shown here is the conversion of all active protons (-OH and -NH) using isotopically labeled methyl iodide (MeI) in the form of <sup>12</sup>C, <sup>13</sup>C, or <sup>2</sup>H in the presence of alkali hydroxide (commonly, NaOH) and an aprotic solvent (dimethyl sulfoxide) under anhydrous conditions.

We have recently implemented differential isotope labeling by permethylation coupled with RPLC-MS/MS for quantitative analysis of intact GSLs. Cognizant of the lack of commercially available <sup>13</sup>C-labeled internal standards for GSLs, and to address the low detectability of GSLs in the presence of total lipids extract, we showed that pooled sample can be used as a universal internal standard. Briefly, aliquots from individual samples are pooled and permethylated with <sup>13</sup>CH<sub>3</sub>I while the individual samples are permethylated using <sup>12</sup>CH<sub>3</sub>I. After pooling the permethylated samples, they were analyzed by RPLC-MS/MS. We observed up to 20-fold increase in signal enhancement between non-permethylated and permethylated samples. We also obtained very good reproducibility and accuracy. The MS/MS fragmentation and retention time information provide different levels of compound identification which provided more confident annotation of detected GSLs in the sample. These results are encouraging and illustrate the usefulness of permethylation for quantitative analysis of low-abundant GSLs in complex mixtures.

### **PAEA labeling**

To improve ionization efficiency of gangliosides, Huang and co-workers developed a labeling approach for monosialogangliosides using 2-(2-Pyridilamino)-ethylamine (PAEA). In this approach, three ganglioside classes, namely GM1, GM2, and GM3 molecular species were successfully quantified and analyzed via RPLC-MS/MS.

In this method, monosialoganglioside (GM) species were derivatized using 4-(4,6-Dimethoxy-1,3,5-triazin-2-yl)-4-methylmorpholinium chloride (DMTMM) and 2-(2-Pyridilamino)ethylamine (PAEA) as derivatizing agents [104] (**Fig. 9**). The labelling agent PAEA attaches to the -COOH functional group of the Neu5Ac. This resulted to 15-fold enhancement of signal intensity in positive mode compared to underivatized analogue. This quantitative UHPLC-MS/MS method was successfully applied to plasma of patients suffering from GM3 synthase deficiency.

### **Isobaric labeling**

Although considered as relatively new tool for GSLs, isobaric labeling has been extensively implemented in proteomics and glycomics. The main goal of this approach is to enable multiplexing at the MS/MS or MS<sup>3</sup> levels. Here, samples are labeled by an isobaric tag that yields reporter ions after being subjected to fragmentation. This tag is multiple versions of the same molecule but differ in the distribution of heavy isotopes such as carbon and nitrogen. Because the arrangement of heavy isotopes can be defined, the resulting fragment ions arising from this label is tuned accordingly. There are two versions of isobaric tag that have been shown to be useful for GSLs. The first one is iTRAQ (isobaric tags for relative and absolute quantitation) and the other is aminoxyTMT (aminoxy tandem mass tag), which are both commercially available (**Fig. 13**)<sup>108,145,208</sup>. The main difference between these two is their reaction

chemistry, iTRAQ reacts with free amines, while aminoxyTMT reacts with reactive carbonyls (aldehyde and ketone). Also, iTRAQ can multiplex up to eight samples while aminoxyTMT, up to six samples, currently.

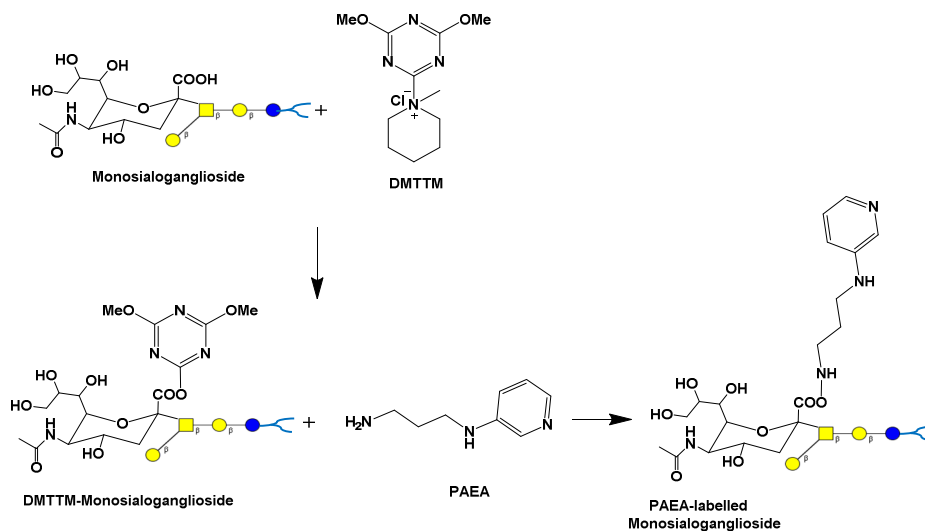


**Figure 12. Labelling of Intact, Monosialoganglioside Using PAEA.**

Nabetani and co-workers demonstrated the use of iTRAQ for the multiplexed analysis of sphingolipids, that includes hexosylceramides (HexCer) derived from cells<sup>108</sup>. To be useful, free amine group must be made available from the analytes, in this case, they used enzymatic hydrolysis via sphingolipid ceramide N-deacylase (SCDase) that cleaves the link between the amino group of the long chain base and the fatty acyl chain. The resulting free amine is then reacted with iTRAQ. Improved sensitivity was observed after iTRAQ labeling and accurate measurement of lipidomic changes was demonstrated.

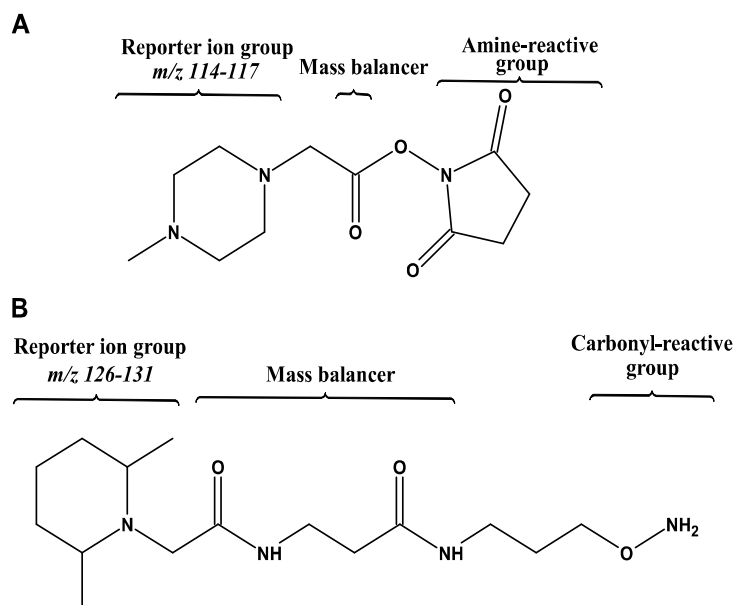


**Figure 13. Chemical Structures of Mass Tags Used for Isobaric Labeling of GSLs.** A) Amine-reactive iTRAQ, and B) Carbonyl-reactive aminoxyTMT. Both isobaric tags are commercially available.

One limitation of this method, however, is the complete neglect of the fatty acyl chain, which may carry important information. One of the challenges in studying metabolism of GSLs is to track them in cell culture experiments and obtain quantitative information of the metabolic products. The use of LacCer analogues labeled with BODIPY has been shown earlier to mimic the native behavior of endogenous LacCer<sup>209,210</sup>. For more accurate quantification of GSLs labeled with BODIPY, Son and co-workers<sup>211</sup> developed a strategy to use iTRAQ. Briefly, by introducing azide functional group to BODIPY, iTRAQ was successfully attached to the BODIPY-LacCer using click chemistry, and analyzed using Q-TOF MS. This approach, same as the previous iTRAQ labeling method on sphingolipids<sup>108</sup>, is not capable to profile endogenous fatty acyls.

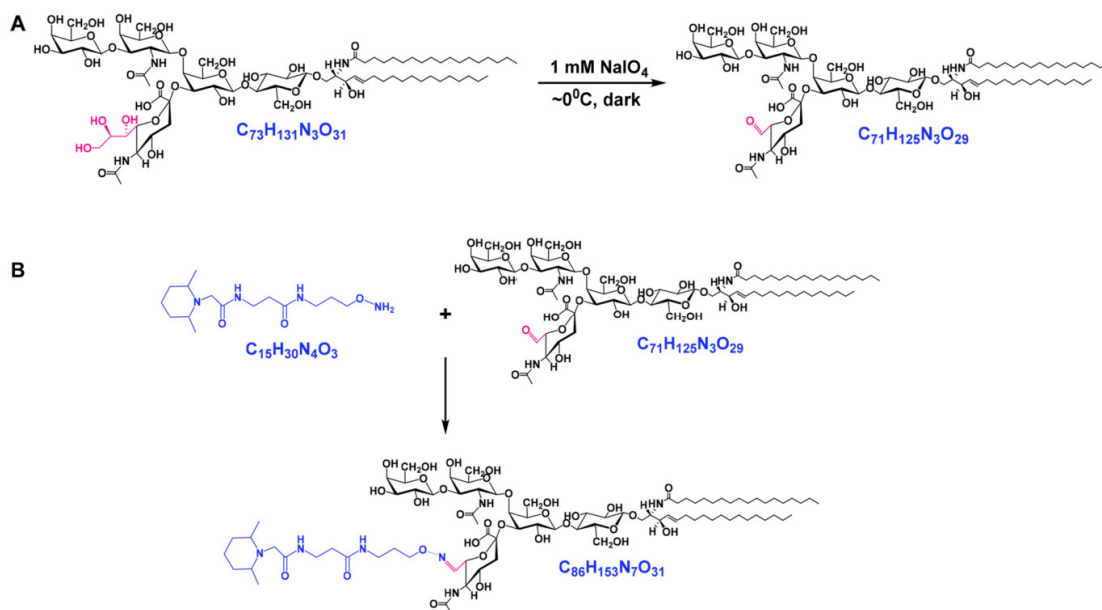


**Figure 14. Isobaric Labeling Based Strategy for Multiplexed Quantification of Intact Gangliosides.** Gangliosides are chemoselectively oxidized at the trihydroxy functional group of sialic acid using  $\text{NaIO}_4$  and the resulting aldehyde is labeled with aminoxyTMT. Reprinted with permission from Barrientos, R.C. & Zhang, Q. *Anal. Chem.* 90, 2578-2586 (2018)<sup>145</sup>, © 2018 American Chemical Society.

Recently, a method using aminoxyTMT for multiplexed analysis of gangliosides was demonstrated by our laboratory<sup>145</sup>. Strictly aimed at analyzing the intact structure of each ganglioside molecular species, chemoselective oxidation followed by aminoxyTMT labeling was exploited to enable analysis of up to six samples in a single LC-MS injection (**Fig. 14**). Improved sensitivity in positive ionization mode was observed (~40x enhancement). Characteristic fragment ions were also noted that allowed the elucidation of both glycan and lipid components. Ultimately, accuracy and precision measurements showed a great promise for its biological applications.

Taken together, these novel labeling approaches helped to improve LC-MS based quantification of GSLs by enhancing the ionization efficiency in positive mode, and enabling multiplexed quantification using permethylation and isobaric labeling.

### **Conclusion and Future Directions**

Our understanding of the biology of GSLs remains scant, specifically, the precise functions of different composition of glycan headgroup, and the diversity of ceramide backbone remain to be fully uncovered. To aid future discoveries, novel approaches are needed, and improvement of existing methodologies are desired. The capabilities allowing intact analysis of GSLs instead of analyzing the lipid and glycan separately would offer more holistic insights about the biology of these molecules. The differentiation of isomers that differ only on the position of carbon-carbon double bonds, or linkage between sugars in the headgroup is an important area of future investigation. As such, modern fragmentation methods such as electron-aided fragmentation, photodissociation, OzID-MS, and IMS would be promising tools for these endeavors.

Often, disease relevant GSLs are of extremely low abundance, as such, it is necessary to use appropriate strategies to detect them. This includes exploitation of powerful separation methods prior to MS, derivatization strategies to improve ionization efficiency, or reduction of analytical background noise via the use of enrichment strategies. One caveat in derivatization, however, is that it alters the mass of analytes and their corresponding fragment ions thus, there is a future need to incorporate them in databases.

Finally, while it is imperative to elucidate the structure of GSLs, it is equally important to know their spatial distribution. In this respect, the use of imaging MS tools such as MALDI and DESI is envisioned to provide novel and meaningful biological insights reflected by the differential distribution of GSLs in various tissues and cells.

Collectively, in this review we presented the current state for determination of GSLs by modern MS strategies. We elaborated on the current available methods for sample preparation, structural characterization and quantification with emphasis on the measurement of intact GSLs. Few impediments remain in each of these areas providing fertile ground for future method development to advance intact GSLs analysis.

### **Acknowledgement**

This work was partially supported by grants from the National Institute of General Medical Sciences (R21 GM104678) and the National Institute of Diabetes and Digestive and Kidney Diseases (R01 DK114345) of the National Institutes of Health.

CHAPTER III  
STRUCTURAL ANALYSIS OF UNSATURATED GLYCOSPHINGOLIPIDS  
USING SHOTGUN OZONE-INDUCED DISSOCIATION  
MASS SPECTROMETRY

This chapter has been published in the *Journal of the American Society for Mass Spectrometry* and is presented in that style. Barrientos, R.C., Vu, N.H., Zhang, Q. *J. Am. Soc. Mass Spectrom.* **2017**, 28, 2330-2343.

**Introduction**

Glycosphingolipids are ubiquitous and localize predominantly on the cell surface and some membrane-bound organelles<sup>15,22,212</sup>. These amphiphilic molecules composed of a glycan head group and ceramide backbone are involved in protein interaction, receptor regulation, initiation and modulation of signal transduction, as well as cell recognition and differentiation<sup>22</sup>. Given these, perturbations in glycosphingolipid metabolism have been recognized as hallmark in a myriad of pathologies including neurological<sup>61,213</sup>, autoimmune<sup>214</sup>, and lysosomal storage diseases<sup>215</sup> among others. Recent literature also indicates their potential use as therapeutic agents in cancer and autoimmune diseases due to their immunogenic characteristics<sup>216</sup>.

Despite the vast number of studies demonstrating the importance of glycosphingolipids, their structural determination has remained relatively underdeveloped compared to other biomolecules, perhaps due to the various structural complexity arising from the glycan and lipid moieties. The glycan may differ in terms of composition and linkage assignments; whereas for the lipid, the long chain base composition as well as double bond location, and stereochemistry in the fatty acyl chain all can vary<sup>212</sup>. Also, as hydroxylation is prevalent in the fatty acyl chain of

these molecules, the presence of this functional group results in the existence of isobaric species thus adding further analytical complexity. While the glycan moiety has been widely studied and possible core structures were identified <sup>15,212</sup>, the lipid backbone is oftentimes overlooked.

Lipid carbon-carbon double bond positional isomers have been shown to possess distinct properties <sup>10</sup>. During biosynthesis, preference for one fatty acid with specific location of unsaturation over the others may reflect normalcy or perturbation of enzymatic activity and metabolic pathways <sup>212,217</sup>. A wealth of evidences further suggests the importance of unsaturation in the overall attributes of these molecules. Besides its conspicuous effect on membrane fluidity <sup>218</sup>, unsaturated glycosphingolipids are also present in specialized tissues/cells such as brain <sup>79</sup>, retina<sup>72</sup>, and sperm <sup>219</sup> thus indicating that olefin in the lipid backbone is an essential motif for highly specialized biological function. The involvement of lipids and glycolipids as antigens has been demonstrated in prior studies further augmenting the relationship between unsaturation and immunogenic behavior. Specifically, different double bond positions could result in distinct structural conformations thus influencing antigenicity and ultimately, recognition by immune cells <sup>32,36,220-222</sup>. Studies also show that some of the potential glycosphingolipid biomarkers of brain development and the underlying diseases are in fact, unsaturated, yet rarely are they identified down to the finest structural detail <sup>79,80,223-225</sup>. As such, comprehensive structural determination of intact glycosphingolipids is warranted.

Mass spectrometry (MS) has been the gold standard for rapid determination of glycosphingolipid molecular species <sup>15,20</sup>. Specifically, gas chromatography-mass spectrometry (GC-MS) was used for a long time to obtain information on both the sequence of the glycan, identity of the fatty acid, and the location of carbon-carbon double bonds after appropriate sample pre-treatment and derivatization <sup>92</sup>. Here, the glycan is typically cleaved off and the lipid backbone is analyzed separately as fatty acid methyl esters, thus losing the intact structural

information. Moreover, *de novo* identification of molecular species using this approach is not possible in the absence of an authentic standard. This is particularly important as limited glycosphingolipid standards are currently available commercially<sup>15</sup>. While early studies of intact glycosphingolipids employed fast atom bombardment (FAB) and liquid secondary ion mass spectrometry, these techniques suffer from low sensitivity and complexity of resulting spectra, thus are now largely replaced by soft ionization methods such as electrospray ionization (ESI)<sup>15,18</sup>.

Shotgun MS is a rapid, separation-free approach involving direct infusion of a complex sample commonly using ESI coupled with tandem mass spectrometry (MS/MS)<sup>19</sup>. In the absence of chromatography, isobaric and isomeric species are co-isolated during precursor ion selection, thus, ability to distinguish them in the resulting MS/MS spectrum is necessary. However, structural information obtained using contemporary techniques such as collision-induced dissociation (CID) and higher collision dissociation (HCD) could not distinguish carbon-carbon double bond positional isomers<sup>10,165,226</sup>. Although the use of lithiated adducts in ESI-MS/MS of intact glycosphingolipids reveals carbon-carbon double bond location resulting from charge-remote fragmentations<sup>227,228</sup>, oftentimes spectra are complex and difficult to interpret. Similarly, other techniques such as electron capture dissociation (ECD)<sup>150</sup>, electron transfer dissociation (ETD)<sup>229</sup>, and electron detachment dissociation (EDD)<sup>150</sup>, reveal only the complexity of the glycan sequence and the composition of the lipid backbone but the exact location of carbon-carbon double bonds cannot be determined. A number of approaches has been exploited to determine double bond positions in lipids as reviewed by Mitchell and colleagues<sup>230</sup>. More recent approaches include Paterno-Buchi reaction coupled with MS<sup>231</sup>, radical-directed dissociation<sup>47,232</sup> and ultraviolet photodissociation (UVPD)<sup>151,153,233,234</sup>. A simple and economical procedure involving air exposure of lipids on a thin layer chromatography plate followed by ESI-MS

analysis could also reveal double bond positions, but data analysis is rather intricate when complex mixture is involved <sup>235</sup>.

Ozone (O<sub>3</sub>) gas was historically employed to determine carbon-carbon double bond position in glycosphingolipids using in-solution ozonolysis, however the technique is laborious and requires relatively large amount of sample <sup>236</sup>. Harnessing this potential using MS, ozone was generated *in situ* during corona discharge using oxygen as nebulizing gas <sup>237</sup> and later directly employed ozone gas with ESI in a technique called ozone-ESI-MS (OzESI-MS) <sup>238</sup>, however, the spectra become increasingly difficult to interpret with increasing sample complexity. Thus, with the advent of ion-molecule reactions, Blanksby and co-workers incorporated ozone gas in an ion trap MS instrument in a technique called ozone-induced dissociation (OzID) <sup>11</sup>. Briefly, in OzID-MS, a precursor ion is mass-isolated followed by selective carbon-carbon double bond reaction with ozone gas which results in formation of characteristic Criegee and aldehyde product ions. The difference in the corresponding mass-to-charge (*m/z*) ratio of the precursor ion and the product ions (neutral losses) are diagnostic of carbon-carbon double bond positions <sup>10</sup>. This simple and rapid technique was successfully implemented in a number of MS platforms <sup>239-243</sup> and applied to characterize isomeric lipids in biological specimens <sup>10,244</sup>.

Recently, we reported the modification and optimization of parameters of a traveling wave-based quadrupole time-of-flight (Q-ToF) mass spectrometer (Synapt™ G2 HDMS, Waters®, UK) to allow the use of ozone as collision gas in the trap and transfer regions <sup>245</sup>. Herein, the said instrument, along with the previously optimized OzID settings <sup>245</sup>, was applied to study the fragmentation of glycosphingolipids and demonstrate its capability to differentiate isobaric and isomeric glycosphingolipid species using shotgun approach.

## **Experimental**

### **Materials**

The following standards and natural mixtures were purchased from Avanti Polar Lipids (Alabaster, AL): *D*-lactosyl- $\beta$ -1,1' *N*-stearoyl-*D*-erythro-sphingosine (LacCer d18:1/18:0, cat. no. 860598), *D*-lactosyl- $\beta$ -1,1' *N*-oleoyl-*D*-erythro-sphingosine (LacCer d18:1/18:1(9Z), cat. no. 860590), *D*-galactosyl- $\beta$ -1,1' *N*-oleoyl-*D*-erythro-sphingosine (GalCer d18:1/18:1(9Z), cat. no. 860546), *D*-galactosyl- $\beta$ -1,1' *N*-stearoyl-*D*-erythro-sphingosine (GalCer d18:1/18:0, cat. no. 860538), *D*-galactosyl- $\beta$ -1,1'-*N*-[2''(*R*)-hydroxystearoyl]-*D*-erythro-sphingosine (GalCer d18:1/18:0(2OH), cat. no. 860840), *D*-galactosyl- $\beta$ -1,1' *N*-nervonoyl-*D*-erythro-sphingosine (GalCer d18:1/24:1(15Z), cat. no. 860546) and *D*-glucosyl- $\beta$ -1,1'*N*-palmitoyl-*D*-erythro-sphingadiene from soy (GlcCer d18:2 (4*E*,8*Z*)/16:0, cat. no. 131304). Bovine brain galactocerebrosides (cat. no. C4905) was purchased from Sigma (St. Louis, MO). Globotetrahexosylceramide (Gb4Cer d18:1/24:1(15Z)(2ROH) from porcine RBC, cat. no. 1068) and Globotriaosylceramide (Gb3Cer d18:1/18:0, from porcine RBC, cat. no. 1529) were obtained from Matreya LLC (State College, PA). All solvents were of LC-MS grade and purchased from Fisher Scientific (Pittsburgh, PA).

### **Preparation of standard solutions and natural mixture sample**

Standard stock solutions were prepared as  $1.0 \mu\text{g} \cdot \mu\text{L}^{-1}$  in chloroform/methanol/water ( $\text{CHCl}_3/\text{MeOH}/\text{H}_2\text{O}$ , 2:1:0.1, v/v) and kept at  $-20^\circ\text{C}$  until further use. Working solutions for direct infusion experiments were made from these solutions by measuring appropriate aliquots in glass vials followed by drying under a stream of nitrogen gas and subsequent reconstitution in acetonitrile/isopropanol/water (ACN/IPA/ $\text{H}_2\text{O}$ , 65/30/10, v/v) to a final concentration of  $10 \text{ pmol} \cdot \mu\text{L}^{-1}$ . Soy and bovine brain galactocerebrosides were prepared as  $0.01 \mu\text{g} \cdot \mu\text{L}^{-1}$  in

ACN/IPA/H<sub>2</sub>O, 65/30/10 (v/v) from corresponding stock solutions in CHCl<sub>3</sub>/MeOH/H<sub>2</sub>O (2:1:0.1, v/v).

### **Instrument set-up**

The OzID-MS experiments were performed on a modified Synapt™ G2 HDMS instrument (Waters, Manchester, UK) as reported previously<sup>245</sup>. Briefly, O<sub>3</sub> MEGA integrated ozone delivery system (MKS Inc., Andover, MA) was connected to the trap and transfer regions of the instrument through a three-way valve. The ozone generator was operated following manufacturer's instructions and produced consistently 6.0 wt% ozone in oxygen at a flow rate of 1.0 slm from high purity oxygen (AirProducts, Indianapolis, IN) at 20 psi, which was used as collision gas in the mass spectrometer at a flow rate of 2.0 mL/min. The resulting pressure in the trap region of Synapt™ G2 was  $\sim 9.9 \times 10^{-3}$  mbar. For safety purposes, the remote switch of the ozone generator was interlocked with an ambient ozone monitoring system (Teledyne, San Diego, CA) and programmed to shut-off production when ambient ozone exceeds safe levels. Excess ozone was destroyed on-line using a destruction catalyst (MKS Inc., Andover, MA) that converts ozone to oxygen.

### **OzID-MS experiments**

Standards and samples were directly infused at 5.0  $\mu$ L/min using an automated syringe pump. The ESI source conditions were optimized and the final working conditions were set at the following values: polarity, positive; spray voltage, 3.0 kV; sampling cone, 30 to 50 V; extraction cone, 6 V; source temperature, 100 °C; desolvation temperature, 200 °C; cone gas flow, 50 L/h; desolvation gas flow, 500 L/h. Isolation of precursor ions was carried out in the quadrupole at  $\sim$  1Th isolation width (LM =16, HM = 15). All spectra were acquired for 1.0 min at 0.5 s/scan. Traveling wave in the trap and transfer regions were operated at the following settings as optimized previously<sup>245</sup>: Entrance, 5.0 V; Bias, 2.0; Trap DC, 0.2; Exit, 0; trap wave velocity, 8

m/s; wave height, 0.2 V; transfer wave velocity, 247 m/s; wave height, 0.4 V. Default instrument settings for all the remaining parameters were applied. Under these settings, the reaction time between ozone and ions is estimated to be  $\sim 16.65$  ms<sup>245</sup>. Instrument was calibrated daily in Resolution mode using sodium formate following manufacturer's instructions obtaining less than 0.6 ppm (0.5 mDa) RMS residual mass. To compensate for the fluctuations of the ambient conditions during mass measurement, lock mass corresponding to leucine enkephalin ( $m/z$  556.2711) was employed. Both the full scan and MS/MS levels were mass-corrected traceable to the reference lock mass using MassLynx v4.1 instrument control software (Waters, Manchester, UK).

### **Nomenclature of glycosphingolipid structures**

The shorthand notations used in this manuscript were based on the recommendations from the LipidMAPS consortium<sup>246</sup>. The CID-MS/MS fragments were annotated according to Domon and Costello<sup>141</sup>, and Ann and Adams<sup>227</sup>. For convenience and intuitive presentation of OzID-MS data, the nomenclature for the position of the carbon-carbon double bond was adopted based on the ( $n-x$ ) system where  $x$  corresponds to the position of unsaturation from the terminal -CH<sub>3</sub> of the hydrocarbon chain, for instance, double bonds in GalCer d18:1(4E)/18:1(9Z) are respectively annotated as  $n-14$  and  $n-9$ .

### **Results and Discussion**

Direct infusion of authentic glycosphingolipid standards yielded predominantly sodiated adducts without addition of sodium ions in solution. Thus, parameters were optimized for [M+Na]<sup>+</sup> and used as precursor ion in the succeeding OzID-MS experiments. Of note, no in-source fragmentation was observed in any of our samples parallel to prior investigations involving oligosaccharides which validated the high stability of this adduct<sup>205</sup>.

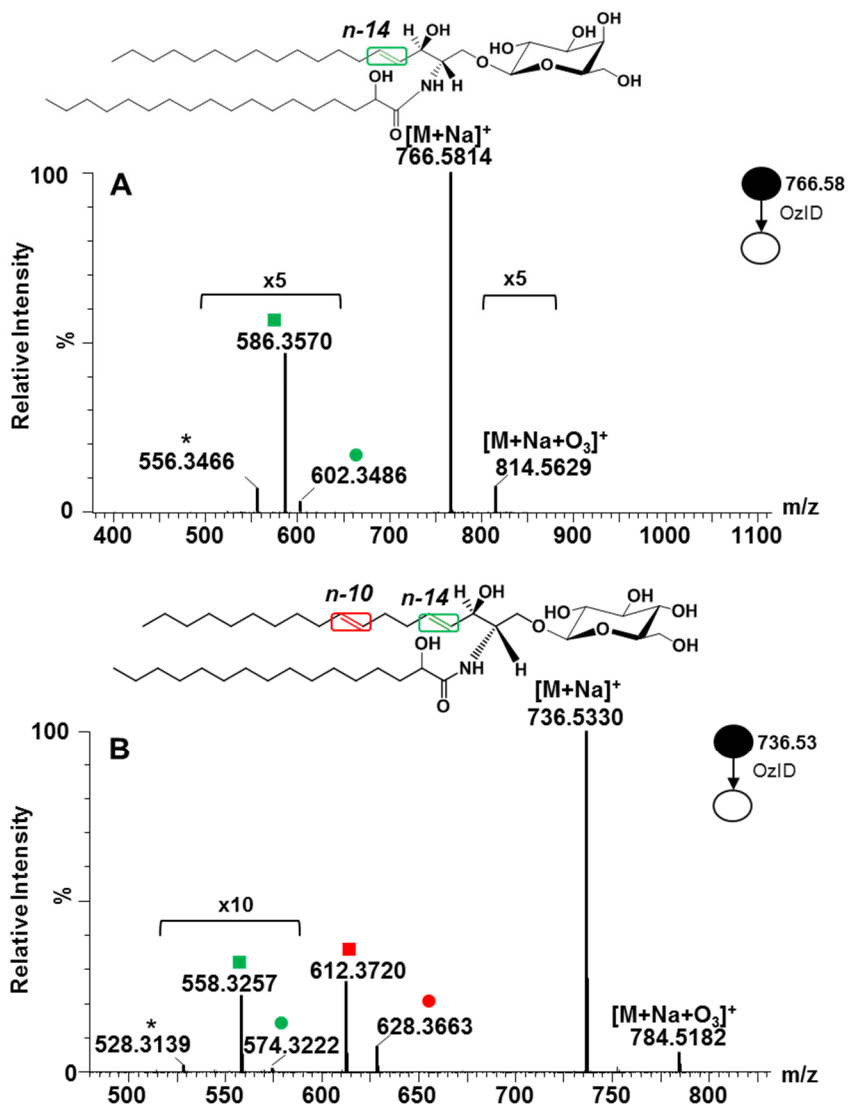


**Figure 15. High Resolution OzID-MS Spectrum of (a) GalCer d18:1/18:0(2OH), and (b) GlcCer d18:2/16:0(2OH) Standards Obtained in Synapt G2™ HDMS.** Criegee and aldehyde product ions are depicted as (●) and (■), respectively. Open square (□) indicates ions generated through elimination of H<sub>2</sub>C=O from the aldehyde ion.

### OzID-MS of common glycosphingolipid long chain bases

Two of the most common long chain bases in glycosphingolipids were chosen to study how these motifs behave in OzID-MS. Specifically, *trans*-4 sphinganine and 4,8-sphingadiene

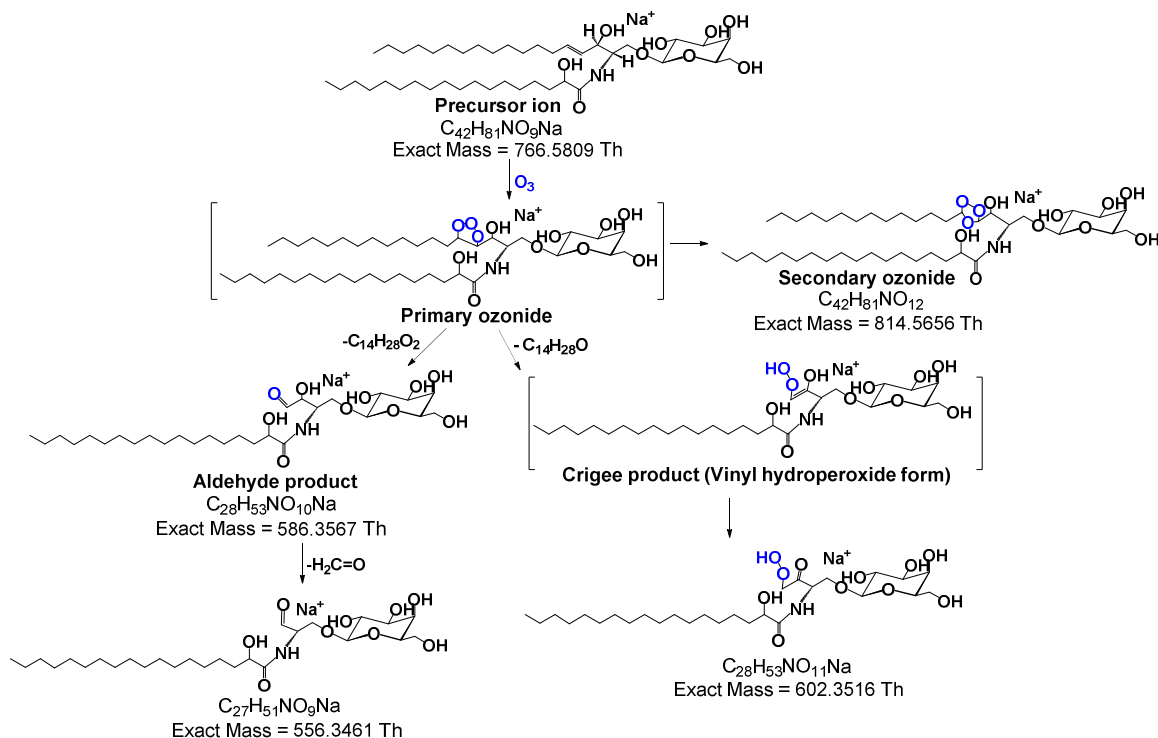


**Figure 16. Proposed Reaction Pathway for the OzID-MS of the  $[M+Na]^+$  of GalCer d18:1/18:0(2OH) ( $m/z$  766.5814).**

### OzID-MS of long chain base *trans*-4 sphingine

The most common glycosphingolipid long chain base in mammals is *trans*-4-sphingine (or simply, sphingosine), designated as d18:1(4E) where the double bond is at *n*-14 with *trans*-stereochemistry<sup>20,212,247</sup>. To determine the behavior of this motif, we first performed OzID-MS of a glycosphingolipid containing saturated fatty acyl chain, GalCer d18:1/18:0(2OH) (**Fig. 15a**). Two low intensity OzID products,  $m/z$  602.3486 (-164 Da) and  $m/z$  586.35470 (-180 Da) which differ by 16 Da were observed. Cognizant of alkene OzID-MS reaction pathway proposed previously<sup>10,11</sup>, those two were assigned as Crigee and aldehyde ions, respectively.

**Table 3. Assignment of OzID-MS Product Ions Based on Accurate Mass Measurement.**

Assignment	Formula	GalCer d18:1/18:0(2OH)		Absolute error ppm
		Theoretical (Th)	Observed (Th)	
[M+Na+O <sub>3</sub> ]	C <sub>42</sub> H <sub>81</sub> NO <sub>12</sub> Na	814.5656	814.5629	3.34
[M+Na] <sup>+</sup>	C <sub>42</sub> H <sub>81</sub> NO <sub>9</sub> Na	766.5809	766.5814	-0.69
Criegee ion ( <i>n-14</i> )	C <sub>28</sub> H <sub>53</sub> NO <sub>11</sub> Na	602.3516	602.3486	5.00
Aldehyde ion ( <i>n-14</i> )	C <sub>28</sub> H <sub>53</sub> NO <sub>10</sub> Na	586.3567	586.357	-0.52
-H <sub>2</sub> CO	C <sub>27</sub> H <sub>51</sub> NO <sub>9</sub> Na	556.3461	556.3466	-0.84
GlcCer d18:2/16:0(2OH)				
[M+O <sub>3</sub> +Na] <sup>+</sup>	C <sub>40</sub> H <sub>75</sub> NO <sub>12</sub> Na	784.518669	784.5182	0.60
[M+Na] <sup>+</sup>	C <sub>40</sub> H <sub>75</sub> NO <sub>9</sub> Na	736.53924	736.533	1.25
Criegee ion ( <i>n-10</i> )	C <sub>30</sub> H <sub>55</sub> NO <sub>11</sub> Na	628.367262	628.3663	1.53
Aldehyde ion ( <i>n-10</i> )	C <sub>30</sub> H <sub>55</sub> NO <sub>10</sub> Na	612.372347	612.372	0.57
Criegee ion ( <i>n-14</i> )	C <sub>26</sub> H <sub>49</sub> NO <sub>11</sub> Na	574.3203144	574.3222	-3.28
Aldehyde ion ( <i>n-14</i> )	C <sub>26</sub> H <sub>49</sub> NO <sub>10</sub> Na	558.3253994	558.3257	-0.54
-H <sub>2</sub> CO	C <sub>25</sub> H <sub>47</sub> NO <sub>9</sub> Na	528.3148352	528.3139	1.77

Interestingly,  $m/z$  556.3466 ion was noted which differs by 30 Da from the aldehyde product and is likely resulted from loss of formaldehyde (H<sub>2</sub>C=O) from  $m/z$  586.35470. Although it could also be directly generated from loss of formic acid (HCOOH) from the Criegee ions, its even higher intensity than the Criegee ion suggests that this may not be the case. Elimination of H<sub>2</sub>C=O was also observed in phosphatidylcholine-derived Criegee ions we reported previously due to high proportion of ozone in our measurement conditions<sup>245</sup>. This similar observation might have been due to the structure similarity between the allylic alcohol-derived aldehyde product and the alkene-derived vinyl hydroperoxide (a form of Criegee ion<sup>10</sup>). Moreover, allylic alcohol-derived Criegee ions can exist as a highly unstable vinyl hydroperoxide product which could further rearrange to form ketone group through keto-enol tautomerization (**Fig. 16**). Of

note, loss of H<sub>2</sub>C=O was only observed from the cleavage products of the long chain base but not from the fatty acyl double bond (vide infra), indicating the role of allylic hydroxyl group in such elimination process. Aside from these fragments, no other side reactions of ozonolysis was observed. Using accurate mass measurements where  $\leq 5$  ppm mass error was consistently obtained, all OzID-MS product ions and their molecular formula as shown in Table 3 were confidently assigned.

The long chain base d18:2(4*E*,8*Z*) also called 4,8-sphingadiene is widespread in plant tissues<sup>212,248,249</sup> and less prominent in mammals<sup>247</sup>. We studied commercial soy glucocerebroside mixture using the most abundant species, GlcCer d18:2/16:0(2OH) with [M+Na]<sup>+</sup> at *m/z* 736.5330. In OzID-MS, the expected products were observed, at *m/z* 628.3663 (-108 Da) and *m/z* 612.3720 (-124 Da) from the oxidative cleavage of *n*-10 double bond followed by *n*-14 double bond at *m/z* 558.3257 (-54 Da) with barely detectable Criegee ion at *m/z* 574.3222 (-38 Da) (**Fig. 15b** and **Fig. 18**). In addition, loss of H<sub>2</sub>C=O from this species at *m/z* 528.3139 was detected, similar as what observed for the glycosphingolipid discussed above (**Fig. 15a**). It is of note that the two double bonds in 4,8-sphingadiene have distinct reactivity toward ozone, with the intensity of OzID products at *n*-10 position (*cis*) about ten-fold higher than that of OzID products originated from the *n*-14 position (*trans*). Although *trans* alkenes are known to be more reactive towards ozone<sup>242</sup>, our observation can be attributed to the distinct electronic and steric influences in these positions that outweigh the contribution of double bond geometric configuration to reactivity.

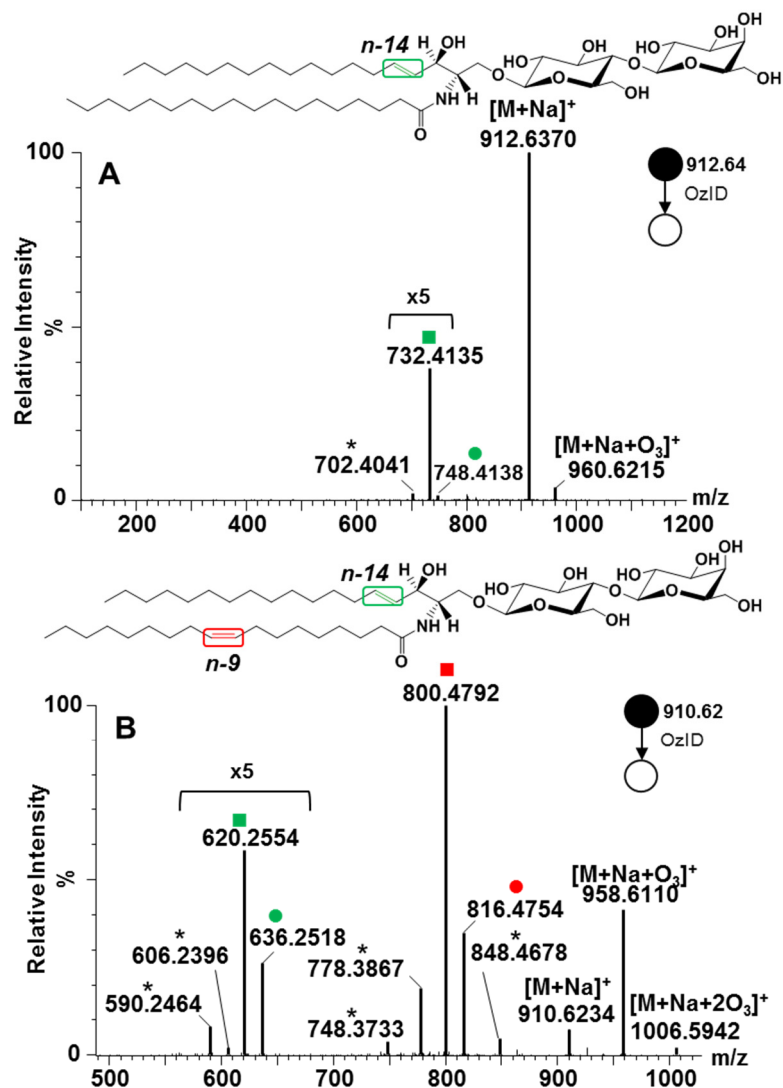


**Figure 17. Comparison of OzID-MS Spectra of (a) LacCer d18:1/18:1(9Z) and (b) LacCer d18:1/18:0.** Criegee and aldehyde product ions are depicted as (●) and (■), respectively. Open square (□) and circle (○) indicate ions generated through elimination of H<sub>2</sub>C=O from the aldehyde ion and Criegee ion, respectively. Asterisk (\*) indicates ions generated through secondary oxidation from [M+Na+O<sub>3</sub>]<sup>+</sup>. Colors represent different double bond locations.

#### OzID-MS of long chain base 4,8-sphingadiene

Sullards and co-workers<sup>248</sup> studied the [M+Li]<sup>+</sup> adduct of GlcCer d18:2/16:0(2OH) using FAB-MS and identified the long chain base double bond positions. Specifically, while

fragmentation of the intact  $[M+Li]^+$  could not directly provide evidence for the precise location of the two double bonds, subjecting the *O* ion (sphingoid base) to fragmentation resulted in characteristic 53 u gap for the  $\Delta^8$  double bond. A distonic allylic radical with  $m/z$  137.2 diagnostic of the  $\Delta^4$  double bond was also apparent indicating that these two double bonds have differential fragmentability. More recently, Ryan *et al.*<sup>153</sup> demonstrated the use of 193 nm UVPD for structural analysis of sphingolipids and showed unique fragments corresponding to cleavage of each double bond in d18:2(4*E*,11*Z*)-sphingadiene. While the two C=C in 4,8-sphingadiene did not show different fragmentation mechanism under OzID, we observed a difference in terms of the double bond reactivity, which is in contrast to the results obtained by Sullards *et al.*<sup>248</sup> and Ryan *et al.*<sup>153</sup>, simpler spectra were also obtained and data interpretation is more straightforward making it useful for both mammalian and non-mammalian glycosphingolipids determination.

Both the  $\Delta^4$  double bond in *trans-4* sphingenine and 4,8-sphingadiene have different reactivity toward ozone than that in alkenes. Zhou and colleagues<sup>235</sup> observed attenuated reactivity of the sphingosine double bond towards oxidation with ozone and singlet oxygen, and rationalized it is due to the electron-withdrawing inductive effect by allylic hydroxyl. This was further supported by recent studies on the free radical-induced oxidation of glycosphingolipids<sup>250,251</sup>. This explanation is consistent with solution-phase ozonolysis of alkenes which showed the electrophilic nature of ozone in the upstream Criegee mechanism<sup>252</sup>. Conversely, gas phase ozonolysis of alkenes with allylic hydroxyl group revealed opposite findings, specifically, unsaturated alcohols were found to be more reactive than the corresponding olefinic analogs<sup>253</sup>.

In their OzESI-MS experiments with sphingomyelin, another lipid class containing the same sphingosine backbone, Thomas and co-workers<sup>238</sup> hypothesized that its gas phase conformation permits hydrogen bonding of the cation in the headgroup to the allylic hydroxyl of sphingosine thus impairing ozone's access to the double bond.

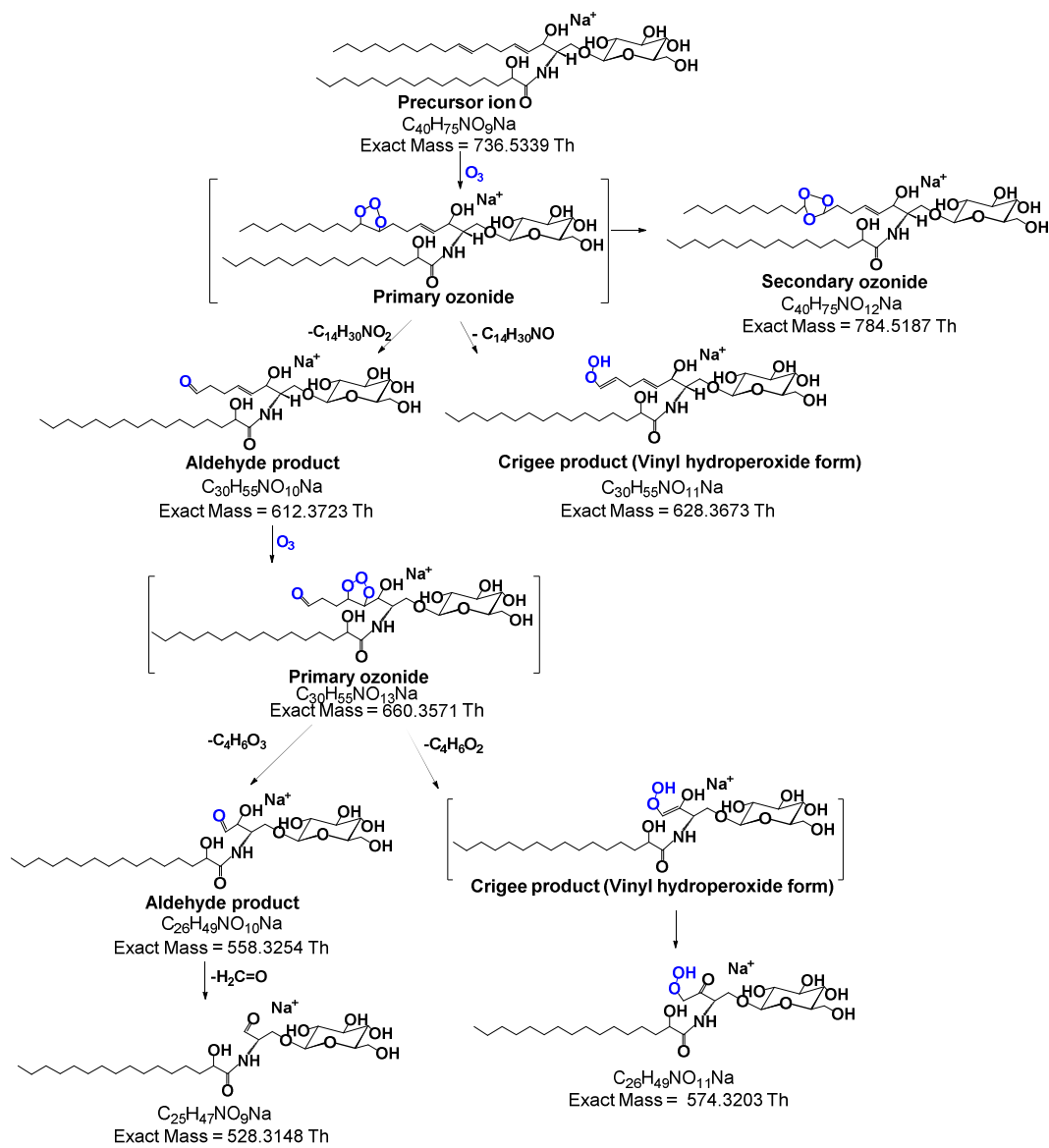


**Figure 18. Proposed Reaction Pathway for the OzID-MS of the  $[M+Na]^+$  of GlcCer d18:2/16:0(2OH) ( $m/z$  736.5330).**

Altogether, these explanations suggest that the peculiar attribute of sphingosine double bond towards oxidation cannot be rationalized in terms of electronic effects of the  $\alpha$ -hydroxyl group alone but rather in conjunction with steric contribution by the head group as a result of its gas phase conformation. Our observation is in agreement with these previous studies<sup>235,238,250-252</sup>.

### **Influence of head group on the cleavage of long chain base double bond**

The proximity of unsaturation in the long chain base to the head group prompted us to study the influence of the glycan on double bond oxidative cleavage. While epimeric sugars glucose and galactose did not show significant difference in OzID-MS features (data not shown), overall, the number of glycan in the head group appeared to influence the reactivity of the sphingosine double bond. Shown in **Fig. S1** are the OzID-MS spectra of glycosphingolipids containing one (GalCer) to three (globotriaosyl ceramide, Gb3) sugar moieties. Notably, the intensity of the ozonide ion along with the OzID diagnostic products is increased with increasing number of sugars. This shows that the head group indeed affects the gas phase ozonolysis of lipids either by influencing electronic density distribution in the proximal double bond as a consequence of gas phase conformation<sup>238</sup> or through its direct involvement in the overall reaction mechanism as recognized previously in other lipid classes<sup>11</sup>. Such concepts require further experimental and computational studies to elucidate the overall mechanistic process. Nevertheless, as diagnostic OzID products are conspicuous despite varying glycan lengths, this technique is undoubtedly applicable to more complex glycosphingolipids.

### **Influence of fatty acyl hydroxylation on the cleavage of long chain base double bond**

Both samples described in **Fig. 15** possess  $\alpha$ -hydroxyl group on the fatty acyl, although the effect is not drastic, its presence appeared to influence the oxidative cleavage of the double bond in the backbone. When GalCer d18:1/18:0(2OH) and GalCer d18:1/18:0 (**Fig. S2**) were compared, about five-fold enhancement of signal intensity of ozonide and aldehyde products and increased intensity ratio of the OzID diagnostic ions to ozonide were observed. This shows that even with the remoteness of the hydroxy group from the double bond, notable influence is apparent.

Taken together, even though the simplified reaction pathways depicted in Schemes I and II clearly illustrate the overall gas phase ozonolysis process, the reaction mechanism might be more complex as we observed that the head group and the remote functional groups also influence the overall steric as well as electronic environment of the double bond. As also acknowledged in the past <sup>11</sup>, these effects, although currently still not quantitative, when carefully considered, could hint on the local environments of the double bond and facilitate glycosphingolipid structural characterization.

### **Comparison between long chain base and fatty acyl unsaturation**

Glycosphingolipid containing unsaturated fatty acyl chain was investigated using the  $[M+Na]^+$  ( $m/z$  910.6234) of standard LacCer d18:1/18:1(9Z). As expected, the Criegee and aldehyde products from *n*-9 double bond in the fatty acyl chain were observed at  $m/z$  816.4754 (-94 Da) and  $m/z$  800.4792 (-110 Da), respectively (**Fig. 17a**). Owing to the two double bonds present, another set of OzID products was identified characteristic of the *n*-14 sphingosine double bond (Criegee ion  $m/z$  636.2518 and aldehyde ion  $m/z$  620.2554) along with a loss of  $H_2C=O$  ( $m/z$  606.2396 and  $m/z$  590.2464) as discussed earlier. Here the presence of two pairs ( $m/z$  636.2518 and  $m/z$  606.2396,  $m/z$  620.2554 and  $m/z$  590.2464) and the consistent intensity ratio within each pair further suggests that  $H_2C=O$  loss from both the aldehyde and Criegee ions is the most probable reaction pathway. It is of note that ions corresponding to fatty acyl double bond were about eight times higher than those of long chain base double bond. Also interestingly, instead of having the anticipated neutral loss of 180 Da and 164 Da directly from the precursor ion, these neutral losses were observed from the OzID products of the fatty acyl double bond. This suggests that oxidative cleavage of these olefins is a non-concerted process, and fatty acyl chain double bond cleavage precedes that of sphingosine analogous to observations with GlcCer d18:2/16:0(2OH) as discussed above (**Fig. 15b**). The relatively low reactivity of this sphingosine

double bond towards oxidation as observed before<sup>235,238,250,251</sup> and in this study, may explain why the unsaturation in the fatty acyl chain is preferentially cleaved off prior to that of the sphingosine. In this respect, Thomas and colleagues performed OzESI-MS of analogous compound sphingomyelin d18:1/18:1(9Z), and showed that only the fatty acyl double bond is prominent<sup>238</sup>. In contrast, our results show the presence of the oxidative cleavage products of both double bonds. While the fatty acyl unsaturation is much more reactive, the difference of reactivity between long chain base double bond and ozone observed by them and us may stem from the different concentrations of ozone used and the different efficiency of OzID reaction in the two OzID-MS instrument platforms. Sequential cleavage of double bonds in OzID-MS of different radyls in phosphatidylcholine was also observed by Poad and co-workers<sup>243</sup>.

Shown in **Fig. 17b** is the OzID-MS of  $m/z$  912.6370, the  $[M+Na]^+$  of LacCer d18:1/18:0. The spectrum shows an ion at  $m/z$  960.6215 corresponding to the ozonide species,  $[M+Na+O_3]^+$ . Two OzID products, a low intensity  $m/z$  748.4138 (-164 Da) and  $m/z$  732.4135 (-180 Da) were observed, assigned as Criegee and aldehyde ions, respectively, along with loss of  $H_2C=O$  at  $m/z$  702.4041.

In contrast to the saturated analog, a remarkable difference in spectrum was distinguished for LacCer d18:1/18:1(9Z) molecule. Specifically, for the unsaturated analog, the precursor ion is almost completely depleted and the  $[M+Na+O_3]^+$  was found to be significantly higher (**Fig. 17a**) than the saturated counterpart (**Fig. 17b**). In addition, another distinct ion at  $m/z$  1006.5942 was observed, albeit low intensity corresponding to  $[M+Na+2O_3]^+$ . In sum, this reflects the high efficiency of ozonolysis reaction under the employed measurement conditions owing to the high proportion of ozone in the collision gas mixture and the increased ozone contact time due to the traveling wave settings in the trap and transfer regions as reported previously<sup>245</sup>. The greater prevalence of ozonide ion (~3 to 4x higher) in the spectrum of unsaturated glycosphingolipid

(**Fig. 17a**) as compared to the saturated analog (**Fig. 17b**) can be rationalized in terms of the increased affinity of this molecule to ozone due to the additional double bond in the fatty acyl chain.

The observed discrepancy in terms of the relative reactivity of the fatty acyl chain and the sphingosine double bonds is analytically advantageous and can be used to distinguish unsaturation between the long chain base and the fatty acyl chain. Prior studies on OzID-MS of phospholipids and triacylglycerols successfully utilized sequential CID/OzID experiments in a linear ion trap instrument to assign double bond position on specific fatty chain<sup>11,240,241,244</sup>. On the other hand, for glycosphingolipids, these sequential steps were deemed unnecessary as differentiation of the backbone and fatty acyl chain is readily observable. Also, as sphingosine marker  $m/z$  264 is sometimes difficult to observe in CID-MS/MS spectrum, OzID-MS is a facile technique for the rapid identification of this long chain base<sup>254</sup>.

Moreover, two sets of OzID-MS products (minor products, labelled with \* in **Fig. 17a**) arising from secondary oxidation cleavages from the ozonide  $[M+Na+O_3]^+$  were evident which were not observed in the saturated counterpart (*cf.* **Fig. 17b**). These minor secondary oxidation products were also detected using analogous instrument in a recent report<sup>243</sup>. The ion with  $m/z$  778.3867 is a putative loss of 180 Da from  $m/z$  958.6110 (**Fig. 17a**). Since the intensity of this ion was observed to increase with increasing ozonide intensity, we hypothesized that it could result from the ozonide and that increasing number of sugar moiety would also increase the intensity of this secondary oxidation products which we have indeed confirmed. Studies on glycosphingolipids exposed to free radicals in the condensed phase reported potential cleavage of the sugar backbone under oxidizing conditions<sup>250,251</sup>. Based on this notion, two sources of the observed neutral loss (-180 Da) from secondary oxidation in OzID are plausible, *first* is the loss of sugar moiety, and *second* is the cleavage of the sphingosine double bond. Clarification of this

ambiguity was greatly facilitated by accurate mass measurements. In the first case, loss of sugar results to an ion with a molecular formula of  $C_{42}H_{77}NO_{10}Na$  ( $m/z$  778.5445) and mass error of 202.69 ppm, while the second case gives  $C_{34}H_{61}NO_{17}Na$  ( $m/z$  778.3837) and a mass error of 3.85 ppm. These results indicate that loss of sugar is unlikely and that the neutral loss of 180 Da from the ozonide results from the cleavage of the sphingosine double bond via secondary oxidation processes. In terms of analytical utility, the low abundance of these secondary products does not complicate data interpretation <sup>243</sup>.

### **Effect of the chain length of unsaturated fatty acyl on OzID product branching**

Comparing different unsaturated standards, interestingly, opposite pattern in the intensity of Criegee and aldehyde ions resulting from fatty acyl double bond was observed between GalCer d18:1/18:1(9Z) and GalCer d18:1/24:1(15Z). In the former, in terms of intensity, the aldehyde > Criegee ion, whereas in the latter, aldehyde < Criegee ion (**Fig. 19a** and **19b**, in red color). Previously, it was reported that phosphoethanolamine (PE) and phosphatidyl inositol (PI) analogs showed opposite intensity ratio of aldehyde and Criegee ions <sup>11</sup>. That difference was rationalized in terms of the gas phase basicities of the different head groups and possible participation of charge in the reaction mechanism. In our present study, analogous pattern was noted notwithstanding the similarity of the head groups indicating the role of hydrocarbon chains in determining the branching ratio. The difference in OzID product intensities we observed could be attributed to the increased flexibility of the fatty acyl chains thus offering greater chance for the double bond to interact with charge, which is in agreement with previous findings that charge carrier participates in OzID mechanism <sup>11</sup>. This was further confirmed when the  $[M+Na]^+$  of one of the most abundant ion in porcine red blood cell globosides, Gb4Cer d18:1/24:1(2OH), was subjected to OzID-MS. As expected, for the 24:1 fatty acyl chain, intensity of Criegee product is higher than the aldehyde (**Fig. 19c**). Moreover, secondary oxidation products are also observed in

agreement with the ones identified in LacCer d18:1/18:1(9Z) thus confirming that an increase in the number of sugar moiety increases propensity towards side reactions. As these products do not impede data interpretation, the utility of this technique for targeted structural analysis of glycolipids containing longer chain glycans is plausible as demonstrated herein.

One remaining challenge in assigning isomeric unsaturated lipids in general and particularly glycosphingolipids, is the stereochemistry of the double bond. The *cis*- and *trans*-isomers are distinguishable using OzID-MS as previously demonstrated<sup>242,245</sup> but requires authentic standards to enable unambiguous assignments. For glycosphingolipids, only the *cis*-isomers are currently available.

#### **Application to bovine brain galactocerebrosides**

The analytical utility of OzID-MS for glycosphingolipids was tested by infusing bovine brain galactocerebrosides. The full scan accurate mass spectrum of the mixture is shown in **Fig. 20a**. Cerebrosides are the simplest yet diverse class of glycosphingolipids with high abundance in the brain and have been implicated in neurodegenerative diseases<sup>255,256</sup>.

The co-existence of isomeric and isobaric galactocerebrosides in this sample makes it an excellent model to demonstrate applicability of OzID-MS in glycosphingolipids. By performing CID-MS/MS of each prominent ion under Argon, we tentatively assigned the identity of each species. Subsequently, OzID-MS was performed by selecting the  $[M+Na]^+$  as precursor ion.

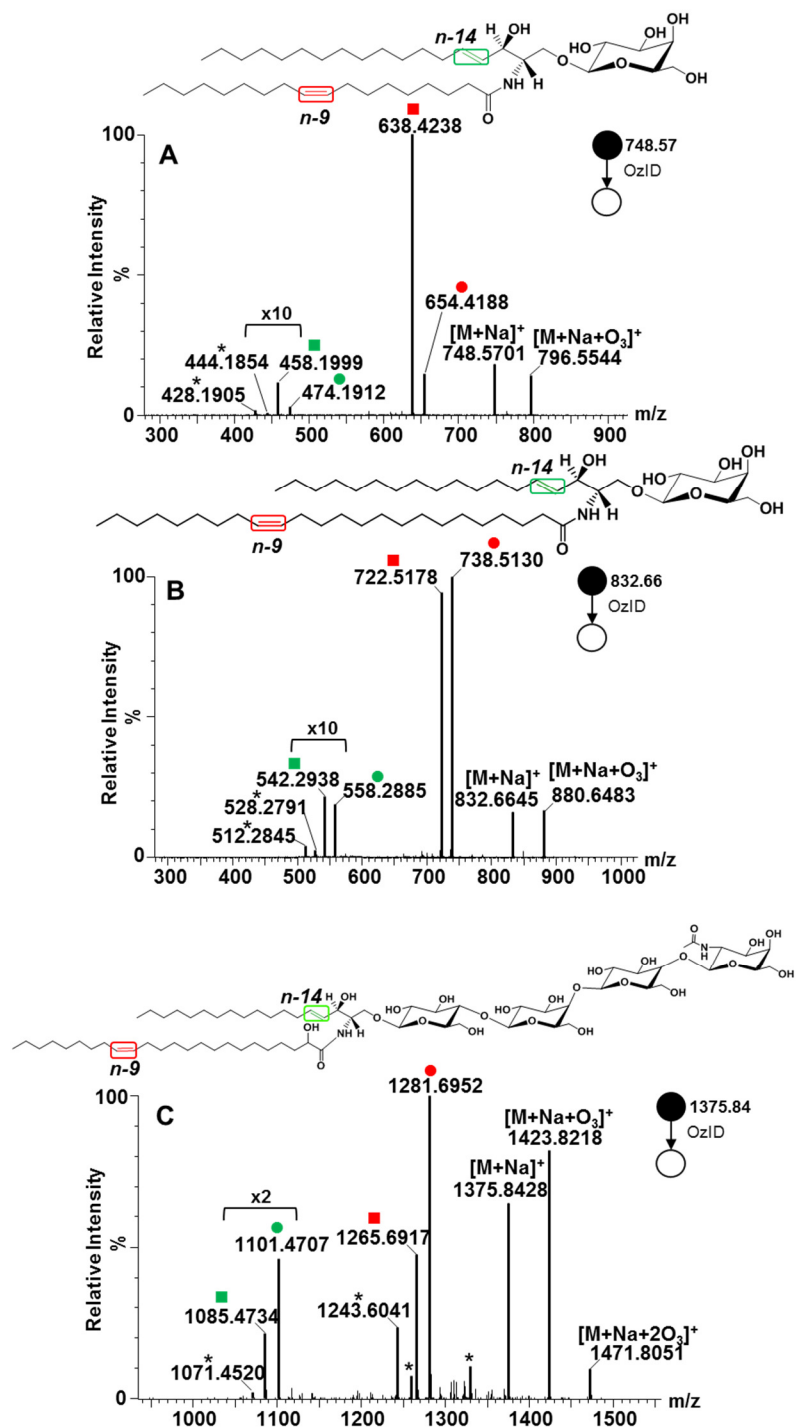
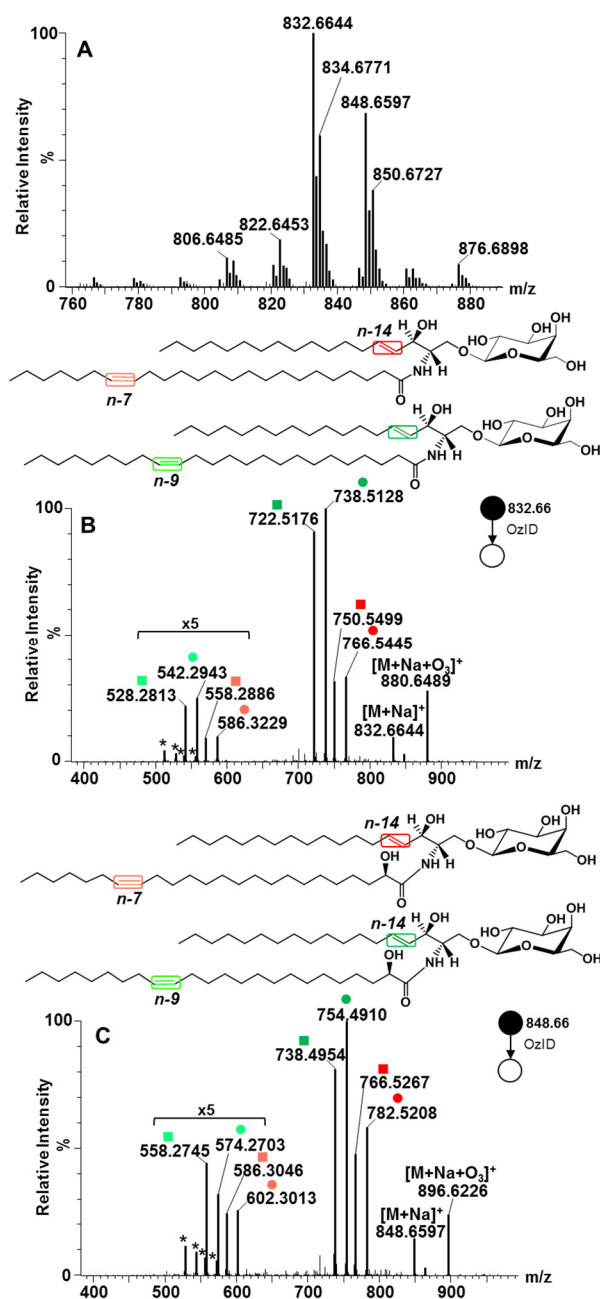


Figure 19. OzID-MS of (a) GalCer d18:1/18:1(9Z), (b) GalCer d18:1/24:1(15Z), and (c) Gb4Cer d18:1/24:1(15Z)(2OH). (Explanation of symbolic representations is described in Figs. 15 and 17).

### OzID-MS of major bovine brain galactocerebroside isomers

The two most abundant galactocerebroside species in bovine brain were  $m/z$  832.6644 and  $m/z$  848.6597. The CID-MS/MS spectrum of  $m/z$  832.6644 showed  $Y_0$  ion at  $m/z$  670.61 and  $Z_0$  ion at  $m/z$  652.60 as well  $m/z$  264.26 diagnostic of the d18:1 long chain base<sup>228,247,254,257</sup>. While important, the latter ion is sometimes hardly observable due to its decreased intensity as the number of glycan head group is increased<sup>254</sup>. The B and C ions corresponding to the sugar head group were also detected (**Fig. S3-a**). This fragmentation data is consistent with previous observations for GalCer d18:1/24:1 and verified using authentic standard shown earlier.

Subjecting  $m/z$  832.6644 to OzID-MS, four distinct pairs of OzID products were found (**Fig. 20b**). The first pair differs from the precursor ion by 66 Da ( $m/z$  766.5445) and 82 Da ( $m/z$  750.5499), characteristic of  $n-7$  double bond. Another pair differs by 94 Da ( $m/z$  738.5128) and 110 Da ( $m/z$  722.5176) from the precursor ion, indicating that another double bond is present at  $n-9$  position. Each of these ions is paired with a set of Criegee and aldehyde ions of neutral loss 164 Da at  $m/z$  586.3229 and  $m/z$  558.2813, and 180 Da at  $m/z$  570.3274 and  $m/z$  542.2943. The lower intensity of the latter ions signify that these are due to the cleavage of the sphingosine double bonds as discussed earlier. Based on this result, these species were assigned as regioisomers GalCer d18:1/24:1(17Z) and GalCer d18:1/24:1(15Z) without ambiguity where only the stereochemistry of the double bond is assumed, consistent with previous findings from GC-MS analysis of bovine brain galactocerebroside<sup>258,259</sup>.



**Figure 20. Application of High Resolution OzID-MS to Major Isomeric Galactocerebroside Species in Bovine Brain.** (a) Full scan MS. (b) OzID-MS spectrum of GalCer d18:1/24:1,  $m/z$  832.6644 with  $n$ -7/ $n$ -14, and  $n$ -9/ $n$ -14 double bonds (fatty acyl chain/long chain base). (c) OzID-MS of  $m/z$  848.6597 GalCer d18:1/24:1(2OH), with  $n$ -7/ $n$ -14, and  $n$ -9/ $n$ -14 double bonds. (Explanation of symbolic representations is described in Figs. 15 and 17).

Using an independent reversed phase liquid chromatography-MS (RPLC-MS) analysis employing a variety of core-shell C<sub>18</sub> and C<sub>30</sub> columns, these two isomers were found to be co-eluted (data not shown). Same as observations by Poad and colleagues of co-eluting phosphatidylcholine isomers in RPLC, our result highlights the importance of OzID-MS in revealing isomers that are otherwise non-distinguishable even with upfront chromatographic separation and contemporary fragmentation technique<sup>243</sup>.

The CID-MS/MS spectrum of  $m/z$  848.6597 is shown in **Fig. S3-b**, with the  $Y_0$  and  $Z_0$  ions at  $m/z$  686.61 and  $m/z$  668.59, respectively. Cleavage of amide bond resulted to formation of  $m/z$  484.33 was also noted indicative of the presence of an  $\alpha$ -hydroxy group. Hsu and Turk<sup>228</sup>, and Hunnam and colleagues<sup>254</sup> also observed the formation of this ion characteristic of glycosphingolipids hydroxylated at carbon atom adjacent to amide carbonyl. Based on this,  $m/z$  848.6597 was tentatively assigned as GalCer d18:1/24:1(2OH). This ion was subjected to OzID-MS and detected two isomers having one double bond in the fatty acyl chain, one at  $n-7$  and another at  $n-9$  as evident by pairs of ions at  $m/z$  782.5208 (-66 Da) and  $m/z$  754.4910 (-82 Da), as well as  $m/z$  766.5267 (-94 Da) and  $m/z$  738.4954 (-110 Da) assigned as Criegee and aldehyde ions, respectively (**Fig. 20c**). The sphingosine double bond (-164Da and -180 Da) was observed at  $m/z$  602.3013, 586.3046, 574.2703 and 558.2745 respectively along with loss of H<sub>2</sub>C=O (30 Da), again with much lower intensity. Taken together, this suggests the presence of two hydroxylated regioisomers, GalCer d18:1/24:1(17Z)(2OH) and GalCer d18:1/24:1(15Z)(2OH) in the sample where only the stereochemistry of the double bond is assumed.

### **Differentiation of major isobaric galactocerebroside species in bovine brain**

One of the challenges in shotgun lipidomics is the co-isolation of isobaric species. For cerebroside, the simplest glycosphingolipids, this may be particularly important, for example, in the co-presence of hydroxylated, unsaturated species and its non-hydroxylated, saturated analog.

Brain cerebroside is an excellent model system to show this capability and here,  $m/z$  834.6771 and  $m/z$  850.6727 were chosen as examples.

In theory, isobaric components can be distinguished at the full scan MS level in high resolution ('W') mode of Synapt™ G2 instrument. Using the 'W' mode, however, two orders of magnitude decline in signal intensity was observed which would require relatively more concentrated sample. Thus, the Resolution ('V') mode was chosen as a trade-off between sensitivity, mass accuracy, and resolution. At this setting on the average, at most ~20,000 full-width at half maximum (FWHM) resolution was achieved and is inadequate to distinguish GalCer d18:1/23:1(2OH) (sodiated adduct,  $m/z$  834.6435) and GalCer d18:1/24:0 (sodiated adduct,  $m/z$  834.6793), which requires at least 24,000 FWHM.

The  $m/z$  834.6771 was tentatively assigned as GalCer d18:1/24:0 based on characteristic fragments identified in its CID-MS/MS spectrum (**Fig. S3-c**). In OzID-MS, *first*, the ion at  $m/z$  654.4553 (-180 Da) was observed along with a low intensity but distinct Criegee ion at  $m/z$  670.4456 (-164 Da) and loss of 30 Da from aldehyde at  $m/z$  624.4434, respectively (**Fig. 21a**). *Second*, two pairs of OzID product ions were recognized corresponding to neutral loss of 66 Da ( $m/z$  768.5538) and 82 Da ( $m/z$  752.5581), and 94 Da ( $m/z$  740.5240) and 110 Da ( $m/z$  724.5289) which reveal the presence of regioisomeric *n*-7 and *n*-9 double bonds. These are paired with another smaller set of Criegee and aldehyde product ions which based on their intensity and accurate mass were identified to correspond to the sphingosine double bond. This indicates that GalCer d18:1/24:0 is co-present with its isobaric analog, GalCer d18:1/23:1(2OH) (**Fig. 21b**). These data showcase the capability of OzID-MS to distinguish isobaric species that are co-isolated during MS/MS step<sup>11</sup> and whose CID-MS/MS spectrum provides low intensity, thus easily overlooked characteristic fragmentations<sup>254</sup>. The lower intensity of the double bond cleavage products (*n*-7, *n*-9) compared to precursor ion further suggests the relatively lower

concentration of these species compared to ones containing saturated fatty acyl chain. In line with our observations, previous reports indicate GalCer d18:1/23:1(2OH) as a minor constituent in the brain while the GalCer d18:1/24:0 as the more abundant species<sup>258,259</sup>. Also, early studies on total mammalian brain sphingolipids have identified the fatty acyl chain 23:1 with double bond positions at *n*-7, *n*-8, *n*-9 and *n*-10<sup>217</sup>.

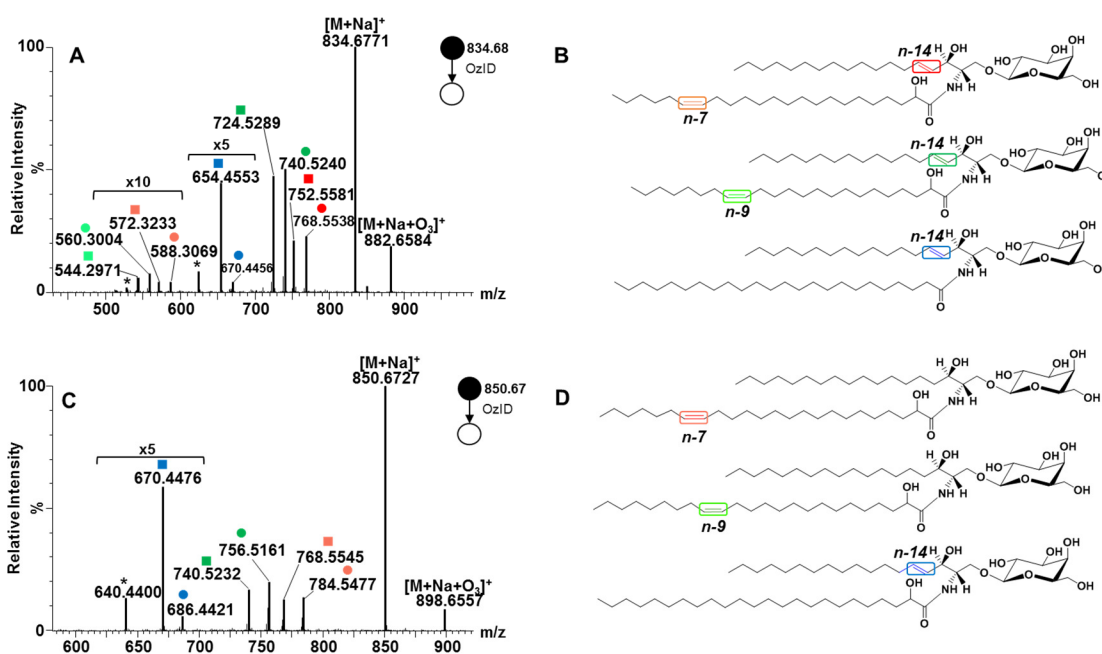


**Figure 21. Application of High Resolution OzID-MS to Major Isomeric and Isobaric Galactocerebroside Species in Bovine Brain.** (a) OzID-MS of *m/z* 834.6771 with *n*-7, *n*-9 (GalCer d18:1/23:1(2OH)), and *n*-14 double bonds (GalCer d18:1/24:0) (b). (c) OzID-MS spectrum of *m/z* 850.6727 with *n*-7, *n*-9 (GalCer d18:0/24:1(2OH)), and *n*-14 (GalCer d18:1/24:0(2OH)) double bonds (d). (Explanation of symbolic representations is described in Figs. 15 and 17).

In our present study, we only detected *n*-7 and *n*-9 positions. This implies that these two fatty acyl chains are favored substrates for glycosylation over the others in the downstream biosynthesis of cerebroside, which indicates that relevant enzymes prefer fatty acyls with specific location of unsaturation. This notion remains a fertile subject of future research.

Another interesting ion,  $m/z$  850.6727 was selected for OzID-MS whose spectrum is shown in **Fig. 21c**. Based on CID-MS/MS pattern (**Fig. S3-d**), this ion was tentatively assigned as GalCer d18:1/24:0(2OH). As before, neutral losses of 164 Da and 180 Da were anticipated along with a high intensity precursor ion due to its expected reduced reactivity with ozone. Indeed, intact precursor ion was observed as the base peak along with the neutral losses of 164 Da and 180 Da at  $m/z$  686.4421 and  $m/z$  670.4476, respectively. Additionally, two pairs of OzID products of low intensity were observed indicative of  $n-7$  and  $n-9$  double bond positions (**Fig. 21d**). For galactocerebroside of mass  $m/z$  850.6727, plausible structures could be the ones containing a hydroxyl group and one double bond. Thus, assignment was made as GalCer d18:0/24:1(17Z)(2OH) and GalCer d18:0/24:1(15Z)(2OH) where the stereochemistry was assumed. Indeed, a very low intensity but distinct fragment ion ( $m/z$  430.36) was noted in its CID-MS/MS spectrum confirming the existence of these species (**Fig. S3-d**). Studies have shown that the sphinganine long chain base (d18:0) in bovine brain sphingolipids is at minimal amount when analyzed by GC following cleavage of the glycan head group<sup>259</sup>. This result clearly highlights the utility of OzID-MS in amplifying the signal of these low-level species and its capability to study intact glycosphingolipids in biological samples.

Taken together, shotgun OzID-MS in conjunction with high resolution and high mass accuracy measurement provides a wealth of information on molecular species that are otherwise hardly achievable using common ion fragmentation tools. Furthermore, as accurate mass measurement is insufficient to distinguish isobaric lipids without adequate resolving power, distinct fragmentations obtained using OzID-MS is a very useful tool for structural elucidation.

### **Conclusion**

Ability to distinguish glycosphingolipid long chain base and fatty acyl unsaturation is needed, especially in non-mammalian systems where a variety of long chain bases coexist that

differ in the position of unsaturation. In this report, for the first time OzID-MS was applied to characterize the structure of intact unsaturated glycosphingolipids. Using this technique, it was possible to rapidly distinguish regiosomeric species in terms of carbon-carbon double bond position of the long chain base and the fatty acyl chain due to their observed differential ozone reactivity. Due to the influence of head group,  $\alpha$ -hydroxylation, and fatty acyl chain length, the subtle reactivity differences on the oxidative cleavage of double bonds provide useful hint on the existence of these molecular features and therefore aid in structural elucidation. Accurate mass measurement in the Q-ToF instrument afforded the assignment of OzID-MS products unambiguously, which greatly facilitated the distinction of isobaric species in a complex mixture in the absence of chromatographic separation. Moreover, the highly efficient ozonolysis reaction in the modified Synapt<sup>TM</sup> G2 instrument enabled the amplification of signals of low abundant species in a complex sample that otherwise would be obscurely identified using CID-MS/MS alone. This shows that OzID and CID, when used as complementary techniques, would enable more comprehensive and definitive structural characterization of glycosphingolipid molecular species in biological samples.

### **Acknowledgement**

This work was partially supported by the National Institute of General Medical Sciences of the National Institutes of Health grant (GM 104678). The authors thank the Triad Mass Spectrometry Facility at the UNCG Chemistry and Biochemistry Department, and Dr. Daniel Todd for help with this work.

CHAPTER IV  
FRAGMENTATION BEHAVIOR AND GAS-PHASE STRUCTURES OF  
CATIONIZED GLYCOSPHINGOLIPIDS IN OZONE-INDUCED  
DISSOCIATION MASS SPECTROMETRY

This chapter has been published in the *Journal of the American Society for Mass Spectrometry* and is presented in that style. Barrientos, R.C. and Zhang, Q. *J. Am. Soc. Mass Spectrom.* **2019**, In Press.

**Introduction**

Glycosphingolipids are complex lipids composed of a ceramide backbone and a glycan headgroup<sup>3,16</sup>. Together with glycoproteins, these molecules form the “glycosynapse” in the surface of eukaryotic cells that assume a plethora of vital biological functions such as cell recognition, cell-cell communication, signal transduction, receptor regulation and others<sup>4</sup>. The structural heterogeneity in glycosphingolipids lies in the glycan headgroup and the lipid tail (**Fig. 22**), both of which dictate the overall biological function of these molecules. This is further evidenced by earlier works that different biological conditions evoke changes not only in the composition of the headgroup but also of the lipid tail<sup>3,5,6,260</sup>. As such, analysis of glycosphingolipids at the intact structure level is warranted.

Generally, in tandem mass spectrometry of glycoconjugates, the type of adducts can significantly affect the fragmentation behavior when being selected for fragmentation under collisional activation techniques<sup>205,261-263</sup>. In this respect, myriad of works have exploited this property to elucidate structure of different molecules. Adducts can remarkably influence not only the energetics of bond cleavage but also the resulting fragmentation mechanism. For example, in

oligosaccharides, protonated adducts typically do not yield the more informative cross-ring cleavages, but these fragments can be observed from sodiated adducts<sup>205</sup>. In lipids, lithium has been frequently used in shotgun analysis and for structural elucidation because it provides more informative fragments that are absent in sodium or protonated forms. Glycosphingolipids in particular have been studied previously using collision-induced dissociation (CID) of different adducts, especially lithium, to yield important fragment ions<sup>228,248,264</sup> that could reveal their intact structure.

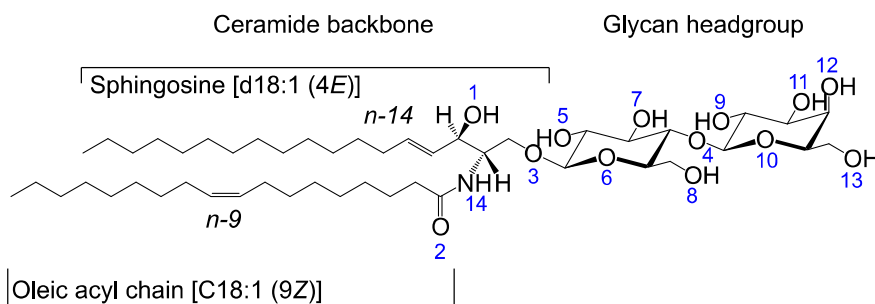


**Figure 22. General Structure of a Glycosphingolipid.** Shown here is LacCer d18:1/18:1(9Z) with glycan headgroup composed of glucose (Glc) and galactose (Gal), and connected to the ceramide backbone. The long chain base shown here is the sphingosine (d18:1) connected to a fatty acyl chain via amide bond. The numbering shown here is used throughout the text to address electronegative atoms.

To rationalize the data obtained experimentally, it is important to obtain the gas-phase structures of ionized molecules from theoretical calculations. Owing to advancements in computational chemistry and availability of powerful computers, a significant amount of work has been pursued to establish gas-phase structures of simple carbohydrates, peptides, and other small molecules, but to our knowledge, not of glycosphingolipids. Ion mobility spectrometry coupled to mass spectrometry (IMS-MS)<sup>265</sup> is generating huge amount of data that are helpful to characterize the size and shape of molecules, such as glycosphingolipids<sup>198,199,201</sup>, but because the theoretical gas-phase structures of a wide selection of ionized lipids are currently not available,

establishing a correlation between experimental data and predicted geometries becomes a challenge.

OzID-MS is a gas-phase fragmentation technique used to pinpoint the location, and in some cases the stereochemistry of carbon-carbon double bonds in unsaturated lipids<sup>10</sup>. This method is based on the highly selective ozone and olefin reaction chemistry<sup>266</sup> and has been implemented in various MS instrument platforms<sup>10-12</sup>. In these implementations, the typical inert collision gas is replaced by a mixture of ozone (O<sub>3</sub>) and oxygen (O<sub>2</sub>) such that ozonolysis can take place inside the collision cell. After precursor ion selection, the ion of interest reacts with O<sub>3</sub> in the collision cell and generates Criegee and aldehyde product ions. The mass difference between the precursor ion and product ions can serve as diagnostic masses to pinpoint the location of the double bonds in the molecular ion<sup>10,12</sup>.

It was previously demonstrated that different adducts could be used for OzID-MS which markedly affect product yield but not the resulting fragmentation patterns in phospholipids and fatty acid methyl esters<sup>11,267</sup>. Previously, we reported the OzID-MS fragmentation of unsaturated glycosphingolipids providing neat spectra of diagnostic OzID-MS ions by selecting the sodiated adduct as precursor ion<sup>9</sup>. In this work, we aimed to study the fragmentation patterns of glycosphingolipids using sodiated, lithiated, and protonated precursors. We observed that the type of adduct clearly influenced the resulting fragmentation pattern. We also carried out theoretical calculations at the semi-empirical level to obtain predicted gas-phase structures of cationized glycosphingolipids that could provide plausible rationalizations of these observations.

## **Experimental Procedures**

### **Materials**

The following standards were purchased from Avanti Polar Lipids (Alabaster, AL): *D*-lactosyl-β-1,1' *N*-oleyl-*D*-erythro-sphingosine (LacCer d18:1/18:1(9Z), cat. no. 860590), *D*-

galactosyl- $\beta$ -1,1' *N*-oleoyl-*D*-erythro-sphingosine (GlcCer d18:1/18:1(9Z), cat. no. 860547), *N*-oleoyl-*D*-erythro-sphingosine (Cer d18:1/18:1(9Z), cat. no. 860519). Lithium chloride was from Sigma-Aldrich, ammonium formate and formic acid were from Fisher Scientific (Pittsburgh, PA). All solvents were of LC-MS grade and purchased from Fisher Scientific (Pittsburgh, PA).

### **Preparation of standard solutions**

Standard stock solutions were prepared as  $1.0 \mu\text{g}\cdot\mu\text{L}^{-1}$  in chloroform/methanol/water ( $\text{CHCl}_3/\text{MeOH}/\text{H}_2\text{O}$ , 2:1:0.1, *v/v*) and kept at  $-20^\circ\text{C}$  until further use. Working solutions for direct infusion experiments were made from these solutions by measuring appropriate aliquots in glass vials followed by drying under a stream of  $\text{N}_2$  gas and subsequent reconstitution in acetonitrile/isopropanol/water ( $\text{ACN}/\text{IPA}/\text{H}_2\text{O}$ , 65/30/10, *v/v*) to a final concentration of  $10 \text{ pmol}\cdot\mu\text{L}^{-1}$ . To induce specific adduct formation,  $\sim 1 \text{ mM LiCl}$  and  $10 \text{ mM NH}_4\text{COOH}$  with  $0.1\%$   $\text{HCOOH}$  was used for  $[\text{M}+\text{Li}]^+$  and  $[\text{M}+\text{H}]^+$ , respectively. For  $[\text{M}+\text{Na}]^+$ , only the neat  $\text{ACN}/\text{IPA}/\text{H}_2\text{O}$  solvent system was used.

### **Instrument set-up**

All experiments described here were carried-out using Synapt<sup>TM</sup> G2 HDMS instrument (Waters, Manchester, UK) modified to allow the use of  $\text{O}_3$  as collision gas as described previously<sup>12</sup>. In this setup,  $\text{O}_3$  MEGA integrated ozone delivery system (MKS Inc., Andover, MA) was connected to the trap and transfer regions of the instrument through a three-way valve. The ozone generator was operated following manufacturer's instructions and produced consistently 6.0-8.0 *wt%*  $\text{O}_3$  in oxygen at a flow rate of  $1.0 \text{ slm}$  from high purity oxygen (AirProducts, Indianapolis, IN) at 20 psi, and used as collision gas in the mass spectrometer at a flow rate of  $2.0 \text{ mL}/\text{min}$ . The pressure in the trap region of Synapt<sup>TM</sup> G2 was  $\sim 9.9 \times 10^{-3} \text{ mbar}$ . For safety purposes, the remote switch of the ozone generator was interlocked with an ambient ozone monitoring system (Teledyne, San Diego, CA) and programmed to shut-off production

when ambient ozone exceeds safe levels. Excess ozone was destroyed on-line using a destruction catalyst (MKS Inc., Andover, MA) that converts ozone to oxygen.

### **OzID-MS experiments**

Standards were directly infused at 5.0  $\mu\text{L}/\text{min}$  using an automated syringe pump. The ESI source conditions were optimized and the final working conditions were set at the following values: polarity, positive; spray voltage, 3.0 kV; sampling cone, 30 to 50 V; extraction cone, 6 V; source temperature, 100  $^{\circ}\text{C}$ ; desolvation temperature, 200  $^{\circ}\text{C}$ ; cone gas flow, 50 L/h; desolvation gas flow, 500 L/h. Isolation of precursor ions was carried out in the quadrupole at  $\sim 1\text{Th}$  isolation width (LM =16, HM = 15). All spectra were acquired for 1.0 min at 0.5 s/scan. The traveling wave in the trap and transfer regions were operated at the following settings as optimized previously<sup>9,12</sup>: Entrance, 5.0 V; Bias, 2.0; Trap DC, 0.2; Exit, 0; trap wave velocity, 8 m/s; wave height, 0.2 V; transfer wave velocity, 247 m/s; wave height, 0.4 V. Default instrument settings for all the remaining parameters were applied. Under these settings, the reaction time between ozone and ions is estimated to be  $\sim 16.65\text{ ms}$ <sup>12</sup>. Instrument was calibrated daily in Resolution mode using sodium formate following manufacturer's instructions obtaining less than 0.6 ppm (0.5 mDa) RMS residual mass. To compensate for the fluctuations of the ambient conditions during mass measurement, lock mass corresponding to leucine enkephalin ( $m/z$  556.2711) was employed. Both the full scan and MS/MS levels were mass-corrected traceable to the reference lock mass using MassLynx v4.1 instrument control software (Waters, Manchester, UK).

### **Theoretical calculations**

All calculations reported here were performed in SCIGRESS vFJ2.8.1 (Fujitsu, Krakow, Poland) using built-in molecular mechanics and semi-empirical methods. Briefly, molecular structures of non-adducted forms were first geometry optimized using the MM3 force fields and the resulting optimized geometry was used to identify the low-energy conformers via CONFLEX

MM3<sup>268</sup> method. In each instance, at least 800 conformers were generated. Of these, only the twenty lowest predicted structures were used for subsequent calculation of the heat of formation ( $\Delta H_f^0$ ) using MO-G, a semi-empirical method based on Molecular Orbital Package (MOPAC) and employing PM6 parameters<sup>269</sup>, both are built-in methods in SCIGRESS. The structure with the lowest heat of formation value was assigned as the most stable conformer of the neutral molecule. This was then used for subsequent calculations to examine preferred localization sites of each adduct.

The preferred localization of adducts was determined by considering all possible sites for adduct attachment, for a total of 14 different sites (*cf.* **Fig. 22**). The ion was positioned at about 2.5 Å for each potential site, followed by geometry optimization using MM3 force fields via molecular mechanics method and conformational search using CONLEX MM3 method<sup>268,270</sup>. Then, the twenty structures with lowest predicted energy were subjected to MO-G PM6 calculations to determine  $\Delta H_f^0$  values.

### **Nomenclature of glycosphingolipid structures**

The shorthand notations used in this manuscript were based on the nomenclatures adapted from the LipidMAPS consortium<sup>246</sup>. For convenience and intuitive presentation of OzID-MS data, the nomenclature for the position of the carbon-carbon double bond was adopted based on the (*n-x*) system where *x* corresponds to the position of unsaturation from the terminal -CH<sub>3</sub> of the hydrocarbon chain, for instance, double bonds in GalCer d18:1(4*E*)/18:1(9*Z*) are respectively annotated as *n-14* and *n-9*.

## Results and Discussion

### Comparison of fragmentation patterns among different cations

Different cations have been previously studied and found to affect gas-phase ozonolysis efficiency in major lipid classes<sup>11,267</sup> but not in glycosphingolipids. We earlier demonstrated the OzID-MS fragmentation of unsaturated neutral glycosphingolipids<sup>9</sup>.

Using sodium adducted species as precursor ions, we have shown that distinct neutral losses in the OzID-MS spectrum pinpoint the location of carbon-carbon unsaturation<sup>9</sup>. In addition, consistent with other works we also reported that sphingosine carbon-carbon double bond is less reactive than the unsaturation in the fatty acyl chain<sup>9</sup>. In this study, we compared the effect of adduct type on the OzID-MS fragmentation of cationized glycosphingolipids.

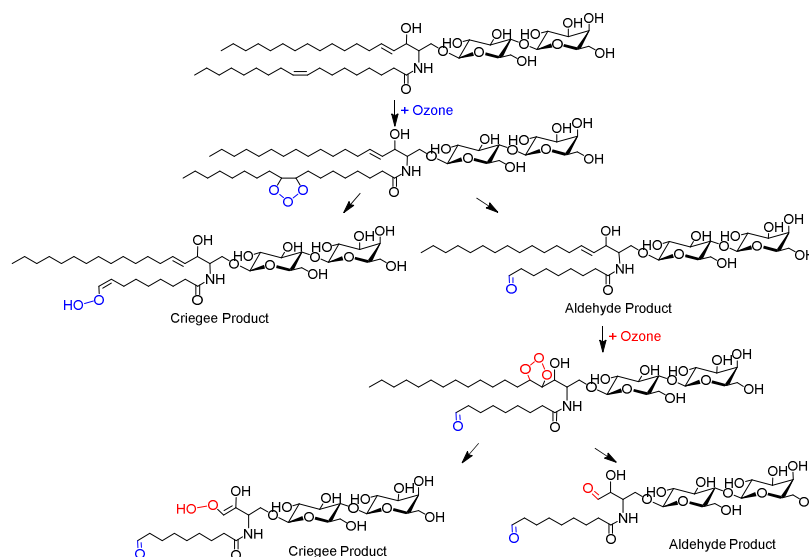


**Figure 23. Overview of the Proposed Pathways Leading to the Formation of Ozonolysis Products Observed in the OzID-MS Spectrum.**

### Lithiated adduct

Lithium has served as a classic cation in the structural elucidation of small molecules including glycosphingolipids by MS<sup>142,164,228,264,271,272</sup>. This metal promotes charge remote

fragmentations that yield informative fragments thus facilitating the structural elucidation of unknown species. Owing to this,  $[M+Li]^+$  has been widely used for characterization of lipids and glycolipids mainly using collisional activation methods<sup>228,264</sup>. Using OzID-MS, Thomas *et al.* showed that the fragmentation of  $[M+Li]^+$  using PC 16:0/18:1 did not yield distinct fragmentation compared to  $[M+Na]^+$ <sup>11</sup>. Phospholipids and glycolipids are structurally distinct owing to the head group diversity and stereochemistry on their backbone<sup>3</sup>. Thus, to determine if glycolipids also show similar behavior as phospholipids in OzID-MS, we infused glycolipid standards and subjected the  $[M+Li]^+$  adducts to OzID-MS fragmentation.

To induce the formation of  $[M+Li]^+$ , the analyte in solution was spiked with ~1 mM LiCl. OzID-MS of  $[M+Li]^+$  showed the expected diagnostic ions, specifically, the ions at  $m/z$  800.51 and  $m/z$  784.51 corresponding to the Criegee and aldehyde ions of the *n*-9 double bond in the fatty acyl chain (**Figure 23 and Fig. 24**). Also, the ions at  $m/z$  620.29 and  $m/z$  604.28, corresponding to the Criegee and aldehyde ions formed from the sequential cleavage of the *n*-14 double bond in the long chain base after cleavage of *n*-9 double bond. Similar to what we reported previously<sup>9</sup>, the *n*-14 sphingosine double bond appeared to be less reactive than the *n*-9 acyl double bond which could be explained from the gas-phase structure of these ions as discussed later in this report.

We found that in contrast to previous reports on OzID of phospholipids<sup>11,267</sup>, glycolipids have a distinct fragmentation pattern when ionized as  $[M+Li]^+$  compared to  $[M+Na]^+$  (**Fig. 24**). The  $[M+Li+O_3]^+$  ion was found to be of higher intensity relative to other fragments within the same spectrum, in contrast to  $[M+Na+O_3]^+$ . Also, when the relative intensities of the Criegee and aldehyde ions were compared with the intensity of the precursor ion, the two adducts showed differential fragmentation efficiency. Specifically, the Criegee and aldehyde ions formed from the cleavage of sphingosine double bond are of higher intensity than those in  $[M+Na]^+$ . As a result,

the intensity difference between the fatty acyl and sphingosine OzID characteristic ions is not as drastic as that in  $[M+Na]^+$ . Previous works by others also demonstrated the peculiar behavior of lithiated adducts in CID and high-energy CID<sup>142,264,273</sup>. This observation can be ascribed to the relative stability of lithiated over sodiated ozonide, presumably because of the lower ionic radii, but higher electronegativity of  $Li^+$  than  $Na^+$ , *i.e.* higher charge density<sup>274</sup>.

The most striking difference between  $[M+Na]^+$  and  $[M+Li]^+$  was the presence of a peak that differ by 180 Da from that of the ozonide, which appeared at  $m/z$  778.38 and  $m/z$  762.42 for the respective adducts (**Supplemental Fig. S4**). Using accurate mass measurements, we showed previously that this fragment originates from the secondary oxidation of the sphingosine carbon-carbon double bond, and could not be due to the loss of one of the monosaccharides in the glycan headgroup, as in the case in sodiated adducts<sup>9</sup>. The only major difference is the relative intensity of this fragment between the two metals, specifically, this fragment had a higher relative intensity in  $[M+Li]^+$  compared to  $[M+Na]^+$ . This suggests that the reactivity of the *n-14* sphingosine double bond is higher in lithiated than in sodiated adduct. We speculate that this differential reactivity stems from higher charge density of lithium ion which translates to a relatively more compact structure, providing closer interaction of the charge carrier with the *n-14* double bond. This is in agreement with our theoretical calculations described in the succeeding sections. Indeed, distinct behavior between these metal ions has been observed not only in glycolipids, but also OzID-MS of lithium and sodium-adducted fatty acid methyl esters<sup>267</sup> and cholesteryl esters<sup>275</sup>. Taken together, these observations highlight that  $Li^+$  and  $Na^+$  ions could affect the efficiency of ozonolysis in the gas-phase.

### **Protonated adduct**

The burgeoning use of protonated adducts in MS stems from the popularity of LC-MS based approaches where often, additives like ammonium formate, ammonium acetate, formic acid

or acetic acid are being used. The presence of these additives suppresses the ubiquitous  $\text{Na}^+$  that is typically observed especially for molecules that have high affinity to these ions. In this respect, we studied the OzID-MS fragmentation of protonated LacCer d18:1/18:1(9Z).

We observed substantially distinct OzID-MS spectra for  $[\text{M}+\text{H}]^+$  compared to  $[\text{M}+\text{Li}]^+$  and  $[\text{M}+\text{Na}]^+$ . Specifically, we observed persistent neutral loss of  $\text{H}_2\text{O}$ , this dehydration is attributed to the lability of the sphingosine hydroxyl<sup>263</sup> as consistently observed in traditional CID and HCD fragmentation of protonated ceramides and glycosphingolipids<sup>115,144,264</sup>. We speculated that the loss of  $\text{H}_2\text{O}$  originated from the sphingosine backbone because infusing Cer d18:1/18:1(9Z) also showed dehydration despite the absence of a glycan headgroup (**Supplemental Fig. S5**). It is interesting to note that the observed dehydration under OzID conditions was not detected with  $[\text{M}+\text{Li}]^+$  or  $[\text{M}+\text{Na}]^+$  (**Fig. 24** and **Supplemental Fig. S5**) although it was observed in collisional activation dissociation (CAD)-based fragmentation<sup>142</sup>. This suggests that the lability of the sphingosine hydroxyl in OzID-MS could be attenuated by metal adducts.

In contrast to sodiated and lithiated adducts, where the precursor ion intensity has dropped significantly, the protonated precursor ions remained abundant in the OzID spectrum (**Fig. 24**). Interestingly, we observed that the ozonide intensity is much weaker compared to that in sodiated and lithiated adducts. Previous OzESI work<sup>238</sup> on sphingomyelin as protonated adduct did not reveal the position of the sphingosine double bond, in contrast, in our work, this double bond is clearly shown, although we failed to detect the Criegee product from this double bond cleavage, probably because of its low stability (**Fig. 24**). This yields two important implications for  $[\text{M}+\text{H}]^+$ , first, its reactivity to ozone is lower than that of  $[\text{M}+\text{Li}]^+$  and  $[\text{M}+\text{Na}]^+$ , and second, ozonolysis of the sphingosine double bond in  $[\text{M}+\text{H}]^+$  is less pronounced compared to that of the alkali metal adducts.

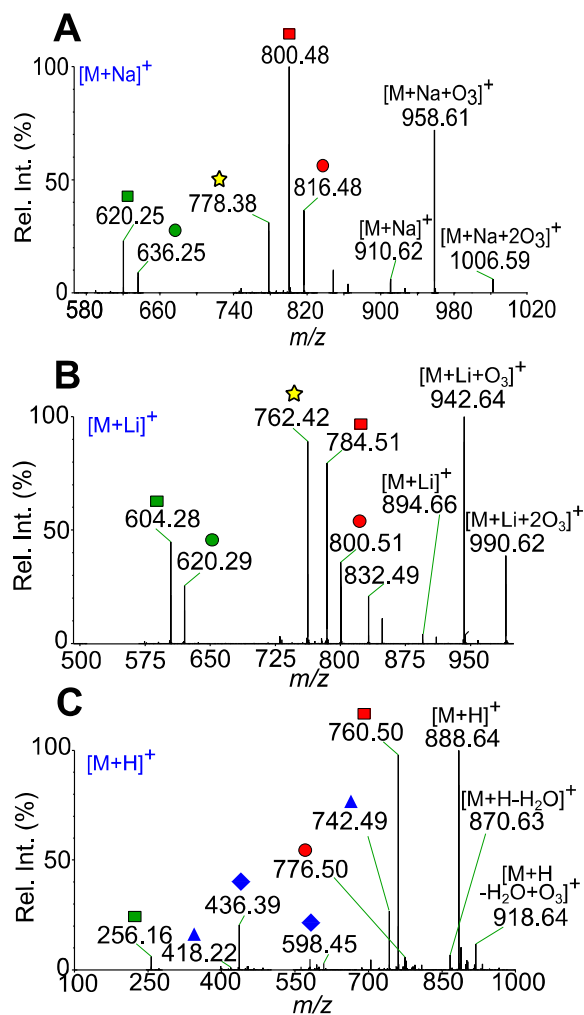
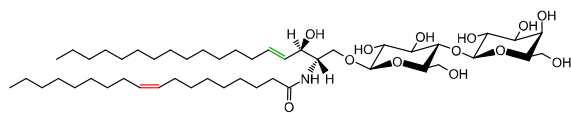


**Figure 24. OzID-MS Spectra of Cationized LacCer d18:1/18:1 (9Z).** The analyte (10 pmol/ $\mu$ L) spiked with  $\sim$ 1 mM LiCl or 10 mM  $\text{NH}_4\text{COOH}/0.1\%$  HCOOH to induce the formation of  $[\text{M}+\text{Li}]^+$  and  $[\text{M}+\text{H}]^+$ , respectively. No spiking of  $\text{Na}^+$ -containing salt was necessary to induce  $[\text{M}+\text{Na}]^+$  formation. Samples were infused using a syringe pump to the ESI source of Synapt G2 HDMS equipped with  $\text{O}_3$  gas in the collision cell. Precursor ions corresponding to different adducts were chosen for OzID-MS. Spectra shown are average of 1.0 min acquisition time. Criegee and aldehyde product ions are depicted as (●) and (■), respectively, as shown in Figure 243. Colors represent different double bond locations. ☆: ozonide stabilized secondary oxidation cleavage product of sphingosine *n*-14 double bond (see Supplemental Figure S4), ◆: loss of hexose, ▲: loss of  $\text{H}_2\text{O}$ .

When protonated adduct was mass-selected for fragmentation, the expected OzID products were observed (**Fig. 24C**). The ion at  $m/z$  776.50 and  $m/z$  760.50 are the Criegee and aldehyde ions corresponding to neutral losses of 94 and 110 Da, respectively, from the dehydrated precursor ion, diagnostic of the *n*-9 double bond at the fatty acyl chain <sup>10</sup>. Interestingly, the expected neutral losses of 180 Da and 164 Da from the *n*-9 cleavage products to locate the *n*-14 sphingosine double bond were not observed. However, two fragment ions,  $m/z$  436 and  $m/z$  256 that differ by 180 Da were apparent, implying that *n*-14 oxidative cleavage in  $[M+H]^+$  adduct occurs differently than that of  $[M+Na]^{+9}$  and  $[M+Li]^+$ .

In addition to the informative OzID fragments corresponding to sphingosine C=C and fatty acyl chain C=C, we observed the formation of a peak that differs by 324 Da from the diagnostic ion for *n*-9 C=C position in LacCer, and 162 Da for GlcCer (**Supplemental Fig. S6**), both have a mass of  $m/z$  436. This ion could result from the loss of the sugar headgroup in a CID-like fragmentation mechanism. To confirm this, we subjected ceramide molecule that contains the same long chain base and fatty acyl chain, Cer d18:1/18:1(9Z) to OzID-MS as  $[M+H]^+$  ions (**Supplemental Fig. S5**). Indeed, the ion  $m/z$  436 was also observed here, verifying that loss of headgroup, and thus, cleavage of Cer-Glc glycosidic bond has occurred and that the  $m/z$  436 corresponds to the aldehyde ion formed by the cleavage of the *n*-14 double bond in sphingosine (*cf.* **Figure 24**). The peak at  $m/z$  598 that differ by 162 Da from the aldehyde product of the oxidative cleavage of *n*-9 double bond ( $m/z$  760) along with the presence of  $m/z$  436 (mass difference of 162 Da from  $m/z$  598) support the potential of identifying the glycan sequence in LacCer d18:1/18:1(9Z).

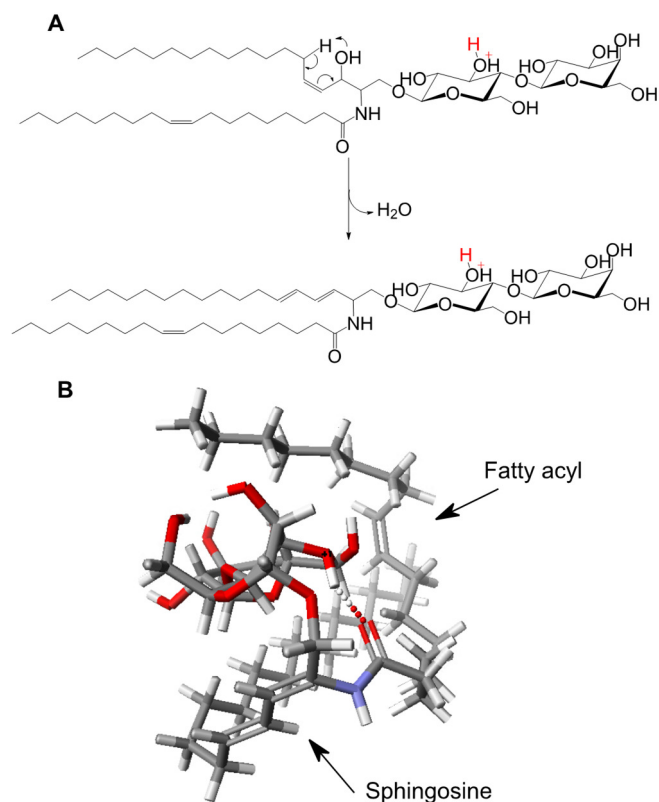


**Figure 25. Calculated Gas-Phase Structure of Dehydrated LacCer d18:1/18:1(9Z).** (A) Proposed elimination of H<sub>2</sub>O from the sphingosine backbone via charge-remote mechanism. (B) Gas-phase structure of dehydrated LacCer d18:1/18:1(9Z) calculated using MO-G with PM6.

We previously showed that using [M+Na]<sup>+</sup>, the sphingosine double bond at *n-14* with a *trans*-configuration is relatively less reactive than that of the *n-9* double bond in the fatty acyl chain<sup>9</sup>. One of the possible explanations offered in the past was the presence of the hydroxyl group adjacent to the original *n-14* double bond along with the possible formation of H-bond between the headgroup and this hydroxyl group as observed using sphingomyelin<sup>11</sup>. In our present results using protonated adduct, the cleavage product of the *n-14* double bond remained lower intensity than that of *n-9* double bond, despite the elimination of the sphingosine hydroxyl suggesting that the presence of the hydroxyl group was not the sole determinant of the low

ozonolysis efficiency at this position. We speculated that the proximity of this unsaturation system to the headgroup has influence on the overall OzID cleavage, this is indeed the case, as we modelled the gas-phase structure of the dehydrated species (**Fig. 25**).

Taken together, these results show that the use of  $[M+H]^+$  adducts in OzID-MS of glycosphingolipids could potentially reveal the sequence of the glycan headgroup and pinpoint the location of the double bonds.

### **Insights on the gas-phase structures of cationized glycosphingolipids**

The gas-phase structures of ionized lipids could explain observations in MS, especially in the era of ion mobility spectrometry<sup>197</sup>; however, to our knowledge, few studies are available in this area. We reasoned that in addition to the known effect of adduct size on the resulting fragmentation patterns evident for oligosaccharides<sup>205</sup>, the localization of the cations could also play a vital role in deciding the fate of fragmentation. Thus, to partially rationalize the observed OzID-MS behavior, we performed theoretical calculations on LacCer d18:1/18:1(9Z).

In this study, we opted to employ molecular mechanics and semiempirical methods to estimate the gas-phase structures of cationized LacCer d18:1/18:1(9Z). Although *ab initio* and density functional theory (DFT) are by far considered to provide relatively more accurate predictions of gas-phase structures of ionized species, molecular mechanics (MM) and semiempirical methods are also suitable and found to be satisfactory by others<sup>270,276-280</sup>. MM3 has been previously shown to be appropriate for disaccharides analysis<sup>281</sup>. Using MM3, we optimized the geometry of our model molecule in its neutral form and performed a conformational search using CONFLEX method utilizing augmented MM3 force fields<sup>268</sup>. The lowest energy conformers were subjected to further optimization using MO-G by employing PM6 parameters to obtain the values of heat of formation ( $\Delta H^0_f$ ). Following geometry optimization, arbitrary dihedrals were chosen for conformational search using CONFLEX MM3 method.

To investigate the preferred localization of cations when complexed with the ligand, we employed the lowest energy conformer of the neutral form as starting point (**Supplemental Fig. S7**). We positioned the cations (Na<sup>+</sup>, Li<sup>+</sup>, H<sup>+</sup>) at ~2.5 Å near each potential cation residence in the LacCer d18:1/18:1(9Z) ligand for a total of 14 different positions and performed identical procedure as mentioned above for the neutral molecule, following an analogous study<sup>282</sup>. Thus, we obtained the low energy structures of cationized LacCer d18:1/18:1(9Z) in the gas-phase using molecular mechanics and semi-empirical calculations as discussed in the subsequent sections.

### **Energetics of cationization**

Cation affinity of ligand *L* with cation *C*<sup>+</sup> is defined as the standard enthalpy change for the following reaction<sup>283</sup>:



Cation affinity is an important parameter that serves as a relative measure of the stability of the adduct and becomes very useful when different cations are being compared. The values of cation affinities for simple carbohydrates have been investigated previously<sup>284-286</sup>, but those of glycosphingolipids remained relatively less studied<sup>287</sup>. In this present work, we used molecular mechanics and semiempirical methods to estimate cation affinity of LacCer d18:1/18:1(9Z) for three cations, H<sup>+</sup>, Li<sup>+</sup> and Na<sup>+</sup>. The calculated values LacCer d18:1/18:1(9Z) (**Table 4**) show that the cation affinities of the ligand for H<sup>+</sup> and Li<sup>+</sup> are greater than that of Na<sup>+</sup> which suggests that formation of [M+H]<sup>+</sup> and [M+Li]<sup>+</sup> adduct is more exothermic than [M+Na]<sup>+</sup>. The values shown here are consistent with experimental data by others<sup>205,274,286</sup> although the values obtained in this work are slightly higher than those of disaccharides, which are expected due to the additional

lipid moiety in glycosphingolipids<sup>284,288</sup>. The high exothermicity of this process along with the size of the adducts were previously associated with increased metastable decay as well as CID fragmentation of [M+H]<sup>+</sup> adducted carbohydrates than their metal-cationized congeners<sup>286,289</sup>.

**Table 4. Estimated Heat of Formation ( $\Delta H_f^0$ ) and Cation Affinities of LacCer d18:1/18:1(9Z) Calculated Using MO-G with PM6.**

	$\Delta H_f^0$ (kJ mol <sup>-1</sup> )		
	Uncomplexed	Complexed	Cation affinity
[M+Na] <sup>+</sup>	-2,400.86	-2,740.33	+339.47
[M+Li] <sup>+</sup>	-2,289.75	-2639.25	+349.50
[M+H] <sup>+</sup>	-1,642.79	-2,445.62	+802.83

Detailed calculations are shown in Appendix C.

#### Calculated gas-phase structure of [M+Na]<sup>+</sup>

Arbitrarily, we considered an atom to be coordinating with the cation if their distance is less than 2.7 Å<sup>282</sup>. In this respect, in the optimized, lowest energy structure of [M+Na]<sup>+</sup>, we observed that Na<sup>+</sup> coordinates to glycosidic oxygen (O4, 2.56 Å), (O12, 1.44 Å), and amide oxygen (O2, 1.23 Å) (**Fig. 26**, for notations, please refer to **Fig. 22**). These values are within reasonable values as previously calculated using more sophisticated DFT methods for carbohydrates<sup>284,285,288</sup>. Of these interactions, the strongest was between Na<sup>+</sup> ion and the amide oxygen (C=O, O2). In a previous study involving oligosaccharides<sup>290</sup> where one of the sugars involved is N-acetyl neuraminic acid, Na<sup>+</sup> was also found to coordinate with the carbonyl oxygen.

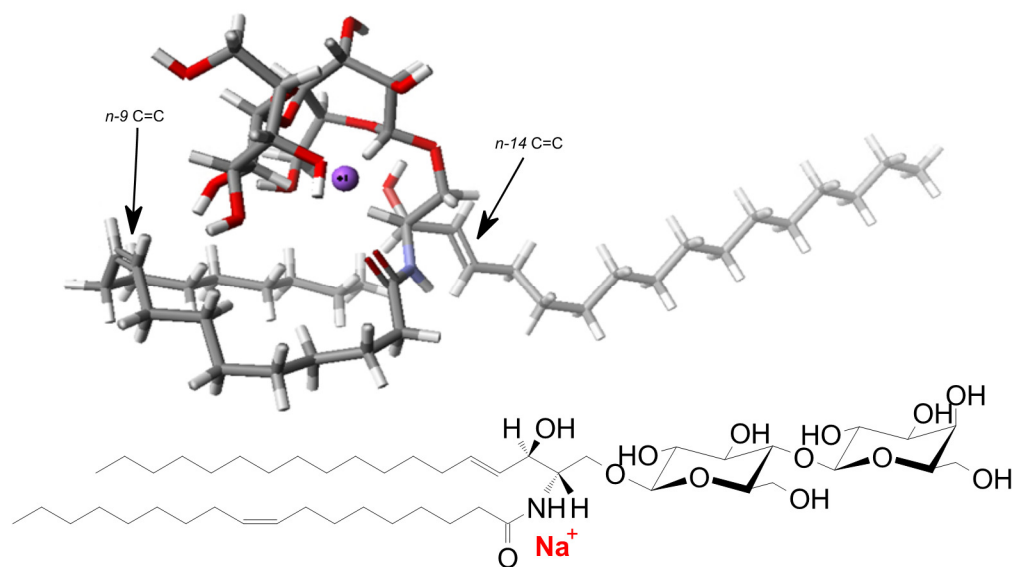


**Figure 26. Most Stable Conformer of  $[M+Na]^+$  of LacCer d18:1/18:1(9Z) Calculated Using MO-G with PM6.** Color indicates different atom (Gray: Carbon, White: Hydrogen, Red: Oxygen, Purple:  $Na^+$ , Cyan: Nitrogen).

In this conformation, we found three prominent intramolecular H-bonding interactions between the sphingosine -OH and the glycosidic oxygen (O3), (O8 and O9), and (O11 and O12). These H-bonding interactions contributed to the stability of this structure in the gas-phase.

The overall 3D spatial distribution of functional groups could significantly dictate the overall gas-phase reactivity. Very clearly, the sodium ion appears to be closer to the acyl chain double bond than the sphingosine double bond, presumably because of the size of the headgroup and the *trans*-configuration of this double bond. Considering that OzID cleavage is charge-induced rather than charge remote<sup>11,275</sup>, the gas-phase structure predicted in our current work offers a plausible explanation to the reduced ozonolysis efficiency of the sphingosine double bond observed previously<sup>9,11,291</sup> and in this study.

### Calculated gas-phase structure of [M+Li]<sup>+</sup>

In the optimized lowest energy structure of [M+Li]<sup>+</sup> adduct, Li<sup>+</sup> ion demonstrated preferential interaction with sphingosine -OH (O1, 1.46 Å), (O11, 2.22 Å), amide oxygen (O2, 1.24 Å), (O12, 2.21 Å), amide nitrogen (N14, 1.48 Å) (**Fig. 26**, for notations, please refer to **Fig. 22**). The overall similarity of Li<sup>+</sup> and Na<sup>+</sup> is manifested by their stronger interaction with the carbonyl oxygen. A landmark study on ceramide fragmentation also hypothesized that Li<sup>+</sup> preferably resides proximal to the carbonyl oxygen<sup>142</sup>. Recent works on disaccharides showed similar conformation regardless of the metal identity, but remarkably distinct to that of proton<sup>284</sup>, as observed in this current work. We also found three prominent intramolecular H-bonding interactions between O12 and O2, O9 and O8, and O6 and O8. Again, the stability of this gas-phase structure could be ascribed, in part, to these H-bonding interactions.

Consistently, the sphingosine double bond is less reactive towards ozonolysis than the fatty acyl chain double bond. Like what was observed in [M+Na]<sup>+</sup>, the sphingosine double bond in [M+Li]<sup>+</sup> appeared to have lower ozonolysis efficiency than *n*-9 fatty acyl chain double bond. This can be explained in a similar manner as above, that the charge-carrier is relatively closer to the *n*-9 acyl double bond than that of *n*-14 sphingosine. The observed higher intensities of the fragment ions in the OzID-MS spectrum could be partly explained by the lower ionic radius but higher charge density of Li<sup>+</sup> ion compared to Na<sup>+</sup> as evidenced by higher cation affinity of Li<sup>+</sup> than Na<sup>+</sup> calculated above (*cf.* **Table 4**) and in previous experimental works<sup>142,228,264,271</sup>.

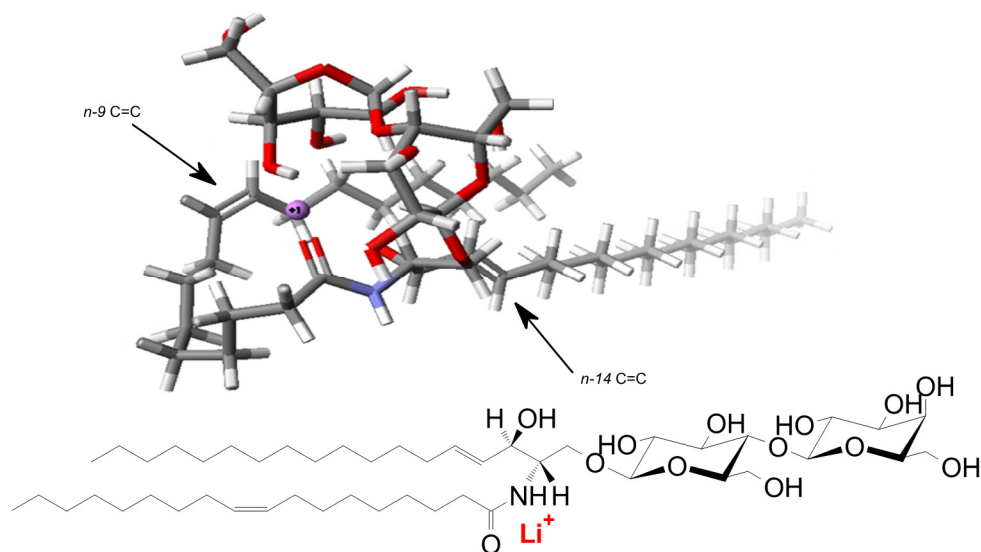


**Figure 27. Most Stable Conformer of  $[M+Li]^+$  of LacCer d18:1/18:1(9Z) Calculated Using MO-G with PM6.** Color indicates different atom (Gray: Carbon, White: Hydrogen, Red: Oxygen, Purple:  $Li^+$ , Cyan: Nitrogen).

#### Calculated gas-phase structure of $[M+H]^+$

The  $[M+H]^+$  has the most distinct gas-phase structure (**Fig. 27**), specifically, in the optimized structure of the lowest energy conformer, we found the localization of the proton to oxygen at O7 position (1.46 Å) (for notations, please refer to **Fig. 22**). This proton is close to the carbonyl oxygen (1.26 Å), sphingosine -OH (1.64 Å), and glucosyl oxygen at O8 (1.43 Å). Further, compared to  $[M+Na]^+$  and  $[M+Li]^+$ , there are more prevalent intramolecular H-bonding interactions, such as O13 and O1, O7 and O13, O1 and O7, O5 and O8, O4 and O8, and O11 and O12. This seemingly peculiar spatial location of the proton compared to  $Na^+$  and  $Li^+$  is analogous to what was observed for saccharides which could be related to the size of the cation<sup>284</sup>.

Overall, comparing the proximity of the acyl double bond to the charge, the cation appears to be closer to the double bond in  $[M+Li]^+$  and  $[M+Na]^+$ , but reasonably distal in  $[M+H]^+$ . This could explain the maximized H-bonding interactions observed in  $[M+H]^+$ . The

larger size of the sodium and lithium compared to proton could have caused the overall more compact structure in  $[M+H]^+$  over  $[M+Na]^+$  and  $[M+Li]^+$ , as predicted by LipidCCS web server (<http://www.metabolomics-shanghai.org/LipidCCS/>) and observed in recent ion mobility experiments of similar GlcCer species<sup>201,292</sup>. Previous work argued that, instead of remote fragmentation, there is a direct role of charge in the mechanism of OzID of ionized lipids<sup>11,238,275</sup>. More recently, a study on the gas-phase structure of 1-deoxysphingosine shows the through-space interaction of charge with the unsaturation site<sup>291</sup>. The gas-phase ion structures we obtained here, clearly support this hypothesis. In this respect, partly, this explains the previous observation that metal adducts provided higher efficiency than protonated adduct.

Seminal works in the past have stressed that protonated species, both in oligosaccharides and in glycolipids<sup>115,286</sup>, could induce substantial fragmentation compared to their metal adduct analogues as observed in MALDI, FAB, and ESI studies. Our results agree with these previous works, and additionally, we provide evidence that not only in collisional activation, but also in OzID-MS that protonated adducts could induce glycosidic bond cleavages.

The intensity of the ozonide ion in  $[M+H]^+$  being almost completely attenuated compared to  $[M+Na]^+$  and  $[M+Li]^+$  (*cf.* **Fig. 24**) could not be a consequence of the increased ozonolysis efficiency, but rather, of the CID-like breakdown of the ozonide ion to cleave the glycan headgroup. We reasoned that both protonation and ozonolysis are highly exothermic processes<sup>293</sup>, releasing energy upon reaction.

This highly energetic process could provide adequate internal energy provoking the cleavage of weak glycosidic linkages. In this respect, it is well-documented<sup>205</sup> that protonated carbohydrates require lower amount of energy to break glycosidic bonds than metal adducts, estimated to be  $138.3 \text{ kJ mol}^{-1}$  and  $245.6 \text{ kJ mol}^{-1}$ , respectively<sup>284</sup> for  $\beta$  anomers.

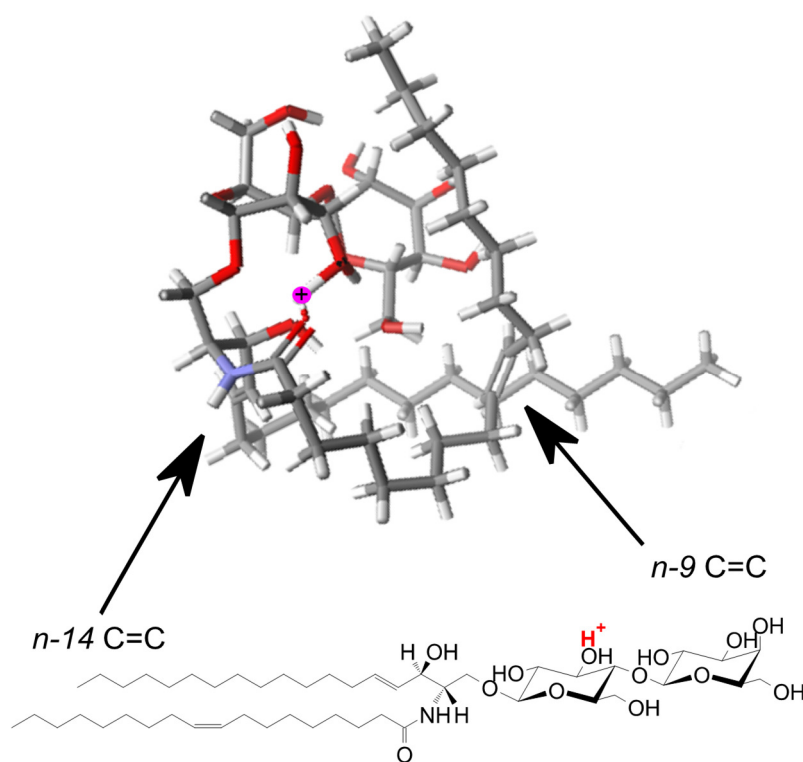


**Figure 28. Most Stable Conformer of  $[M+H]^+$  of LacCer d18:1/18:1(9Z) Calculated Using MO-G with PM6.** Color indicates different atom (Gray: Carbon, White: Hydrogen, Red: Oxygen, Purple:  $H^+$ , Cyan: Nitrogen).

Taken together, these results suggest that the high charge density of the  $H^+$  ion along with the highly exothermic nature of ozonolysis, could induce glycosidic bond cleavages which are absent in metal-adducted species. This can offer a possibility to determine the location of double bonds, and sequence the glycan headgroup in OzID-MS of intact, unsaturated glycosphingolipids.

### Conclusion

This study demonstrated the distinct fragmentation behavior of cationized ( $Na^+$ ,  $Li^+$ ,  $H^+$ ) glycosphingolipids in OzID-MS. While similar fragmentation patterns were observed between sodiated and lithiated adducts in terms of the presence of diagnostic OzID ions, relative intensities of these fragments were remarkably different. Protonated adducts gave the most

striking difference in the fragmentation pattern as evidenced by the presence of ions resulting from cleavage of the glycosidic bonds. Molecular modeling using molecular mechanics and semiempirical methods show that the size of the cation could influence the gas-phase structures of the cationized glycosphingolipids. This, along with the exothermic nature of cationization, presumably has induced glycosidic cleavages and charge-induced ozonolysis of the carbon-carbon double bonds. This is especially the case for the  $[M+H]^+$  ion where the high charge density of the proton and its peculiar localization close to glycosidic oxygen evoked the breaking of the glycosidic bonds. Thus, the use of  $[M+H]^+$  could provide both double bond locations and sequence of the glycan headgroup. Taken together, our work contributes to the current understanding of OzID-MS, gas-phase ion structures of neutral glycosphingolipids, and has potential to be extended to other glycoconjugates.

### **Acknowledgement**

This work was partially supported by the National Institute of General Medical Sciences of the National Institutes of Health grant (R21 GM104678). The authors thank the Triad Mass Spectrometry Facility at the UNCG Chemistry and Biochemistry Department, Ngoc Vu, and Dr. Daniel Todd for help with this work.

CHAPTER V

ISOBARIC LABELING OF INTACT GANGLIOSIDES TOWARD MULTIPLEXED  
LC-MS/MS BASED QUANTITATIVE ANALYSIS

This chapter has been published in the journal *Analytical Chemistry* and is presented in that style. Barrientos, R.C., and Zhang, Q. *Anal. Chem.* **2018**, 90, 2578-2586.

**Introduction**

Gangliosides are glycosphingolipids composed of a ceramide backbone and a glycan head group that carries at least one sialic acid moiety. In mammals, the most abundant form of the latter is *N*-acetyl neuraminic acid (Neu5Ac) (**Fig.29a**)<sup>64,294</sup>. These ubiquitous molecules are recognized to play important role in biological processes, and perturbation of their metabolism is often associated with human diseases. Despite this, they remain relatively underexplored due to their compositional and structural complexity. In general, the overall biological function of glycosphingolipids is influenced by both the structures of the lipid and glycan, thus they warrant to be determined as intact molecular species<sup>9,295,296</sup>.

Traditional analysis of gangliosides involves cleavage of the lipid from the glycan head group followed by gas chromatography–mass spectrometry (GC-MS)<sup>297</sup>. In recent years, the use of liquid chromatography–mass spectrometry (LC-MS) based approaches namely reversed-phase (RPLC)<sup>155,171,298,299</sup>, and hydrophilic interaction (HILIC)<sup>143,157,170,172,174</sup> as well as chip-based technologies<sup>154,163</sup> have made it possible to analyze intact gangliosides<sup>15,173</sup>. Despite these developments, quantification of these biomolecules has remained a challenging task due to limited availability of standards, variability of ionization efficiency across ganglioside classes,



instrument response since samples are ionized simultaneously in a single injection. This technique has also been shown to greatly improve measurement accuracy, precision, and throughput<sup>13,303</sup>. In this respect, stable isotope labeling for multiplexed relative quantification in proteomics, metabolomics, and glycomics has been well demonstrated.

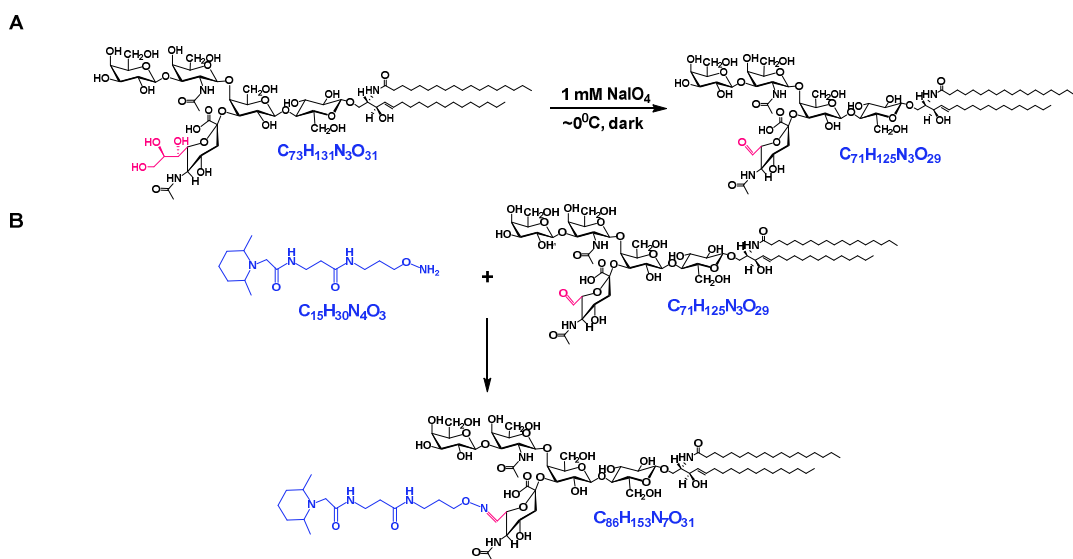


**Figure 30. Reactions Involved in the Oxidation and Isobaric Labeling Technique Implemented in this Study.** Shown here is GM1a d18:1/18:0 as an example. Chemoselective oxidation of sialic acid side chain to generate aldehyde functional group (a). The afforded product undergoes aminoxyTMT labeling at the reactive aldehyde via oxime bond formation (b).

In glycomics, multiplexing is commonly exploited using carbonyl-reactive isobaric mass tags<sup>302,304,305</sup> such as aminoxy tandem mass tag (aminoxyTMT) reagent<sup>301,306,307</sup>. The latter contains a carbonyl-reactive moiety, a mass normalizer, and a reporter ion group, which fragments upon ion activation through collision-induced dissociation (CID), higher-energy collisional dissociation (HCD) or electron-transfer dissociation (ETD)<sup>301,306,307</sup> (**Fig. 29b**). To use this reagent, glycans should contain a free carbonyl group at the reducing terminus to enable its attachment through a stable oxime bond<sup>301</sup>. Thus, enzymatic or chemical modification is

commonly employed, *e.g.* glycopeptides/glycoproteins are digested with peptide *N*-glycosidase F (PNGase F)<sup>301,302,306,307</sup> to release *N*-glycans. If glycolipids are desired to be labeled with aminoxyTMT, treatment with endoglycoceramidases (EDCase)<sup>111</sup> would be necessary. Not only this technique eliminates the lipid structural information, but also the use of enzyme requires longer sample preparation time which typically takes ~18 hours.

Selective oxidation of vicinal diols using sodium metaperiodate (NaIO<sub>4</sub>) has been known in organic chemistry for decades<sup>14,308,309</sup> and was utilized for labeling of live cells through bioconjugation of cell-surface sialic acids<sup>14,310,311</sup>. Under properly controlled conditions, Neu5Ac side chain can be selectively cleaved to form aldehyde at C-7 position leaving the remainder of the molecule unaltered (**Fig.29c**)<sup>14,310,311</sup>. In this paper, we applied this approach to label gangliosides with aminoxyTMT reagent (Scheme 4) followed by RPLC-MS/MS analysis. This facile strategy enabled the simultaneous analysis of ganglioside molecular species from multiple samples in one injection.

## **Experimental Procedures**

### **Materials and reagents**

The following glycosphingolipid standards and lipid extracts were purchased from Avanti Polar Lipids (Alabaster, AL): *D*-galactosyl- $\beta$ -1,1'-*N*-stearoyl-*D*-erythro-sphingosine (GalCer d18:1/18:0, cat. no. 860844), *D*-galactosyl- $\beta$ -1-1'-*N*-[2''(R)-hydroxystearoyl]-*D*-erythro-sphingosine (GalCer d18:1/18:0 (2ROH), cat. no. 860840), total gangliosides extract (porcine brain, cat. no. 860053), total lipid extract (porcine brain, cat. no. 131101). *N*-stearoyl-globotriaosylceramide (Gb3Cer d18:1/18:0, cat. no. 1529), *N*-stearoyl-sphingosyl- $\beta$ -*D*-galactoside-3-sulfate (Sulfatide d18:1/18:0, cat. no. 1932), and ganglioside standard mixtures containing different acyl chain lengths and long chain bases (*e.g.* d18:1 and d20:1): monosialoganglioside GM1a (bovine, NH<sub>4</sub><sup>+</sup> salt, cat. no. 1061), monosialoganglioside GM3

(bovine buttermilk,  $\text{NH}_4^+$  salt, cat. no. 1503), disialoganglioside GD3 (bovine buttermilk,  $\text{NH}_4^+$  salt, cat. no. 1527), disialoganglioside GD1a (bovine,  $\text{NH}_4^+$  salt, cat. no. 1062), disialoganglioside GD1b (bovine,  $\text{NH}_4^+$  salt, cat. no. 1501), and trisialoganglioside GT1b (bovine,  $\text{NH}_4^+$  salt, cat. no. 1063) were obtained from Matreya, LLC (State College, PA). Sodium metaperiodate ( $\text{NaIO}_4$ ), Glycerin, sodium acetate ( $\text{CH}_3\text{COONa}$ ), glacial acetic acid ( $\text{CH}_3\text{COOH}$ ), aminoxyTMT<sup>0</sup> (cat. no. PI90400) and aminoxyTMT 6-plex reagent (cat. no. PI90401), and all solvents (at least HPLC or LC-MS grade) were obtained from Fisher Scientific (Pittsburgh, USA) unless stated otherwise. Structure and systematic name of gangliosides discussed in the text are provided in Supplemental Table S1.

### **Chemoselective oxidation**

The protocol described by Hermanson was adopted with modifications<sup>14</sup>. Briefly, aliquots equivalent to 1.0 nmol to 5.0 nmol of individual ganglioside standards or porcine brain ganglioside extract (1.9  $\mu\text{g}$  to 9.4  $\mu\text{g}$ ) were transferred to glass vials from 1.0  $\mu\text{g}/\mu\text{L}$  stock solutions in chloroform/methanol/water ( $\text{CHCl}_3/\text{CH}_3\text{OH}/\text{H}_2\text{O}$ , 2:1:0.1, v/v), and dried under a stream of nitrogen ( $\text{N}_2$ ) gas. The dried samples were reconstituted in 250  $\mu\text{L}$  of oxidation buffer, 0.1 M  $\text{CH}_3\text{COONa}/\text{CH}_3\text{COOH}$  (pH ~5.5) and then added with 12.5  $\mu\text{L}$  of 20 mM  $\text{NaIO}_4$  prepared in the same buffer. After vortexing for five seconds, the vial was kept in an ice bath ( $\sim 0^\circ\text{C}$ ) in the dark. After incubation for 60 minutes, the reaction was quenched by adding 2.5  $\mu\text{L}$  of 100 mM aqueous glycerol, incubated for another 60 minutes and then subjected to solid-phase extraction (SPE) to remove salts and dried to eliminate by-products of the oxidation process.

### **SPE clean-up**

A 1.0 mL capacity Isolute C18 SPE cartridge (Biotage) was activated using 2.5 mL of  $\text{CH}_3\text{OH}$  and conditioned with 2.5 mL of  $\text{CH}_3\text{OH}/\text{H}_2\text{O}$  (10/90, v/v). The oxidized ganglioside was loaded in the cartridge and desalted by washing five times with 1.0 mL of  $\text{H}_2\text{O}$ . Finally, the

oxidized gangliosides were eluted using 1.0 to 3.0 mL of CHCl<sub>3</sub>/CH<sub>3</sub>OH/H<sub>2</sub>O (5:5:0.5, v/v), dried under N<sub>2</sub> or vacuum, and kept at -20°C until further processing.

### **Isobaric labeling**

Labeling using aminoxyTMT was performed following manufacturer's instructions with minor modifications. Briefly, the labeling reagent was dissolved in 200 µL of 95% CH<sub>3</sub>OH with 0.1% CH<sub>3</sub>COOH, vortexed, and mixed with oxidized gangliosides for 10 mins at room temperature. The solvent was removed under vacuum followed by re-dissolving the sample in 200 µL of 95% CH<sub>3</sub>OH and vortexed for 10 min to ensure complete labeling. Thereafter, the sample was dried under N<sub>2</sub> or vacuum. Excess labeling reagent was scavenged by adding 100 µL of 10% acetone in 95% CH<sub>3</sub>OH/H<sub>2</sub>O, pooled, dried under N<sub>2</sub> and finally reconstituted in LC-MS mobile phase.

### **LC-MS/MS analysis**

A binary Acquity UPLC system (Waters, Milford, MA) coupled with LTQ Orbitrap XL (Thermo Scientific, Bremen, Germany) was used to monitor the progress of chemoselective oxidation of ganglioside standards. For TMT-labeling experiments, a Vanquish UHPLC system (Thermo Scientific) coupled with Q Exactive HF (Thermo Scientific) was employed. In either case, a Cortecs C18 column (2.6 mm ID x 100 mm, 1.6 µm) (Waters) and the following mobile phases were used<sup>312,313</sup>: A (60/40 CH<sub>3</sub>CN/H<sub>2</sub>O with 10 mM NH<sub>4</sub>COOH and 0.1% HCOOH), B (90/10 isopropanol/CH<sub>3</sub>CN with 10 mM NH<sub>4</sub>COOH and 0.1% HCOOH). The gradient was 30% B (0 min), 50% B (1 min), 70% B (7 min), 99% B (13 min), 30% B (13.1 min), and column equilibration for additional 2 min at 30% B. The column was maintained at 40°C and a flow rate of 350 µL/min. The injection volume was 5.0 µL.

Both mass spectrometers were operated using heated electrospray ionization (HESI) source in positive and negative ion modes. Since native gangliosides ionize more efficiently as

negative ions<sup>154</sup>, oxidation reaction was monitored in ESI- mode, while TMT-labeled gangliosides are characterized in the ESI+ mode. In LTQ Orbitrap XL, the following parameters were used: Spray voltage 3.5 kV, vaporizer temperature 300<sup>0</sup>C, sheath gas 40 arb. units (au), auxiliary gas 20 au, sweep gas 1 au, ion transfer capillary temperature 300<sup>0</sup>C, tube lens voltage 100V, and resolution setting of 100,000. The Q Exactive HF settings were spray voltage 3.0 kV, vaporizer temperature 400<sup>0</sup>C, sheath gas 20 au, auxiliary gas 5 au, sweep gas 1 au, ion transfer capillary temperature 350<sup>0</sup>C, S-lens RF voltage 50V, and resolution 120,000. Fragmentation of TMT-labeled gangliosides was performed using parallel reaction monitoring (PRM) of pre-determined inclusion list. The following settings were used for HCD fragmentation: maximum injection time 100 ms, automatic gain control (AGC) 1e5, and resolution of 15,000.

## **Results and Discussion**

### **Optimization of oxidation conditions**

We found that the optimum condition to oxidize Neu5Ac side chain to C-7 aldehyde involves incubation of the sample with 1 mM NaIO<sub>4</sub> for 60 min in the dark at ~ 0<sup>0</sup>C, followed by quenching with glycerol, and further incubation for 60 min. Prolonged incubation prior to quenching resulted to a decline in the yield of the C-7 aldehyde which probably due to side reactions. Performing the reaction at room temperature led to formation of side products that could affect the downstream labeling steps. It also appeared that the use of CH<sub>3</sub>COONa/CH<sub>3</sub>COOH buffer is an important component during the oxidation process. Changing the solvent to purely organic or purely aqueous resulted to low yields and even side reactions involving opening of the susceptible neutral sugar rings at the non-reducing terminus (data not shown). We monitored the reaction progress using RPLC-MS/MS with LTQ Orbitrap XL as detector. Based on accurate mass data, conversion of the C-7 hydroxyl group of the model compound GM1a d18:1/18:0 to C-7 aldehyde was judged to be complete with nearly negligible

side products (**Fig. 31a-b**). This result demonstrates that the target species has been efficiently converted to aldehyde-containing product.

Inefficient or incomplete oxidation can be easily identified as manifested by the presence of other products resulting from the stepwise cleavage of the C-8 and C-9, which can be determined in a straightforward manner based on the mass difference of 14 Da, 18 Da, and 30 Da from the precursor ion, for example when the reaction is carried out at suboptimum conditions; these side products are speculated to originate from geminal diol intermediates which result from well-known hydration of aldehydes in aqueous medium (**Supplemental Fig. S8**). It is of note that in GD1a, the Neu5Ac connected to the terminal Gal unit oxidized more efficiently than the one connected to the internal Gal (**Supplemental Fig. S9d**). Furthermore, no degradation of labile Neu5Ac was observed both during oxidation and ionization in HESI. Based on the peak area of the substrate before and after oxidation, gangliosides were oxidized with an efficiency of at least ~ 90% across different classes investigated (*vide infra*). Reuter *et al.*<sup>314</sup> showed that the Neu5Ac in GM1a ganglioside is hardly oxidizable; however, using our method, we observed highly efficient oxidation of this analyte. Notably, their method uses lower periodate: substrate molar ratio (10:1) while ours uses high enough periodate: substrate ratio (200:1) leading to efficient oxidation to take place but low enough to prevent unwanted side reactions to occur.

### **Chemoselectivity of oxidation**

While the widely accepted mechanism of  $\text{IO}_4^-$  oxidation involves the cleavage of vicinal diols, other structural motifs could also be oxidized<sup>14,309</sup>. For example, it is possible that common structural features in glycosphingolipids such as *cis*- or *trans*- diols in the neutral carbohydrate ring, and hydroxyl group adjacent to carbonyl in the fatty acyl chain could all be affected by  $\text{IO}_4^-$  oxidation. Thus, we subjected representative glycosphingolipids possessing these common structural features under the same conditions we employed for gangliosides. Specifically, we

investigated GlcCer d18:1/18:0, Sulfatide d18:1/18:0, Gb3Cer d18:1/18:0, and GalCer d18:1/18:0(2ROH). Absolute abundance and peak area comparison between NaIO<sub>4</sub>-treated and control (only in oxidation buffer) show that effects of dilute NaIO<sub>4</sub> to these motifs are negligible and remained intact under the conditions optimized for gangliosides (**Supplemental Fig. S8**). Minimal difference in peak area and absolute intensity could be attributed to sample handling such as transfer from one container to the next and SPE steps which we consider to be acceptable and suffice to show that the oxidation process under these conditions are not detrimental to these motifs. This validates previous studies about the selectivity of mild periodate oxidation<sup>14,310,311</sup>.

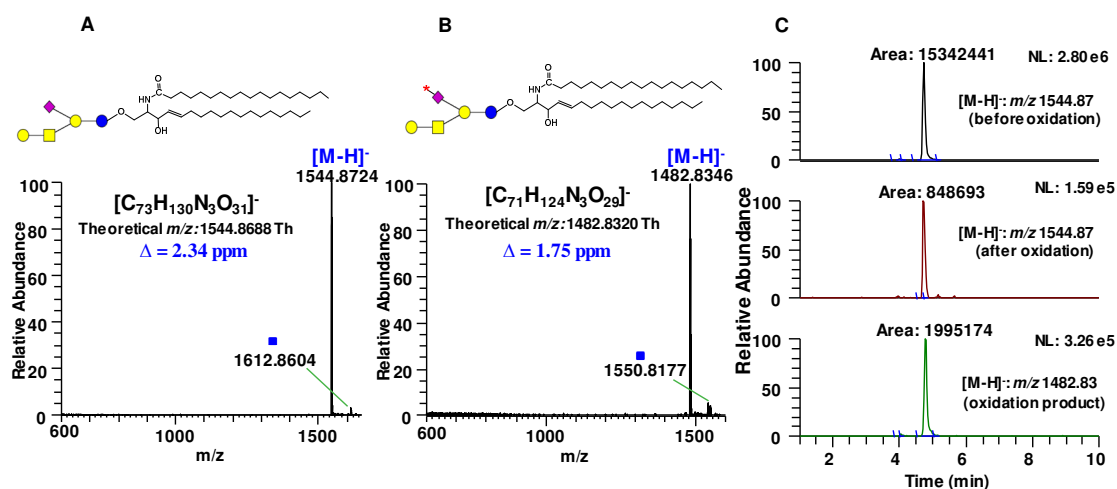


**Figure 31. Full Scan MS Spectrum of Unoxidized (a) and Oxidized (b) Ganglioside GM1a d18:1/18:0 Acquired Using LTQ Orbitrap XL Demonstrating Almost Negligible Side Reactions.** (c) Representative extracted ion chromatograms (EIC's) of GM1a d18:1/18:0 substrate before oxidation (panel 1), residual unoxidized substrate left after incubation with 1mM NaIO<sub>4</sub> (panel 2), and the resulting product of oxidation (panel 3). Guide to symbols: \*: aldehyde at C-7 position of Neu5Ac side chain; Δ: absolute mass error; ■: tentatively assigned as sodium formate adduct, [M+HCOO+Na<sup>+</sup>-H]<sup>-</sup> based on accurate mass measurement and isotopic distribution. Structure and systematic name of gangliosides are shown in Supplemental Table S1. Full scan mass range of other gangliosides subjected to NaIO<sub>4</sub> oxidation is shown in Supplemental Fig. S10 & S11.

## Oxidation of different ganglioside classes

To test the applicability of the oxidation process to different classes of ganglioside, we used the optimum condition to oxidize commercially available standards individually.

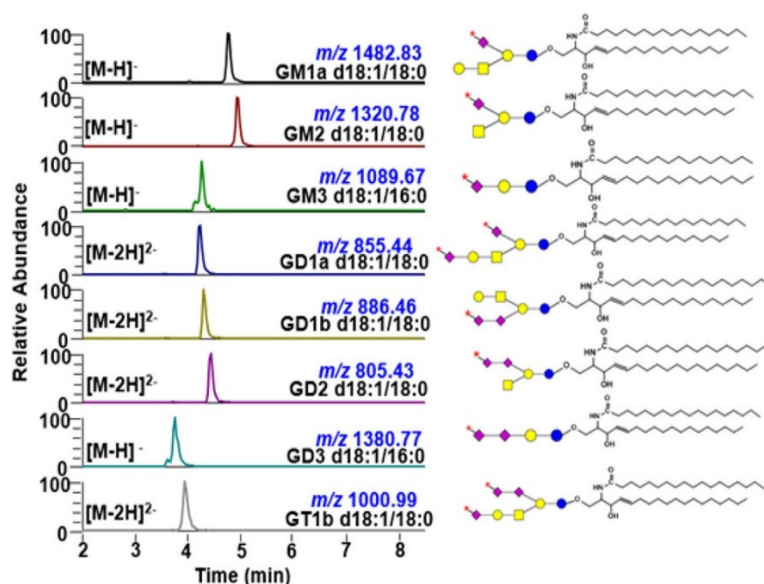


**Figure 32. Extracted Ion Chromatograms (EIC) of Individual Ganglioside Standards Oxidized Using 1 mM NaIO<sub>4</sub> Demonstrating its Applicability Across Different Core Structures.** Asterisk (\*) on the Neu5Ac symbol indicates aldehyde at C-7 position. Corresponding total ion chromatograms and full mass ranges are shown in the Supplemental Figs. S9-S10.

Our results show that this procedure is applicable to different classes of ganglioside such as monosialogangliosides (contain one Neu5Ac) GM1a, GM2 and GM3, disialogangliosides (contain two Neu5Ac) GD1a, GD1b, GD2, and GD3, and trisialoganglioside (contains three Neu5Ac) GT1b (**Fig. 32** and **Supplemental Fig. S9**). These constitute the predominant mammalian core structures<sup>25</sup> that are commonly analyzed both qualitatively and quantitatively in milk<sup>298,299</sup>, biofluids (cerebrospinal fluid, serum and plasma)<sup>170-172,315,316</sup>, and tissues<sup>172,174,317</sup>. It is noteworthy that when more than one Neu5Ac is present, the number of oxidizable Neu5Ac is dependent on how the C-7, C-8, and C-9 are used for glycosidic bonding or *O*-acetylation. Our

results show that C-7 aldehyde is produced only when C-8 is free, consistent with the known mechanism of  $\text{IO}_4^-$  oxidation<sup>309</sup>. For example, GD1a has two oxidizable Neu5Ac whereas GD1b, GD2, and GD3 only have one since their Neu5Ac's are connected through  $\alpha(2-8)$  linkage (Supplemental Table S1)<sup>318</sup>.

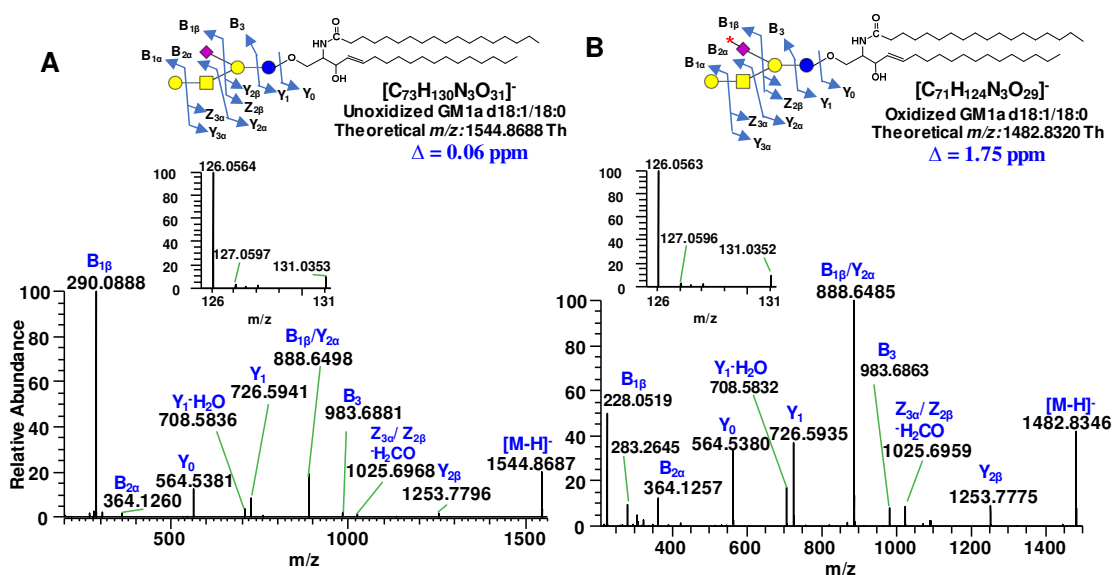


**Figure 33. Negative ESI-MS/MS Spectra of Unoxidized (a) and Oxidized (b) Ganglioside GM1a d18:1/18:0 Acquired Using Q Exactive HF.** Asterisk (\*) on the Neu5Ac symbol indicates aldehyde at C-7 position. Insets show the magnified  $m/z$  126-131 region.  $\Delta$  indicates absolute mass error. Fragments are labeled according to Domon and Costello nomenclature<sup>43</sup>. Structure and systematic name of gangliosides are shown in Supplemental Table S1.

To verify that aldehyde group is generated at the C-7 position of Neu5Ac side chain, we compared the fragmentation pattern of oxidized and unoxidized analytes. An observed neutral loss of 62.04 Da ( $-\text{C}_2\text{H}_6\text{O}_2$ ) from the  $[\text{M}-\text{H}]^-$  ion or 31.02 Da from the corresponding  $[\text{M}-2\text{H}]^{2-}$  ion confirmed that C-8 and C-9 of sialic acid have been cleaved off. For unoxidized analyte, using GM1a d18:1/18:0 as a model,  $Y_n$  ions due to glycosidic bond cleavages and ceramide backbone were observed (annotated according to nomenclature proposed by Domon and Costello<sup>141</sup>, and

Ann and Adams<sup>264</sup>). More importantly, loss of 291.0891 Da from the precursor ion, characteristic of Neu5Ac, generated the  $Y_{2\beta}$  fragment at  $m/z$  1253.7796, (**Fig. 33a**).

When subjected to  $\text{IO}_4^-$  oxidation, instead of 291.0891, loss of 229.0571 Da was observed to yield the same  $Y_{2\beta}$  fragment while majority of the ions remained the same for both analytes suggesting that loss of  $\text{C}_2\text{H}_6\text{O}_2$  originates from Neu5Ac (**Fig. 33b**). Moreover, the  $B_{1\beta}$  fragment ( $m/z$  290.0888) known as Neu5Ac marker<sup>143,154,172,298</sup> is absent in the oxidized species, instead the corresponding  $m/z$  228.0519 was observed (*cf.* **Fig. 33a-b**).

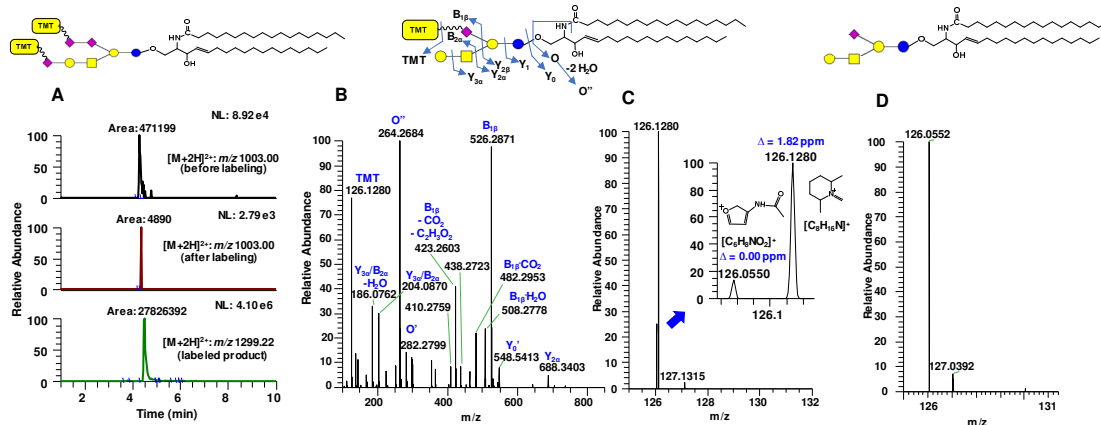


**Figure 34. EIC of Representative Oxidized Ganglioside GT1b d18:1/18:0.** (a) Before Labeling (panel 1), Residual Oxidized Species Left After Labeling (panel 2) and the Resulting AminoxyTMT<sup>0</sup> Labeled Product (panel 3) where Notable Enhancement in Ionization is Apparent. Representative MS/MS spectrum of the  $[\text{M}+2\text{H}]^{2+}$  of aminoxyTMT<sup>0</sup>-labeled GM1a d18:1/18:0 (b). The TMT reporter ion region of (b) is magnified to show the presence of interfering peak from GalNAc ( $m/z$  126.0550) and its baseline resolution with the reporter ion  $m/z$  126.1280; data were acquired at 15,000 resolution setting at  $\text{MS}^2$  level using Q Exactive HF (c);  $\Delta$  indicates absolute mass error. Also observed is the contribution of the isotopic  $[\text{M}+1]$  peak of the aminoxyTMT label at  $m/z$  127.1315. Reporter ion region of the  $[\text{M}+\text{H}]^+$  of unlabeled GM1a d18:1/18:0 (d) (for reference, the full MS/MS fragmentation of  $[\text{M}+\text{H}]^+$  ion of the unlabeled ganglioside is shown in Supplemental Fig. S9b). This indicates that the most significant interfering ion for the analysis of gangliosides using the aminoxyTMT labeling in positive ion mode is the GalNAc-derived oxonium ion as described in the present work.

Based on its accurate mass, this ion was assigned to be due to  $C_9H_{10}NO_6$  (Neu5Ac  $B_{1\beta}$  ion -  $C_2H_6O_2$ ) with an absolute mass error of 0.83 ppm. This further confirms that  $IO_4^-$  oxidation took place selectively at the Neu5Ac portion of the molecule and that aldehyde is generated at C-7 position consistent with the results of earlier reports<sup>310,311</sup>. Fragmentation of precursor ions in negative mode of oxidized and unoxidized gangliosides generated peaks that are isobaric to TMT reporter ions (**Fig. 33a-b**, inset).

By comparing individual carbohydrate standards, we deduced that  $m/z$  131.03 originates from Hexose (Gal or Glc) fragment while  $m/z$  126.05 originates mainly from Neu5Ac with minor contribution from GalNAc. Surprisingly, we also observed that  $m/z$  126.05 appears in positive ionization polarity, which could pertain to species having the same molecular formula but differ in mass by  $\sim 2$  electrons, so-called “twin ions”<sup>319</sup> (*cf.* **Fig. 33a-b** and **Fig. 34d**). However, only  $m/z$  126.05 in the TMT reporter ion region was observed after aminoxyTMT labeling upon fragmentation of  $[M+2H]^{2+}$  ions as discussed below. Since quantification using isobaric tag is carried out almost exclusively in positive ion mode<sup>301,306,307</sup>, the presence of these interfering ions in negative mode does not jeopardize the utilization of this technique.

### **Isobaric labeling of ganglioside standards**

Commercially available carbonyl-reactive aminoxyTMT<sup>0</sup> was used to label the oxidized individual standard gangliosides GM1a, GM2, GM3, GD1a, GD1b, GD2, GD3, and GT1b (**Supplemental Fig. S8**). We observed the TMT-labeled species as  $[M+2H]^{2+}$  ions in positive ion mode, and  $[M-H]^-$  in the negative ion mode. Based on the peak area of unlabeled gangliosides before and after reaction with aminoxyTMT<sup>0</sup>, efficiency of labeling was estimated to be greater than 95%. This highly efficient labeling is attributed to the rapid oxime bond formation using aminoxy functional group in the isobaric tag<sup>301</sup>. Also, compared to unlabeled gangliosides, significant increase in ionization efficiency in the positive mode was observed (**Fig. 34a**). This is

expected since the aminoxyTMT label made the analyte relatively more hydrophobic and enhanced its proton affinity. Zhou *et al.*<sup>307</sup> and Zhong *et al.*<sup>306</sup> showed that TMT-labeled glycans could exist in multiple charge states with varying number of proton and sodium adducts during ionization in ESI. In contrast, our mobile phase<sup>312</sup> which is supplemented with 10 mM NH<sub>4</sub>COOH allowed ionization of TMT-labeled gangliosides as mostly in protonated form with minimal (<30% of the intensity of the protonated form) to no detectable sodium adducts in some species, thus allowing better quantification. Although gangliosides ionize better as negative ions<sup>298</sup>, the TMT reporter ions were only observed in the positive ion mode<sup>306,307,320</sup>, hence, the latter was used for the fragmentation of TMT-labeled gangliosides.

Successful ligation of aminoxyTMT<sup>0</sup> to the oxidized monosialoganglioside GM1a was confirmed from the HCD fragmentation of [M+2H]<sup>2+</sup> ions measured at a resolution setting of 15,000 FWHM at the MS<sup>2</sup> level. We observed highly abundant *B*<sub>1β</sub> fragment at *m/z* 526.2871 (theoretical formula: C<sub>24</sub>H<sub>40</sub>N<sub>5</sub>O<sub>8</sub>, absolute mass error = 1.09 ppm) corresponding to the C-7 aldehyde linked to TMT via oxime bond. The high abundance of this fragment could be attributed to the lability of the Neu5Ac moiety during collisional dissociation. These results suggest that the aminoxyTMT<sup>0</sup> label was successfully attached to the C-7 aldehyde of the oxidized Neu5Ac unit. The presence of *B*<sub>1β</sub> fragment in conjunction with reporter ions is useful as diagnostic markers for the straightforward identification of TMT-labeled ganglioside (**Fig. 34b**). Also, information about the composition of the lipid backbone is easily identified from *Y*<sub>0</sub> or dehydrated *Y*<sub>0</sub> (*Y*<sub>0</sub>' ) and *O*<sup>''</sup> ions, the latter being diagnostic of the long chain base<sup>143,155</sup>. For instance, the *Y*<sub>0</sub>' ion (*m/z* 548.5413, theoretical formula: C<sub>36</sub>H<sub>70</sub>NO<sub>2</sub>, absolute mass error = 1.23 ppm) in **Fig. 34b** indicates a lipid composition of 36:1 (total carbon: number of unsaturation), which could correspond to either d18:1/18:0, d20:1/16:0, or d16:1/20:0 and so on. The presence of the *O*<sup>''</sup> ion in the MS/MS spectrum at *m/z* 264.2684 (theoretical formula: C<sub>18</sub>H<sub>34</sub>N, absolute mass error = 2.69 ppm)

facilitated the unequivocal assignment of the lipid moiety as d18:1/18:0. Likewise, GM1a d20:1/18:0 was identified using the  $m/z$  292.2995 ( $O''$  ion, theoretical formula:  $C_{20}H_{38}N$ , absolute mass error = 3.11 ppm) resulting from double dehydration of the eicosasphingosine (d20:1) long chain base (**Supplemental Fig. S10a**). More complex gangliosides GD1a, GD1b and GT1b were also successfully tagged with aminoxyTMT (*vide infra*). Like GM1a, diagnostic fragment  $B_{1\beta}$  (or  $B_{1a}$ ) along with reporter ion was observed indicating that the aminoxyTMT<sup>0</sup> reagent was attached to the C-7 aldehydes (**Supplemental Fig. S11a-c**).

While previous studies<sup>306,307</sup> employed sodiated adduct to obtain high intensity reporter ions, our results show that for TMT-labeled gangliosides, high enough intensity of reporter ions can also be obtained using  $[M+2H]^{2+}$  as precursor ions by applying relatively lower collision energy. This difference from their study and ours can be attributed to the type of analytes and how the TMT label is connected to the molecule. It was suggested by Zhou *et al.*<sup>307</sup> that the fragment ion yield of the TMT reporter ions is related to degree of branching, molecular weight, and strength of the reporter ion bond. In this respect, the ligation of TMT to the labile Neu5Ac could have aided the cleavage of reporter ions more easily. We found that by varying the normalized collision energy (NCE) between 20 to 35 arb. units, different levels of structural information can be obtained ranging from the glycan, lipid, and TMT reporter ions; increasing the NCE value yields higher reporter ion intensity and consequently lower signals due to glycan fragmentation (**Supplemental Fig. S12**). Also, one potential interference for the reporter ion  $m/z$  126.13 is the isobaric oxonium ion ( $m/z$  126.05) derived from Neu5Ac and GalNAc fragment<sup>321</sup>. The resolution we employed at the MS/MS level,  $R = 15,000$  FWHM is more than sufficient to distinguish these two fragments (**Fig. 34c**), like those previously achieved<sup>306,307</sup>. Taken together, this indicates a need for a high-resolution mass spectrometer in order for this technique to be useful.

### **Isobaric labeling of total ganglioside extract from porcine brain**

The developed strategy using aminoxyTMT<sup>0</sup> was applied to porcine brain total ganglioside extract. The major classes that comprise ~97% of gangliosides in mammalian brain include GM1a, GD1b, GD1a, and GT1b, in decreasing abundance, respectively<sup>25</sup>. We successfully labeled these gangliosides and confirmed their identity based on accurate mass (**Supplemental Table S2**) and HCD fragmentation data (**Supplemental Fig. S14**). Two Neu5Ac (one terminal, and one internal) in GD1a are oxidizable and only one in GD1b (**Supplemental Table S1**). This results to different products of oxidation which could be potentially used to differentiate them. However, the internal Neu5Ac in GD1a is less exposed towards oxidation which is oxidized more slowly than the terminal Neu5Ac. Due to this differential reactivity, GD1a could contribute certain amount of oxidation products isomeric to the product of GD1b upon oxidation that co-elute during RPLC separation and could be co-isolated for fragmentation (**Supplemental Fig. S9d and S10c**). Hence, the use of MS data alone could overestimate GD1b. Since GD1b has only one oxidizable Neu5Ac unit, we verified that it does not generate oxidation product isomeric to that of GD1a, thus the latter can be effectively quantified using the present approach. To quantitate GD1b using the described technique, appropriate separation method is thus recommended. Using RPLC, separation of GD1a and GD1b isomers is not possible<sup>155</sup>, but in our preliminary experiments using HILIC mode, these two gangliosides and their oxidation products were easily distinguishable (data not shown). This issue is not observed in other structures included in this study that contain multiple Neu5Ac units. This result highlights the potential of chemoselective oxidation followed by TMT labeling of gangliosides in mixtures; and application of this strategy in HILIC mode or ion mobility spectrometry<sup>198</sup> would be a fertile ground for future method development.

### **Oxidation and labeling of gangliosides in total lipids extract**

To investigate whether oxidation followed by TMT labeling workflow can be used even without prior isolation and purification of gangliosides, we directly oxidized total porcine brain lipid extract containing phosphatidylcholine (PC), phosphatidylethanolamine (PE), phosphatidylinositol (PI), phosphatidylserine (PS), and phosphatidic acid (PA) spiked with 1.0 to 5.0 nmol of porcine brain ganglioside mixture. During  $\text{IO}_4^-$  oxidation and subsequent TMT labeling, no appreciable interference from the other lipid species was observed. However, slight ion suppression was apparent which probably caused by phospholipids due to competitive process during ionization. For more reliable quantification, sample purification is recommended especially when low abundant ganglioside species are sought.

### **Feasibility for multiplexed relative quantification**

To test the practical utility of our technique, using separate preparations of porcine brain gangliosides extract in two different ratios by weight, chemoselective oxidation and labeling using aminoxyTMT<sup>6</sup> reagents were performed (**Fig. 35a**). We noted that this approach can be applied to limited amounts of ganglioside extract as low as 1.0  $\mu\text{g}$  of starting material even in the presence of total lipids extract. One-to-one volumetric ratio of the resulting solutions were combined and analyzed by RPLC-MS/MS. Using a pre-determined inclusion list for HCD fragmentation in PRM mode we extracted the intensities of reporter ions, calculated the experimental ratios and compared them to the theoretical value for GM1a d18:1/18:0, GM1a d20:1/18:0, GD1a d18:1/18:0, GD1a d20:1/18:0, GT1b d18:1/18:0 and GT1b d20:1/18:0 (**Fig. 35b**). We obtained a mean error of 5.68% and 8.42%, and mean relative standard deviation (RSD) of 4.88% and 11.29% for theoretical ratios 1:1:1:1:1 and 1:1:3:3:5:5, respectively, indicating the feasibility of this technique for reliable relative quantification of multiple samples

(Fig. 35c-f). Collectively, these results highlight the potential of  $\text{IO}_4^-$  oxidation followed by TMT labeling for relative quantification of ganglioside at the molecular species level using tandem mass spectrometry.

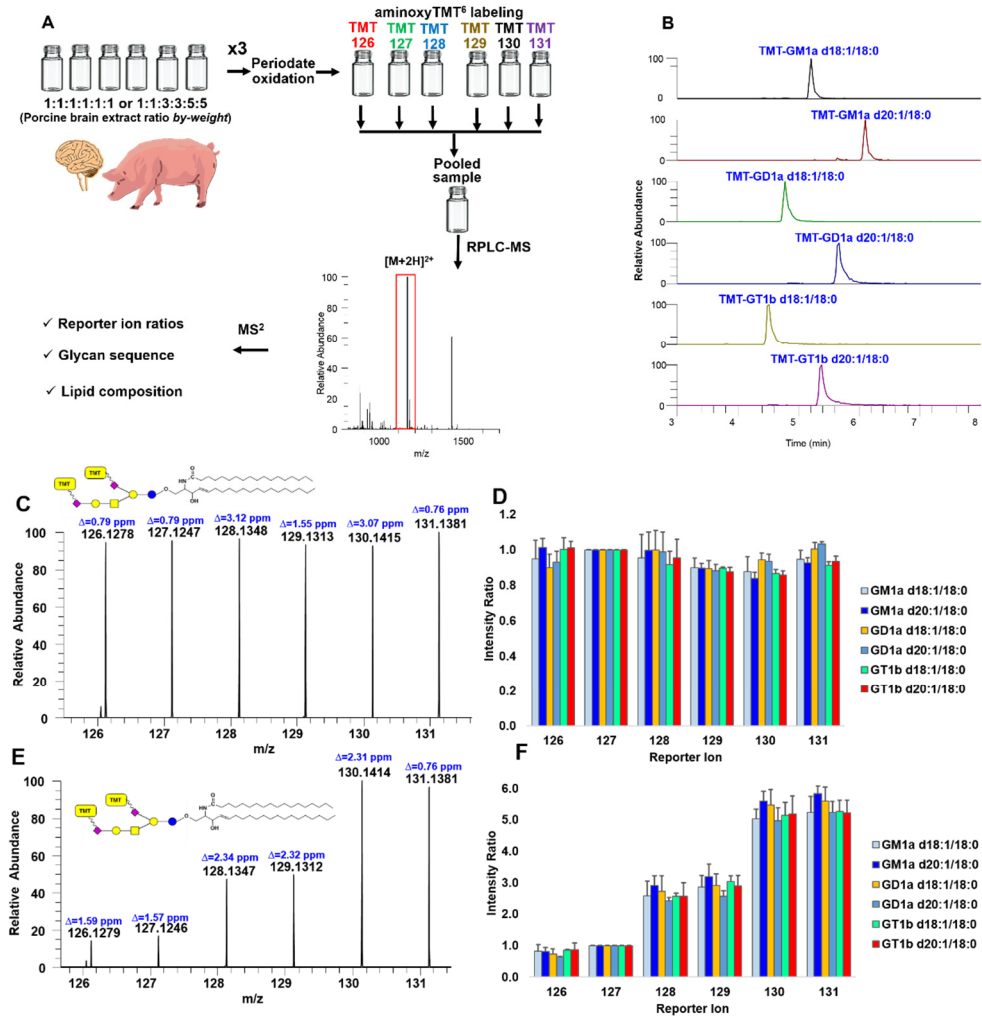


**Figure 35. Workflow Employed to Demonstrate Feasibility of Multiplexed Experiment Using Porcine Brain Extract** (a). Resulting EIC of major ganglioside components in porcine brain labeled with aminoxyTMT<sup>6</sup> (b). Representative reporter ion region of aminoxyTMT<sup>6</sup>-labeled GD1a d20:1/18:0 in porcine brain extract mixed in 1:1:1:1:1 (c) and 1:1:3:3:5:5 (e) ratios *by-weight* for the channels indicated. Calculated intensity ratios plotted as overall mean  $\pm$  standard deviation ( $n=3$ , triplicate preparations, each injected twice) relative to arbitrary reference channel, TMT-127 (d and f).  $\Delta$  indicates absolute mass error.

## **Conclusion**

In this paper, we demonstrated a strategy to label major mammalian ganglioside core structures to allow the use of commercially available isobaric mass tag reagent without removing the lipid backbone. Under conditions described in this paper,  $\text{NaIO}_4$  is chemoselective to the C-7 side chain of Neu5Ac to form aldehyde functional group without affecting other structural motifs. The oxidizability of Neu5Ac depends on the availability of free hydroxy at C-8, which could be exploited to aid the structural characterization of the connectivity of Neu5Ac in the glycan moiety. Attachment of the isobaric label is straightforward and found to be advantageous to increase the ionization efficiency of complex gangliosides. The high-resolution, accurate mass measurements afforded the baseline resolution of interfering ions that are isobaric to TMT reporter ions. Multiplexed analysis is an efficient and sensitive technique for relative quantification of gangliosides. Using this methodology, not only can we analyze six samples simultaneously, but also determine both the glycan and lipid compositions. This promising approach can be used to compare gangliosides composition across different samples, biological treatments, or temporal studies involving longitudinal research design. Moreover, as this strategy is selective to sialic acid group, it could also be extended to other biomolecules of interest such as glycopeptides or others that commonly possess sialic acids. Future application of this novel strategy to answer relevant biological questions is expected.

## **Acknowledgement**

This work was partially supported by grants from the National Institute of General Medical Sciences (GM 104678) and the National Institute of Diabetes and Digestive and Kidney Diseases (R01 DK114345) of the National Institutes of Health. The authors are also grateful for Triad Mass Spectrometry Facility of the UNCG Department of Chemistry and Biochemistry and Dr. Daniel Todd.

CHAPTER VI  
DIFFERENTIAL ISOTOPE LABELING BY PERMETHYLATION AND  
REVERSED-PHASE LC/MS FOR RELATIVE QUANTIFICATION  
OF INTACT NEUTRAL GLYCOLIPIDS  
IN MAMMALIAN CELLS

This chapter has been published in the journal *Analytical Chemistry* and is presented in that style. Barrientos, R.C., and Zhang, Q. *Anal. Chem.*, **2019**, In Press.

**Introduction**

Glycolipids, also termed glycosphingolipids, are biologically important glycoconjugates that play crucial roles in cell health and disease<sup>3,8</sup>. They can be classified according to the head group composition as acidic or neutral glycolipids. The former class contains carbohydrate moieties with at least one sialic acid (gangliosides) or sulfate functional group (sulfatides) while the latter does not carry any of these features. Abnormal metabolism of these molecules, especially neutral glycolipids, has been implicated in numerous diseases such as lysosomal storage, Parkinson's, and Alzheimer's among others<sup>8,27,322</sup>. The specific roles of the glycan head group and the lipid backbone in biology remains elusive but current evidences clearly highlight the importance of both features in biological processes<sup>3,7</sup>. Therefore, structural characterization and quantitation of glycolipids need to be performed at intact structural level, where the linkage between the glycan and lipid moieties is kept during analysis.

Glycolipids are chemically diverse and structurally heterogeneous. Traditionally, structures of glycolipids are determined using mass spectrometry (MS) by separately identifying

glycan and lipid structures after hydrolysis, which only works for highly purified compound if complete molecular structural information is desired<sup>9,15,18,323</sup>. In addition, one general challenge in glycoconjugate analysis by MS is the low sensitivity due to the poor ionization efficiency of these molecules. Various sample derivatization approaches<sup>114,128</sup> have been developed to address this. Among them, permethylation is a well-studied reaction that involves methylation of all active protons in the form of hydroxyl and amide hydrogens in the molecule<sup>202,324-327</sup>. It has been widely used for the MS-based characterization of glycans cleaved from glycoconjugates<sup>128</sup>. However, its application to glycolipids was rare and limited only to structural determination of highly purified, individual glycolipids<sup>115,325</sup>.

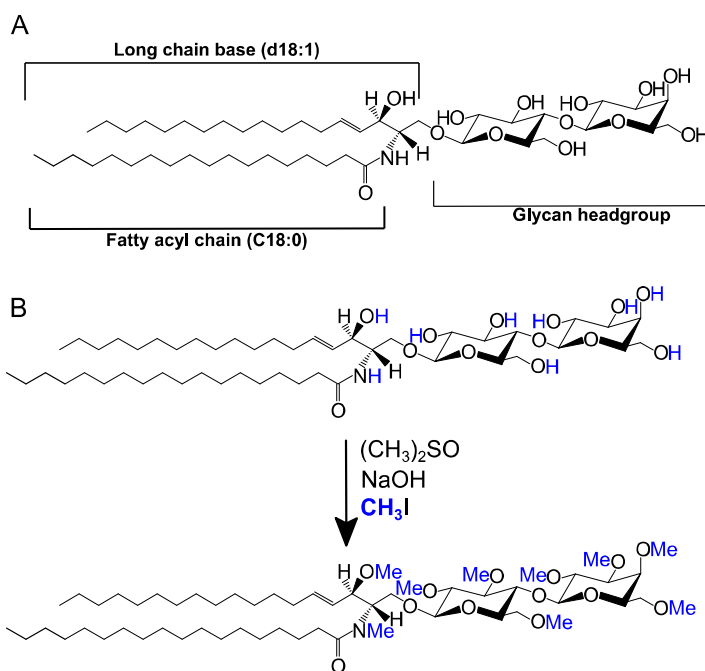


**Figure 36. Schematic of Reaction Workflow Implemented in this Work.** A) General structure of a neutral glycolipid, shown is *D*-lactosyl- $\beta$ -1,1' *N*-stearoyl-*D*-erythro-sphingosine abbreviated as LacCer d18:1/18:0. B) Overview of permethylation reaction where all active protons (-OH and -NH) are converted to methyl groups by  $\text{CH}_3\text{I}$ .

Quantification of glycoconjugates has been greatly facilitated by recent developments in MS methodologies and instrumentation<sup>114</sup>. By far the most reliable method for quantification is isotope dilution using stable isotope labeled internal standards. These internal standards mimic the physical and chemical properties of the analytes during measurements and therefore serve as reliable reference when comparing multiple samples. However, having pure isotopically labeled standards for all target molecules remains a bottleneck as oftentimes these standards are not commercially available. Thus, differential isotope labeling was introduced to address this issue. In this approach, different samples are labeled with different isotopes either through a labeling reagent or through cell culture, followed by mixing the samples and then analysis by MS. Although this strategy has been adapted in the field of metabolomics<sup>328</sup>, glycomics<sup>13,206,207,329,330</sup>, and proteomics<sup>331</sup>, currently it has very limited use in lipidomics<sup>332,333</sup>, especially in glycolipids analysis.

In this work, we demonstrate differential isotope labeling technique by exploiting permethylation using  $^{12}\text{CH}_3\text{I}$  and  $^{13}\text{CH}_3\text{I}$  as a facile approach for relative quantification of intact neutral glycolipids (**Fig. 36**). Robustness of the method in both structural characterization as well as quantification has been achieved using commercially available glycolipid standards and total lipid extracts derived from mammalian cells.

## **Experimental Procedures**

### **Materials and reagents**

The following standards were purchased from Avanti Polar Lipids (Alabaster, AL): D-lactosyl- $\beta$ -1,1' N-stearoyl-D-erythro-sphingosine (LacCer d18:1/18:0, cat. no. 860598), D-galactosyl- $\beta$ -1,1' N-stearoyl-D-erythro-sphingosine (GalCer d18:1/18:0, cat. no. 860538), D-galactosyl- $\beta$ 1-1'-N-[2''(R)-hydroxystearoyl]-D-erythro-sphingosine (GalCer d18:1/18:0(2OH), cat. no. 860840), 1-(1Z-octadecenyl)-2-oleoyl-*sn*-glycero-3-phosphoethanolamine (C18(Plasm)-

18:1 PE, cat. no. 852758), 1,2-dioleoyl-*sn*-glycero-3-phosphocholine (18:1 ( $\Delta^9$ -Cis) PC, cat. no. 850375). Due to the unavailability of synthetic Globotetrahexosylceramide (Gb4), a well-characterized commercial mixture of Gb4 (porcine RBC, cat. no. 1068) from Matreya LLC (State College, PA) was used. Globotriaosylceramide (Gb3Cer d18:1/18:0, porcine RBC, cat. no. 1529) was obtained from Matreya LLC (State College, PA). Sodium hydroxide pellets and dimethylsulfoxide were from Fisher Scientific. The  $^{12}\text{C}$ -methyl iodide and  $^{13}\text{C}$ -methyl iodide (99% atom) containing copper stabilizer were purchased from Sigma-Aldrich (Milwaukee, WI) and used without any further purification. All solvents used for extraction steps were at least HPLC grade while solvents and reagents used for RPLC-MS analysis were LC-MS grade and purchased from Fisher Scientific (Pittsburgh, PA).

### **Permethylation**

We followed the methods of Ciucanu and Kerek<sup>202</sup> and Gunnarsson<sup>203</sup> in this work with slight modifications. Briefly, aliquots equivalent to 0.1  $\mu\text{g}$  to 100.0  $\mu\text{g}$  of glycolipids were measured from stock solutions in  $\text{CHCl}_3/\text{CH}_3\text{OH}/\text{H}_2\text{O}$  (2:1:0.1 v/v) and dried using a stream of  $\text{N}_2$  gas. For cells, lipid extracts equivalent to 250  $\mu\text{g}$  protein were used. In a glass HPLC sample vial, the dried glycolipids were reconstituted in 300  $\mu\text{L}$  of anhydrous dimethylsulfoxide (DMSO) that has been previously dried over molecular sieves. Fine NaOH powder (~40 mg) were added and vortexed briefly. Then, 20  $\mu\text{L}$  of  $^{12}\text{CH}_3\text{I}$  or  $^{13}\text{CH}_3\text{I}$  was added, incubated for 30 minutes at room temperature. This was followed by additional 20  $\mu\text{L}$  of  $\text{CH}_3\text{I}$  and incubated for another 30 minutes at room temperature. The reaction was quenched by adding 995  $\mu\text{L}$  of cold water and immediately extracted with 400  $\mu\text{L}$  of dichloromethane ( $\text{CH}_2\text{Cl}_2$ ). The organic phase was washed three times with water and dried under a stream of  $\text{N}_2$  gas. The residue was reconstituted in  $\text{CH}_3\text{CN}/2\text{-propanol}/\text{H}_2\text{O}$  (65/30/5, v/v) and analyzed by RPLC-MS/MS.

### **Cell culture**

Wild-type murine macrophage cell line, RAW 264.7 was a generous gift from Dr. Michael Brenner (Brigham and Women's Hospital, Boston, MA). Cells were grown<sup>334</sup> using Dulbecco's Modified Eagle's medium (DMEM) (ATCC, Manassas, VA) supplemented with 10% fetal bovine serum (Gibco), 2 mM L-glutamine (Gibco), 100 U/mL Penicillin (Gibco) and 100 µg/mL Streptomycin (Gibco) in a humidified cell culture incubator at 37°C and 5% CO<sub>2</sub>. After reaching ~80% confluency on a 10-cm dish, cells were treated with or without 100 µM conduritol B epoxide (EMD Millipore) for 3, 6, 12, 48, and 72 h. Then, cells were washed three times using 0.1 M phosphate buffered saline (PBS, pH 7.4) and scraped off. Following centrifugation at 500 xg for 5 mins, cells were immediately subjected to total lipids extraction as described below.

### **Lipid extraction**

The method described by Löfgren *et al.* was used for the extraction of total lipids<sup>90</sup>. Briefly, cells were homogenized in the presence of 500 µL of cold 1-butanol/methanol (3:1, v/v). Then, 500 µL of heptane/ethyl acetate (3:1, v/v) and 500 µL 1% aqueous acetic acid were sequentially added. Upper layer was collected, and the lower layer was re-extracted with 500 µL heptane/ethyl acetate (3:1, v/v). The pooled upper phases were dried down under a stream of N<sub>2</sub> gas and immediately analyzed by RPLC-MS/MS or subjected to permethylation as described above. Resulting protein pellets were quantified and used for sample normalization<sup>335</sup>.

### **Protein quantification**

Cell pellets were denatured using 200 µL of 1X RIPA lysis buffer overnight at 4°C. Total protein was quantified using bicinchoninic acid (BCA) assay kit (Thermo Scientific) following manufacturer's instructions. Protein content was used as sample normalization factor.

### **Cell viability assay**

Appropriate dose for treatment was determined using cell counting kit-8 (CCK-8) reagent (Dojindo Molecular Technologies, Rockville, MD). This assay relies on the reduction of 2-(2-methoxy-4-nitrophenyl)-3-(4-nitrophenyl)-5-(2,4-disulfophenyl)-2H-tetrazolium, monosodium salt (WST-8) reagent to form colored formazan dye by dehydrogenases in viable cells which can be measured spectrophotometrically. Briefly, RAW 264.7 cells ( $2 \times 10^4$  cells/well) were incubated on a clear flat bottom 96 well plate (Nunc) and incubated at 37°C and 5% CO<sub>2</sub>/95% humidified air overnight. Next, cells were treated with or without 100 μM CBE at specified exposure times (3h, 6h, 12h, 48h, 72h) and measured using Cytation 5 plate reader (Biotek) at  $\lambda=450$  nm.

### **β-glucocerebrosidase assay**

Following the method of van Es *et al.*<sup>336</sup>, after treating the cells with or without 100 μM CBE, 10 μM of fluorescein di-β-D-glucopyranoside (FDGlu)<sup>336</sup> (Molecular Probes) was added to each well and further incubated for 1 hr before reading the samples using flow cytometer (Guava Incyte, Millipore) using the Fluorescence Channel 1 (Green Fluorescence).

### **RPLC-MS/MS analysis**

A Vanquish UHPLC system (Thermo Scientific) coupled with Q Exactive HF (Thermo Scientific) was employed. Cortecs C18 column (2.6 mm ID x 100 mm, 1.6 μm, Waters) and the following mobile phases were used<sup>145,312</sup>: A (60/40 CH<sub>3</sub>CN/H<sub>2</sub>O with 10 mM NH<sub>4</sub>COOH and 0.1% HCOOH), B (90/10 isopropanol/CH<sub>3</sub>CN with 10 mM NH<sub>4</sub>COOH and 0.1% HCOOH). The gradient was 30% B (0 min), 50% B (1 min), 70% B (7 min), 99% B (13 min), 30% B (13.1 min), and column equilibration for additional 2 min at 30% B. The column was maintained at 40°C and a flow rate of 350 μL/min. The injection volume was 10.0 μL. The Q Exactive HF settings were: spray voltage 3.0 kV, vaporizer temperature 400 °C, sheath gas 20 au, auxiliary gas 5 au, sweep

gas 1 au, ion transfer capillary temperature 350 °C, S-lens rf voltage 50 V. Data-dependent acquisition using the top 10 most abundant ions was performed at a full MS resolution of 120,000, MS<sup>2</sup> resolution of 15,000, isolation window of 1.4 *m/z* and dynamic exclusion setting of 15.0 s. For targeted fragmentation studies, the following HCD settings were used: maximum injection time 100 ms, automatic gain control (AGC)  $1 \times 10^5$ , and resolution of 15,000.

### **Data analysis**

Evaluation of extracted ion chromatograms and MS/MS spectra were carried out using XCalibur (Thermo Scientific). For quantification, TraceFinder 4.1 SP2 software (Thermo Scientific) was used to integrate peak areas, extract accurate mass, and retention time of target analytes. The ratios of <sup>12</sup>C- and <sup>13</sup>C- permethylated analytes were then calculated using these peak areas and used for downstream statistical analyses as log-transformed values in MetaboAnalyst 4.0<sup>337</sup>. Univariate statistical tests employed unpaired Student's *t* test at  $\alpha=0.05$  in Prism 6 (GraphPad Software, Inc.).

## **Results and Discussion**

### **Optimization of reaction conditions**

Permethylation is commonly used for derivatization of glycoconjugates and a few recipes have been developed for this reaction. Initially, we employed the modified method of Ciucanu and Costello<sup>324</sup> that incorporates trace amount of water in the reaction. The reaction efficiency is high as previously reported with all substrate completely reacted (**Fig. 37A**). However, we observed that in the presence of water, two main products of permethylation were present for glycolipids, one where only the glycan hydroxyls being methylated (per-*O*-methylated), and the other with all hydroxyls and the amide -NH in the ceramide backbone (per-*N,O*-methylated) (**Fig. 37B**).

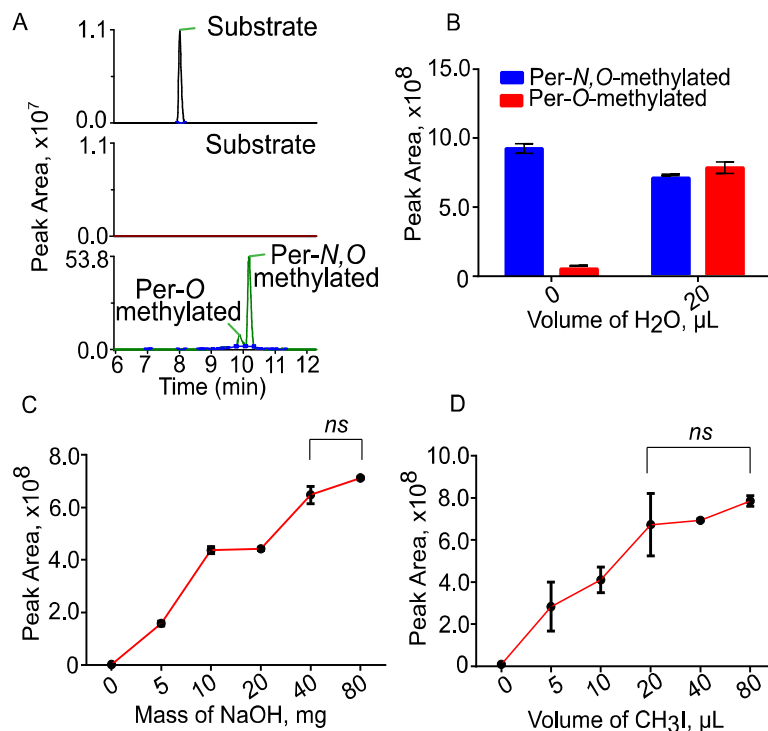


**Figure 37. Effect of Reaction Conditions on the Efficiency of Permethylation.** Different standard glycolipids, shown here is LacCer d18:1/18:0, were permethylated using <sup>12</sup>CH<sub>3</sub>I under various conditions and analyzed by RPLC-MS. A) Extracted ion chromatogram of LacCer d18:1/18:0 substrate (*m/z* 890.66) under untreated (top panel) and treated (middle panel) conditions, the permethylated products are also shown (bottom panel). B) Effect of trace amount of water on the quantitative conversion of glycolipids to >95% per-*N,O*-methylated product. C) Effect of the amount of NaOH on the yield of permethylated product. D) Effect of the amount of CH<sub>3</sub>I on the yield of permethylated product. Range of tested amounts of glycolipids is 0.1 μg to 100 μg. *ns*: not statistically significant ( $\alpha=0.05$ ).

This is because, unlike the –OH protons that can be easily deprotonated, the N-H protons are not readily deprotonated due to the adjacent C=O group. Analytically, this could be a challenge for quantification since the substrate is not quantitatively converted into a single derivative. Under anhydrous conditions using DMSO dried over molecular sieves, the per-*O*-methylated derivative was substantially suppressed and the per-*N,O*-methylated product remained the major species (**Fig. 37B**).

Further, we investigated the effect of various parameters on the efficiency of full-permethylation of glycolipids, which include the amount of CH<sub>3</sub>I, amount of powdered NaOH, and incubation time. Among these tested parameters, the most crucial factors are the amount of CH<sub>3</sub>I and NaOH, which should be in huge molar excess. We observed that, consistent with previous works<sup>202,325</sup>, excess amount of CH<sub>3</sub>I and NaOH did not significantly deteriorate the yield of permethylation. Thus, we fixed the amounts of these reagents to 40 mg for NaOH and 40 μL for CH<sub>3</sub>I (**Fig. 37C-D**). When the samples were incubated for 60 mins using a thermomixer set at room temperature (~25<sup>0</sup>C), up to 100 μg of glycolipids can be efficiently permethylated with negligible level of unreacted substrate left after permethylation. This amount is typical for glycolipids derived from cell culture work.

Permethylation of glycolipids under the optimum conditions generated no degradation products and minimal by-products. We monitored the formation of potential products of the “peeling” reactions in glycolipids analogous to that of *O*-glycans from glycopeptides or of free-reducing end carbohydrates<sup>324</sup>, but we did not observe them suggesting that under the experimental conditions employed in this study, “peeling” reactions are negligible. However, some levels of by-products were formed, specifically as mentioned above, up to ~5% of undermethylated (per-*O*-methylated) product was detected, although it is still better compared to recent work<sup>326</sup> on *N*-glycan permethylation analysis that yielded 32% undermethylated products. Aside from these undermethylated products, no other by-products were found. This confirms the neatness and suitability<sup>338,339</sup> of this reaction for glycolipids analysis as already demonstrated in the past<sup>203,327</sup>.

Additionally, since the entire permethylation, extraction, and reconstitution steps were carried out in one HPLC sample vial, it avoided the potential sample loss that could result from transfer of samples from one container to another. The recent work on the automated

permethylation by Shubhakar and co-workers could also be potentially applied in this context<sup>326</sup> allowing potential automation of this process.

### **RPLC retention characteristics of permethylated glycolipids**

Previous works on permethylated glycolipids have focused on structural analysis without any chromatographic separation<sup>74,115,340,341</sup>. For quantitative purposes, particularly with limited amount of samples, chromatography prior to MS detection offers a great advantage in terms of improving the sensitivity of analysis due to chromatographic focusing, and it also allows resolution of possible isobaric compounds. Reversed-phase column for separation prior to MS analysis is ideal for permethylated glycoconjugates owing to their increased hydrophobicity<sup>342,343</sup>. In this study, we used Cortecs C18 RPLC column. Shown in **Supplemental Fig. S16A** are the extracted ion chromatograms of glycolipids containing 1 to 4 sugars with identical lipid composition. We observed that each sugar moiety resulted to ~0.50 min decrease in retention time. Specifically, Gb4Cer d18:1/18:0 eluted the earliest, followed by Gb3Cer d18:1/18:0, LacCer d18:1/18:0, and GlcCer d18:1/18:0. On the other hand, increase of one -CH<sub>2</sub>- unit in the fatty acyl is equivalent to ~0.40 min increase in retention time for glycolipids of the same glycan head group, e.g. HexCer with different fatty acyl chain length (**Supplemental Fig. S16B**). Also as expected, the <sup>12</sup>C and <sup>13</sup>C-permethylated glycolipids coeluted in RPLC and the relative abundances of the monoisotopic peaks agreed well with the theoretical ratio (**Fig. 38A-B**). The co-elution ensures uniform MS detector response between the two derivatives and is more applicable for RPLC-MS-based quantitation, which is a great advantage over the previous method employed for *O*-glycan analysis where, instead of <sup>13</sup>CH<sub>3</sub>I, CD<sub>3</sub>I was used which could have noticeable isotopic effects if it were coupled with chromatography<sup>207</sup>. The increased retention of permethylated glycolipids also has an added benefit, as we observed, there are less interferences coeluting with glycolipids at the high organic portion of the gradient. Overall, the uniform

retention behavior and predictability of retention time are useful criteria to validate results in RPLC-MS analysis of permethylated glycolipids.

### **Ionization and fragmentation pattern of permethylated [M+H]<sup>+</sup> ions using HCD**

Similarly, as previously reported<sup>340,344</sup>, permethylation has increased the ionization efficiency of glycolipids by at least ten-fold, which greatly facilitated the detection of low abundant species in complex samples.

Fragmentation of permethylated glycolipids has been studied in the past mainly as metal adducts generated under direct infusion conditions<sup>18,323,341</sup>, using CID and high-energy CID. Under the LC mobile phase and gradient conditions used in this work where additives such as ammonium formate and formic acid are used<sup>28,29</sup>, permethylated glycolipids almost exclusively exist as [M+H]<sup>+</sup> with negligible level of [M+Na]<sup>+</sup><sup>145,312</sup>.

To study the fragmentation pattern of permethylated glycolipids with different levels of structural complexity, commercially available standards GlcCer d18:1/18:0, LacCer d18:1/18:0, Gb3Cer d18:1/18:0, and Gb4Cer d18:1/18:0 were permethylated and their [M+H]<sup>+</sup> ions were selected for HCD fragmentation (**Fig. 38 and Supplemental Fig. S17**). The nominal mass increment represents the number of active protons present in the native form of the structure. After differential permethylation using CH<sub>3</sub>I, we observed corresponding mass shifts of the relevant neutral losses and fragment ions. For example, in permethylated LacCer d18:1/18:0, the mass increments for *Y*<sub>0</sub> and *Y*<sub>1</sub> ions were 2 and 5 Da, respectively, which indicates that two methyl groups were attached to the sphingosine backbone and additional three methyl groups were attached to the internal hexose unit. In addition, the shift of neutral loss of internal hexose unit from 204 Da to 207 Da, further confirmed that three methyl groups have been substituted in this hexose moiety (**Fig. 38 D-E**).

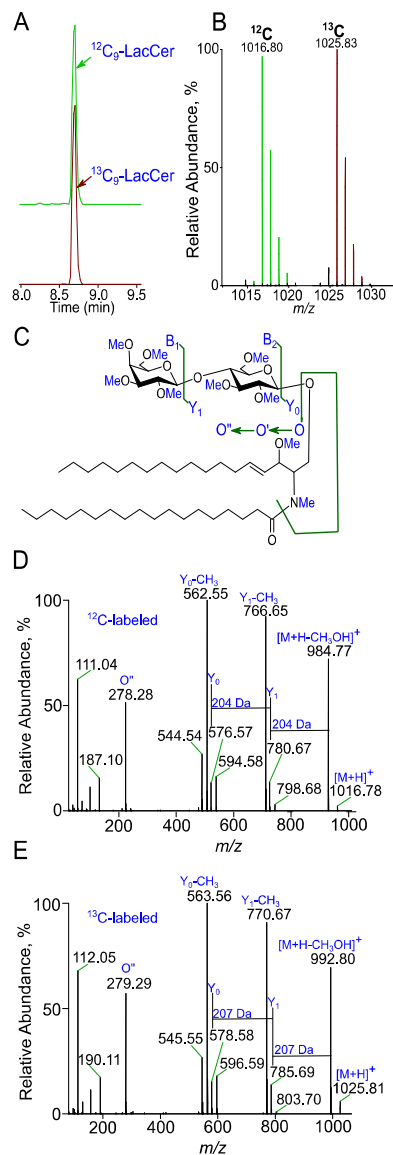


**Figure 38. Coelution and Fragmentation Behavior of Permethylated Glycolipid.** Standard glycolipids were permethylated according to the optimized conditions. A) Coelution of [ $^{12}\text{C}_9$ ] and [ $^{13}\text{C}_9$ ]-LacCer18:1/18:0 mixed at 1:1 ratio by weight. The subscripts indicate the number of active protons that have been replaced by methyl group. B) Mass spectrum of the chromatographic peaks shown in A. C) Nomenclature of fragments according to Domon and Costello, and Ann and Adams. D) Fragmentation of [ $^{12}\text{C}_9$ ]-LacCer18:1/18:0. E) Fragmentation of [ $^{13}\text{C}_9$ ]-LacCer18:1/18:0. Both spectra were acquired by selecting the  $[\text{M}+\text{H}]^+$  ion using HCD at normalized collision energy (NCE) = 20 in a hybrid orbitrap instrument (QExactive HF). Fragmentation of other glycolipids possessing different structural features is shown in Supplemental Fig. S17.

Also, the sphingosine marker *O*<sup>+</sup> at  $m/z$  278.2846 with  $^{12}\text{C}$ -labeled shifted to  $m/z$  279.2880 with  $^{13}\text{C}$ -labeled, this mass difference ( $\Delta m = 1.0034$  Th) can be accounted for by the presence of one methyl substitution. Previous work<sup>341</sup> on permethylated glycolipids proposed the cleavage of the C(3) methoxy group of the long chain base sphinganine. Consequently, only one methyl group is left, which explains the 1 Th shift of the *O*<sup>+</sup> ion. Overall, the differential mass shifts of either molecular or fragment ions are analytically useful for structural characterization and could benefit structural studies of novel glycolipids.

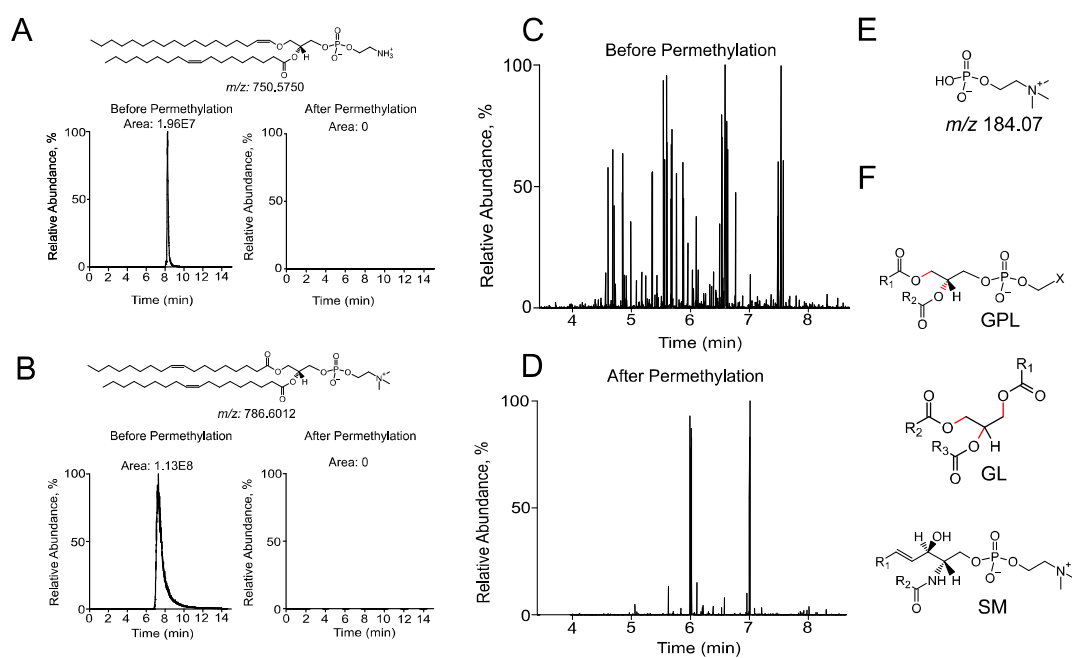


**Figure 39. Simultaneous Elimination of Dominant Phospholipids During Permethylation.** Phospholipid standard mixtures were prepared and subjected to the optimized permethylation reaction conditions. A) Extracted ion chromatograms (EIC) of phosphatidyl ethanolamine, before and after permethylation. B) EIC of phosphatidyl choline before and after permethylation. This also holds in a real sample as verified from the MS/MS TIC trace of  $m/z$  184.07 (mass tolerance = 5.0 ppm) of RAW264.7 total lipids extract. Total lipids from RAW264.7 cells were extracted and analyzed before (C) and after (D) permethylation. E) Structure of  $m/z$  184.07, diagnostic of phosphocholine-containing lipids. F) General structure of common lipids present in cells where the chemical bonds highlighted in red are alkaline-labile bonds and are expected to break as a result of the highly basic conditions employed during the permethylation step (GPL: Glycerophospholipids; GL: Glycerolipids; SM: Sphingomyelin).

## Elimination of ester-linked lipids in sample matrix

Previous works using permethylation for structural elucidation of glycolipids involved tedious purification steps prior to permethylation. With the goal of high throughput, straightforward analysis of glycolipids in a complex total lipid extract, we show here that direct permethylation is an effective process in eliminating the interfering lipids. For example, phospholipids ionize better than glycolipids and ionization of the latter could be suppressed when both are present.

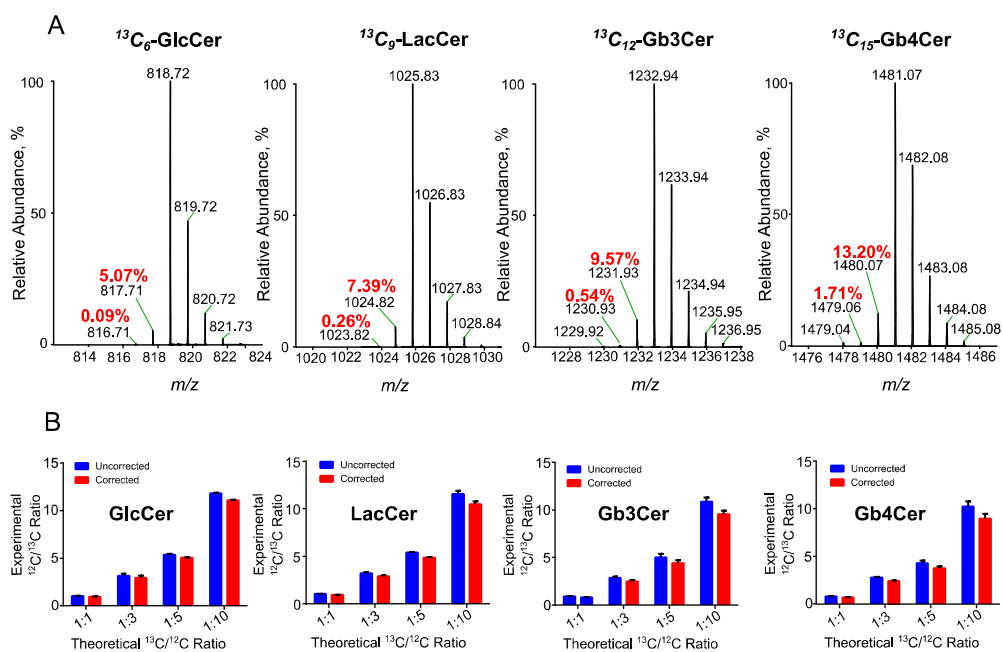


**Figure 40. Evaluation of Quantitative Ability of  $^{12}\text{C}$  and  $^{13}\text{C}$  Permethylation.** Standard glycolipids were independently permethylated using  $^{12}\text{CH}_3\text{I}$  and  $^{13}\text{CH}_3\text{I}$ , pooled at different ratios and analyzed by RPLC-MS as described in the experimental section. A) Effect of  $^{12}\text{C}$  impurity in the overall isotopic distribution of different glycolipids. Shown in red are the relative abundances of the peaks 1  $m/z$  and 2  $m/z$  lower than the monoisotopic peak of fully  $^{13}\text{C}$  permethylated product. The subscript indicates the number of active protons that have been replaced by methyl group. B) Effect of performing correction due to the presence of  $^{12}\text{C}$  impurity. Actual values of the ratios and standard deviations are shown in Supplemental Table S3.

Cognizant that amide bonds are relatively more stable than ester bonds under alkaline conditions<sup>345</sup>, we found that most naturally occurring phospholipids, such as phosphatidylcholine (PC), phosphatidylethanolamine (PE), and phosphatidylinositol (PI) could be eliminated in the permethylation step.

To illustrate, first we compared a mixture of phospholipid standards with and without permethylation (**Fig. 39A-B**). Our results, by monitoring the specific ions of the phospholipid standards, clearly showed the depletion of these species during the permethylation step (**Supplemental Fig. S20**). The same was observed in total lipids extract from RAW264.7 cells where we used the intensity of the phosphocholine fragment ion<sup>346</sup> -  $m/z$  184.07 to indicate the abundance of PC before and after permethylation (**Fig. 39C-E**).

Again, the abundances of precursor ions producing  $m/z$  184.07 were dramatically reduced. This is expected because of the highly alkaline condition<sup>144,345</sup> in this process, which cleaved ester bonds that are present in PC but spared the amide bonds in glycolipids (**Fig. 39F**). The incomplete disappearance of  $m/z$  184.07 in RAW264.7 cell extracts (**Fig. 39D**) is due to the presence of sphingomyelins (SM) that do not possess ester linkages. It is of note that the highly alkaline condition can hydrolyze all ester-linked lipids, in this respect, not only phospholipids, but also other glycerol lipids, such as triacylglycerols are also being hydrolyzed. Because of this, elimination of most interferents and consequently, reduced analytical background greatly improved sensitivity in detection of low abundant glycolipids in complex biological samples. Thus, permethylation offers a quick, one-step sample preparation for analysis of glycolipids starting from crude, total lipids extract.

#### **Effect of isotopic impurity on the overall quantification accuracy**

To demonstrate the quantitative aspects of this method, we prepared a mixture of known glycolipids, including GlcCer d18:1/18:0, LacCer d18:1/18:0, Gb3Cer d18:1/18:0, and Gb4Cer

d18:1/18:0, permethylated either with  $^{12}\text{CH}_3\text{I}$  or  $^{13}\text{CH}_3\text{I}$  and pooled at various ratios, namely 1:1, 1:3, 1:5, and 1:10 ( $^{13}\text{C}/^{12}\text{C}$ -) in triplicate experiments. Across the different glycolipids tested, a more accurate quantification at the chromatogram level showed that the observed ratio between the  $^{13}\text{CH}_3$ - and  $^{12}\text{CH}_3$ -labeled is slightly higher than the theoretical ratio (**Fig. 40B**), implying the effect of trace amounts of  $^{12}\text{CH}_3\text{I}$  present in the  $^{13}\text{CH}_3\text{I}$  reagent. This is further illustrated in the resulting spectra of  $^{13}\text{C}$ -permethylation products (**Fig. 40A**) where peaks that are one and two  $m/z$  units lower than the monoisotopic peaks are apparent. This was verified using *in silico* simulation of natural isotopic distribution pattern of the expected products as well as the various isotopomers that resulted from  $^{12}\text{CH}_3\text{I}$  as impurities in the  $^{13}\text{CH}_3\text{I}$  reagent (**Supplemental Fig. S18**). Using the sum of the natural relative abundances of both  $^{12}\text{C}$  and  $^{13}\text{C}$  isotopic clusters as correction factor, we calculated the ratio (**Supplemental Fig. S18**) and found significant improvement in accuracy in all glycolipids tested (**Fig. 40B**) compared with using the monoisotopic peak alone. It is of note that excellent linear correlation between expected and theoretical ratios still holds even without using correction (**Supplemental Fig. S19**). Our observation is consistent with the work done by Alvarez-Manilla and colleagues for permethylated glycans<sup>206</sup> where they recommended the use of the sum of isotopic peaks to improve accuracy. Thus, isotopic correction factor should be applied to improve the accuracy of measurements for permethylated glycoconjugates.

### **Linearity and reproducibility of the method**

After correction, as shown in **Supplemental Table S3**, for GlcCer d18:1/18:0, the experimental ratios displayed very close to the four theoretical ratios with coefficient of variation (CV) of <2%. For LacCer d18:1/18:0, CV is <3.5%. More complex glycolipids Gb3Cer d18:1/18:0 and Gb4Cer d18:1/18:0 gave slightly larger CV of <5.5%. Generally, all standard glycolipids tested gave <5.5% CV. Our results provided more reproducible results when compared to similar work by others<sup>206,207</sup>, where permethylation was applied for relative

quantification of released glycans from glycoproteins using MALDI and ESI. Taken together, this illustrates that the coupling of RPLC to ESI-MS offers higher level of accuracy and reproducibility for the relative quantification of permethylated glycolipids.

#### **Application of differential isotope permethylation to profile glycolipid changes in CBE-treated murine macrophage cells**

To further demonstrate the utility of this technique in profiling glycolipids in biological samples (**Fig. 41A**), we used a cell culture model system by inhibiting the breakdown of neutral glycolipids using CBE, a highly specific inhibitor of lysosomal  $\beta$ -glucocerebrosidase<sup>347,348</sup>. This enzyme is involved in the catabolism of glucocerebrosides, thus inhibition of this enzyme results to accumulation of this type of glycolipids (**Fig. 41B**). Gaucher's disease, the pathological condition associated with the inhibition of this enzyme, is characterized by the buildup of glucocerebrosides in various cells such as macrophages<sup>349</sup>. To investigate the temporal changes of glycolipids during inhibition of  $\beta$ -glucocerebrosidase activity, RAW 264.7 cells were treated with 100  $\mu$ M CBE at different exposure times (3h, 6h, 12h, 48h, 72h). For biological and quality control purposes, a negative control (untreated cells) and reagent blank (cell-free) were co-incubated with the treated cells. We confirmed from cell viability and  $\beta$ -glucocerebrosidase inhibition assays that treatment was successful indicating no change in cell viability within the duration of the experiment, and that the target enzyme was inhibited progressively with increasing incubation time (**Supplemental Fig. S21A-B**). This agrees with earlier works that used similar approach<sup>347,350</sup>.

After treatment, cells were scraped off, lysed and an aliquot from each sample was pooled together. The total lipid extract from each individual sample, after normalizing by protein content, were permethylated using  $^{12}\text{CH}_3\text{I}$ , while the pooled sample was permethylated using

$^{13}\text{CH}_3\text{I}$  to serve as internal standard. The  $^{13}\text{C}$ -permethylated pooled sample was spiked in equal amounts to each of the individual samples and analyzed by RPLC-MS/MS (**Fig. 41A**). Target list of glycolipids was based on previous lipidomics work<sup>351,352</sup> on the same cell line as well as additional species theoretically expected based on the existing knowledge on sphingolipids<sup>3</sup>. Peak areas were extracted using TraceFinder software and were used for calculation of  $^{12}\text{C}/^{13}\text{C}$  ratios. To ensure the high quality of the data, only those peaks that met the following criteria were considered: 1) contain both expected masses of  $^{12}\text{C}$  and  $^{13}\text{C}$ -permethylated glycolipids and coelute; 2) the fully  $^{12}\text{C}$ -labeled glycolipid should be absent both in  $^{13}\text{C}$ -permethylated sample injected alone and in the reagent blank; 3) matched with the retention time of a permethylated commercial standard (if available); 4) MS/MS fragmentation contains diagnostic ions. For example, to annotate the peak at 8.60 min in the RAW264.7 cells, the retention time was matched with the permethylated standard LacCer $d_{18:1/18:0}$  as well as accurate mass (**Supplemental Fig. S22A**). Under this chromatographic peak, both the expected [ $^{12}\text{C}_9$ ] and [ $^{13}\text{C}_9$ ] products were present and that [ $^{12}\text{C}_9$ ] peak was absent in reagent blank and in [ $^{13}\text{C}$ ] pooled sample (**Supplemental Fig. S22B-C**). Because our method could not distinguish epimeric hexoses, this peak was annotated as Hex $_2$ Cer $d_{18:1/18:0}$  after inspecting MS/MS fragmentation. Indeed, this species showed significant accumulation after 72h of treatment, compared with negative control (**Supplemental Fig. S23C**).

In total, we identified 40 glycolipid species excluding potential isomers that could not be independently quantified due to their coelution in RPLC-MS, and tracked their time-dependent accumulation in response to CBE treatment (examples are shown in **Supplemental Fig. S23**). Overall, monohexosylceramides and dihexosylceramides levels increased with prolonged incubation times with CBE because of attenuated  $\beta$ -glucocerebrosidase activity<sup>347</sup>. On the other

hand, the more complex glycolipids which result from successive glycosylation downstream of the metabolic pathway (Fig. 41B) such as Hex<sub>3</sub>HexNAcCer species appeared unaffected by the treatment (Supplemental Fig. S23D).

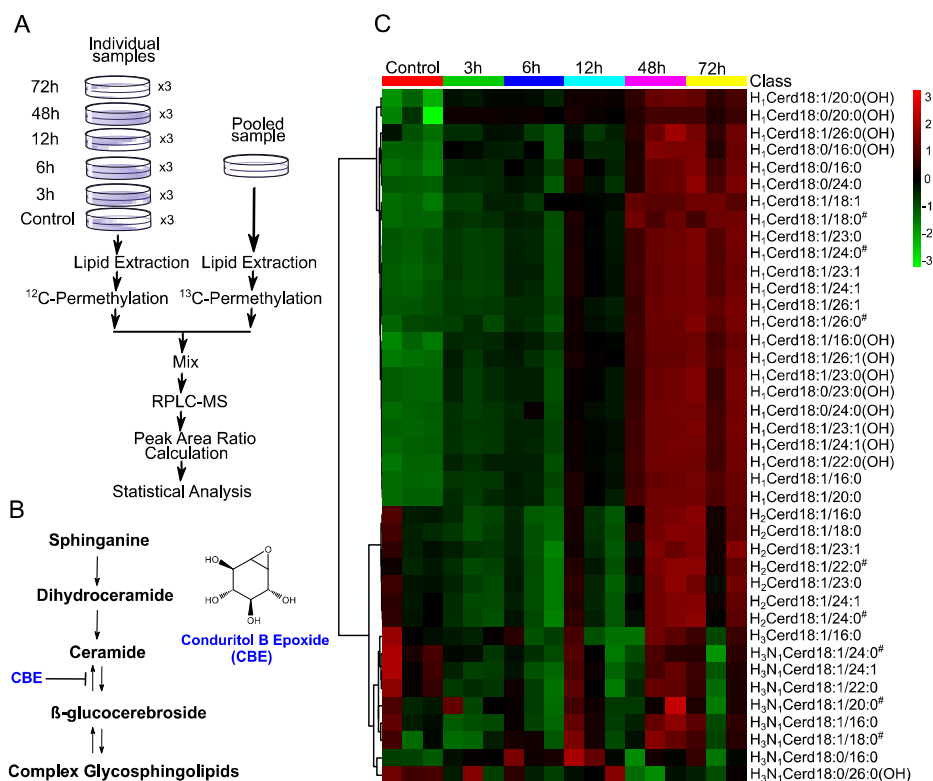


**Figure 41. Accumulation of Glycolipids in CBE-Treated RAW264.7 Cells.** A) Schematic of the methodology as detailed in the experimental section. Briefly, individual samples (normalized to protein content) are permethylated using <sup>12</sup>CH<sub>3</sub>I and a pooled aliquot of each sample is permethylated using <sup>13</sup>CH<sub>3</sub>I to serve as internal standard. The <sup>13</sup>C-labeled pooled sample is spiked to each of the individual samples and analyzed by RPLC-MS or MS/MS. Peak areas corresponding to <sup>12</sup>C and <sup>13</sup>C target analytes are measured and the ratios calculated are used for downstream statistical analysis. B) Overview of the mammalian glycosphingolipid metabolism showing the important step catalyzed by β-glucocerebrosidase and its well-known inhibitor, conduritol B epoxide (CBE). Calculated peak area ratios of target glycolipids were used for downstream statistical analyses using MetaboAnalyst 4.0. C) Overview of the changes in the relative levels of glycolipids across different treatment times. Glycolipid annotations were abbreviated as H: hexosyl, and N: N-acetylhexosamine; #: potential isomers non-resolvable by RPLC could be present. The detailed dataset is shown in Supplemental Table S6.

This could be attributed to CBE inhibitor's specificity to  $\beta$ -glucocerebrosidase, as previously demonstrated<sup>348</sup>. Multivariate statistical analyses of all the annotated glycolipids using PCA (**Supplemental Fig. S22D**) and One-way ANOVA (**Supplemental Fig. S22E & Supplemental Table S6**) indicate clear distinction of treated versus control groups and that 30 out of 40 species were significantly changed, respectively. These results are even clearer when presented as a heatmap (**Fig. 41C**) where there is a time-dependent increase of glycolipid levels following the duration of CBE treatment.

Previous works utilizing isotopic permethylation for glycomics<sup>206,207</sup> have mainly focused on direct infusion analysis and on comparing two different samples at a time therefore, comparison of multiple samples is not straightforward. Our approach of using a pooled sample labeled with <sup>13</sup>C to serve as internal standard has allowed the straightforward comparison of multiple samples (shown in our RAW264.7 cells,  $n=21$ ). This highlights the practical utility of this approach in facilitating the analysis of glycolipids in multiple samples. In summary, these results showcase the usefulness of this approach as a simple way for relative quantification of glycolipids in mammalian cells.

## **Conclusion**

In this work, we presented a strategy for relative quantification of intact neutral glycolipids using differential isotope labeling by permethylation and RPLC-MS. The increased ionization efficiency, chromatographic focusing and separation ability via RPLC, as well as analytical background reduction by elimination of major ester-linked lipids during the permethylation process will allow more sensitive determination of low abundant glycosphingolipid species. This work also addressed the limited availability of isotopically labeled internal standards by using a pooled sample labeled with heavy isotope to serve as omnipresent internal standard. The systematic mass shifts of the MS/MS fragments of

differentially labeled glycolipids allow more confident structural characterization of permethylated species. Finally, we successfully demonstrated the ability of this method to both identify and quantify the changes in glycolipid profile in mammalian cells. Taken together, this method has potential applications in evaluating the effect of inhibitors on enzymes involved in glycolipid metabolism, in comparison of cells from different pathological conditions, and could also be extended to analysis of neutral glycolipids from different sample matrices other than cells. It is of note that this method may also be applied to other glycosphingolipids, such as gangliosides, however, optimization of reaction conditions is suggested in order to achieve full permethylation.

#### **Acknowledgment**

This work was partially supported by grants from the National Institute of General Medical Sciences (R21 GM104678) of the National Institutes of Health. The authors are also grateful for Dr. Guan-yuan Chen and Dr. Liuyi Hao for technical assistance.

## CHAPTER VII

### CONCLUDING REMARKS

The methodologies developed in this dissertation addressed the fundamental issues in intact glycolipids analysis. Chapter III explored the application of OzID-MS to pinpoint the location of carbon-carbon double bonds in intact, unsaturated glycolipids. The differential reactivity observed between double bonds in different locations afforded the straightforward differentiation of long chain base and fatty acyl unsaturation. This method revealed isomeric and isobaric species that would otherwise be non-distinguishable with current existing MS approaches. Furthermore, while lithiated and sodiated adducts did not reveal the composition of glycan head group, the use of protonated adducts provided hints on the structure of the glycan sequence. Chapter IV provided theoretical foundations to rationalize the observed unique behavior of protonated glycolipids in OzID-MS compared to the metal cationized congeners.

Chapter V described the development and application of a novel isobaric labeling strategy for multiplexed quantification of intact gangliosides using RPLC-MS/MS. Using chemoselective oxidation, attachment of aldehyde-reactive isobaric tag was achieved and enabled the analysis of up to six samples in one RPLC-MS/MS injection. The increased hydrophobicity of the labeled gangliosides afforded at least ~40-fold enhancement in sensitivity and allowed the sequencing of the glycan headgroup and identifying the composition of the lipid tail in a single MS/MS spectrum. While helpful for gangliosides, this method failed when extending to non-sialic acid containing glycolipids. This was addressed in Chapter VI via differential isotope labeling method that exploits permethylation using light and heavy isotope-labeled methyl iodide

This method also successfully demonstrated the use of pooled sample as universal internal standards for glycolipid analysis providing excellent reproducibility and sensitivity.

Taken together, the innovative methods presented here showcased the power and flexibility of MS to uncover the complexity of glycolipids. Moving forward, as these tools become increasingly adapted, databases, especially for isobaric labeled and permethylated glycolipids would be greatly needed. The ability to enhance detectability, facilitate structural analysis, and improve quantification of glycolipids in its intact, native form will unlock exciting future applications in life science research.

## REFERENCES

- (1) Marx, V. *Nature Methods* **2017**, *14*, 667.
- (2) National Research Council . Committee on Assessing the, I.; Impact of, G.; Glycosciences. National Academies Press: Washington, D.C., 2012.
- (3) Merrill, A. H. *Chem. Rev.* **2011**, *111*, 6387–6422.
- (4) Hakomori, S. *Proc. Nat. Acad. Sci. USA* **2002**, *99*, 225-232.
- (5) Lingwood, C. A. *Cold Spring Harb. Perspect. Biol.* **2011**, *3*, a004788.
- (6) Hakomori, S. *Glycoconj. J.* **2000**, *17*, 627-647.
- (7) Hakomori, S.-i. *Biochim. Biophys. Acta* **2008**, *1780*, 325-346.
- (8) D'Angelo, G.; Capasso, S.; Sticco, L.; Russo, D. *FEBS J.* **2013**, *280*, 6338-6353.
- (9) Barrientos, R. C.; Vu, N.; Zhang, Q. *J. Am. Soc. Mass Spectrom.* **2017**, *28*, 2330-2343.
- (10) Brown, S. H. J.; Mitchell, T. W.; Blanksby, S. J. *Bioch. Biophys. Acta Mol. Cell Biol. Lipids* **2011**, *1811*, 807-817.
- (11) Thomas, M. C.; Mitchell, T. W.; Harman, D. G.; Deeley, J. M.; Nealon, J. R.; Blanksby, S. J. *Anal. Chem.* **2008**, *80*, 303-311.
- (12) Vu, N.; Brown, J.; Giles, K.; Zhang, Q. *Rapid Commun. Mass Spectrom.* **2017**, *31*, 1415-1423.
- (13) Atwood, J. A.; Cheng, L.; Alvarez-Manilla, G.; Warren, N. L.; York, W. S.; Orlando, R. J. *Proteome Res.* **2008**, *7*, 367-374.
- (14) Hermanson, G. T. *Bioconjugate Techniques (3)*; Academic Press: San Diego, US, 2013.
- (15) Farwanah, H.; Kolter, T. *Metabolites* **2012**, *2*, 134-164.
- (16) Schnaar, R. L.; Kinoshita, T. In *Essentials of Glycobiology*, Varki, A.; Cummings, R. D.; Esko, J. D.; Stanley, P.; Hart, G. W.; Aebi, M.; Darvill, A. G.; Kinoshita, T.; Packer, N. H.; Prestegard, J. H.; Schnaar, R. L.; Seeberger, P. H., Eds.; Cold Spring Harbor Laboratory Press: Cold Spring Harbor (NY), 2015, pp 125-135.
- (17) Thudichum, J. L. W. *A treatise on the chemical constitution of the brain*; Bailliere, Tindall and Cox: London, 1884.
- (18) Levery, S. B. *Methods Enzymol.* **2005**, *405*, 300-369.
- (19) Blanksby, S. J.; Mitchell, T. W. *Annual Review of Analytical Chemistry* **2010**, *3*, 433-465.
- (20) Haynes, C. A.; Allegood, J. C.; Park, H.; Sullards, M. C. *J. Chromatogr. B* **2009**, *877*, 2696-2708.
- (21) Farwanah, H.; Kolter, T.; Sandhoff, K. *Biochimica et Biophysica Acta (BBA) - Molecular and Cell Biology of Lipids* **2011**, *1811*, 854-860.
- (22) Varki, A.; Cummings, R.; Esko, J. *Essentials of Glycobiology 2nd Edition*; Cold Spring Harbor Laboratory Press: Cold Spring Harbor, New York, 2009.
- (23) Fahy, E.; Subramaniam, S.; Murphy, R. C., *et al.* *J. Lipid Res.* **2009**, *50 Suppl*, S9-14.
- (24) Spassieva, S.; Bieberich, E. *J. Neurosci. Res.* **2016**, *94*, 974-981.
- (25) Schnaar, R. L.; Gerardy-Schahn, R.; Hildebrandt, H. *Physiol. Rev.* **2014**, *94*, 461–518.
- (26) Takahashi, T.; Suzuki, T. *J. Lipid Res.* **2012**, *53*, 1437-1450.
- (27) Wennekes, T.; van den Berg, R. J. B. H. N.; Boot, R. G.; van der Marel, G. A.; Overkleeft, H. S.; Aerts, J. M. F. G. *Angew. Chem. Int. Ed.* **2009**, *48*, 8848-8869.

- (28) Sandhoff, R.; Sandhoff, K. *FEBS Lett.* **2018**, *592*, 3835-3864.
- (29) Xu, Y. H.; Barnes, S.; Sun, Y.; Grabowski, G. A. *J. Lipid Res.* **2010**, *51*, 1643-1675.
- (30) Svennerholm, L. *J. Lipid Res.* **1964**, *5*, 145-155.
- (31) *Eur. J. Biochem.* **1998**, *257*, 293-298.
- (32) De Libero, G.; Mori, L. *FEBS Lett.* **2006**, *580*, 5580-5587.
- (33) Porubsky, S.; Speak, A. O.; Salio, M., *et al.* *Journal of immunology (Baltimore, Md. : 1950)* **2012**, *189*, 3007-3017.
- (34) Garcia-Ruiz, C.; Morales, A.; Fernández-Checa, J. C. *Apoptosis* **2015**, *20*, 607-620.
- (35) Iwabuchi, K.; Nakayama, H.; Oizumi, A.; Suga, Y.; Ogawa, H.; Takamori, K. *Mediators of Inflammation* **2015**, *2015*, 120748.
- (36) Kiarash, A.; Boyd, B.; Lingwood, C. A. *J. Biol. Chem.* **1994**, *269*, 11138-11146.
- (37) Zamfir, A. D. In *Advancements of Mass Spectrometry in Biomedical Research*, Woods, A. G.; Darie, C. C., Eds.; Springer International Publishing: Cham, 2014, pp 153-204.
- (38) Sandhoff, K.; Harzer, K. *The Journal of Neuroscience* **2013**, *33*, 10195-10208.
- (39) Zhuo, D.; Li, X.; Guan, F. *Frontiers in physiology* **2018**, *9*, 466-466.
- (40) Carreno, L. J.; Saavedra-Avila, N. A.; Porcelli, S. A. *Clin Trans Immunol* **2016**, *5*, e69.
- (41) Durrant, L. G.; Noble, P.; Spendlove, I. *Clinical and experimental immunology* **2012**, *167*, 206-215.
- (42) Tyler, A.; Johansson, A.; Karlsson, T.; Gudey, S. K.; Brännström, T.; Grankvist, K.; Behnam-Motlagh, P. *Experimental Cell Research* **2015**, *336*, 23-32.
- (43) Folch, J.; Lees, M.; Sloane Stanley, G. H. *J. Biol. Chem.* **1957**, *226*, 497-509.
- (44) Li, Y.; Zhou, D.; Xia, C.; Wang, P. G.; Levery, S. B. *Glycobiology* **2008**, *18*, 166-176.
- (45) Kolter, T. *ISRN biochemistry* **2012**, *2012*, 506160.
- (46) Nakajima, K.; Akiyama, H.; Tanaka, K.; Kohyama-Koganeya, A.; Greimel, P.; Hirabayashi, Y. *J. Chromatogr. B* **2016**, *1031*, 146-153.
- (47) Pham, H. T.; Julian, R. R. *The Analyst* **2016**, *141*, 1273-1278.
- (48) Kirsch, S.; Muthing, J.; Peter-Katalinic, J.; Bindila, L. *Biol. Chem.* **2009**, *390*, 657-672.
- (49) Boutin, M.; Sun, Y.; Shacka, J. J.; Auray-Blais, C. *Anal. Chem.* **2016**, *88*, 1856-1863.
- (50) Hanamatsu, H.; Nishikaze, T.; Miura, N., *et al.* *Anal. Chem.* **2018**, *90*, 13193-13199.
- (51) Brennan, P. J.; Cheng, T.-Y.; Pellicci, D. G., *et al.* *Proceedings of the National Academy of Sciences* **2017**, *114*, 8348-8353.
- (52) Quehenberger, O.; Dennis, E. A. *The New England journal of medicine* **2011**, *365*, 1812-1823.
- (53) Guo, X.; Lankmayr, E. *Bioanalysis* **2011**, *3*, 349-352.
- (54) Kaneko, T.; Tsubakihara, Y.; Fushimi, H., *et al.* *Clin. Exp. Nephrol.* **2015**, *19*, 403-410.
- (55) Zhang, Y.; Wang, J.; Liu, J. a.; Han, J.; Xiong, S.; Yong, W.; Zhao, Z. *Scientific reports* **2016**, *6*, 25289.
- (56) Kanda, T.; Ariga, T.; Kubodera, H., *et al.* *J. Neurosci. Res.* **2004**, *78*, 141-150.
- (57) Lam, S. M.; Wang, Y.; Duan, X., *et al.* *Neurobiology of aging* **2014**, *35*, 2369-2381.
- (58) Valdes-Gonzalez, T.; Goto-Inoue, N.; Hirano, W.; Ishiyama, H.; Hayasaka, T.; Setou, M.; Taki, T. *J. Neurochem.* **2011**, *116*, 678-683.
- (59) Mlinac, K.; Fabris, D.; Vukelic, Z.; Rozman, M.; Heffer, M.; Bogner, S. K. *Carbohydr. Res.* **2013**, *382*, 1-8.
- (60) Bian, L.; Yang, J.; Sun, Y. *Biomed. Chromatogr.* **2015**, *29*, 1604-1611.
- (61) Chan, R. B.; Oliveira, T. G.; Cortes, E. P., *et al.* *J. Biol. Chem.* **2012**, *287*, 2678-2688.
- (62) Sato, Y.; Bernier, F.; Suzuki, I.; Kotani, S.; Nakagawa, M.; Oda, Y. *J. Lipid. Res.* **2013**, *54*, 2687-2696.

- (63) Moyano, A. L.; Li, G.; Lopez-Rosas, A.; Mansson, J. E.; van Breemen, R. B.; Givogri, M. I. *Anal. Biochem.* **2014**, *467*, 31-39.
- (64) Schnaar, R. L. *J. Mol. Biol.* **2016**, *428*, 3325-3336.
- (65) Zamfir, A. D.; Serb, A.; Vukeli, Z., *et al.* *J. Am. Soc. Mass. Spectrom.* **2011**, *22*, 2145-2159.
- (66) Barone, A.; Benktander, J.; Teneberg, S.; Breimer, M. E. *Xenotransplantation* **2014**, *21*, 510-522.
- (67) Beausoleil, H. E.; Lepine, F.; Dubreuil, J. D. *FEMS Microbiol. Lett.* **2002**, *209*, 183-188.
- (68) Joo, E. J.; Weyers, A.; Li, G., *et al.* *Omics* **2014**, *18*, 231-241.
- (69) Holst, S.; Stavenhagen, K.; Balog, C. I., *et al.* *Molecular & cellular proteomics : MCP* **2013**, *12*, 3081-3093.
- (70) Ruh, H.; Sandhoff, R.; Meyer, B.; Gretz, N.; Hopf, C. *Anal. Chem.* **2013**, *85*, 6233-6240.
- (71) Marsching, C.; Jennemann, R.; Heilig, R.; Grone, H. J.; Hopf, C.; Sandhoff, R. *J. Lipid Res.* **2014**, *55*, 2343-2353.
- (72) Brush, R. S.; Tran, J.-T. A.; Henry, K. R.; McCellan, M. E.; Elliott, M. H.; Mandal, M. N. A. *Invest Ophthalmol Vis Sci. Data* **2010**, *51*, 4422-4431.
- (73) Liu, Y.; Chen, Y.; Momin, A., *et al.* *Mol Cancer* **2010**, *9*, 186.
- (74) Rajanayake, K. K.; Taylor, W. R.; Isailovic, D. *Carbohydr. Res.* **2016**, *431*, 6-14.
- (75) Yang, L.; Cui, X.; Zhang, N., *et al.* *Anal Bioanal Chem* **2015**, *407*, 5065-5077.
- (76) Stimmer, L.; Dehay, S.; Nemati, F., *et al.* *BMC Cancer* **2014**, *14*, 916.
- (77) Liang, Y. J.; Ding, Y.; Levery, S. B.; Lobaton, M.; Handa, K.; Hakomori, S. I. *Proc Natl Acad Sci U S A* **2013**, *110*, 4968-4973.
- (78) Zhu, T.; Xu, L.; Xu, X., *et al.* *Carbohydr. Res.* **2015**, *402*, 189-199.
- (79) Sarbu, M.; Robu, A. C.; Ghiulai, R. M.; Vukelić, Ž.; Clemmer, D. E.; Zamfir, A. D. *Anal. Chem.* **2016**, *88*, 5166-5178.
- (80) Ghiulai, R. M.; Sarbu, M.; Vukelić, Ž.; Ilie, C.; Zamfir, A. D. *Glycoconjugate J.* **2014**, *31*, 231-245.
- (81) Podbielska, M.; Dasgupta, S.; Levery, S. B.; Tourtellotte, W. W.; Annuk, H.; Moran, A. P.; Hogan, E. L. *J. Lipid Res.* **2010**, *51*, 1394-1406.
- (82) Moyano, A. L.; Pituch, K.; Li, G.; van Breemen, R.; Mansson, J. E.; Givogri, M. I. *J. Neurochem.* **2013**, *127*, 600-604.
- (83) Moyano, A. L.; Li, G.; Boullerne, A. I.; Feinstein, D. L. **2016**, *94*, 1579-1587.
- (84) Mirzaian, M.; Kramer, G.; Poorthuis, B. J. *J. Lipid Res.* **2015**, *56*, 936-943.
- (85) Furukawa, J.; Sakai, S.; Yokota, I., *et al.* *J. Lipid Res.* **2015**, *56*, 2399-2407.
- (86) Tiphara, P.; Thongboonkerd, V. In *Lipidomics in Health & Disease: Methods & Application*, Wang, X.; Wu, D.; Shen, H., Eds.; Springer Singapore: Singapore, 2018, pp 97-111.
- (87) Barcenas, M.; Suhr, T. R.; Scott, C. R.; Turecek, F.; Gelb, M. H. *Clin. Chim. Acta* **2014**, *433*, 39-43.
- (88) Lydic, T. A.; Busik, J. V.; Reid, G. E. *J. Lipid Res.* **2014**, *55*, 1797-1809.
- (89) Bligh, E. G.; Dyer, W. J. *Canadian Journal of Biochemistry and Physiology* **1959**, *37*, 911-917.
- (90) Löfgren, L.; Forsberg, G.-B.; Ståhlman, M. *Sci. Rep.* **2016**, *6*, 27688.
- (91) Yin, B.; Hawke, D.; Zhou, D. *Journal of visualized experiments : JoVE* **2013**, 10.3791/4224.
- (92) Gregson, N. A. In *Biomembrane Protocols: I. Isolation and Analysis*, Graham, J. M.; Higgins, J. A., Eds.; Humana Press: Totowa, NJ, 1993, pp 287-301.
- (93) Schnaar, R. L. In *Methods Enzymol.*; Academic Press, 1994, pp 348-370.
- (94) Svennerholm, L.; Fredman, P. *Biochim. Biophys. Acta* **1980**, *617*, 97-109.
- (95) Schwarz, A.; Terstappen, G. C.; Futerman, A. H. *Anal. Biochem.* **1997**, *254*, 221-225.

- (96) Svennerholm, L.; Thorin, H. *J. Lipid Res.* **1962**, *3*, 483-485.
- (97) Hara, A.; Radin, N. S. *Anal. Biochem.* **1979**, *100*, 364-370.
- (98) Spacil, Z.; Babu Kumar, A.; Liao, H. C., *et al.* *Clin. Chem.* **2016**, *62*, 279-286.
- (99) Radin, N. S. *J. Lipid Res.* **1976**, *17*, 290-293.
- (100) Schnaar, R. L.; Needham, L. K. In *Methods Enzymol.*; Academic Press, 1994, pp 371-389.
- (101) Bodennec, J.; Koul, O.; Aguado, I.; Brichon, G.; Zwingelstein, G.; Portoukalian, J. *J. Lipid Res.* **2000**, *41*, 1524-1531.
- (102) Mirzaian, M.; Wisse, P.; Ferraz, M. J., *et al.* *Blood Cells, Molecules, and Diseases* **2015**, *54*, 307-314.
- (103) Noda, A.; Kato, M.; Miyazaki, S.; Kyogashima, M. *Glycoconjugate J.* **2018**, *35*, 493-498.
- (104) Nagahori, N.; Abe, M.; Nishimura, S.-I. *Biochemistry* **2009**, *48*, 583-594.
- (105) Anugraham, M.; Everest-Dass, A. V.; Jacob, F.; Packer, N. H. *Rapid Commun. Mass Spectrom.* **2015**, *29*, 545-561.
- (106) Albrecht, S.; Vainauskas, S.; Stöckmann, H.; McManus, C.; Taron, C. H.; Rudd, P. M. *Anal. Chem.* **2016**, *88*, 4795-4802.
- (107) Arigi, E.; Blixt, O.; Buschard, K.; Clausen, H.; Levery, S. B. *Glycoconjugate J.* **2012**, *29*, 1-12.
- (108) Nabetani, T.; Makino, A.; Hullin-Matsuda, F., *et al.* *J. Lipid Res.* **2011**, *52*, 1294-1302.
- (109) Song, X.; Ju, H.; Lasanajak, Y.; Kudelka, M. R.; Smith, D. F.; Cummings, R. D. *Nat Meth* **2016**, *13*, 528-534.
- (110) Furukawa, J.-i.; Shinohara, Y.; Kuramoto, H., *et al.* *Anal. Chem.* **2008**, *80*, 1094-1101.
- (111) Fujitani, N.; Takegawa, Y.; Ishibashi, Y., *et al.* *J. Biol. Chem.* **2011**, *286*, 41669-41679.
- (112) Zaia, J. *Chemistry & Biology* **2008**, *15*, 881-892.
- (113) Wuhrer, M. *Glycoconjugate J.* **2013**, *30*, 11-22.
- (114) Kailemia, M. J.; Ruhaak, L. R.; Lebrilla, C. B.; Amster, I. J. *Anal. Chem.* **2014**, *86*, 196-212.
- (115) Dell, A. In *Adv. Carbohydr. Chem. Biochem.*, Tipson, R. S.; Horton, D., Eds.; Academic Press, 1987, pp 19-72.
- (116) Farwanah, H.; Wirtz, J.; Kolter, T.; Raith, K.; Neubert, R. H. H.; Sandhoff, K. *J. Chromatogr. B* **2009**, *877*, 2976-2982.
- (117) Delobel, A.; Roy, S.; Touboul, D., *et al.* *J. Mass Spectrom.* **2006**, *41*, 50-58.
- (118) Wilm, M. *Molecular & Cellular Proteomics* **2011**, *10*.
- (119) Cech, N. B.; Enke, C. G. *Mass Spectrom. Rev.* **2001**, *20*, 362-387.
- (120) Ikeda, K.; Taguchi, R. *Rapid Commun. Mass Spectrom.* **2010**, *24*, 2957-2965.
- (121) Hillenkamp, F.; Karas, M. In *MALDI MS*; Wiley-VCH Verlag GmbH & Co. KGaA, 2007, pp 1-28.
- (122) Harvey, D. J. *Mass Spectrom. Rev.* **1999**, *18*, 349-451.
- (123) Harvey, D. J. *Mass Spectrom. Rev.* **2006**, *25*, 595-662.
- (124) Harvey, D. J. *Mass Spectrom. Rev.* **2012**, *31*, 183-311.
- (125) Harvey, D. J. *Mass Spectrom. Rev.* **2015**, *34*, 268-422.
- (126) O'Connor, P. B.; Mirgorodskaya, E.; Costello, C. E. *J. Am. Soc. Mass. Spectrom.* **2002**, *13*, 402-407.
- (127) Zhang, J.; LaMotte, L.; Dodds, E. D.; Lebrilla, C. B. *Anal. Chem.* **2005**, *77*, 4429-4438.
- (128) Harvey, D. J. *J. Chromatogr. B* **2011**, *879*, 1196-1225.
- (129) Torretta, E.; Fania, C.; Vasso, M.; Gelfi, C. *ELECTROPHORESIS* **2016**, *37*, 2036-2049.
- (130) Harvey, D. J.; Scarff, C. A.; Crispin, M.; Scanlan, C. N.; Bonomelli, C.; Scrivens, J. H. *J. Am. Soc. Mass Spectrom.* **2012**, *23*, 1955-1966.

- (131) Zarei, M.; Kirsch, S.; Muthing, J.; Bindila, L.; Peter-Katalinic, J. *Anal Bioanal Chem* **2008**, *391*, 289-297.
- (132) Caughlin, S.; Hepburn, J. D.; Park, D. H.; Jurcic, K.; Yeung, K. K. C.; Cechetto, D. F.; Whitehead, S. N. *PLOS ONE* **2015**, *10*, e0130364.
- (133) Ruh, H.; Salonikios, T.; Fuchser, J., *et al. J. Lipid Res.* **2013**, *54*, 2785-2794.
- (134) Chen, Y.; Allegood, J.; Liu, Y., *et al. Anal. Chem.* **2008**, *80*, 2780-2788.
- (135) Karlsson, O.; Michno, W.; Ransome, Y.; Hanrieder, J. *Biochimica et Biophysica Acta (BBA) - Proteins and Proteomics.*
- (136) Vens-Cappell, S.; Kouzel, I. U.; Ketting, H., *et al. Anal. Chem.* **2016**, *88*, 5595-5599.
- (137) Kouzel, I. U.; Soltwisch, J.; Pohlentz, G.; Schmitz, J. S.; Karch, H.; Dreisewerd, K.; Muthing, J. *Int. J. Mass spectrom.*
- (138) Norris, J. L.; Caprioli, R. M. *Chem. Rev.* **2013**, *113*, 2309-2342.
- (139) He, H.; Emmett, M. R.; Nilsson, C. L.; Conrad, C. A.; Marshall, A. G. *Int. J. Mass spectrom.* **2011**, *305*, 116-119.
- (140) Schwartz, J.; Syka, J.; Quarmby, S. *San Antonio, Texas* **2005**.
- (141) Domon, B.; Costello, C. *Glycoconjugate J.* **1988**, *5*, 397-409.
- (142) Ann, Q.; Adams, J. *Anal. Chem.* **1993**, *65*, 7-13.
- (143) Masson, E. A.; Sibille, E.; Martine, L.; Chaux-Picquet, F.; Bretillon, L.; Berdeaux, O. *J. Lipid Res.* **2015**, *56*, 1821-1835.
- (144) Peng, B.; Weintraub, S. T.; Coman, C., *et al. Anal. Chem.* **2017**, *89*, 12480-12487.
- (145) Barrientos, R. C.; Zhang, Q. *Anal. Chem.* **2018**, *90*, 2578-2586.
- (146) Haynes, C. A.; Allegood, J. C.; Park, H.; Sullards, M. C. *J Chromatogr B Analyt Technol Biomed Life Sci* **2009**, *877*, 2696-2708.
- (147) Qi, Y.; Volmer, D. A. *Mass Spectrom. Rev.* **2017**, *36*, 4-15.
- (148) Fort, K. L.; Cramer, C. N.; Voinov, V. G.; Vasil'ev, Y. V.; Lopez, N. I.; Beckman, J. S.; Heck, A. J. R. *Journal of proteome research* **2018**, *17*, 926-933.
- (149) Kim, M.-S.; Pandey, A. *Proteomics* **2012**, *12*, 530-542.
- (150) McFarland, M. A.; Marshall, A. G.; Hendrickson, C. L.; Nilsson, C. L.; Fredman, P.; Månsson, J.-E. *J. Am. Soc. Mass. Spectrom.* **2005**, *16*, 752-762.
- (151) O'Brien, J. P.; Brodbelt, J. S. *Anal. Chem.* **2013**, *85*, 10399-10407.
- (152) Reilly, J. P. *Mass Spectrom. Rev.* **2009**, *28*, 425-447.
- (153) Ryan, E.; Nguyen, C. Q. N.; Shiea, C.; Reid, G. E. *J. Am. Soc. Mass. Spectrom.* **2017**, *28*, 1406-1419.
- (154) Lee, H.; Lerno, L. A., Jr.; Choe, Y., *et al. Anal. Chem.* **2012**, *84*, 5905-5912.
- (155) Ikeda, K.; Shimizu, T.; Taguchi, R. *J. Lipid Res.* **2008**, *49*, 2678-2689.
- (156) Kruger, R.; Bruns, K.; Grunhage, S.; Rossmann, H.; Reinke, J.; Beck, M.; Lackner, K. J. *Clin Chem Lab Med* **2010**, *48*, 189-198.
- (157) Ikeda, K.; Taguchi, R. *Rapid Comm. Mass Spectrom.* **2010**, *24*, 2957-2965.
- (158) Oedit, A.; Vulto, P.; Ramautar, R.; Lindenburg, P. W.; Hankemeier, T. *Curr. Opin. Biotechnol.* **2015**, *31*, 79-85.
- (159) Feng, X.; Liu, B.-F.; Li, J.; Liu, X. *Mass Spectrom. Rev.* **2015**, *34*, 535-557.
- (160) Sarbu, M.; Zamfir, A. D. In *Nanoparticles' Promises and Risks: Characterization, Manipulation, and Potential Hazards to Humanity and the Environment*, Lungu, M.; Neculae, A.; Bunoiu, M.; Biris, C., Eds.; Springer International Publishing: Cham, 2015, pp 137-165.
- (161) Kirsch, S.; Bindila, L. *Bioanalysis* **2009**, *1*, 1307-1327.
- (162) Bindila, L.; Peter-Katalinić, J. *Mass Spectrom. Rev.* **2009**, *28*, 223-253.

- (163) Zamfir, A.; Vukelić, Ž.; Bindila, L.; Peter-Katalinić, J.; Almeida, R.; Sterling, A.; Allen, M. *J. Am. Soc. Mass Spectrom.* **2004**, *15*, 1649-1657.
- (164) Han, X.; Cheng, H. *J. Lipid Res.* **2005**, *46*, 163-175.
- (165) Kirsch, S.; Zarei, M.; Cindrić, M.; Müthing, J.; Bindila, L.; Peter-Katalinić, J. *Anal. Chem.* **2008**, *80*, 4711-4722.
- (166) Daikoku, S.; Ono, Y.; Ohtake, A., *et al.* *The Analyst* **2011**, *136*, 1046-1050.
- (167) Ohtake, A.; Daikoku, S.; Suzuki, K.; Ito, Y.; Kanie, O. *Anal. Chem.* **2013**, *85*, 8475-8482.
- (168) Sueoka, H.; Aoki, M.; Tsukimura, T.; Togawa, T.; Sakuraba, H. *PLOS ONE* **2015**, *10*, e0144958.
- (169) Sueoka, H.; Ichihara, J.; Tsukimura, T.; Togawa, T.; Sakuraba, H. *PLOS ONE* **2015**, *10*, e0127048.
- (170) Garcia, A.; Chavez, J.; Mechref, Y. *J. Chromatogr. B.* **2014**, *947-948*, 1-7.
- (171) Huang, Q.; Zhou, X.; Liu, D.; Xin, B.; Cechner, K.; Wang, H.; Zhou, A. *Anal. Biochem.* **2014**, *455*, 26-34.
- (172) Hajek, R.; Jirasko, R.; Lisa, M.; Cifkova, E.; Holcapek, M. *Anal. Chem.* **2017**, *89*, 12425-12432.
- (173) Sisu, E.; Flangea, C.; Serb, A.; Rizzi, A.; Zamfir, A. D. *Electrophoresis* **2011**, *32*, 1591-1609.
- (174) Fong, B.; Norris, C.; Lowe, E.; McJarrow, P. *Lipids* **2009**, *44*, 867-874.
- (175) Dossarps, D.; Martine, L.; Berdeaux, O., *et al.* *Ophthalmic Res* **2016**, *56*, 41-48.
- (176) Pintado-Sierra, M.; García-Álvarez, I.; Bribián, A., *et al.* *Anal. Chim. Acta* **2017**, *951*, 89-98.
- (177) von Gerichten, J.; Schlosser, K.; Lamprecht, D., *et al.* *J. Lipid Res.* **2017**, *58*, 1247-1258.
- (178) Zhang, W.; Hankemeier, T.; Ramautar, R. *Curr. Opin. Biotechnol.* **2017**, *43*, 1-7.
- (179) Zaia, J. In *Capillary Electrophoresis of Biomolecules: Methods and Protocols*, Volpi, N.; Maccari, F., Eds.; Humana Press: Totowa, NJ, 2013, pp 13-25.
- (180) Sarver, S. A.; Keithley, R. B.; Essaka, D. C., *et al.* *J. Chromatogr. A* **2012**, *1229*, 268-273.
- (181) Essaka, D. C.; Prendergast, J.; Keithley, R. B.; Palcic, M. M.; Hindsgaul, O.; Schnaar, R. L.; Dovichi, N. J. *Anal. Chem.* **2012**, *84*, 2799-2804.
- (182) Keithley, R. B.; Rosenthal, A. S.; Essaka, D. C., *et al.* *The Analyst* **2013**, *138*, 164-170.
- (183) Zamfir, A. D.; Flangea, C.; Serb, A.; Zagrean, A.-M.; Rizzi, A. M.; Sisu, E. In *Mass Spectrometry of Glycoproteins: Methods and Protocols*, Kohler, J. J.; Patrie, S. M., Eds.; Humana Press: Totowa, NJ, 2013, pp 145-169.
- (184) Harstad, R. K.; Johnson, A. C.; Weisenberger, M. M.; Bowser, M. T. *Anal. Chem.* **2016**, *88*, 299-319.
- (185) Ju, D. D.; Lai, C. C.; Her, G. R. *J. Chromatogr. A* **1997**, *779*, 195-203.
- (186) Zamfir, A.; Vukelić, Ž.; Peter-Katalinić, J. *ELECTROPHORESIS* **2002**, *23*, 2894-2903.
- (187) Ito, E.; Nakajima, K.; Waki, H., *et al.* *Anal. Chem.* **2013**, *85*, 7859-7865.
- (188) Müthing, J.; Distler, U. *Mass Spectrom. Rev.* **2010**, *29*, 425-479.
- (189) Fuchs, B.; Schiller, J.; Suss, R.; Schurenberg, M.; Suckau, D. *Anal Bioanal Chem* **2007**, *389*, 827-834.
- (190) Torretta, E.; Vasso, M.; Fania, C., *et al.* *Electrophoresis* **2014**, *35*, 1319-1328.
- (191) Park, H.; Zhou, Y.; Costello, C. E. *J. Lipid Res.* **2014**, *55*, 773-781.
- (192) Seng, J. A.; Ellis, S. R.; Hughes, J. R.; Maccarone, A. T.; Truscott, R. J.; Blanksby, S. J.; Mitchell, T. W. *Biochim. Biophys. Acta* **2014**, *1841*, 1285-1291.
- (193) Wong, M.; Xu, G.; Park, D.; Barboza, M.; Lebrilla, C. B. *Scientific reports* **2018**, *8*, 10993.
- (194) Hofmann, J.; Pagel, K. *Angew. Chem. Int. Ed.* **2017**, *56*, 8342-8349.

- (195) Gray, C. J.; Thomas, B.; Upton, R.; Migas, L. G.; Eyers, C. E.; Barran, P. E.; Flitsch, S. L. *Biochimica et Biophysica Acta (BBA) - General Subjects* **2016**, *1860*, 1688-1709.
- (196) Struwe, W. B.; Pagel, K.; Benesch, J. L. P.; Harvey, D. J.; Campbell, M. P. *Glycoconjugate J.* **2016**, *33*, 399-404.
- (197) Lanucara, F.; Holman, S. W.; Gray, C. J.; Eyers, C. E. *Nature chemistry* **2014**, *6*, 281-294.
- (198) Wojcik, R.; Webb, I.; Deng, L., et al. *Int. J. Mol. Sci.* **2017**, *18*, 183.
- (199) Jackson, S. N.; Colsch, B.; Egan, T.; Lewis, E. K.; Schultz, J. A.; Woods, A. S. *The Analyst* **2011**, *136*, 463-466.
- (200) Xu, H.; Boucher, F. R.; Nguyen, T. T., et al. *J. Lipid Res.* **2019**, *60*, 200-211.
- (201) Leaptrot, K. L.; May, J. C.; Dodds, J. N.; McLean, J. A. *Nat. Comm.* **2019**, *10*, 985.
- (202) Ciucanu, I.; Kerek, F. *Carbohydr. Res.* **1984**, *131*, 209-217.
- (203) Gunnarsson, A. *Glycoconjugate J.* **1987**, *4*, 239-245.
- (204) Zaia, J. *OMICs : a Journal of Integrative Biology* **2010**, *14*, 401-418.
- (205) Zaia, J. *Mass Spectrom. Rev.* **2004**, *23*, 161-227.
- (206) Alvarez-Manilla, G.; Warren, N. L.; Abney, T., et al. *Glycobiology* **2007**, *17*, 677-687.
- (207) Kang, P.; Mechref, Y.; Kyselova, Z.; Goetz, J. A.; Novotny, M. V. *Anal. Chem.* **2007**, *79*, 6064-6073.
- (208) Ross, P. L.; Huang, Y. N.; Marchese, J. N., et al. *Molecular & cellular proteomics : MCP* **2004**, *3*, 1154-1169.
- (209) Whitmore, C. D.; Hindsgaul, O.; Palcic, M. M.; Schnaar, R. L.; Dovichi, N. J. *Anal. Chem.* **2007**, *79*, 5139-5142.
- (210) Keithley, R. B.; Rosenthal, A. S.; Essaka, D. C., et al. *The Analyst* **2013**, *138*, 164-170.
- (211) Son, S.-H.; Daikoku, S.; Ohtake, A.; Suzuki, K.; Kabayama, K.; Ito, Y.; Kanie, O. *Chem. Commun.* **2014**, *50*, 3010-3013.
- (212) Alfred H. Merrill, J. *Chem. Rev.* **2011**, *111*, 6387-6422.
- (213) Boomkamp, S. D.; Butters, T. D. In *Lipids in Health and Disease*, Quinn, P. J.; Wang, X., Eds.; Springer Netherlands: Dordrecht, 2008, pp 441-467.
- (214) Misasi, R.; Dionisi, S.; Farilla, L.; Carabba, B.; Lenti, L.; Mario, U. D.; Dotta, F. *Diabetes/Metabolism Reviews* **1997**, *13*, 163-179.
- (215) Boutin, M.; Auray-Blais, C. *J. Am. Soc. Mass. Spectrom.* **2015**, *26*, 499-510.
- (216) Yu, A. L.; Hung, J. T.; Ho, M. Y.; Yu, J. *Stem Cells Dev* **2016**.
- (217) Kishimoto, Y.; Radin, N. S. *J. Lipid Res.* **1963**, *4*, 437-443.
- (218) Stillwell, W. *Scandinavian Journal of Food and Nutrition* **2006**, *50*, 107-113.
- (219) Sandhoff, R.; Geyer, R.; Jennemann, R., et al. *J. Biol. Chem.* **2005**, *280*, 27310-27318.
- (220) Yu, K. O. A.; Im, J. S.; Molano, A., et al. *Proceedings of the National Academy of Sciences of the United States of America* **2005**, *102*, 3383-3388.
- (221) Mahfoud, R.; Manis, A.; Lingwood, C. A. *J. Lipid Res.* **2009**, *50*, 1744-1755.
- (222) Watkins, Erik B.; Gao, H.; Dennison, Andrew J. C., et al. *Biophys. J.* **2014**, *107*, 1146-1155.
- (223) Schiopu, C.; Vukelic, Z.; Capitan, F.; Kalanj-Bognar, S.; Sisu, E.; Zamfir, A. D. *Electrophoresis* **2012**, *33*, 1778-1786.
- (224) Serb, A. F.; Sisu, E.; Vukelić, Ž.; Zamfir, A. D. *J. Mass Spectrom.* **2012**, *47*, 1561-1570.
- (225) Schiopu, C.; Flangea, C.; Capitan, F., et al. *Analytical and Bioanalytical Chemistry* **2009**, *395*, 2465-2477.
- (226) Olling, A.; Breimer, M. E.; Peltomaa, E.; Samuelsson, B. E.; Ghardashkhani, S. *Rapid Commun. Mass Spectrom.* **1998**, *12*, 637-645.

- (227) Ann, Q.; Adams, J. *Journal of the American Society for Mass Spectrometry* **1992**, *3*, 260-263.
- (228) Hsu, F. F.; Turk, J. *J. Am. Soc. Mass. Spectrom.* **2001**, *12*, 61-79.
- (229) Han, L.; Costello, C. E. *J. Am. Soc. Mass. Spectrom.* **2011**, *22*, 997-1013.
- (230) Mitchell, T. W.; Pham, H.; Thomas, M. C.; Blanksby, S. J. *J. Chromatogr. B* **2009**, *877*, 2722-2735.
- (231) Ma, X.; Chong, L.; Tian, R.; Shi, R.; Hu, T. Y.; Ouyang, Z.; Xia, Y. *Proceedings of the National Academy of Sciences* **2016**, *113*, 2573-2578.
- (232) Pham, H. T.; Ly, T.; Trevitt, A. J.; Mitchell, T. W.; Blanksby, S. J. *Anal. Chem.* **2012**, *84*, 7525-7532.
- (233) Morrison, L. J.; Parker, W. R.; Holden, D. D.; Henderson, J. C.; Boll, J. M.; Trent, M. S.; Brodbelt, J. S. *Anal. Chem.* **2016**, *88*, 1812-1820.
- (234) Klein, D. R.; Brodbelt, J. S. *Anal. Chem.* **2017**, *89*, 1516-1522.
- (235) Zhou, Y.; Park, H.; Kim, P.; Jiang, Y.; Costello, C. E. *Anal. Chem.* **2014**, *86*, 5697-5705.
- (236) Kishimoto, Y.; Radin, N. S. *J. Lipid Res.* **1963**, *4*, 437-443.
- (237) Thomas, M. C.; Mitchell, T. W.; Blanksby, S. J. *J. Am. Chem. Soc.* **2006**, *128*, 58-59.
- (238) Thomas, M. C.; Mitchell, T. W.; Harman, D. G.; Deeley, J. M.; Murphy, R. C.; Blanksby, S. J. *Anal. Chem.* **2007**, *79*, 5013-5022.
- (239) Kozłowski, R. L.; Mitchell, T. W.; Blanksby, S. J. *Eur. J. Mass Spectrom.* **2015**, *21*, 191-200.
- (240) Kozłowski, R. L.; Campbell, J. L.; Mitchell, T. W.; Blanksby, S. J. *Analytical and Bioanalytical Chemistry* **2015**, *407*, 5053-5064.
- (241) Pham, H. T.; Maccarone, A. T.; Thomas, M. C.; Campbell, J. L.; Mitchell, T. W.; Blanksby, S. J. *The Analyst* **2014**, *139*, 204-214.
- (242) Poad, B. L. J.; Pham, H. T.; Thomas, M. C.; Nealon, J. R.; Campbell, J. L.; Mitchell, T. W.; Blanksby, S. J. *J. Am. Soc. Mass. Spectrom.* **2010**, *21*, 1989-1999.
- (243) Poad, B. L. J.; Green, M. R.; Kirk, J. M.; Tomczyk, N.; Mitchell, T. W.; Blanksby, S. J. *Anal. Chem.* **2017**, *89*, 4223-4229.
- (244) Marshall, D. L.; Pham, H. T.; Bhujel, M., *et al.* *Anal. Chem.* **2016**, *88*, 2685-2692.
- (245) Vu, N.; Brown, J.; Giles, K.; Zhang, Q. *Rapid Communications in Mass Spectrometry*, In press, DOI: 10.1002/rcm.7920.
- (246) Liebisch, G.; Vizcaíno, J. A.; Köfeler, H., *et al.* *J. Lipid Res.* **2013**, *54*, 1523-1530.
- (247) Colsch, B.; Afonso, C.; Popa, I.; Portoukalian, J.; Fournier, F.; Tabet, J. C.; Baumann, N. *J. Lipid Res.* **2004**, *45*, 281-286.
- (248) Sullards, M. C.; Lynch, D. V.; Merrill, A. H.; Adams, J. *J. Mass Spectrom.* **2000**, *35*, 347-353.
- (249) Wang, R.-F.; Wu, X.-W.; Geng, D. *Molecules* **2013**, *18*, 1181.
- (250) Couto, D.; Melo, T.; Maciel, E., *et al.* *J. Am. Soc. Mass. Spectrom.* **2016**, *27*, 1965-1978.
- (251) Couto, D.; Santinha, D.; Melo, T., *et al.* *Chem. Phys. Lipids* **2015**, *191*, 106-114.
- (252) Fliszar, S.; Granger, M. *J. Am. Chem. Soc.* **1970**, *92*, 3361-3369.
- (253) Grosjean, E.; Grosjean, D. *KIN International Journal of Chemical Kinetics* **1994**, *26*, 1185-1191.
- (254) Hunnam, V.; Harvey, D. J.; Priestman, D. A.; Bateman, R. H.; Bordoli, R. S.; Tyldesley, R. *J. Am. Soc. Mass. Spectrom.* **2001**, *12*, 1220-1225.
- (255) Boutin, M.; Sun, Y.; Shacka, J. J.; Auray-Blais, C. *Analytical Chemistry* **2016**, *88*, 1856-1863.

- (256) Couttas, T. A.; Kain, N.; Suchowerska, A. K., *et al. Neurobiology of Aging* **2016**, *43*, 89-100.
- (257) Shaner, R. L.; Allegood, J. C.; Park, H., *et al. J. Lipid Res.* **2009**, *50*, 1692-1707.
- (258) Murata, T.; Ariga, T.; Oshima, M.; Miyatake, T. *J. Lipid Res.* **1978**, *19*, 370-374.
- (259) Abe, T.; Norton, W. T. *J. Neurochem.* **1979**, *32*, 823-832.
- (260) Tanaka, K.; Yamada, M.; Tamiya-Koizumi, K.; Kannagi, R.; Aoyama, T.; Hara, A.; Kyogashima, M. *Glycoconj J* **2011**, *28*, 67-87.
- (261) Fujii, T. *Mass Spectrom. Rev.* **2000**, *19*, 111-138.
- (262) Cancilla, M. T.; Wong, A. W.; Voss, L. R.; Lebrilla, C. B. *Anal. Chem.* **1999**, *71*, 3206-3218.
- (263) Murphy, R. C. *Tandem mass spectrometry of lipids: molecular analysis of complex lipids*; Royal Society of Chemistry, 2014.
- (264) Ann, Q.; Adams, J. J. *Am. Soc. Mass Spectrom.* **1992**, *3*, 260-263.
- (265) Kyle, J. E.; Zhang, X.; Weitz, K. K., *et al. The Analyst* **2016**, *141*, 1649-1659.
- (266) Criegee, R. *Angew. Chem. Int. Ed.* **1975**, *14*, 745-752.
- (267) Pham, H. T.; Maccarone, A. T.; Campbell, J. L.; Mitchell, T. W.; Blanksby, S. J. *J. Am. Soc. Mass. Spectrom.* **2013**, *24*, 286-296.
- (268) Goto, H.; Osawa, E. *J. Chem. Soc. Perkin Trans.* **1993**, 187-198.
- (269) Stewart, J. J. P. *J. Mol. Model.* **2007**, *13*, 1173-1213.
- (270) Huczynski, A.; Przybylski, P.; Brzezinski, B.; Bartl, F. *Biopolymers* **2006**, *81*, 282-294.
- (271) Hsu, F.; Turk, J.; Stewart, M. E.; Downing, D. T. *J. Am. Soc. Mass. Spectrom.* **2002**, *13*, 680-695.
- (272) Tatituri, R. V. V.; Brenner, M. B.; Turk, J.; Hsu, F.-F. *J. Mass Spectrom.* **2012**, *47*, 115-123.
- (273) Adams, J.; Gross, M. L. *J. Am. Chem. Soc.* **1986**, *108*, 6915-6921.
- (274) Cancilla, M. T.; Penn, S. G.; Carroll, J. A.; Lebrilla, C. B. *J. Am. Chem. Soc.* **1996**, *118*, 6736-6745.
- (275) Hancock, S. E.; Maccarone, A. T.; Poad, B. L. J.; Trevitt, A. J.; Mitchell, T. W.; Blanksby, S. J. *Chem. Phys. Lipids* **2019**, *221*, 198-206.
- (276) Franski, R.; Eitner, K.; Schroeder, G.; Sz wajka, O. P. *J. Am. Soc. Mass. Spectrom.* **2003**, *14*, 289-294.
- (277) Amorim Madeira, P. J.; Vaz, P. D.; Bettencourt da Silva, R. J. N.; Florêncio, M. H. *ChemPlusChem* **2013**, *78*, 1149-1156.
- (278) Gierczyk, B.; Schroeder, G.; Przybylski, P.; Brzezinski, B.; Bartl, F.; Zundel, G. *J. Mol. Struct.* **2005**, *738*, 261-270.
- (279) Hofmeister, G. E.; Zhou, Z.; Leary, J. A. *J. Am. Chem. Soc.* **1991**, *113*, 5964-5970.
- (280) Wright, P.; Alex, A.; Pullen, F. *Rapid Commun. Mass Spectrom.* **2014**, *28*, 1127-1143.
- (281) Stortz, C. A.; Johnson, G. P.; French, A. D.; Csonka, G. I. *Carbohydr. Res.* **2009**, *344*, 2217-2228.
- (282) Colas, C.; Bouchonnet, S.; Rogalewicz-Gilard, F.; Popot, M.; Ohanessian, G. *J. Phys. Chem. A* **2006**, *110*, 7503-7508.
- (283) Ervin, K. M. *Chem. Rev.* **2001**, *101*, 391-444.
- (284) Bythell, B. J.; Abutokaikah, M. T.; Wagoner, A. R.; Guan, S.; Rabus, J. M. *J. Am. Soc. Mass. Spectrom.* **2017**, *28*, 688-703.
- (285) Rabus, J. M.; Abutokaikah, M. T.; Ross, R. T.; Bythell, B. J. *Phys. Chem. Chem. Phys.* **2017**, *19*, 25643-25652.
- (286) Ngoka, L. C.; Gal, J. F.; Lebrilla, C. B. *Anal. Chem.* **1994**, *66*, 692-698.

- (287) Rožman, M. *J. Am. Soc. Mass. Spectrom.* **2016**, *27*, 91-98.
- (288) Cerda, B. A.; Wesdemiotis, C. *Int. J. Mass spectrom.* **1999**, *189*, 189-204.
- (289) Harvey, D. J. *J. Mass Spectrom.* **2000**, *35*, 1178-1190.
- (290) Penn, S. G.; Cancilla, M. T.; Lebrilla, C. B. *Int. J. Mass spectrom.* **2000**, *195-196*, 259-269.
- (291) Poad, B. L. J.; Maccarone, A. T.; Yu, H., *et al.* *Anal. Chem.* **2018**, *90*, 5343-5351.
- (292) Zhou, Z.; Tu, J.; Xiong, X.; Shen, X.; Zhu, Z. *J. Anal. Chem.* **2017**, *89*, 9559-9566.
- (293) Nangia, P. S.; Benson, S. W. *J. Am. Chem. Soc.* **1980**, *102*, 3105-3115.
- (294) Fong, B. Y.; Ma, L.; Khor, G. L.; van der Does, Y.; Rowan, A.; McJarrow, P.; MacGibbon, A. K. *J. Agric. Food Chem.* **2016**, *64*, 6295-6305.
- (295) Krengel, U.; Bousquet, P. A. *Front. Immunol.* **2014**, *5*, 325.
- (296) Oikawa, N.; Matsubara, T.; Fukuda, R., *et al.* *PLoS One* **2015**, *10*, e0121356.
- (297) Argia, T.; Yu, R. K.; Miyatake, T. *J. Lipid. Res.* **1984**, *25*, 1096-1101.
- (298) Lee, H.; German, J. B.; Kjelden, R.; Lebrilla, C. B.; Barile, D. *J. Agric. Food Chem.* **2013**, *61*, 9689-9696.
- (299) Sørensen, L. K. *Rapid Comm. Mass Spectrom.* **2006**, *20*, 3625-3633.
- (300) Zhou, S.; Tello, N.; Harvey, A.; Boyes, B.; Orlando, R.; Mechref, Y. *Electrophoresis* **2016**, *37*, 1489-1497.
- (301) Hahne, H.; Neubert, P.; Kuhn, K.; Etienne, C.; Bomgarden, R.; Rogers, J. C.; Kuster, B. *Anal. Chem.* **2012**, *84*, 3716-3724.
- (302) Yang, S.; Wang, M.; Chen, L., *et al.* *Sci. Rep.* **2015**, *5*, 17585.
- (303) Rauniyar, N.; Yates, J. R. *J. Proteome Res.* **2014**, *13*, 5293-5309.
- (304) Yang, S.; Yuan, W.; Yang, W., *et al.* *Anal. Chem.* **2013**, *85*, 8188-8195.
- (305) Cai, Y.; Jiao, J.; Bin, Z.; Zhang, Y.; Yang, P.; Lu, H. *Chem. Comm.* **2015**, *51*, 772-775.
- (306) Zhong, X.; Chen, Z.; Snovida, S.; Liu, Y.; Rogers, J. C.; Li, L. *Anal. Chem.* **2015**, *87*, 6527-6534.
- (307) Zhou, S.; Hu, Y.; Veillon, L.; Snovida, S. I.; Rogers, J. C.; Saba, J.; Mechref, Y. *Anal. Chem.* **2016**, *88*, 7515-7522.
- (308) Thaysen-Andersen, M.; Larsen, M. R.; Packer, N. H.; Palmisano, G. *RSC Adv.* **2013**, *3*, 22683-22705.
- (309) Sudalai, A.; Khenkin, A.; Neumann, R. *Org. Biol. Chem.* **2015**, *13*, 4374-4394.
- (310) Zeng, Y.; Ramya, T. N. C.; Dirksen, A.; Dawson, P. E.; Paulson, J. C. *Nat. Meth.* **2009**, *6*, 207-209.
- (311) Ramya, T. N. C.; Weerapana, E.; Cravatt, B. F.; Paulson, J. C. *Glycobiology* **2013**, *23*, 211-221.
- (312) Narvaez-Rivas, M.; Zhang, Q. *J. Chromatogr. A* **2016**, *1440*, 123-134.
- (313) Narvaez-Rivas, M.; Vu, N.; Chen, G. Y.; Zhang, Q. *Anal. Chim. Acta* **2017**, *954*, 140-150.
- (314) Reuter, G.; Schauer, R.; Szeiki, C.; Kamerling, J. P.; Vliegenthart, J. F. *Glycoconjugate J.* **1989**, *6*, 35-44.
- (315) Fuller, M.; Duplock, S.; Hein, L. K.; Rigat, B. A.; Mahuran, D. J. *Anal. Biochem.* **2014**, *458*, 20-26.
- (316) Gu, J.; Tiffit, C. J.; Soldin, S. J. *Clin. Biochem.* **2008**, *41*, 413-417.
- (317) Robu, A. C.; Vukelić, Ž.; Schiopu, C.; Capitan, F.; Zamfir, A. D. *Anal. Biochem.* **2016**, *509*, 1-11.
- (318) Schengrund, C. *Trends Biochem. Sci.* **2015**, *40*, 397-406.
- (319) Ferrer, I.; Thurman, E. M. *Anal. Chem.* **2005**, *77*, 3394-3400.
- (320) Afiuni-Zadeh, S.; Rogers, J. C.; Snovida, S. I.; Bomgarden, R. D.; Griffin, T. J. *Biotechniques* **2016**, *60*, 186-188, 190, 192-186.

- (321) Yu, J.; Schorlemer, M.; Gomez Toledo, A., *et al. Chem. Eur. J.* **2016**, *22*, 1114-1124.
- (322) Platt, F. M.; Boland, B.; van der Spoel, A. C. *J. Cell Biol.* **2012**, *199*, 723-734.
- (323) Costello, C. E.; Vath, J. E. In *Methods Enzymol.*, 1990, pp 738-768.
- (324) Ciucanu, I.; Costello, C. E. *J. Am. Chem. Soc.* **2003**, *125*, 16213-16219.
- (325) Ciucanu, I. *Anal. Chim. Acta* **2006**, *576*, 147-155.
- (326) Shubhakar, A.; Kozak, R. P.; Reiding, K. R.; Royle, L.; Spencer, D. I. R.; Fernandes, D. L.; Wuhrer, M. *Anal. Chem.* **2016**, *88*, 8562-8569.
- (327) Larson, G.; Karlsson, H.; Hansson, G. C.; Pimlott, W. *Carbohydr. Res.* **1987**, *161*, 281-290.
- (328) Guo, K.; Li, L. *Anal. Chem.* **2009**, *81*, 3919-3932.
- (329) Pabst, M.; Benesova, I.; Fagerer, S. R., *et al. J. Proteome Res.* **2016**, *15*, 326-331.
- (330) Orlando, R.; Lim, J.-M.; Atwood, J. A., 3rd, *et al. J. Proteome Res.* **2009**, *8*, 3816-3823.
- (331) Gevaert, K.; Impens, F.; Ghesquière, B.; Van Damme, P.; Lambrechts, A.; Vandekerckhove, J. *Proteomics* **2008**, *8*, 4873-4885.
- (332) Triebl, A.; Wenk, M. R. *Biomolecules* **2018**, *8*, 151.
- (333) Holčapek, M.; Liebisch, G.; Ekroos, K. *Anal. Chem.* **2018**, *90*, 4249-4257.
- (334) Wolf, B. J.; Tatituri, R. V. V.; Almeida, C. F., *et al. J. Immunol.* **2015**, *195*, 2540-2551.
- (335) Sullards, M. C.; Liu, Y.; Chen, Y.; Merrill, A. H., Jr. *Biochim. Biophys. Acta* **2011**, *1811*, 838-853.
- (336) van Es, H. H. G.; Veldwijk, M.; Havenga, M.; Valerio, D. *Anal. Biochem.* **1997**, *247*, 268-271.
- (337) Chong, J.; Soufan, O.; Li, C., *et al. Nucleic Acids Res.* **2018**, *46*, W486-W494.
- (338) Hu, Y.; Borges, C. R. *The Analyst* **2017**, *142*, 2748-2759.
- (339) Shajahan, A.; Supekar, N. T.; Heiss, C.; Ishihara, M.; Azadi, P. *Anal. Chem.* **2017**, *89*, 10734-10743.
- (340) Doman, B.; Vath, J. E.; Costello, C. E. *Anal. Biochem.* **1990**, *184*, 151-164.
- (341) Ju, D. D.; Wei, G. J.; Her, G. R. *J. Am. Soc. Mass. Spectrom.* **1994**, *5*, 558-563.
- (342) Zhou, S.; Hu, Y.; Mechref, Y. *Electrophoresis* **2016**, *37*, 1506-1513.
- (343) Zhou, S.; Dong, X.; Veillon, L.; Huang, Y.; Mechref, Y. *Anal. Bioanal. Chem.* **2017**, *409*, 453-466.
- (344) Costello, C. E.; Contado-Miller, J. M.; Cipollo, J. F. *J. Am. Soc. Mass. Spectrom.* **2007**, *18*, 1799-1812.
- (345) Brockerhoff, H. *J. Lipid Res.* **1963**, *4*, 96-99.
- (346) Chao, H. C.; Chen, G. Y.; Hsu, L. C., *et al. Anal. Chim. Acta* **2017**, *971*, 68-77.
- (347) Newburg, D. S.; Shea, T. B.; Yatziv, S.; Raghavan, S. S.; McCluer, R. H. *Exp. Mol. Pathol.* **1988**, *48*, 317-323.
- (348) Grabowski, G. A.; Osiecki-Newman, K.; Dinur, T.; Fabbro, D.; Legler, G.; Gatt, S.; Desnick, R. J. *J. Biol. Chem.* **1986**, *261*, 8263-8269.
- (349) Brady, R. O.; Kanfer, J. N.; Shapiro, D. *Biochem. Biophys. Res. Commun.* **1965**, *18*, 221-225.
- (350) Henriques, A.; Huebecker, M.; Blasco, H., *et al. Scientific reports* **2017**, *7*, 5235.
- (351) Dennis, E. A.; Deems, R. A.; Harkewicz, R., *et al. J. Biol. Chem.* **2010**, *285*, 39976-39985.
- (352) Andreyev, A. Y.; Fahy, E.; Guan, Z., *et al. J. Lipid Res.* **2010**, *51*, 2785-2797.
- (353) Varki, A.; Cummings, R. D.; Aebi, M., *et al. Glycobiology* **2015**, *25*, 1323-1324.
- (354) Clark, G.; The Open, U.; Smart, L. E. *Mechanism and Synthesis*; Royal Society of Chemistry: Cambridge, 2003.
- (355) Kensil, C. R.; Dennis, E. A. *Biochemistry* **1981**, *20*, 6079-6085.

## APPENDIX A

### SUPPLEMENTAL TABLES

Table S1. Structure of Gangliosides Discussed in the Text.

Table S2. Major Ganglioside Components in AminoxyTMT<sup>0</sup>-Labeled Porcine Brain Gangliosides Extract.

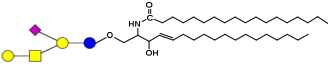
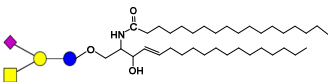
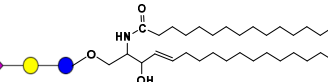
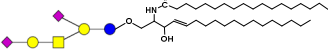
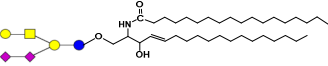
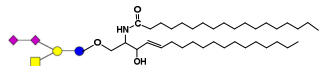
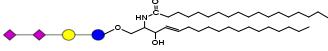
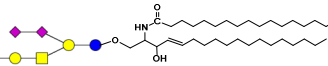
Table S3. List of Glycolipid Standards Used for Method Development.

Table S4. Accurate Mass and Retention Time of <sup>12</sup>C and <sup>13</sup>C Permethylated Glycolipid Standards.

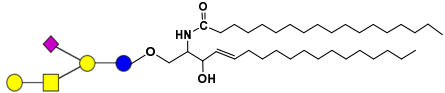
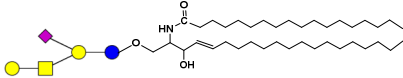
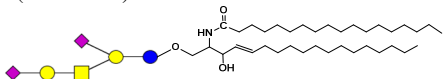
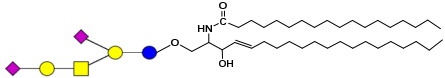
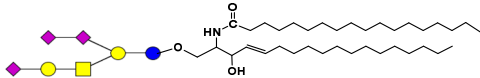
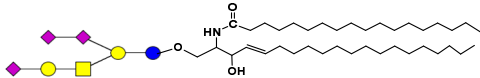
Table S5. Accuracy and Reproducibility of the RPLC-MS Based Relative Quantification of [<sup>12</sup>C] and [<sup>13</sup>C] Permethylated Glycolipid Standards.

Table S6. Significantly Changed Glycolipids in CBE-Treated RAW264.7 Cells Identified Using One-Way Analysis of Variance (ANOVA) at 5% False Discovery Rate (FDR).

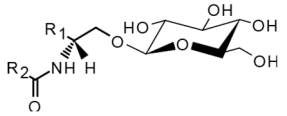
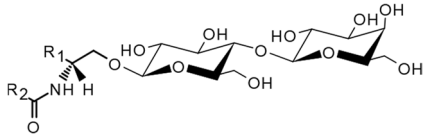
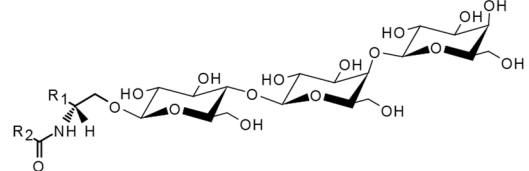
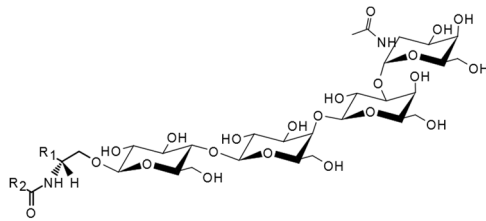
**Table S1. Structure of Gangliosides Discussed in the Text.**

Ganglioside	LIPIDMAPS ID <sup>23</sup>	Structure/Systematic Name	Molecular Formula	Exact Mass (Da)
GM1a d18:1/18:0	LMSP0601AP02	 Galβ1-3GalNAcβ1-4(NeuAcα2-3)Galβ1-4Glcβ-Cer(d18:1/18:0)	C <sub>73</sub> H <sub>131</sub> N <sub>3</sub> O <sub>31</sub>	1545.8766
GM2 d18:1/18:0	LMSP0601AM02	 GalNAcβ1-4(NeuAcα2-3)Galβ1-4Glcβ-Cer(d18:1/18:0)	C <sub>67</sub> H <sub>121</sub> N <sub>3</sub> O <sub>26</sub>	1383.8238
GM3 d18:1/16:0	LMSP0601AJ01	 NeuAcα2-3Galβ1-4Glcβ-Cer(d18:1/16:0)	C <sub>57</sub> H <sub>104</sub> N <sub>2</sub> O <sub>21</sub>	1152.7131
GD1a d18:1/18:0	LMSP0601AS02	 NeuAcα2-3Galβ1-3GalNAcβ1-4(NeuAcα2-3)Galβ1-4Glcβ-Cer(d18:1/18:0)	C <sub>84</sub> H <sub>148</sub> N <sub>4</sub> O <sub>39</sub>	1836.9720
GD1b d18:1/18:0	LMSP0601AQ02	 Galβ1-3GalNAcβ1-4(NeuAcα2-8NeuAcα2-3)Galβ1-4Glcβ-Cer(d18:1/18:0)	C <sub>84</sub> H <sub>148</sub> N <sub>4</sub> O <sub>39</sub>	1836.9720
GD2 d18:1/18:0	LMSP0601AN02	 GalNAcβ1-4(NeuAcα2-8NeuAcα2-3)Galβ1-4Glcβ-Cer(d18:1/18:0)	C <sub>78</sub> H <sub>138</sub> N <sub>4</sub> O <sub>34</sub>	1674.9192
GD3 d18:1/16:0	LMSP0601AK01	 NeuAcα2-8NeuAcα2-3Galβ1-4Glcβ-Cer(d18:1/16:0)	C <sub>68</sub> H <sub>121</sub> N <sub>3</sub> O <sub>29</sub>	1443.8085
GT1b d18:1/18:0	LMSP0601AT02	 NeuAcα2-3Galβ1-3GalNAcβ1-4(NeuAcα2-8NeuAcα2-3)Galβ1-4Glcβ-Cer(d18:1/18:0)	C <sub>95</sub> H <sub>165</sub> N <sub>5</sub> O <sub>47</sub>	2128.0674

**Table S2. Major Ganglioside Components in AminoxyTMT<sup>0</sup>-Labeled Porcine Brain Gangliosides Extract.**

Ganglioside	Structure	Molecular Formula (aminoxyTMT <sup>0</sup> labeled)	Adduct	Theoretical <i>m/z</i>	Experimental <i>m/z</i>	Mass error (ppm)
GM1a d18:1/18:0		C <sub>86</sub> H <sub>153</sub> N <sub>7</sub> O <sub>31</sub>	[M+2H] <sup>2+</sup>	891.0383	891.03625	2.35
GM1a d20:1/18:0		C <sub>88</sub> H <sub>157</sub> N <sub>7</sub> O <sub>31</sub>	[M+2H] <sup>2+</sup>	905.0540	905.05261	1.53
GD1a d18:1/18:0		C <sub>110</sub> H <sub>192</sub> N <sub>12</sub> O <sub>39</sub>	[M+2H] <sup>2+</sup>	1153.6783	1153.67676	1.31
GD1a d20:1/18:0		C <sub>112</sub> H <sub>196</sub> N <sub>12</sub> O <sub>39</sub>	[M+2H] <sup>2+</sup>	1167.6939	1167.69238	1.32
GT1b d18:1/18:0		C <sub>121</sub> H <sub>209</sub> N <sub>13</sub> O <sub>47</sub>	[M+2H] <sup>2+</sup>	1299.2260	1299.22449	1.15
GT1b d20:1/18:0		C <sub>123</sub> H <sub>213</sub> N <sub>13</sub> O <sub>47</sub>	[M+2H] <sup>2+</sup>	1313.2416	1313.24048	0.87
	NeuAcα2-3Galβ1-3GalNAcβ1-4(NeuAcα2-3)Galβ1-4Glcβ-Cer(d18:1/18:0)					
	NeuAcα2-3Galβ1-3GalNAcβ1-4(NeuAcα2-3)Galβ1-4Glcβ-Cer(d20:1/18:0)					
	NeuAcα2-3Galβ1-3GalNAcβ1-4(NeuAcα2-8NeuAcα2-3)Galβ1-4Glcβ-Cer(d18:1/18:0)					
	NeuAcα2-3Galβ1-3GalNAcβ1-4(NeuAcα2-8NeuAcα2-3)Galβ1-4Glcβ-Cer(d20:1/18:0)					

**Table S3. List of Glycolipid Standards Used for Method Development.**

Analyte	Headgroup structure showing active protons (-OH and -NH) <sup>a</sup>	Native Molecular Formula	Native Exact Mass (Da)	No. of active protons
GlcCer d18:1/18:0		C <sub>42</sub> H <sub>81</sub> NO <sub>8</sub>	727.5962	6
LacCer d18:1/18:0		C <sub>48</sub> H <sub>91</sub> NO <sub>13</sub>	889.6490	9
Gb3Cer d18:1/18:0		C <sub>54</sub> H <sub>101</sub> NO <sub>18</sub>	1051.7018	12
Gb4Cer d18:1/18:0		C <sub>62</sub> H <sub>114</sub> N <sub>2</sub> O <sub>23</sub>	1254.7810	15

<sup>a</sup>R<sub>1</sub> = sphingosine backbone; R<sub>2</sub> = C18:0 fatty acyl chain

**Table S4. Accurate Mass and Retention Time of <sup>12</sup>C and <sup>13</sup>C Permethylated Glycolipid Standards.**

Analyte	Permethylated Molecular Formula	<sup>12</sup> C]-Permethylated				<sup>13</sup> C]-Permethylated			
		Theoretical [M+H] <sup>+</sup> (Th)	Experimental [M+H] <sup>+</sup> (Th)	Mass Error (ppm)	Ret. Time (min)	Theoretical [M+H] <sup>+</sup> (Th)	Experimental [M+H] <sup>+</sup> (Th)	Mass Error (ppm)	Ret. Time (min)
GlcCer d18:1/18:0	C <sub>48</sub> H <sub>93</sub> NO <sub>8</sub>	812.6979	812.6965	-1.72	9.36	818.7180	818.7167	-1.59	9.36
LacCer d18:1/18:0	C <sub>57</sub> H <sub>109</sub> NO <sub>13</sub>	1016.7977	1016.7964	-1.28	8.83	1025.8279	1025.8265	-1.36	8.83
Gb3Cer d18:1/18:0	C <sub>66</sub> H <sub>125</sub> NO <sub>18</sub>	1220.8974	1220.8970	-0.33	8.70	1232.9377	1232.9374	-0.24	8.70
Gb4Cer d18:1/18:0	C <sub>77</sub> H <sub>144</sub> N <sub>2</sub> O <sub>23</sub>	1466.0238	1466.0228	-0.68	8.15	1481.0741	1481.0730	-0.74	8.15

**Table S5. Accuracy and Reproducibility of the RPLC-MS Based Relative Quantification of [<sup>12</sup>C] and [<sup>13</sup>C] Permethyated Glycolipid Standards.**

Analyte	Theoretical	Uncorrected		Corrected	
	Ratio	$\bar{x}$	CV	$\bar{x}$	CV
	( <sup>13</sup> C: <sup>12</sup> C)	Experimental		Experimental	
		Ratio <sup>a</sup>		Ratio <sup>a,b</sup>	
		( <sup>13</sup> C: <sup>12</sup> C)		( <sup>13</sup> C: <sup>12</sup> C)	
GlcCer	1	1.0	1.9	1.0	1.9
d18:1/18:0	3	3.1	6.8	2.9	6.6
	5	5.4	7.0	5.0	1.2
	10	11.8	0.4	11.1	0.5
LacCer	1	1.1	0.9	1.0	0.9
d18:1/18:0	3	3.2	3.4	2.9	3.4
	5	5.4	0.9	4.9	1.0
	10	11.5	2.4	10.5	2.5
Gb3Cer	1	0.9	3.3	0.8	3.3
d18:1/18:0	3	2.9	4.1	2.5	4.0
	5	5.0	5.4	4.4	5.4
	10	10.9	3.1	9.6	3.1
Gb4Cer	1	1.1	5.5	0.9	5.5
d18:1/18:0	3	3.7	2.4	3.2	2.4
	5	5.7	4.9	5.0	4.8
	10	13.7	4.4	12.0	4.3

<sup>a</sup>Average of triplicate measurements.

<sup>b</sup>Correction is based on the sum of isotopic clusters.

**Table S6. Significantly Changed Glycolipids in CBE-Treated RAW264.7 Cells Identified Using One-Way Analysis of Variance (ANOVA) at 5% False Discovery Rate (FDR).**

No.	Analyte	p-Value	log <sub>10</sub> (p)	FDR	Between-treatment comparisons identified as significant using Fisher's LSD <i>post-hoc</i>
1	H1Cerd181/181	5.24E-09	8.2803	2.10E-07	3Hrs vs Control; 6Hrs vs Control; 12Hrs vs Control; 48Hrs vs Control; 72Hrs vs Control; 12Hrs vs 3Hrs; 48Hrs vs 3Hrs; 72Hrs vs 3Hrs; 48Hrs vs 6Hrs; 72Hrs vs 6Hrs; 48Hrs vs 12Hrs; 72Hrs vs 12Hrs
2	H1Cerd181/160	2.49E-08	7.6034	3.11E-07	3Hrs vs Control; 6Hrs vs Control; 12Hrs vs Control; 48Hrs vs Control; 72Hrs vs Control; 12Hrs vs 3Hrs; 48Hrs vs 3Hrs; 72Hrs vs 3Hrs; 12Hrs vs 6Hrs; 48Hrs vs 6Hrs; 72Hrs vs 6Hrs; 48Hrs vs 12Hrs; 72Hrs vs 12Hrs
3	H1Cerd181/261OH	3.05E-08	7.5159	3.11E-07	3Hrs vs Control; 6Hrs vs Control; 12Hrs vs Control; 48Hrs vs Control; 72Hrs vs Control; 12Hrs vs 3Hrs; 48Hrs vs 3Hrs; 72Hrs vs 3Hrs; 12Hrs vs 6Hrs; 48Hrs vs 6Hrs; 72Hrs vs 6Hrs; 48Hrs vs 12Hrs; 72Hrs vs 12Hrs
4	H1Cerd181/160OH	3.11E-08	7.507	3.11E-07	3Hrs vs Control; 6Hrs vs Control; 12Hrs vs Control; 48Hrs vs Control; 72Hrs vs Control; 12Hrs vs 3Hrs; 48Hrs vs 3Hrs; 72Hrs vs 3Hrs; 12Hrs vs 6Hrs; 48Hrs vs 6Hrs; 72Hrs vs 6Hrs; 48Hrs vs 12Hrs; 72Hrs vs 12Hrs
5	H1Cerd181/231	5.39E-08	7.2685	3.47E-07	6Hrs vs Control; 12Hrs vs Control; 48Hrs vs Control; 72Hrs vs Control; 12Hrs vs 3Hrs; 48Hrs vs 3Hrs; 72Hrs vs 3Hrs; 12Hrs vs 6Hrs; 48Hrs vs 6Hrs; 72Hrs vs 6Hrs; 48Hrs vs 12Hrs; 72Hrs vs 12Hrs
6	H1Cerd181/261	5.85E-08	7.2325	3.47E-07	12Hrs vs Control; 48Hrs vs Control; 72Hrs vs Control; 12Hrs vs 3Hrs; 48Hrs vs 3Hrs; 72Hrs vs 3Hrs; 12Hrs vs 6Hrs; 48Hrs vs 6Hrs; 72Hrs vs 6Hrs; 48Hrs vs 12Hrs; 72Hrs vs 12Hrs
7	H1Cerd181/241OH	6.86E-08	7.1635	3.47E-07	3Hrs vs Control; 6Hrs vs Control; 12Hrs vs Control; 48Hrs vs Control; 72Hrs vs Control; 12Hrs vs 3Hrs; 48Hrs vs 3Hrs; 72Hrs vs 3Hrs; 12Hrs vs 6Hrs; 48Hrs vs 6Hrs; 72Hrs vs 6Hrs; 48Hrs vs 12Hrs; 72Hrs vs 12Hrs
8	H1Cerd181/231OH	7.13E-08	7.1472	3.47E-07	3Hrs vs Control; 6Hrs vs Control; 12Hrs vs Control; 48Hrs vs Control; 72Hrs vs Control; 12Hrs vs 3Hrs; 48Hrs vs 3Hrs; 72Hrs vs 3Hrs; 12Hrs vs 6Hrs; 48Hrs vs 6Hrs; 72Hrs vs 6Hrs; 48Hrs vs 12Hrs; 72Hrs vs 12Hrs
9	H1Cerd181/241	7.80E-08	7.1081	3.47E-07	6Hrs vs Control; 12Hrs vs Control; 48Hrs vs Control; 72Hrs vs Control; 12Hrs vs 3Hrs; 48Hrs vs 3Hrs; 72Hrs vs 3Hrs; 12Hrs vs 6Hrs; 48Hrs vs 6Hrs; 72Hrs vs 6Hrs; 48Hrs vs 12Hrs; 72Hrs vs 12Hrs
10	H1Cerd181/180	1.35E-07	6.8707	5.04E-07	3Hrs vs Control; 6Hrs vs Control; 12Hrs vs Control; 48Hrs vs Control; 72Hrs vs Control; 12Hrs vs 3Hrs; 48Hrs vs 3Hrs; 72Hrs vs 3Hrs; 12Hrs vs 6Hrs; 48Hrs vs 6Hrs; 72Hrs vs 6Hrs; 48Hrs vs 12Hrs; 72Hrs vs 12Hrs
11	H1Cerd181/230	1.38E-07	6.8587	5.04E-07	12Hrs vs Control; 48Hrs vs Control; 72Hrs vs Control; 12Hrs vs 3Hrs; 48Hrs vs 3Hrs; 72Hrs vs 3Hrs; 12Hrs vs 6Hrs; 48Hrs vs 6Hrs; 72Hrs vs 6Hrs; 48Hrs vs 12Hrs; 72Hrs vs 12Hrs
12	H1Cerd181/240	1.57E-07	6.8049	5.22E-07	12Hrs vs Control; 48Hrs vs Control; 72Hrs vs Control; 12Hrs vs 3Hrs; 48Hrs vs 3Hrs; 72Hrs vs 3Hrs; 12Hrs vs 6Hrs; 48Hrs vs 6Hrs; 72Hrs vs 6Hrs; 48Hrs vs 12Hrs; 72Hrs vs 12Hrs

Table S6 (continued)					
13	H1Cerd181/220OH	2.07E-07	6.684	6.37E-07	3Hrs vs Control; 6Hrs vs Control; 12Hrs vs Control; 48Hrs vs Control; 72Hrs vs Control; 48Hrs vs 3Hrs; 72Hrs vs 3Hrs; 12Hrs vs 6Hrs; 48Hrs vs 6Hrs; 72Hrs vs 6Hrs; 48Hrs vs 12Hrs; 72Hrs vs 12Hrs
14	H1Cerd181/200	2.61E-07	6.5839	7.45E-07	3Hrs vs Control; 6Hrs vs Control; 12Hrs vs Control; 48Hrs vs Control; 72Hrs vs Control; 12Hrs vs 3Hrs; 48Hrs vs 3Hrs; 72Hrs vs 3Hrs; 12Hrs vs 6Hrs; 48Hrs vs 6Hrs; 72Hrs vs 6Hrs; 48Hrs vs 12Hrs; 72Hrs vs 12Hrs
15	H1Cerd181/260	3.36E-07	6.4739	8.95E-07	12Hrs vs Control; 48Hrs vs Control; 72Hrs vs Control; 12Hrs vs 3Hrs; 48Hrs vs 3Hrs; 72Hrs vs 3Hrs; 12Hrs vs 6Hrs; 48Hrs vs 6Hrs; 72Hrs vs 6Hrs; 48Hrs vs 12Hrs; 72Hrs vs 12Hrs
16	H1Cerd181/200OH	1.13E-06	5.9452	2.84E-06	3Hrs vs Control; 6Hrs vs Control; 12Hrs vs Control; 48Hrs vs Control; 72Hrs vs Control; 48Hrs vs 3Hrs; 72Hrs vs 3Hrs; 48Hrs vs 6Hrs; 72Hrs vs 6Hrs; 48Hrs vs 12Hrs; 72Hrs vs 12Hrs
17	H1Cerd181/230OH	1.61E-06	5.7929	3.66E-06	3Hrs vs Control; 6Hrs vs Control; 12Hrs vs Control; 48Hrs vs Control; 72Hrs vs Control; 48Hrs vs 3Hrs; 72Hrs vs 3Hrs; 48Hrs vs 6Hrs; 72Hrs vs 6Hrs; 48Hrs vs 12Hrs; 72Hrs vs 12Hrs
18	H1Cerd180/230OH	1.65E-06	5.7838	3.66E-06	3Hrs vs Control; 6Hrs vs Control; 12Hrs vs Control; 48Hrs vs Control; 72Hrs vs Control; 48Hrs vs 3Hrs; 72Hrs vs 3Hrs; 48Hrs vs 6Hrs; 72Hrs vs 6Hrs; 48Hrs vs 12Hrs; 72Hrs vs 12Hrs
19	H1Cerd180/240OH	1.80E-06	5.7443	3.79E-06	6Hrs vs Control; 12Hrs vs Control; 48Hrs vs Control; 72Hrs vs Control; 48Hrs vs 3Hrs; 72Hrs vs 3Hrs; 48Hrs vs 6Hrs; 72Hrs vs 6Hrs; 48Hrs vs 12Hrs; 72Hrs vs 12Hrs
20	H1Cerd180/160	1.49E-05	4.8254	2.99E-05	3Hrs vs Control; 6Hrs vs Control; 12Hrs vs Control; 48Hrs vs Control; 72Hrs vs Control; 48Hrs vs 3Hrs; 72Hrs vs 3Hrs; 48Hrs vs 6Hrs; 72Hrs vs 6Hrs; 48Hrs vs 12Hrs; 72Hrs vs 12Hrs
21	H1Cerd180/240	2.80E-05	4.5522	5.34E-05	12Hrs vs Control; 48Hrs vs Control; 72Hrs vs Control; 48Hrs vs 3Hrs; 72Hrs vs 3Hrs; 48Hrs vs 6Hrs; 72Hrs vs 6Hrs; 48Hrs vs 12Hrs; 72Hrs vs 12Hrs
22	H1Cerd180/160OH	1.90E-04	3.7214	3.45E-05	3Hrs vs Control; 12Hrs vs Control; 48Hrs vs Control; 72Hrs vs Control; 48Hrs vs 3Hrs; 72Hrs vs 3Hrs; 48Hrs vs 6Hrs; 72Hrs vs 6Hrs; 48Hrs vs 12Hrs; 72Hrs vs 12Hrs
23	H1Cerd181/260OH	2.43E-04	3.6134	4.23E-04	48Hrs vs Control; 72Hrs vs Control; 48Hrs vs 3Hrs; 72Hrs vs 3Hrs; 48Hrs vs 6Hrs; 72Hrs vs 6Hrs; 48Hrs vs 12Hrs; 72Hrs vs 12Hrs
24	H1Cerd180/200OH	1.10E-03	2.9586	1.83E-03	3Hrs vs Control; 6Hrs vs Control; 12Hrs vs Control; 48Hrs vs Control; 72Hrs vs Control
25	H2Cerd181/180	3.69E-03	2.4329	5.91E-03	48Hrs vs Control; 48Hrs vs 3Hrs; 72Hrs vs 3Hrs; 48Hrs vs 6Hrs; 72Hrs vs 6Hrs; 48Hrs vs 12Hrs; 72Hrs vs 12Hrs
26	H2Cerd181/220	5.21E-03	2.2831	8.01E-03	48Hrs vs Control; 72Hrs vs Control; 48Hrs vs 3Hrs; 72Hrs vs 3Hrs; 48Hrs vs 6Hrs; 72Hrs vs 6Hrs; 48Hrs vs 12Hrs; 72Hrs vs 12Hrs
27	H2Cerd181/241	7.14E-03	2.1463	1.06E-02	48Hrs vs 3Hrs; 72Hrs vs 3Hrs; 48Hrs vs 6Hrs; 72Hrs vs 6Hrs; 48Hrs vs 12Hrs; 72Hrs vs 12Hrs
28	H2Cerd181/160	8.39E-03	2.0761	1.20E-02	48Hrs vs 3Hrs; 72Hrs vs 3Hrs; 48Hrs vs 6Hrs; 72Hrs vs 6Hrs; 48Hrs vs 12Hrs; 72Hrs vs 12Hrs

<sup>a</sup>H: Hexosyl

## APPENDIX B

### SUPPLEMENTAL FIGURES

Figure S1. Effect of Glycan Head Group on the Oxidative Cleavage of Sphingosine Double Bond.

Figure S2. Effect of Fatty Acyl Chain  $\alpha$ -Hydroxyl Group on the Oxidative Cleavage of Sphingosine Double Bond.

Figure S3. Collision-Induced Dissociation (CID) MS/MS Spectra of Galactocerebroside  $m/z$  832.66 in Bovine Brain Obtained in Argon Gas at CID 55 eV.

Figure S4. Overview of the Proposed Pathways Leading to the Formation of Secondary Ozonolysis Products Observed in the OzID-MS Spectrum.

Figure S5. OzID-MS Spectra of Cationized Cer d18:1/18:1(9Z).

Figure S6. OzID-MS Spectra of Cationized GlcCer d18:1/18:1(9Z).

Figure S7. Most Stable Conformer of Neutral Form of LacCer d18:1/18:1(9Z) Calculated Using MO-G with PM6.

Figure S8. Demonstration of Incomplete Oxidation of Ganglioside GM1a d18:1/18:0 After Subjecting to 1mM NaIO<sub>4</sub> for Only 30 Minutes Incubation in Ice Bath ( $\sim 0^{\circ}\text{C}$ ).

Figure S9. Chemoselectivity of NaIO<sub>4</sub> Oxidation Under Mild Conditions.

Figure S10. Total ion chromatograms (TIC) of Oxidized Gangliosides.

Figure S11. Full Scan Mass Range of Unoxidized (Left Column) and Oxidized (Right Column) Gangliosides Based on the Peak Indicated by Asterisk (\*) in the Right Column of Fig. S3.

Figure S12. Total Ion Chromatograms of Ganglioside Standard Mixtures Labeled with AminoxyTMT<sup>0</sup>.

Figure S13. MS/MS Spectrum of AminoxyTMT<sup>0</sup>-Labeled GM1a d20:1/18:0 Using the  $[\text{M}+2\text{H}]^{2+}$  ( $m/z$  905.05) as Precursor Ion Showing the  $O''$  ion at  $m/z$  292.2995 Diagnostic of the Long Chain Base d20:1 (A).

Figure S14. Representative HCD-MS/MS (Stepped NCE 22,26,30) of AminoxyTMT<sup>0</sup>-Labeled Gangliosides from Porcine Brain Extract.

Figure S15. HCD-MS/MS Spectra of AminoxyTMT<sup>0</sup>-Labeled Ganglioside GM1a d18:1/18:0 at Different Normalized Collision Energy (NCE) Values.

Figure S16. Elution Behavior of Permethylated Glycolipids in a Cortecs C18 Column.

Figure S17. Higher Energy Collisional Dissociation (HCD) Fragmentation Characteristics of Permethylated Glycolipid Standards.

Figure S18. Effect of  $^{12}\text{C}$  Impurity in the Resultant Isotopic Distribution Pattern of [ $^{13}\text{C}$ ]-Labeled Glycolipid.

Figure S19. Regression Curves Based on Corrected (Top) and Uncorrected (Bottom)  $^{12}\text{C}/^{13}\text{C}$  Ratios.

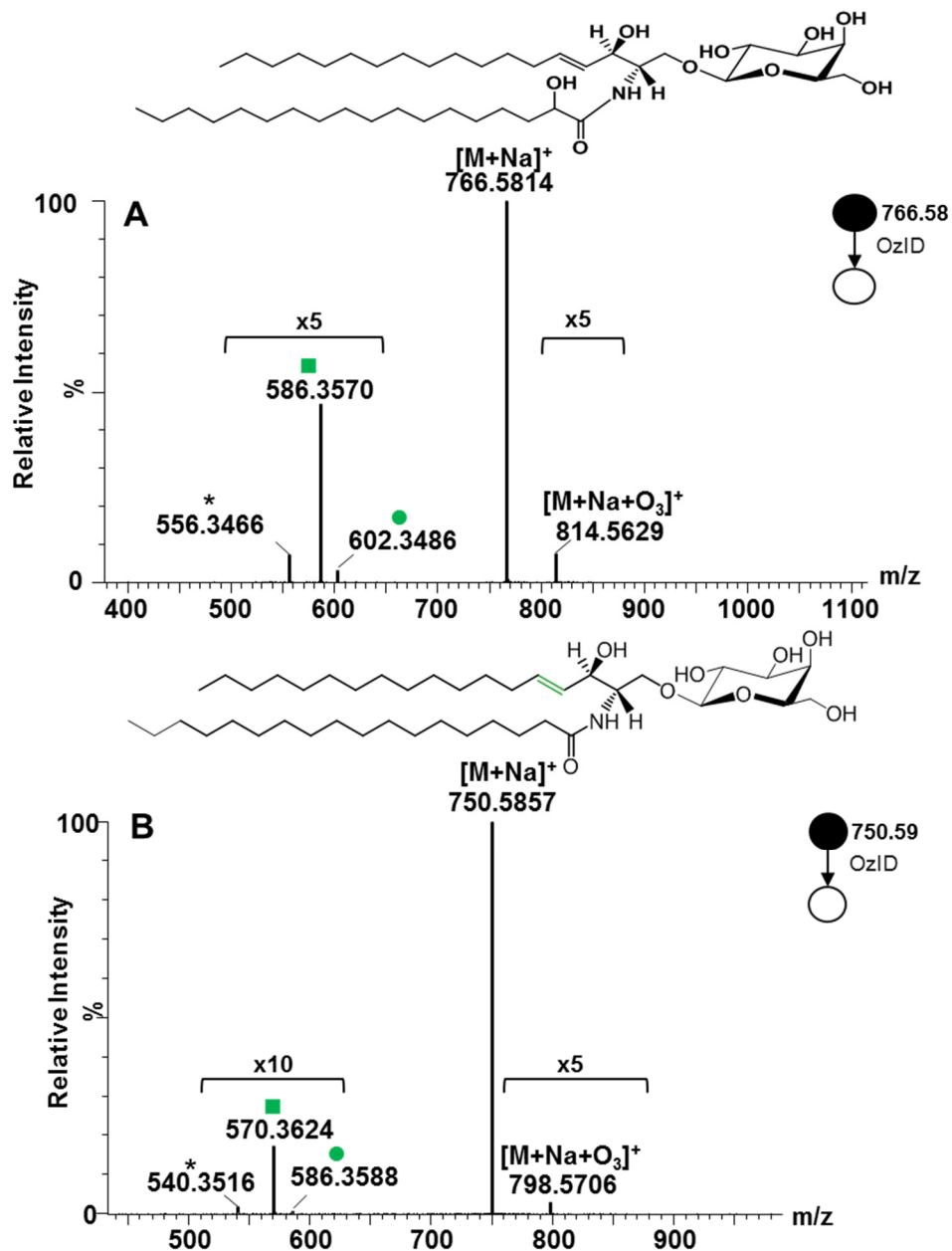
Figure S20. Proposed Pathway for the Breakdown of Phospholipids Under Alkaline Conditions.

Figure S21. Application of Stable Isotope Labeling by Permethylation and RPLC-MS for Relative Quantification of Neutral Glycolipids in Mammalian Cells.

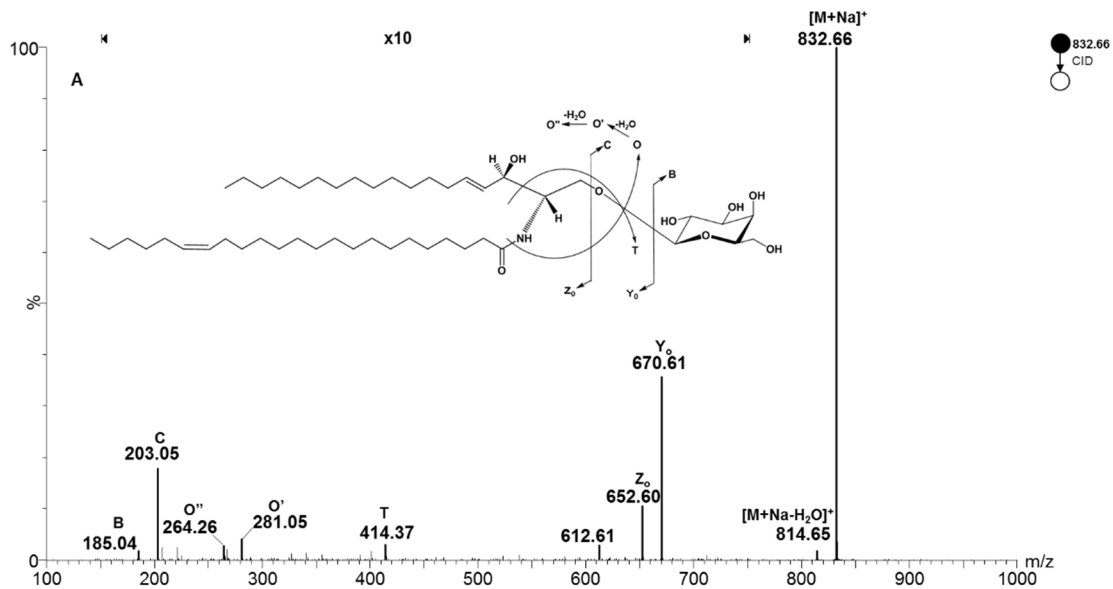
Figure S22. Accumulation of Glycolipids in CBE-Treated RAW264.7 Cells.

Figure S23. Representative Glycolipids Detected and Annotated in CBE-Treated RAW 264.7 Cells.





**Figure S2. Effect of Fatty Acyl Chain  $\alpha$ -Hydroxyl Group on the Oxidative Cleavage of Sphingosine Double Bond.** (a) Hydroxylated, GalCer d18:1/18:0(2OH), and (b) Non-hydroxylated, GalCer d18:1/18:0. (Explanation of symbolic representations is described in Fig. S1).



**Figure S3a. Collision-Induced Dissociation (CID) MS/MS Spectra of Galactocerebroside  $m/z$  832.66 in Bovine Brain Obtained in Argon Gas at CID 55 eV.** Nomenclature was based on the system developed by Domon and Costello<sup>141</sup> and Ann and Adams<sup>227</sup>. In all cases where isomers exist as discussed in the text, only one scheme is shown in each panel.

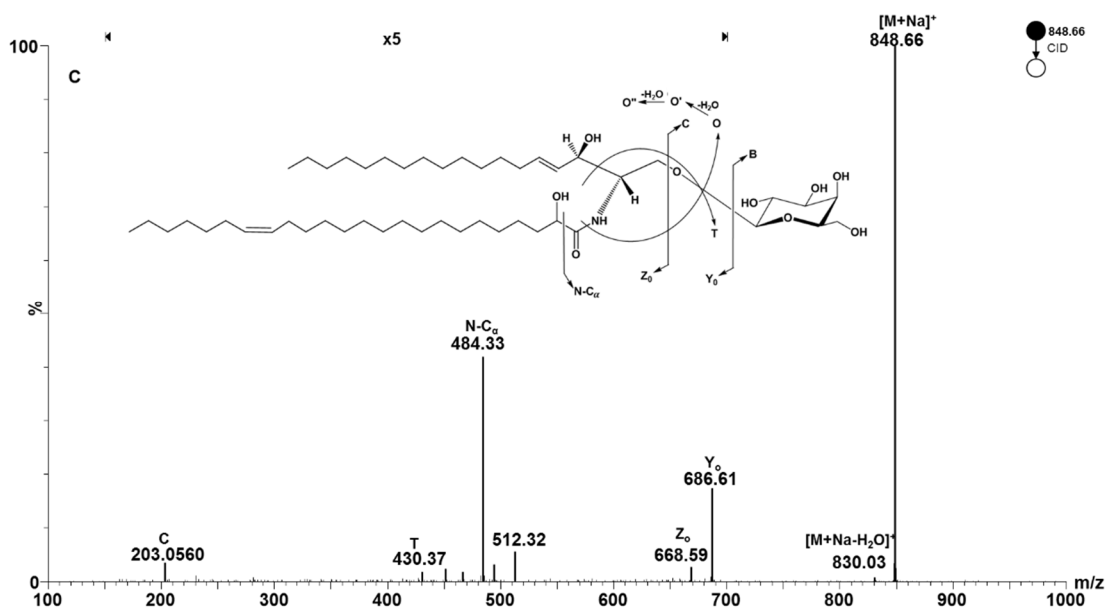


**Figure S3b. Collision-Induced Dissociation (CID) MS/MS Spectra of Galactocerebroside  $m/z$  848.66 in Bovine Brain Obtained in Argon Gas at CID 55 eV.** Nomenclature was based on the system developed by Domon and Costello<sup>141</sup> and Ann and Adams<sup>227</sup>. In all cases where isomers exist as discussed in the text, only one scheme is shown in each panel.

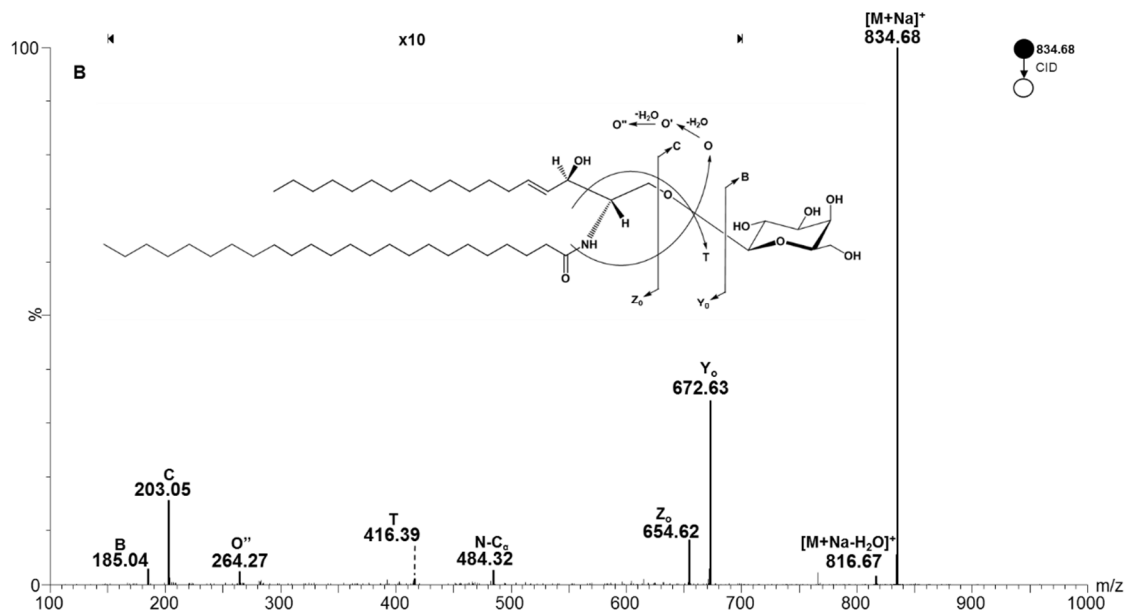


**Figure S3c. Collision-Induced Dissociation (CID) MS/MS Spectra of Galactocerebroside  $m/z$  834.68 in Bovine Brain Obtained in Argon Gas at CID 55 eV.** Nomenclature was based on the system developed by Domon and Costello<sup>141</sup> and Ann and Adams<sup>227</sup>. In all cases where isomers exist as discussed in the text, only one scheme is shown in each panel.

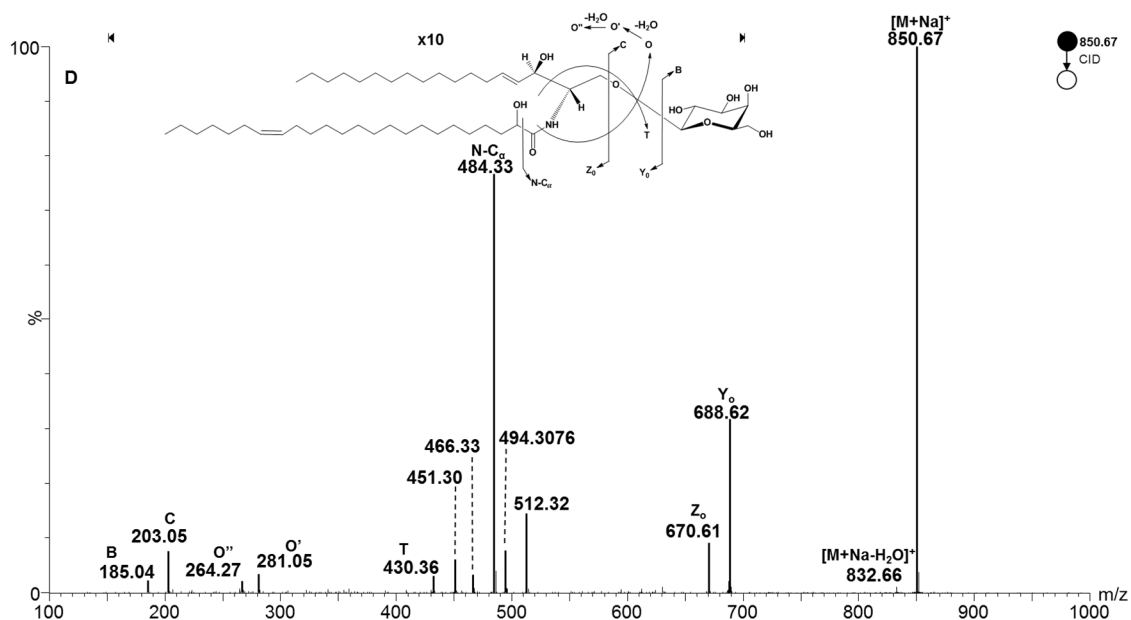


**Figure S3d. Collision-Induced Dissociation (CID) MS/MS Spectra of Galactocerebroside  $m/z$  850.67 in Bovine Brain Obtained in Argon Gas at CID 55 eV.** Nomenclature was based on the system developed by Domon and Costello<sup>141</sup> and Ann and Adams<sup>227</sup>. In all cases where isomers exist as discussed in the text, only one scheme is shown in each panel.

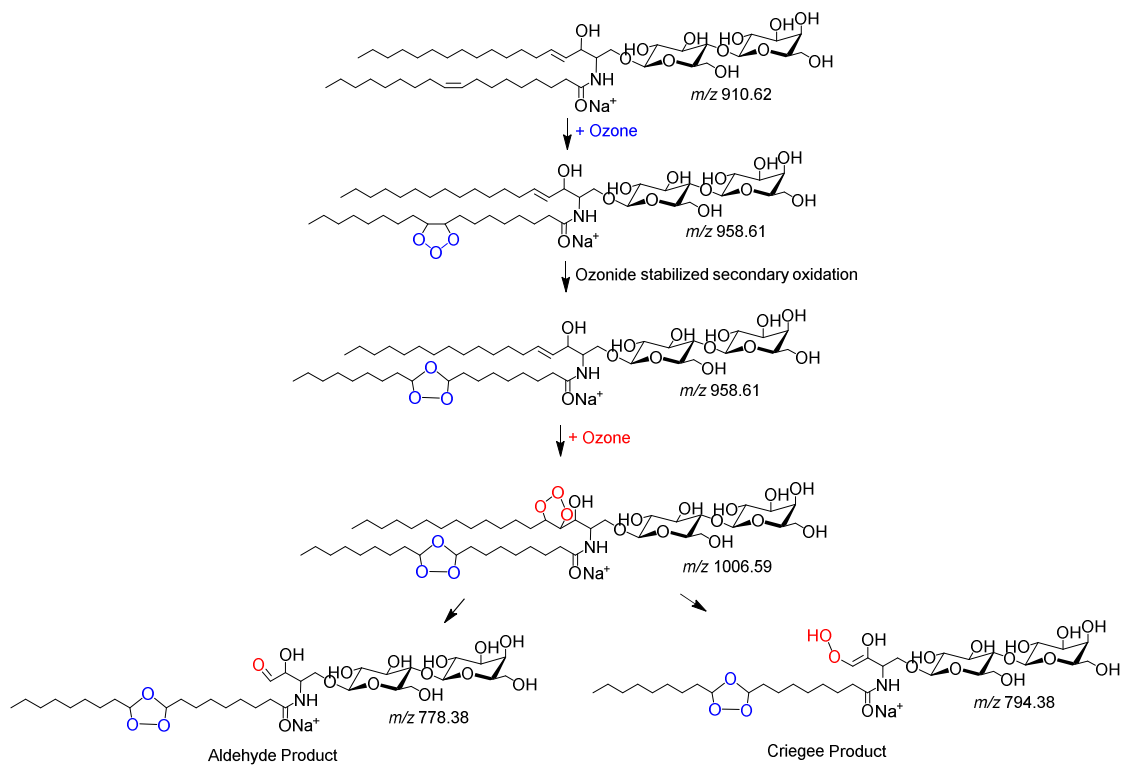


**Figure S4. Overview of the Proposed Pathways Leading to the Formation of Secondary Ozonolysis Products Observed in the OzID-MS Spectrum.**

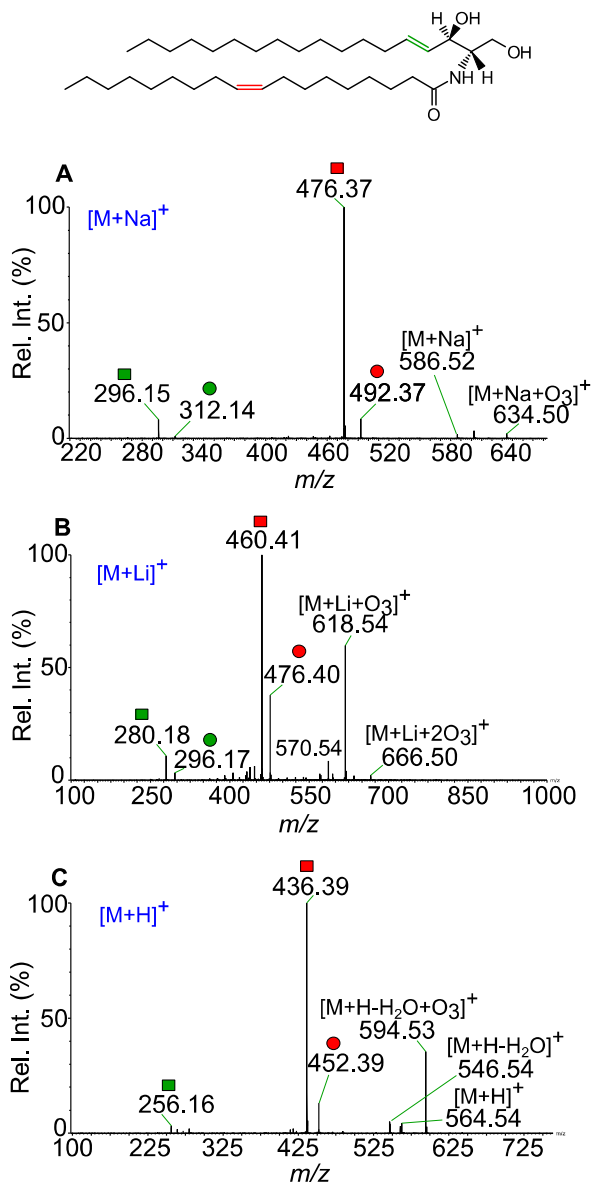


**Figure S5. OzID-MS Spectra of Cationized Cer d18:1/18:1(9Z).** The analyte (10 pmol/ $\mu$ L) spiked with  $\sim$ 1 mM LiCl or 10 mM  $\text{NH}_4\text{COOH}/0.1\%$  HCOOH to induce the formation of  $[\text{M}+\text{Li}]^+$  and  $[\text{M}+\text{H}]^+$ , respectively. No spiking of  $\text{Na}^+$ -containing salt was necessary to induce  $[\text{M}+\text{Na}]^+$  formation. Samples were infused using a syringe pump to the ESI source of Synapt G2 HDMS equipped with  $\text{O}_3$  gas in the collision cell. Precursor ions corresponding to different adducts were chosen for OzID-MS. Spectra shown are average of 1.0 min acquisition time.

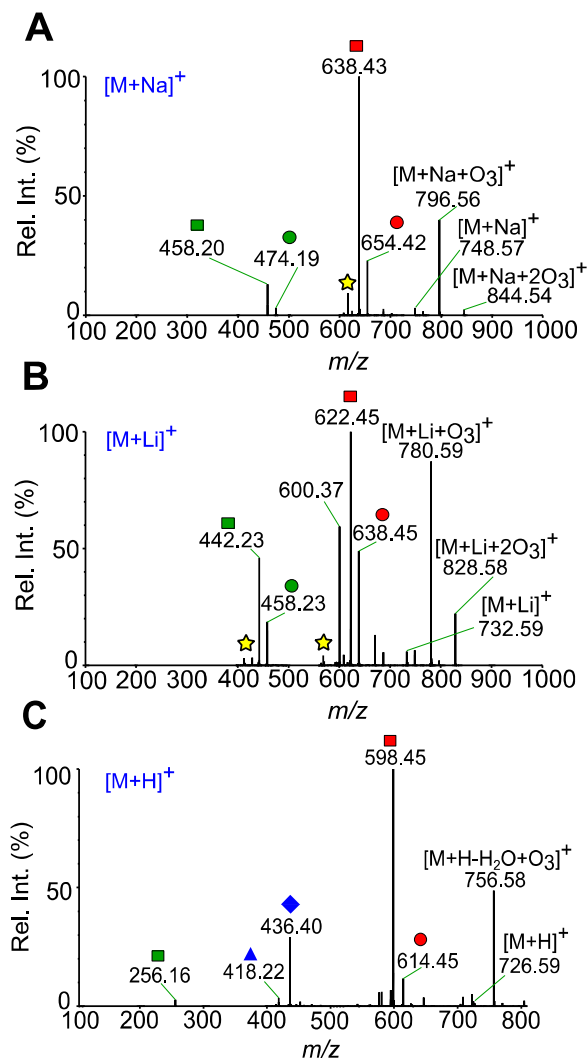
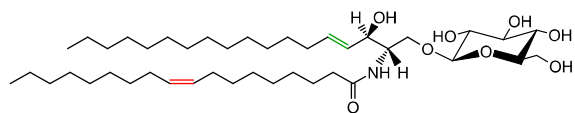


**Figure S6. OzID-MS Spectra of Cationized GlcCer d18:1/18:1(9Z).** The analyte (10 pmol/ $\mu$ L) spiked with  $\sim$ 1 mM LiCl or 10 mM  $\text{NH}_4\text{COOH}/0.1\%$   $\text{HCOOH}$  to induce the formation of  $[\text{M}+\text{Li}]^+$  and  $[\text{M}+\text{H}]^+$ , respectively. No spiking of  $\text{Na}^+$ -containing salt was necessary to induce  $[\text{M}+\text{Na}]^+$  formation. Samples were infused using a syringe pump to the ESI source of Synapt G2 HDMS equipped with  $\text{O}_3$  gas in the collision cell. Precursor ions corresponding to different adducts were chosen for OzID-MS. Spectra shown are average of 1.0 min acquisition time.  $\star$ : ozonide stabilized secondary oxidation cleavage product of sphingosine *n*-14 double bond (see Fig. 22),  $\blacklozenge$ : loss of glycan headgroup,  $\blacktriangle$ : loss of  $\text{H}_2\text{O}$ .

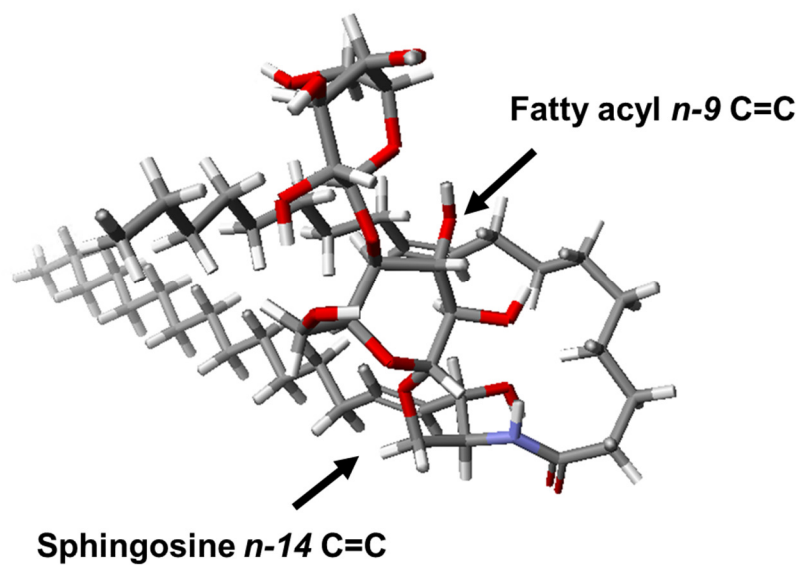


**Figure S7. Most Stable Conformer of Neutral Form of LacCer d18:1/18:1(9Z) Calculated Using MO-G with PM6.** Color indicates different atom (Gray: Carbon, White: Hydrogen, Red: Oxygen, Purple: H<sup>+</sup>, Cyan: Nitrogen).

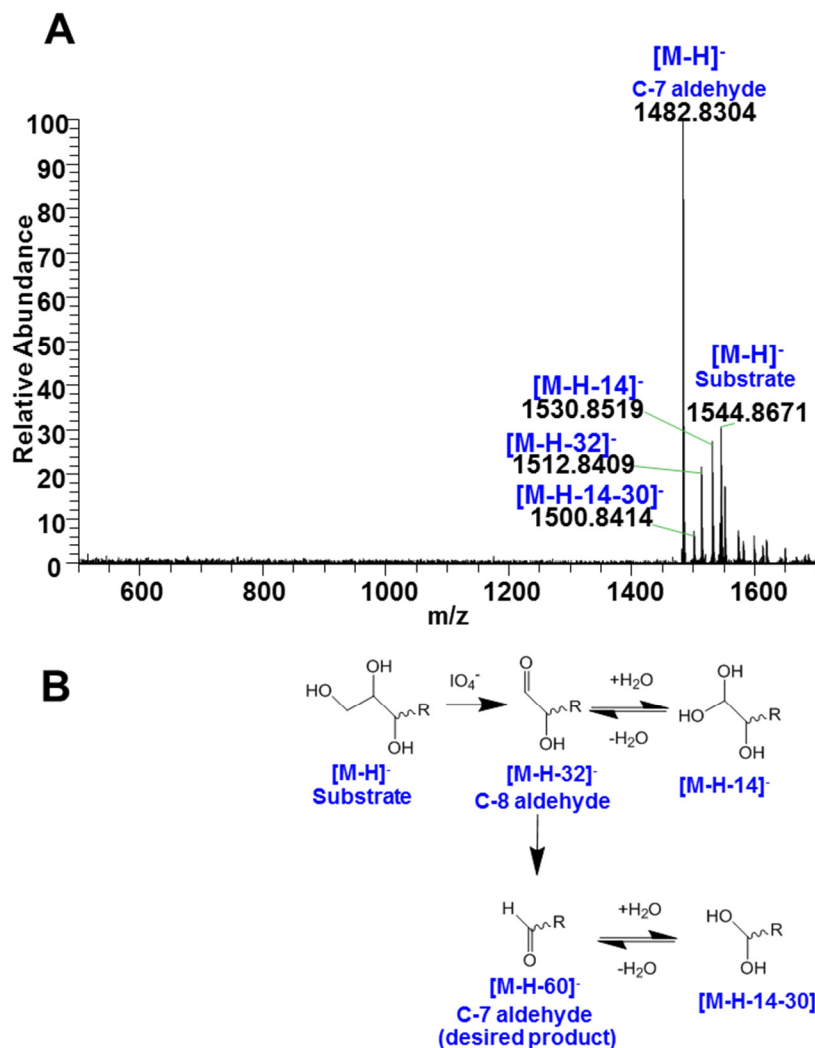


**Figure S8. Demonstration of Incomplete Oxidation of Ganglioside GM1a d18:1/18:0 After Subjecting to 1mM NaIO<sub>4</sub> for Only 30 Minutes Incubation in Ice Bath (~0°C).** (A) full scan mass range showing the presence of unwanted products of incomplete oxidation; (B) plausible origin of the observed side products, aldehydes are known to undergo geminal diol formation in aqueous medium<sup>354</sup> analogous to hemiacetals which could subsequently undergo dehydration to yield the observed side products. Notably, when incubation is done under optimum conditions (*i.e.* 60 minutes at ~0°C as discussed in the text, almost exclusively C-7 aldehyde was obtained (see main text).

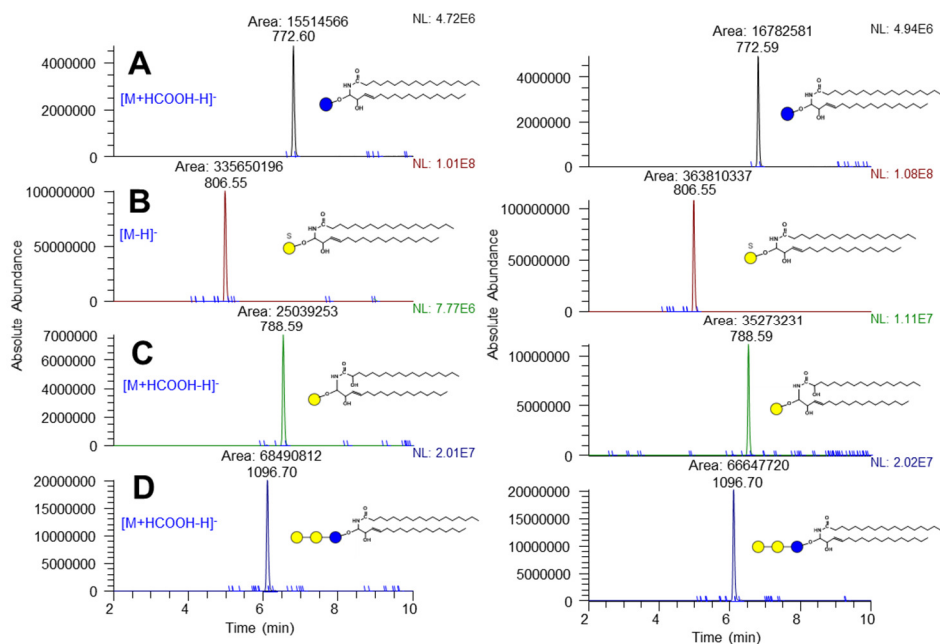


**Figure S9. Chemoselectivity of NaIO<sub>4</sub> Oxidation Under Mild Conditions.** Left column shows the extracted ion chromatograms of unoxidized glycosphingolipids in oxidation buffer alone. Right column shows the extracted ion chromatograms of the same compounds after 60 mins incubation with 1 mM NaIO<sub>4</sub>. Comparable peak areas and absolute ion abundance were obtained between these two sets of data indicating the treatment does not significantly affect these structural motifs. Difference in the observed abundance and peak area could be attributed to sample handling including solid-phase extraction (SPE) and transfer of sample from one container to the other. (A), GlcCer d18:1/18:0 (contains only vicinal diols); (B), Sulfatide d18:1/18:0 (contains a sulfate group); (C), GalCer d18:1/18:0(2ROH) (contains  $\alpha$ -hydroxyl group in the fatty acyl chain); (D), Gb3Cer d18:1/18:0 (contains vicinal diols and longer glycan chain). Symbols are defined in Fig. 1 of the main text.

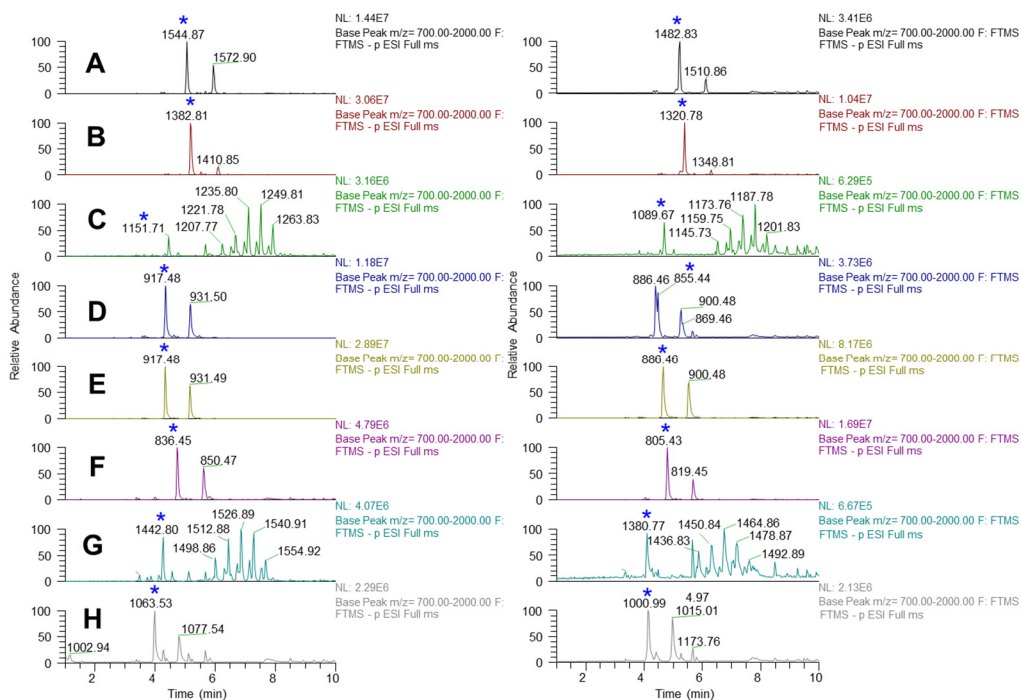


**Figure S10. Total ion chromatograms (TIC) of Oxidized Gangliosides.** Left column represents the of the unoxidized gangliosides with a mass range of  $m/z$  700-2000. The right column represents the corresponding TIC of oxidized gangliosides. The major components of each mixture corresponding to the EIC shown in Fig. 3 are marked with asterisk (\*). In each case, a loss of 62.04 Da (from  $[M-H]^-$ ) or 32.02 Da (from  $[M-2H]^{2-}$ ) was observed. (A), GM1a,  $[M-H]^-$ ; (B), GM2,  $[M-H]^-$ ; (C), GM3,  $[M-H]^-$ ; (D), GD1a,  $[M-2H]^{2-}$ ; (E), GD1b,  $[M-2H]^{2-}$ ; (F), GD2,  $[M-2H]^{2-}$ ; (G), GD3,  $[M-H]^-$ ; (H), GT1b,  $[M-2H]^{2-}$ .

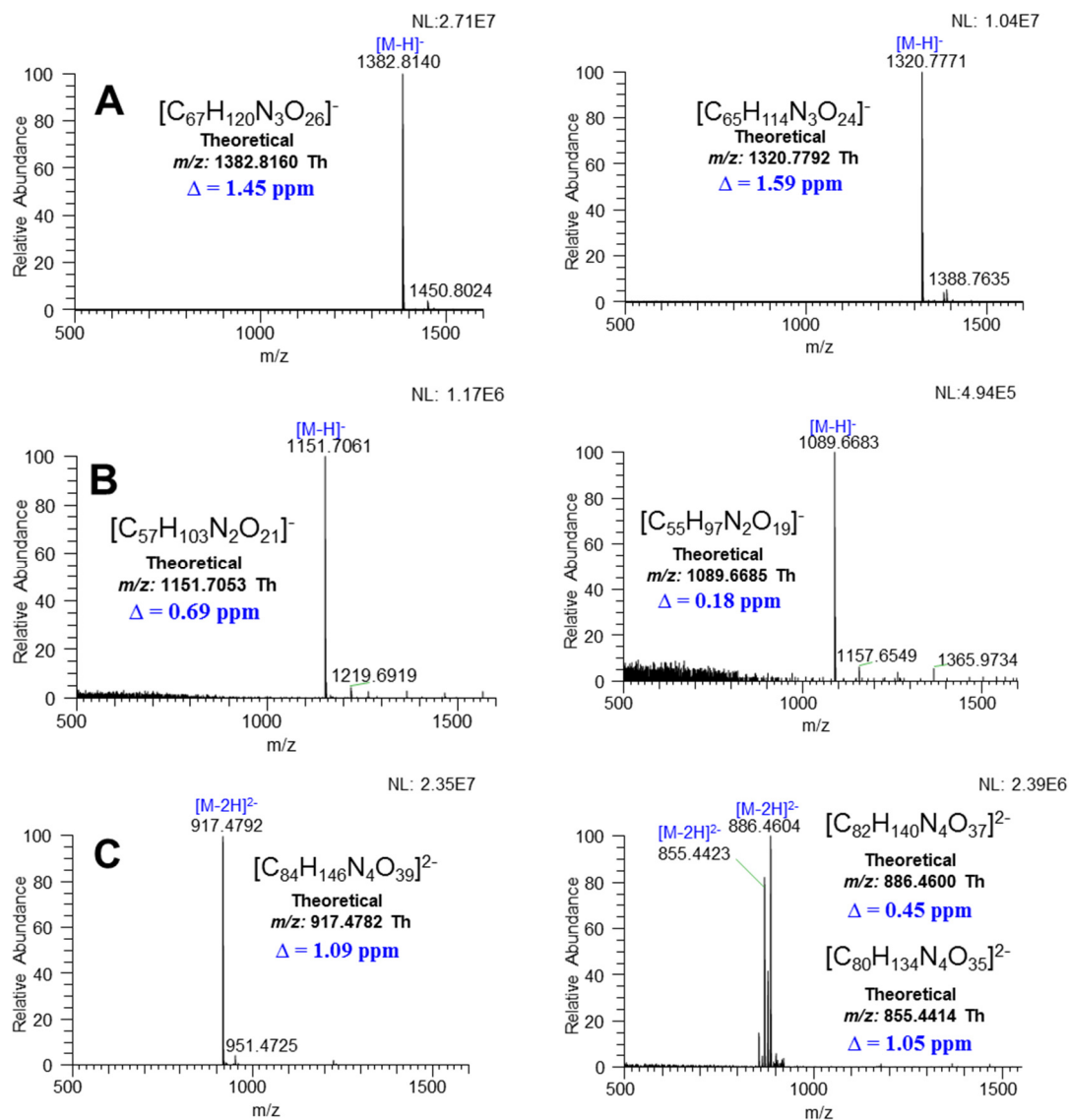


**Figure S11. Full Scan Mass Range of Unoxidized (Left Column) and Oxidized (Right Column) Gangliosides Based on the Peak Indicated by Asterisk (\*) in the Right Column of Fig. S3. (A), GM2 d18:1/18:0; (B), GM3 d18:1/16:0; (C), GD1a d18:1/18:0; (D), GD1b d18:1/18:0; (E), GD2 d18:1/18:0; (F), GD3 d18:1/16:0; (G), GT1b d18:1/18:0.  $\Delta$  indicates absolute mass error.**

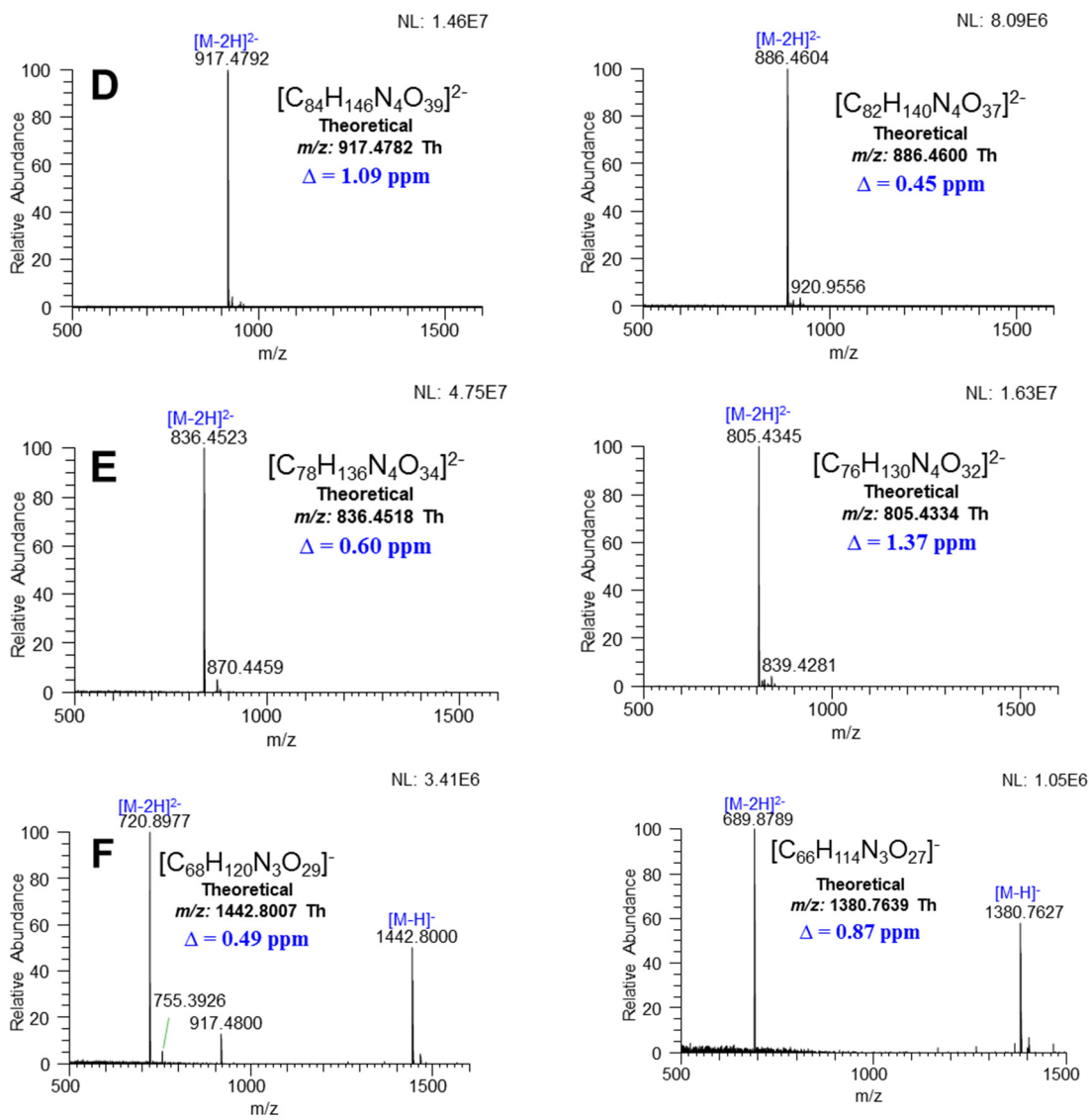
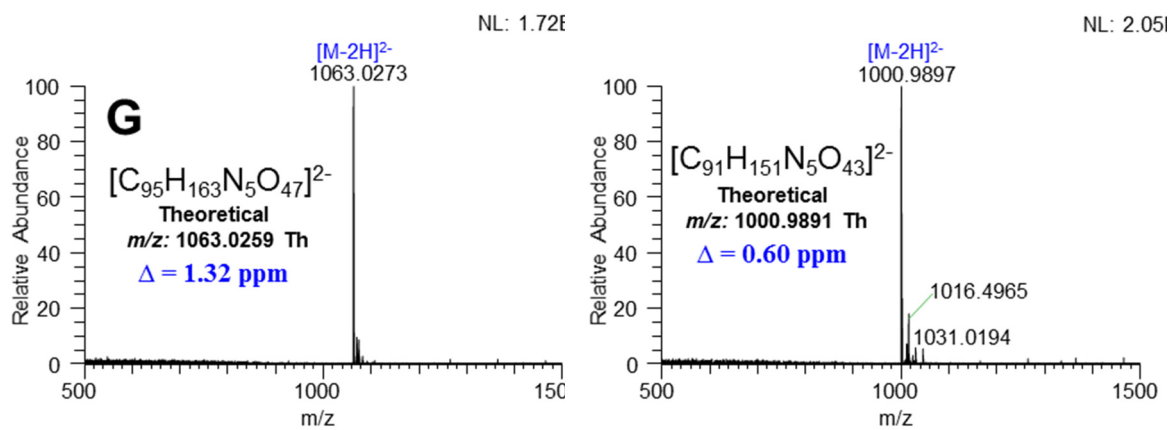
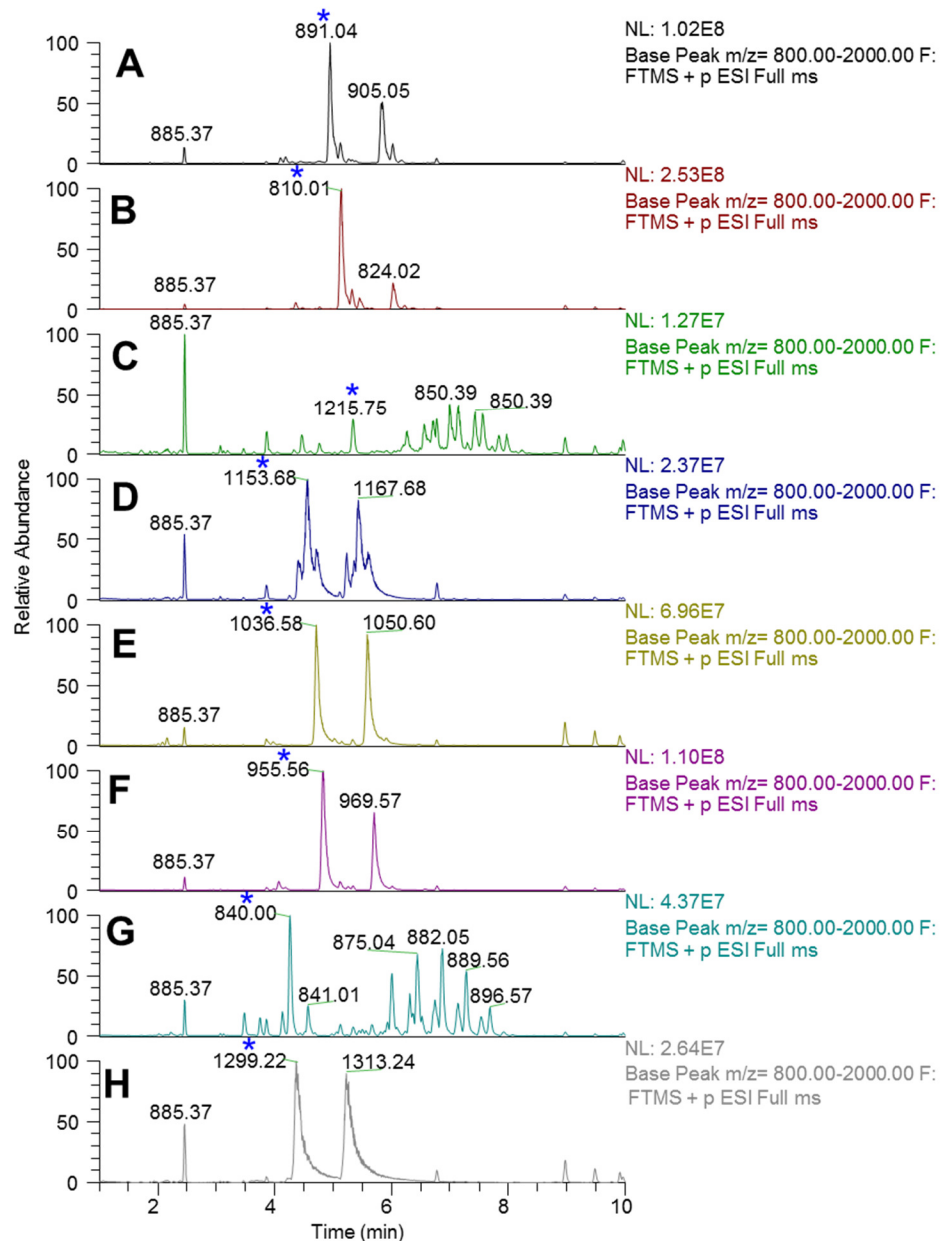


Figure S11 (Continued).



**Figure S11 (Continued).**



**Figure S12. Total Ion Chromatograms of Ganglioside Standard Mixtures Labeled with AminoxyTMT<sup>0</sup>.** The major components of each mixture corresponding to the unoxidized and oxidized gangliosides whose EIC's are shown in Fig. S3 are marked with asterisk (\*). (A), GM1a; (B), GM2; (C), GM3; (D), GD1a; (E), GD1b; (F), GD2; (G), GD3; (H), GT1b. All masses shown are  $[M+2H]^{2+}$ , ion with  $m/z$  885.37 and peaks above 8.5 min have been detected in the reagent blanks and not a component of ganglioside standards.

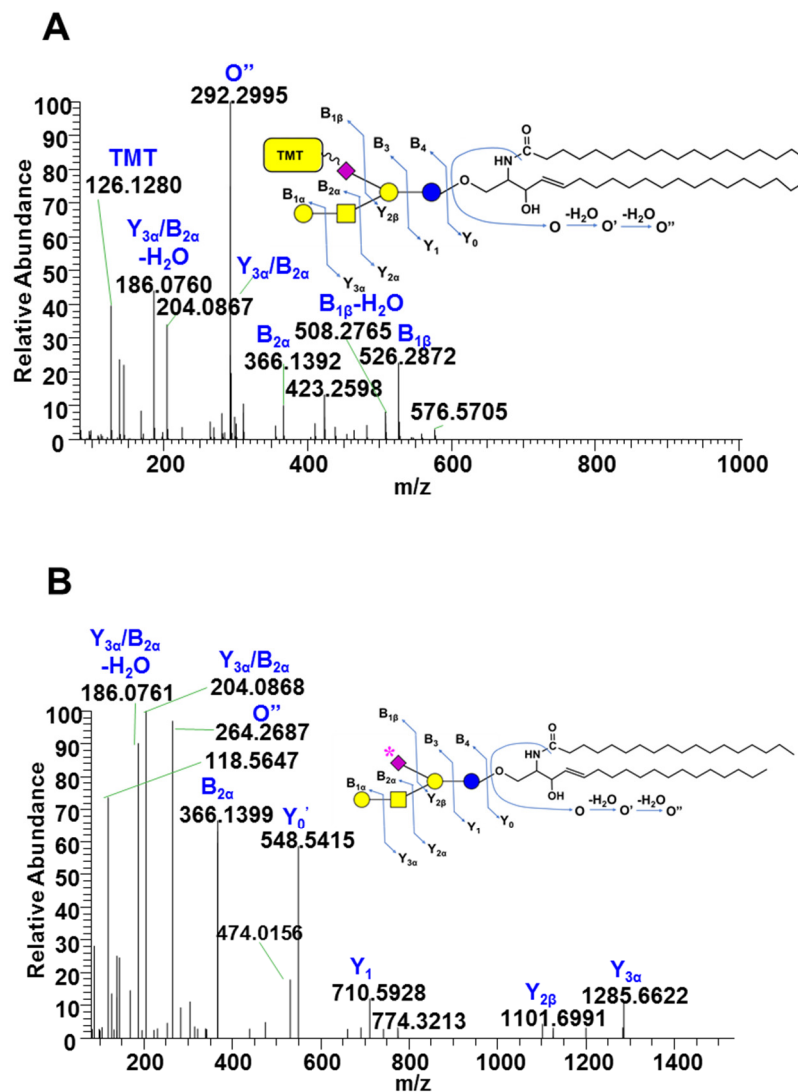


**Figure S13. MS/MS Spectrum of AminoxyTMT<sup>0</sup>-Labeled GM1a d20:1/18:0 Using the [M+2H]<sup>2+</sup> ( $m/z$  905.05) as Precursor Ion Showing the O'' ion at  $m/z$  292.2995 Diagnostic of the Long Chain Base d20:1 (A). MS/MS spectrum of oxidized (unlabeled) GM1a d18:1/18:0 using the [M+H]<sup>+</sup> as precursor ion (B).**

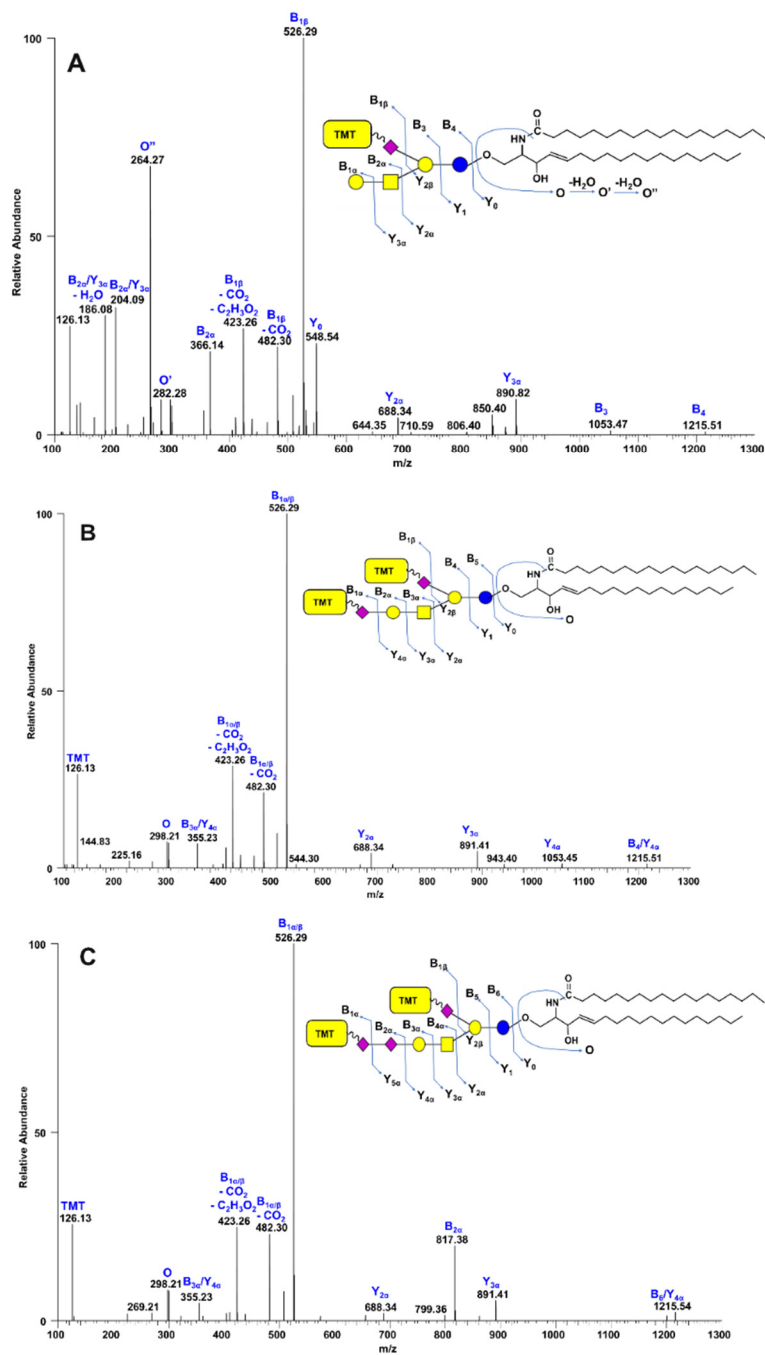


**Figure S14. Representative HCD-MS/MS (Stepped NCE 22,26,30) of AminoxyTMT<sup>0</sup>-Labeled Gangliosides from Porcine Brain Extract.** GM1a d18:1/18:0 (A), GD1a d18:1/18:0 (B), and GT1b d18:1/18:0 (C). All precursor ions used are  $[M+2H]^{2+}$ .

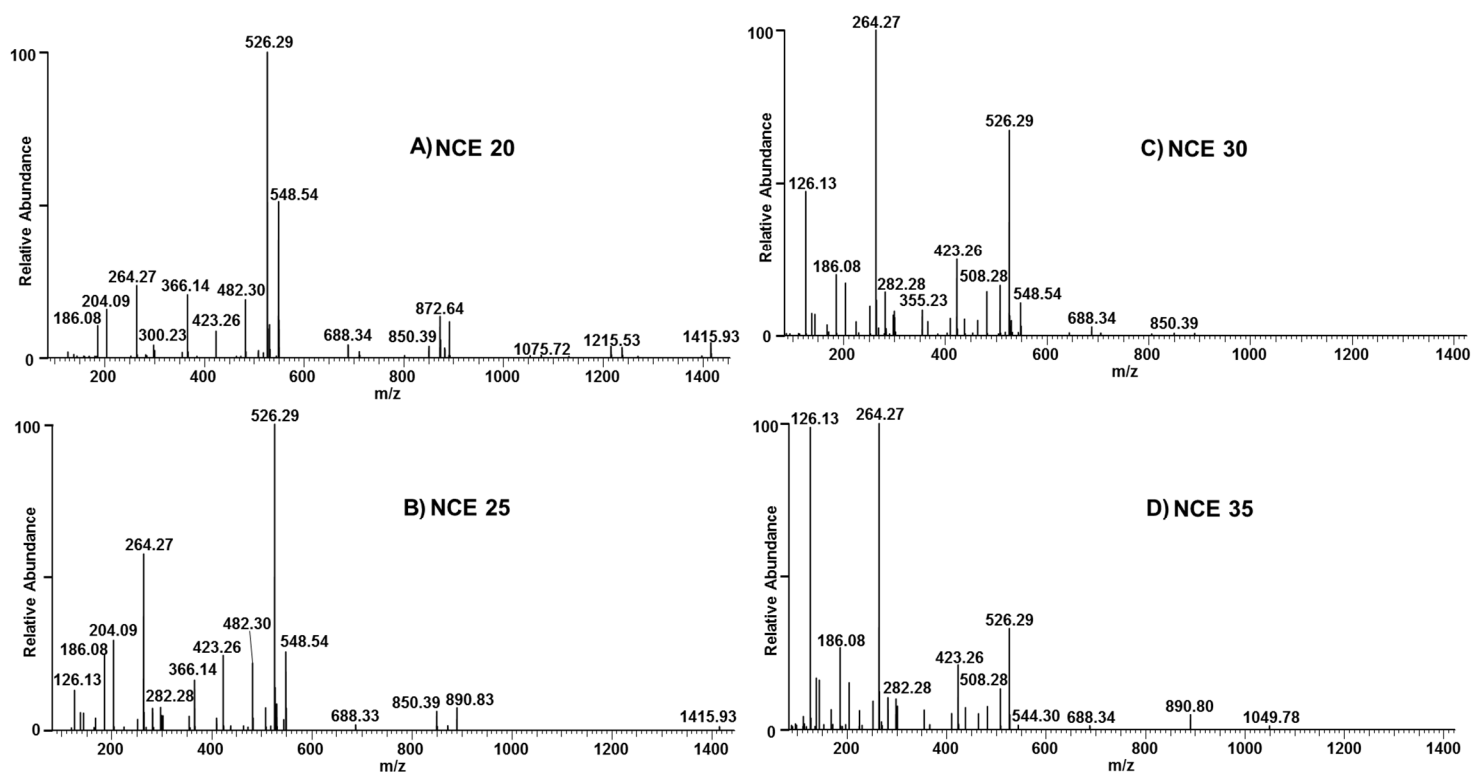


**Figure S15. HCD-MS/MS Spectra of AminoxyTMT<sup>0</sup>-Labeled Ganglioside GM1a d18:1/18:0 at Different Normalized Collision Energy (NCE) Values. (A) NCE 20; (B) NCE 25; (C) NCE 30; (D) NCE 35. Increasing the NCE values generate higher yield of reporter ion region along with a corresponding decrease in the intensity of glycan-informative fragments. Depending on the analytical purpose, appropriate collision energy values can be used.**

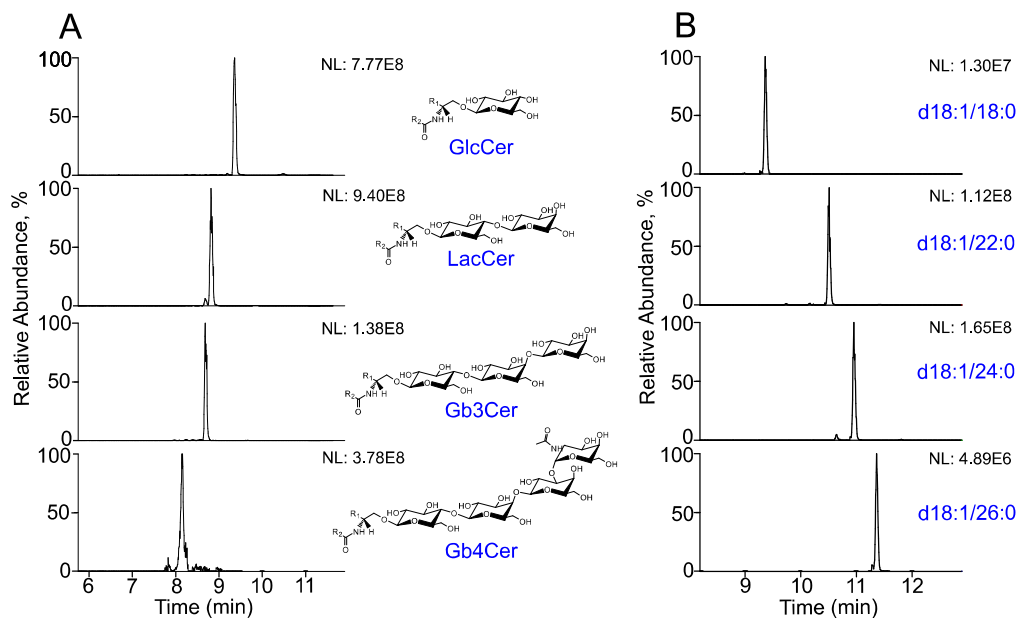


**Figure S16. Elution Behavior of Permethyated Glycolipids in a Cortecs C18 Column.** A) Extracted ion chromatograms (EIC) of standard glycolipids all possessing d18:1/18:0 ceramide backbone. B) EIC of HexCer from RAW264.7 cell extract carrying different ceramide backbone (mass tolerance: 5 ppm, identity validated from MS/MS spectra).

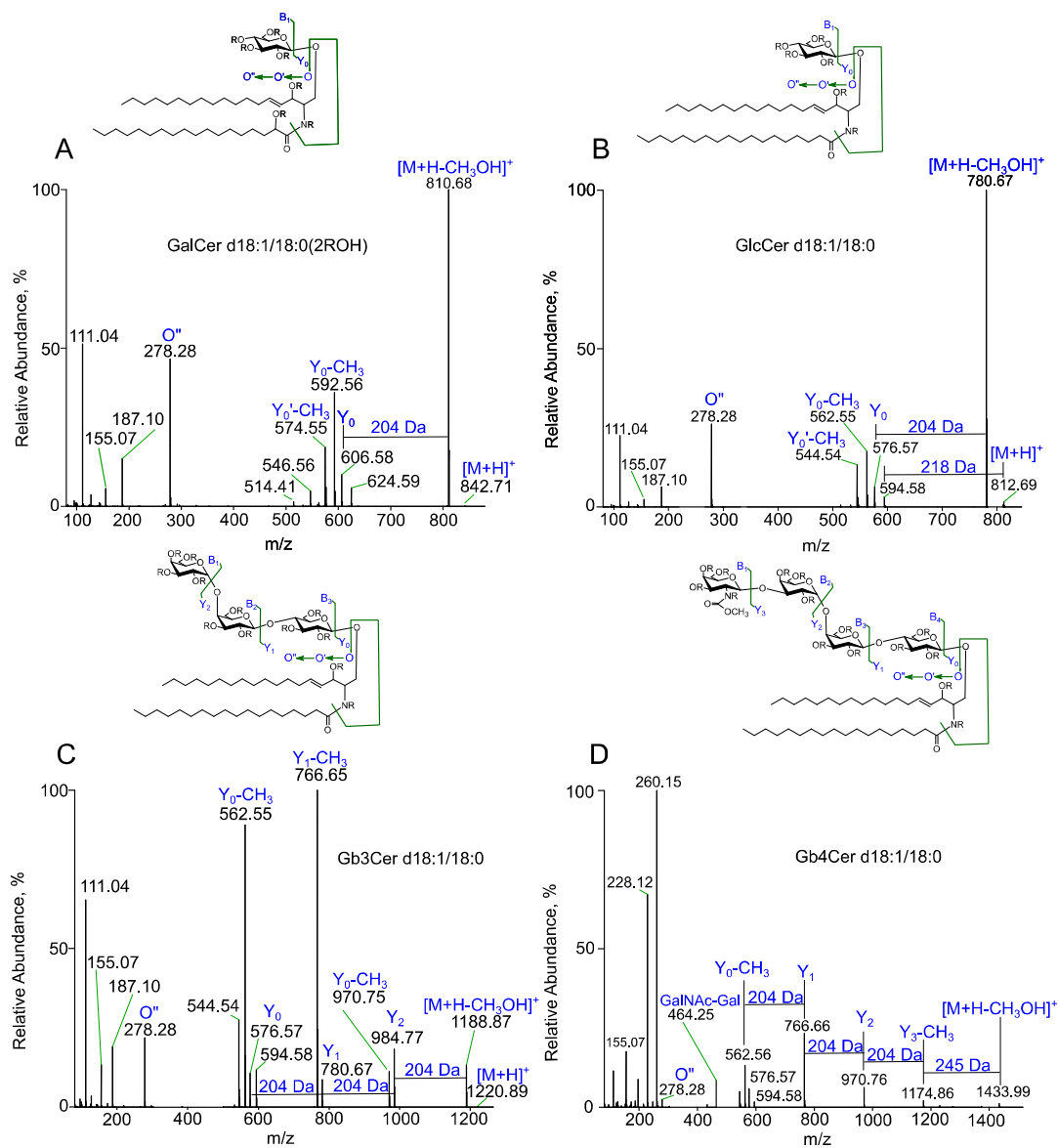


**Figure S17. Higher Energy Collisional Dissociation (HCD) Fragmentation Characteristics of Permethylated Glycolipid Standards.** A) Hydroxylated glycolipid, [ $^{13}\text{C}_7$ ]-GalC18:1/18:0(2ROH). B) Monohexosyl glycolipid, [ $^{13}\text{C}_6$ ]-GlcC18:1/18:0. C) Trihexosyl glycolipid, [ $^{13}\text{C}_{12}$ ]-Gb3C18:1/18:0. D) N-acetylhexosamine containing glycolipid, [ $^{13}\text{C}_{15}$ ]-Gb4C18:1/18:0. All spectra were recorded at NCE=20 in a QExactive HF instrument. Fragmentation annotation is according to Domon and Costello<sup>141</sup> and Ann and Adams<sup>264</sup> nomenclature. R:  $-\text{CH}_3$  group.

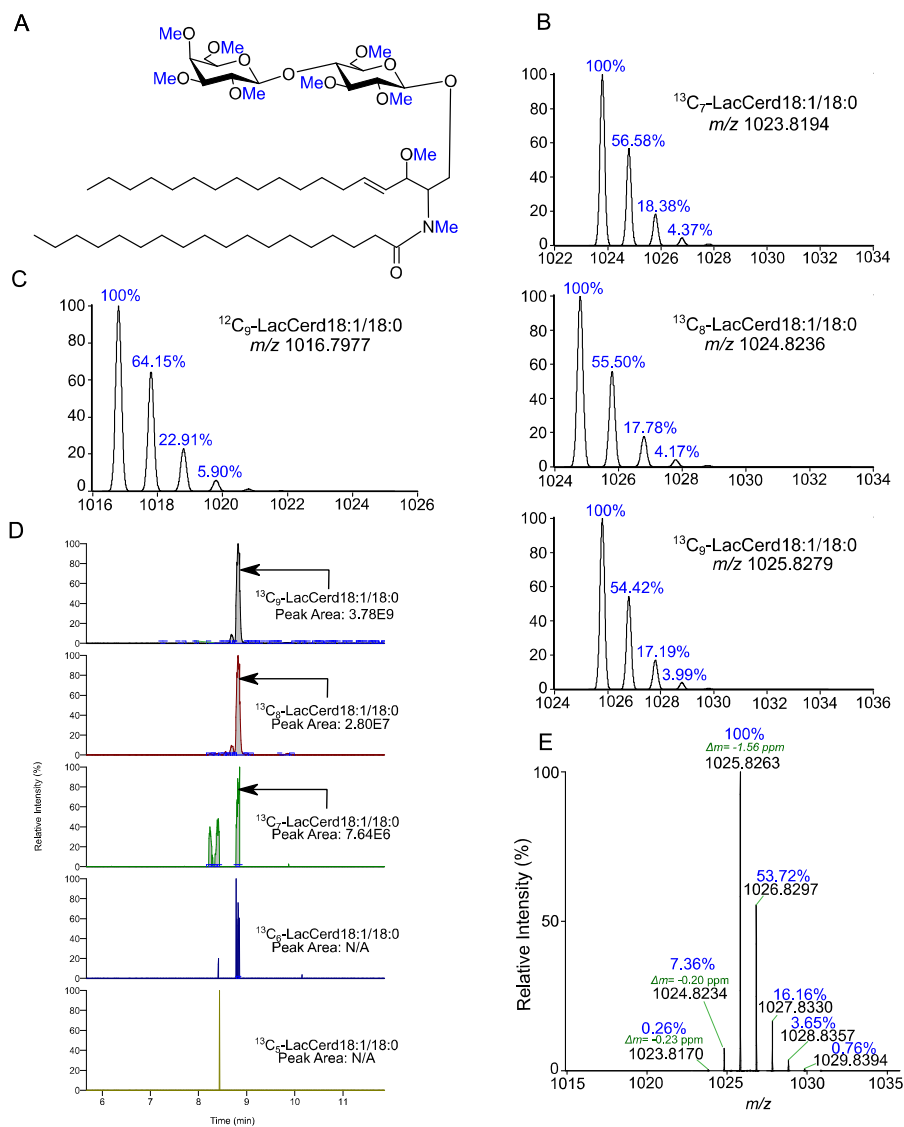
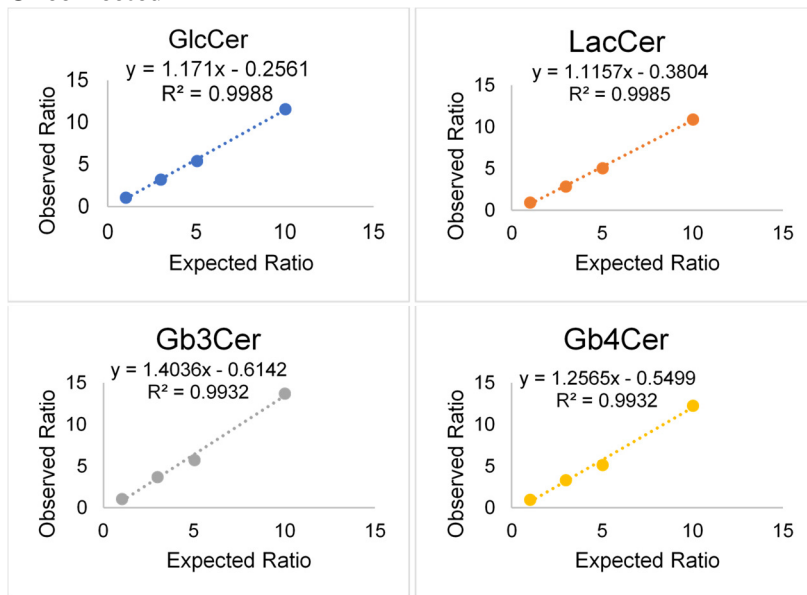


**Figure S18. Effect of  $^{12}\text{C}$  Impurity in the Resultant Isotopic Distribution Pattern of [ $^{13}\text{C}$ ]-Labeled Glycolipid.** A) Structure of representative glycolipid, LacCer d18:1/18:0 showing the theoretical maximum number of  $^{13}\text{C}$  that can be attached by permethylation using  $^{13}\text{CH}_3\text{I}$  (highlighted in blue). B) *In-silico* natural isotope distribution pattern of LacCer d18:1/18:0 with specified number of  $^{13}\text{C}$  atoms. C) *In-silico* isotopic distribution pattern of  $^{12}\text{C}$ -permethylated LacCer d18:1/18:0 obtained using the isotopic distribution modeling function of Molecular Weight Calculator v6.5 showing the isotopomers that overlap with the monoisotopic peak of fully- $^{13}\text{C}$  permethylated species. D) Extracted ion chromatograms of monoisotopic peaks of  $^{13}\text{C}_5$  to  $^{13}\text{C}_9$  labeled LacCer d18:1/18:0 (mass tolerance = 5.0 ppm) with their peak areas. E) Experimental isotopic distribution pattern of  $^{13}\text{C}$ -labeled LacCer d18:1/18:0 along with the mass accuracy of peaks depicted in B.

### Uncorrected



### Corrected

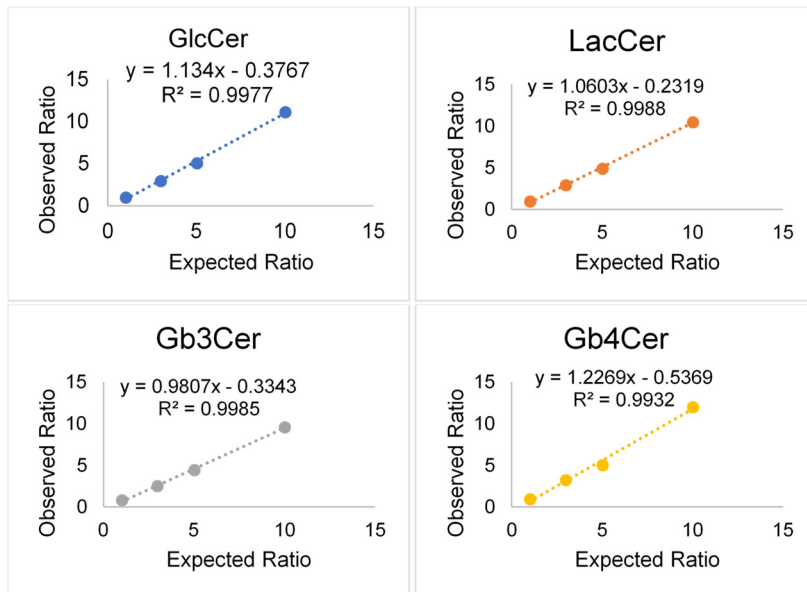
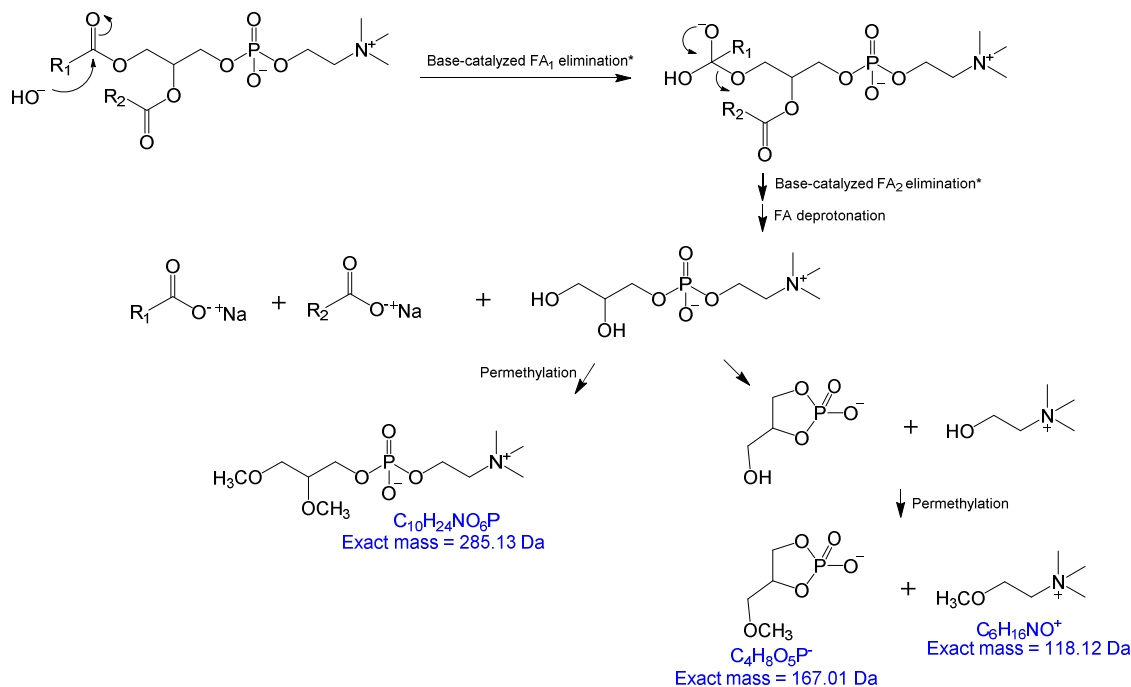


**Figure S19. Regression Curves Based on Corrected (Top) and Uncorrected (Bottom) <sup>12</sup>C/<sup>13</sup>C Ratios.** Standard glycolipids were independently permethylated using <sup>12</sup>CH<sub>3</sub>I and <sup>13</sup>CH<sub>3</sub>I, pooled at different ratios and analyzed by RPLC-MS as described in the experimental section.



\*FA<sub>1</sub> and FA<sub>2</sub> elimination is a concerted process.

**Figure S20. Proposed Pathway for the Breakdown of Phospholipids Under Alkaline Conditions.** As an example, shown here is the structure of phosphatidylcholine (PC) which undergoes alkali-induced ester hydrolysis causing elimination of both fatty acyl chains<sup>345,355</sup> and a glycerophosphocholine (GPC). The GPC could further breakdown<sup>345</sup> to cyclic phosphate ester and choline. These products (GPC, cyclic phosphate ester, and choline) could undergo methylation in the presence of CH<sub>3</sub>I.

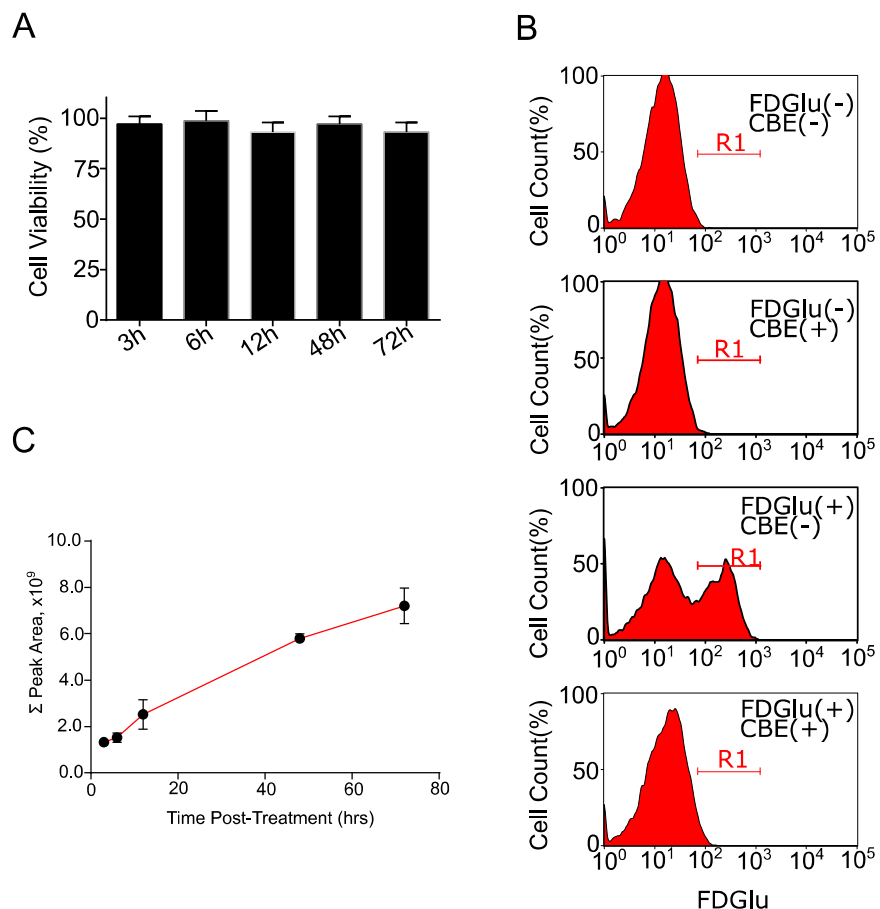


**Figure S21. Application of Stable Isotope Labeling by Permethylation and RPLC-MS for Relative Quantification of Neutral Glycolipids in Mammalian Cells.** A) Viability of RAW264.7 cells throughout the three-day study period measured using CCK-8 test kit. B) Flow cytometry-based functional validation of the inhibitory effect of CBE toward  $\beta$ -glucocerebrosidase in RAW264.7 cells using fluorescein di- $\beta$ -D-glucopyranoside (FDGlu), a highly specific substrate that becomes fluorescent after being cleaved by  $\beta$ -glucocerebrosidase. C) Measurement of summed peak areas of permethylated glycolipids in individual samples showing their increased abundance with increasing incubation time.

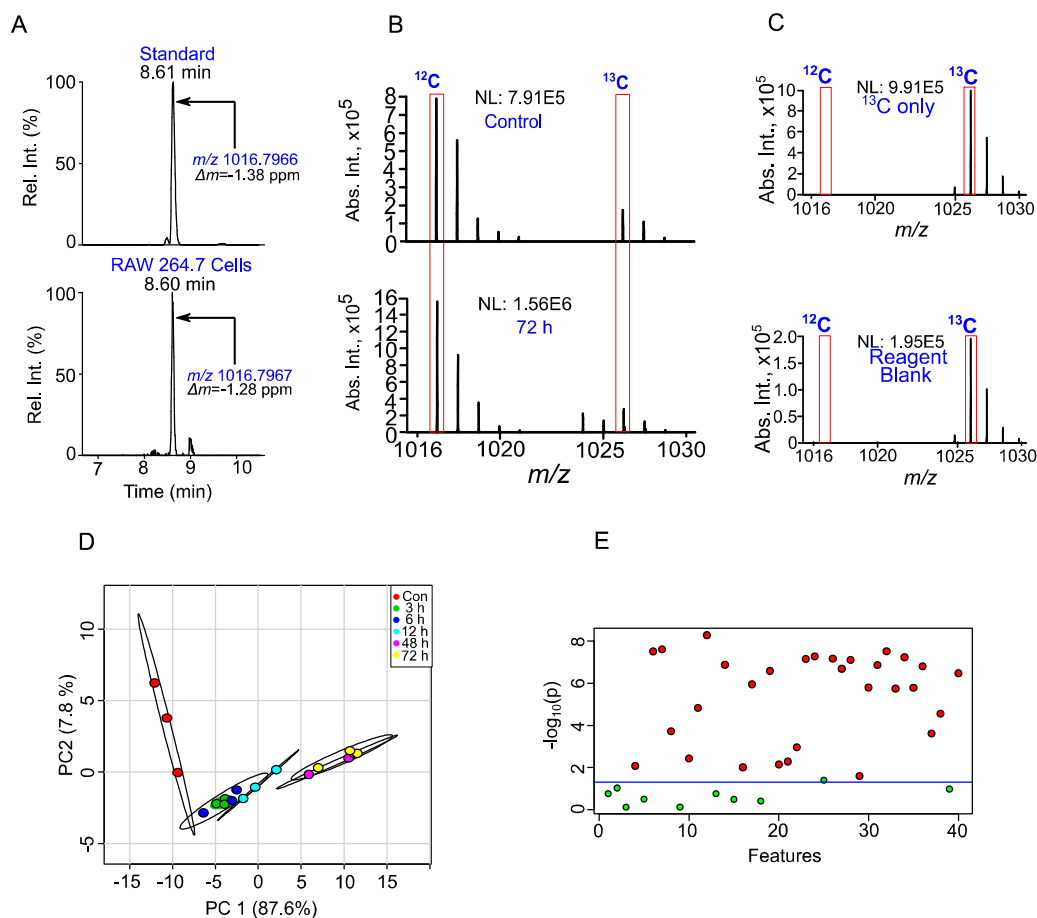


**Figure S22. Accumulation of Glycolipids in CBE-Treated RAW264.7 Cells.** A) Example of a glycolipid from RAW264.7 cells eluting at 8.60 min. The composition of this peak was verified using an authentic standard, LacCer18:1/18:0 based on retention time and accurate mass measurement. This peak was annotated as Hex<sub>2</sub>Cer18:1/18:0 based on MS/MS spectrum. B) Shown are the MS spectra for the same chromatographic peak at 8.60 min, in Control (untreated) and CBE-treated RAW264.7 cells where the y-axis is labeled with absolute intensity. Verification of the authenticity of signals observed in RAW264.7 cells. C) (Top) Spectrum of the peak at 8.60 min of the <sup>13</sup>C-permethylated pooled sample only, as described in the main text. (Bottom) Spectrum of the peak at 8.60 min of the reagent blank and [<sup>13</sup>C]-permethylated pooled sample, as described in the main text. The absence of any [<sup>12</sup>C]-labeled component in the top and bottom panels but presence in the cell-containing samples validate that the glycolipids observed originate from the cells and not from the reagents used throughout the cell culture, lipid extraction, or RPLC-MS analysis. D) Principal component analysis (PCA) of all measured ratios for each sample. E) One-way analysis of variance (ANOVA) of all the measured ratios where the blue dashed lines indicate the threshold cutoff ( $p < 0.05$ ).

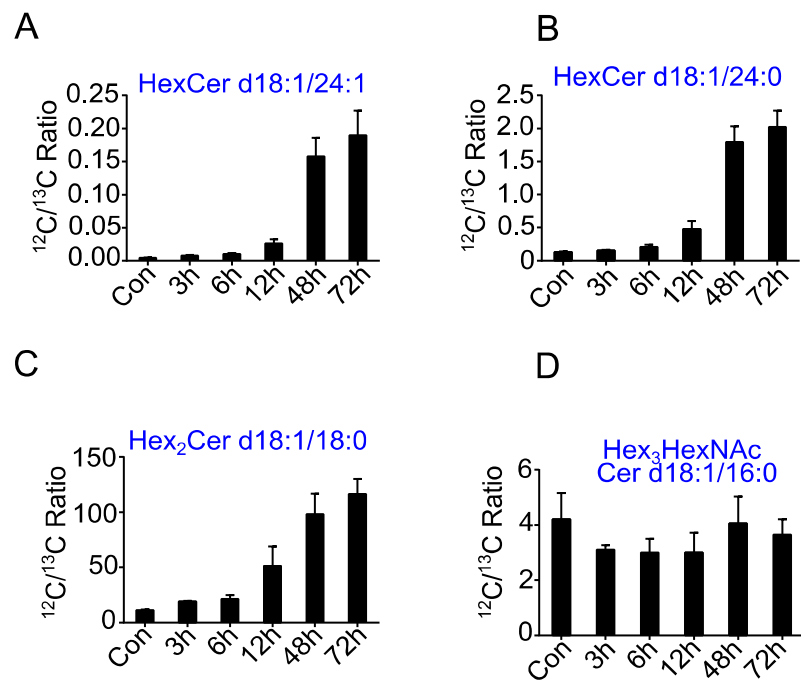


**Figure S23. Representative Glycolipids Detected and Annotated in CBE-Treated RAW 264.7 Cells.** A) HexCer d18:1/24:1, B) HexCer d18:1/24:0, C) Hex<sub>2</sub>Cer d18:1/18:0, D) Hex<sub>3</sub>HexNAcCer d18:1/16:0.

## APPENDIX C

### SUPPLEMENTARY CALCULATIONS

#### Calculation of Cation Affinities



Where: L = glycolipid, C<sup>+</sup> = cation (H<sup>+</sup>, Na<sup>+</sup>, Li<sup>+</sup>)

$$\Delta H^0 = [\Delta H^0_L + \Delta H^0_{C^+}] - \Delta H^0_{LC}$$

Where:  $\Delta H^0$  = cation affinity (kJ·mol<sup>-1</sup>)  
 $[\Delta H^0_L + \Delta H^0_{C^+}]$  = uncomplexed glycolipid + cation (kJ·mol<sup>-1</sup>)  
 $\Delta H^0_L$  = heat of formation of glycolipid (kJ·mol<sup>-1</sup>)  
 $\Delta H^0_{C^+}$  = heat of formation of cation (kJ·mol<sup>-1</sup>)  
 $\Delta H^0_{LC^+}$  = heat of formation of cation-glycolipid complex (kJ·mol<sup>-1</sup>)

	$\Delta H^0_L$ (kJ·mol <sup>-1</sup> )	$\Delta H^0_{C^+}$ (kJ·mol <sup>-1</sup> )	$\Delta H^0_{LC}$ (kJ·mol <sup>-1</sup> )
Na <sup>+</sup>	-2945.95	+545.09	-2740.33
Li <sup>+</sup>	-2945.95	+656.20	-2639.25
H <sup>+</sup>	-2945.95	+1303.16	-2445.62

*\*Calculations were performed using MOPAC with PM6 Hamiltonians in SCIGRESS*

$$\begin{aligned} [M+Na]^+: \quad \Delta H^0 &= [-2945.95 + 545.09] - (-2740.33) \\ \Delta H^0 &= -2400.86 + 2740.33 \\ \Delta H^0 &= + 339.47 \text{ (kJ·mol}^{-1}\text{)} \end{aligned}$$

$$\begin{aligned} [M+Li]^+: \quad \Delta H^0 &= [-2945.95 + 656.20] - (-2639.25) \\ \Delta H^0 &= -2289.75 + 2639.25 \\ \Delta H^0 &= + 349.50 \text{ (kJ·mol}^{-1}\text{)} \end{aligned}$$

$$\begin{aligned} [M+H]^+: \quad \Delta H^0 &= [-2945.95 + 1303.16] - (-2445.62) \\ \Delta H^0 &= -1642.79 + 2445.62 \\ \Delta H^0 &= + 802.83 \text{ (kJ·mol}^{-1}\text{)} \end{aligned}$$

APPENDIX D  
COPYRIGHT PERMISSIONS

	Page
Cold Spring Harbor Perspectives in Biology .....	201
Nature Reviews Cancer.....	203
Journal of the American Society for Mass Spectrometry .....	206
Analytical Chemistry .....	209
Analytical Chemistry .....	210



Rodell Barrientos &lt;rcbarrie@uncg.edu&gt;

**FW: CSHL Press Reprint Permission Request Form**

2 messages

**Brown, Carol** <brown@cshl.edu>  
 To: "rcbarrie@uncg.edu" <rcbarrie@uncg.edu>

Mon, Apr 8, 2019 at 3:03 PM

Hello Rodell,

This figure was modified and used with permission from several other sources - please see figure legend for details. I can grant permission for the use described below on behalf of Cold Spring Harbor Perspective in Biology, however, you will need to reach out to Macmillan to secure the necessary rights from them for the other two journals that were original sources for this figure.

Kind regards,

Carol C. Brown  
 Permissions Coordinator  
 Cold Spring Harbor Laboratory Press  
 500 Sunnyside Blvd  
 Woodbury, New York 11797  
 516 422 4038 ph.  
 516 422 4095 fx.  
[brown@cshl.edu](mailto:brown@cshl.edu)

-----Original Message-----

From: [reprint@cshl.edu](mailto:reprint@cshl.edu) [mailto:[reprint@cshl.edu](mailto:reprint@cshl.edu)]  
 Sent: Monday, April 08, 2019 11:35 AM  
 To: Reprint  
 Subject: CSHL Press Reprint Permission Request Form

Default Intro  
 Default Intro - line2

Name: Rodell Barrientos  
 Company/Institution: University of North Carolina at Greensboro  
 Library Address: 500 Laureate Way, North Carolina Research Campus,  
 Library Address (line 2): Suite 4226  
 City: Kannapolis  
 State (US and Canada): NC  
 Country: United States  
 Zip: 28081  
 Title:  
 Lab/Department:  
 Phone: 3365874210  
 Fax:  
 Email: [rcbarrie@uncg.edu](mailto:rcbarrie@uncg.edu)  
 Title of Publication: Modern Methods for Improved Determination of Intact Glycosphingolipids by Mass Spectrometry  
 Authors/Editors: Rodell Barrientos and Qibin Zhang  
 Date of Publication: 2019  
 Publisher: Elsevier  
 Title of CSHLP Journal/Book: Essentials of Glycobiology, Third edition  
 Title of Article/Chapter: Chapter 1 Historical Background and Overview  
 CSHL Authors/Editors: Ajit Varki and Stuart Kornfeld  
 Page Numbers: 1-20  
 Figure Numbers: 1.6  
 Figure Page Numbers:

<https://mail.google.com/mail/u/0/?ik=ce66afd8ea&view=pt&search=all&permthid=thread-f%3A1630273764914753084&siml=msg-f%3A16302737649...> 1/2

4/8/2019

UNCG Mail - FW: CSHL Press Reprint Permission Request Form

Copyright Date: 2015-2017  
Language: English  
Territory: United States  
Format: print and electronic  
Additional comments: Permission is requested to use for a review article, intended for submission to Analytica Chimica Acta, 2019, subject for the journal's usual peer review policy.

ipaddress: 204.084.006.016  
Default Footer  
Default Footer - line2

---

Rodell Barrientos <rbarrie@uncg.edu>  
To: "Brown, Carol" <brown@cshl.edu>

Mon, Apr 8, 2019 at 3:15 PM

Hi Carol, thanks for the information. I will reach out to Macmillan accordingly.

Thank you.

Best,  
Rodell  
[Quoted text hidden]  
--

**Rodell C. Barrientos**  
PhD candidate, Zhang Research Group  
Department of Chemistry and Biochemistry

Research Assistant,  
Center for Translational Biomedical Research

Office: 500 Laureate Way, NC Research Campus, Kannapolis, NC 28081  
E-mail: [rbarrie@uncg.edu](mailto:rbarrie@uncg.edu)



**SPRINGER NATURE LICENSE  
TERMS AND CONDITIONS**

Apr 08, 2019

This Agreement between Mr. Rodell Barrientos ("You") and Springer Nature ("Springer Nature") consists of your license details and the terms and conditions provided by Springer Nature and Copyright Clearance Center.

License Number	4564380081459
License date	Apr 08, 2019
Licensed Content Publisher	Springer Nature
Licensed Content Publication	Nature Reviews Cancer
Licensed Content Title	The sweet and sour of cancer: glycans as novel therapeutic targets
Licensed Content Author	Mark M. Fuster, Jeffrey D. Esko
Licensed Content Date	Jul 1, 2005
Licensed Content Volume	5
Licensed Content Issue	7
Type of Use	Thesis/Dissertation
Requestor type	academic/university or research institute
Format	print and electronic
Portion	figures/tables/illustrations
Number of figures/tables/illustrations	1
High-res required	no
Will you be translating?	no
Circulation/distribution	<501
Author of this Springer Nature content	no
Title	INNOVATIVE METHODS TO ADVANCE THE ANALYSIS OF INTACT GLYCOLIPIDS BY MASS SPECTROMETRY
Institution name	University of North Carolina at Greensboro
Expected presentation date	Jun 2019
Order reference number	1
Portions	Figure 1. Important glycans involved in tumour progression
Requestor Location	Mr. Rodell Barrientos 500 Laureate Way Suite 4226  KANNAPOLIS, NC 28081 United States Attn: Mr. Rodell Barrientos
Total	0.00 USD
Terms and Conditions	

**Springer Nature Terms and Conditions for RightsLink Permissions**

**Springer Nature Customer Service Centre GmbH (the Licensor)** hereby grants you a non-exclusive, world-wide licence to reproduce the material and for the purpose and requirements specified in the attached copy of your order form, and for no other use, subject to the conditions below:

1. The Licensor warrants that it has, to the best of its knowledge, the rights to license reuse of this material. However, you should ensure that the material you are requesting is original to the Licensor and does not carry the copyright of another entity (as credited in the published version).  
  
If the credit line on any part of the material you have requested indicates that it was reprinted or adapted with permission from another source, then you should also seek permission from that source to reuse the material.
2. Where **print only** permission has been granted for a fee, separate permission must be obtained for any additional electronic re-use.
3. Permission granted **free of charge** for material in print is also usually granted for any electronic version of that work, provided that the material is incidental to your work as a whole and that the electronic version is essentially equivalent to, or substitutes for, the print version.
4. A licence for 'post on a website' is valid for 12 months from the licence date. This licence does not cover use of full text articles on websites.
5. Where '**reuse in a dissertation/thesis**' has been selected the following terms apply: Print rights of the final author's accepted manuscript (for clarity, NOT the published version) for up to 100 copies, electronic rights for use only on a personal website or institutional repository as defined by the Sherpa guideline ([www.sherpa.ac.uk/romeo/](http://www.sherpa.ac.uk/romeo/)).
6. Permission granted for books and journals is granted for the lifetime of the first edition and does not apply to second and subsequent editions (except where the first edition permission was granted free of charge or for signatories to the STM Permissions Guidelines <http://www.stm-assoc.org/copyright-legal-affairs/permissions/permissions-guidelines/>), and does not apply for editions in other languages unless additional translation rights have been granted separately in the licence.
7. Rights for additional components such as custom editions and derivatives require additional permission and may be subject to an additional fee. Please apply to [Journalpermissions@springernature.com](mailto:Journalpermissions@springernature.com)/[bookpermissions@springernature.com](mailto:bookpermissions@springernature.com) for these rights.
8. The Licensor's permission must be acknowledged next to the licensed material in print. In electronic form, this acknowledgement must be visible at the same time as the figures/tables/illustrations or abstract, and must be hyperlinked to the journal/book's homepage. Our required acknowledgement format is in the Appendix below.
9. Use of the material for incidental promotional use, minor editing privileges (this does not include cropping, adapting, omitting material or any other changes that affect the meaning, intention or moral rights of the author) and copies for the disabled are permitted under this licence.
10. Minor adaptations of single figures (changes of format, colour and style) do not require the Licensor's approval. However, the adaptation should be credited as shown in Appendix below.

#### Appendix — Acknowledgements:

##### **For Journal Content:**

Reprinted by permission from [the Licensor]: [Journal Publisher (e.g.

Nature/Springer/Palgrave)) [JOURNAL NAME] [REFERENCE CITATION  
(Article name, Author(s) Name), [COPYRIGHT] (year of publication)

**For Advance Online Publication papers:**

Reprinted by permission from [the Licensor]: [Journal Publisher (e.g. Nature/Springer/Palgrave)] [JOURNAL NAME] [REFERENCE CITATION  
(Article name, Author(s) Name), [COPYRIGHT] (year of publication), advance  
online publication, day month year (doi: 10.1038/sj.[JOURNAL ACRONYM].)

**For Adaptations/Translations:**

Adapted/Translated by permission from [the Licensor]: [Journal Publisher (e.g. Nature/Springer/Palgrave)] [JOURNAL NAME] [REFERENCE CITATION  
(Article name, Author(s) Name), [COPYRIGHT] (year of publication)

**Note: For any republication from the British Journal of Cancer, the following credit line style applies:**

Reprinted/adapted/translated by permission from [the Licensor]: on behalf of Cancer Research UK: : [Journal Publisher (e.g. Nature/Springer/Palgrave)] [JOURNAL NAME] [REFERENCE CITATION (Article name, Author(s) Name), [COPYRIGHT] (year of publication)

**For Advance Online Publication papers:**

Reprinted by permission from The [the Licensor]: on behalf of Cancer Research UK: [Journal Publisher (e.g. Nature/Springer/Palgrave)] [JOURNAL NAME] [REFERENCE CITATION (Article name, Author(s) Name), [COPYRIGHT] (year of publication), advance online publication, day month year (doi: 10.1038/sj.[JOURNAL ACRONYM])

**For Book content:**

Reprinted/adapted by permission from [the Licensor]: [Book Publisher (e.g. Palgrave Macmillan, Springer etc) [Book Title] by [Book author(s)] [COPYRIGHT] (year of publication)

**Other Conditions:**

Version 1.1

Questions? [customercare@copyright.com](mailto:customercare@copyright.com) or +1-855-239-3415 (toll free in the US) or +1-978-646-2777.

**SPRINGER NATURE LICENSE  
TERMS AND CONDITIONS**

Apr 08, 2019

This Agreement between Mr. Rodell Barrientos ("You") and Springer Nature ("Springer Nature") consists of your license details and the terms and conditions provided by Springer Nature and Copyright Clearance Center.

License Number	4564380812773
License date	Apr 08, 2019
Licensed Content Publisher	Springer Nature
Licensed Content Publication	Journal of The American Society for Mass Spectrometry
Licensed Content Title	Structural Analysis of Unsaturated Glycosphingolipids Using Shotgun Ozone-Induced Dissociation Mass Spectrometry
Licensed Content Author	Rodell C. Barrientos, Ngoc Vu, Qibin Zhang
Licensed Content Date	Jan 1, 2017
Licensed Content Volume	28
Licensed Content Issue	11
Type of Use	Journal/Magazine
Requestor type	publisher
Publisher	Elsevier
Format	print and electronic
Portion	figures/tables/illustrations
Number of figures/tables/illustrations	2
Will you be translating?	no
Circulation/distribution	<501
Author of this Springer Nature content	yes
Title of new article	Modern Methods for Improved Determination of Intact Glycosphingolipids by Mass Spectrometry
Lead author	Rodell Barrientos
Title of targeted journal	Analytica Chimica Acta
Publisher	Elsevier
Expected publication date	Jul 2019
Order reference number	2
Portions	Figure 2 Comparison of OzID-MS spectra of (a) LacCer d18:1/18:1(9Z) and (b) LacCer d18:1/18:0.
Requestor Location	Mr. Rodell Barrientos 500 Laureate Way Suite 4226  KANNAPOLIS, NC 28081 United States Attn: Mr. Rodell Barrientos

Total 0.00 USD

[Terms and Conditions](#)

### Springer Nature Terms and Conditions for RightsLink Permissions

Springer Nature Customer Service Centre GmbH (the Licensor) hereby grants you a non-exclusive, world-wide licence to reproduce the material and for the purpose and requirements specified in the attached copy of your order form, and for no other use, subject to the conditions below:

1. The Licensor warrants that it has, to the best of its knowledge, the rights to license reuse of this material. However, you should ensure that the material you are requesting is original to the Licensor and does not carry the copyright of another entity (as credited in the published version).  
  
If the credit line on any part of the material you have requested indicates that it was reprinted or adapted with permission from another source, then you should also seek permission from that source to reuse the material.
2. Where **print only** permission has been granted for a fee, separate permission must be obtained for any additional electronic re-use.
3. Permission granted **free of charge** for material in print is also usually granted for any electronic version of that work, provided that the material is incidental to your work as a whole and that the electronic version is essentially equivalent to, or substitutes for, the print version.
4. A licence for 'post on a website' is valid for 12 months from the licence date. This licence does not cover use of full text articles on websites.
5. Where '**reuse in a dissertation/thesis**' has been selected the following terms apply: Print rights of the final author's accepted manuscript (for clarity, NOT the published version) for up to 100 copies, electronic rights for use only on a personal website or institutional repository as defined by the Sherpa guideline ([www.sherpa.ac.uk/romeo/](http://www.sherpa.ac.uk/romeo/)).
6. Permission granted for books and journals is granted for the lifetime of the first edition and does not apply to second and subsequent editions (except where the first edition permission was granted free of charge or for signatories to the STM Permissions Guidelines <http://www.stm-assoc.org/copyright-legal-affairs/permissions/permissions-guidelines/>), and does not apply for editions in other languages unless additional translation rights have been granted separately in the licence.
7. Rights for additional components such as custom editions and derivatives require additional permission and may be subject to an additional fee. Please apply to [Journalpermissions@springernature.com](mailto:Journalpermissions@springernature.com)/[bookpermissions@springernature.com](mailto:bookpermissions@springernature.com) for these rights.
8. The Licensor's permission must be acknowledged next to the licensed material in print. In electronic form, this acknowledgement must be visible at the same time as the figures/tables/illustrations or abstract, and must be hyperlinked to the journal/book's homepage. Our required acknowledgement format is in the Appendix below.
9. Use of the material for incidental promotional use, minor editing privileges (this does not include cropping, adapting, omitting material or any other changes that affect the meaning, intention or moral rights of the author) and copies for the disabled are permitted under this licence.
10. Minor adaptations of single figures (changes of format, colour and style) do not require the Licensor's approval. However, the adaptation should be credited as shown in Appendix below.

#### Appendix — Acknowledgements:

##### For Journal Content:

Reprinted by permission from [the Licensor]: [Journal Publisher (e.g. Nature/Springer/Palgrave)]  
[JOURNAL NAME] [REFERENCE CITATION (Article name, Author(s) Name), [COPYRIGHT]  
(year of publication)]

##### For Advance Online Publication papers:

Reprinted by permission from [the Licensor]: [Journal Publisher (e.g. Nature/Springer/Palgrave)]

[JOURNAL NAME] [REFERENCE CITATION (Article name, Author(s) Name), [COPYRIGHT] (year of publication), advance online publication, day month year (doi: 10.1038/sj.[JOURNAL ACRONYM].)]

**For Adaptations/Translations:**

Adapted/Translated by permission from [the Licensor]: [Journal Publisher (e.g. Nature/Springer/Palgrave)] [JOURNAL NAME] [REFERENCE CITATION (Article name, Author(s) Name), [COPYRIGHT] (year of publication)]

**Note: For any republication from the British Journal of Cancer, the following credit line style applies:**

Reprinted/adapted/translated by permission from [the Licensor]: on behalf of Cancer Research UK: : [Journal Publisher (e.g. Nature/Springer/Palgrave)] [JOURNAL NAME] [REFERENCE CITATION (Article name, Author(s) Name), [COPYRIGHT] (year of publication)]

**For Advance Online Publication papers:**

Reprinted by permission from The [the Licensor]: on behalf of Cancer Research UK: [Journal Publisher (e.g. Nature/Springer/Palgrave)] [JOURNAL NAME] [REFERENCE CITATION (Article name, Author(s) Name), [COPYRIGHT] (year of publication), advance online publication, day month year (doi: 10.1038/sj.[JOURNAL ACRONYM].)]

**For Book content:**

Reprinted/adapted by permission from [the Licensor]: [Book Publisher (e.g. Palgrave Macmillan, Springer etc) [Book Title] by [Book author(s)] [COPYRIGHT] (year of publication)]

**Other Conditions:**

Version 1.1

Questions? [customercare@copyright.com](mailto:customercare@copyright.com) or +1-855-239-3415 (toll free in the US) or +1-978-646-2777.



RightsLink®

[Home](#)[Create Account](#)[Help](#)ACS Publications  
Most Trusted. Most Cited. Most Read.**Title:** Structural Characterization of Gangliosides and Glycolipids via Ultraviolet Photodissociation Mass Spectrometry**Author:** John P. O'Brien, Jennifer S. Brodbelt**Publication:** Analytical Chemistry**Publisher:** American Chemical Society**Date:** Nov 1, 2013

Copyright © 2013, American Chemical Society

## LOGIN

If you're a [copyright.com](#) user, you can login to RightsLink using your [copyright.com](#) credentials. Already a [RightsLink](#) user or want to [learn more?](#)

**PERMISSION/LICENSE IS GRANTED FOR YOUR ORDER AT NO CHARGE**

This type of permission/license, instead of the standard Terms & Conditions, is sent to you because no fee is being charged for your order. Please note the following:

- Permission is granted for your request in both print and electronic formats, and translations.
- If figures and/or tables were requested, they may be adapted or used in part.
- Please print this page for your records and send a copy of it to your publisher/graduate school.
- Appropriate credit for the requested material should be given as follows: "Reprinted (adapted) with permission from (COMPLETE REFERENCE CITATION). Copyright (YEAR) American Chemical Society." Insert appropriate information in place of the capitalized words.
- One-time permission is granted only for the use specified in your request. No additional uses are granted (such as derivative works or other editions). For any other uses, please submit a new request.

If credit is given to another source for the material you requested, permission must be obtained from that source.

[BACK](#)[CLOSE WINDOW](#)

Copyright © 2019 [Copyright Clearance Center, Inc.](#) All Rights Reserved. [Privacy statement](#). [Terms and Conditions](#). Comments? We would like to hear from you. E-mail us at [customercare@copyright.com](mailto:customercare@copyright.com)



# RightsLink®

[Home](#)
[Create Account](#)
[Help](#)


**ACS Publications**  
Most Trusted. Most Cited. Most Read.

**Title:** Isobaric Labeling of Intact Gangliosides toward Multiplexed LC-MS/MS-Based Quantitative Analysis

**Author:** Rodell C. Barrientos, Qibin Zhang

**Publication:** Analytical Chemistry

**Publisher:** American Chemical Society

**Date:** Feb 1, 2018

Copyright © 2018, American Chemical Society

#### LOGIN

If you're a [copyright.com](#) user, you can login to RightsLink using your [copyright.com](#) credentials. Already a [RightsLink](#) user or want to [learn more?](#)

#### PERMISSION/LICENSE IS GRANTED FOR YOUR ORDER AT NO CHARGE

This type of permission/license, instead of the standard Terms & Conditions, is sent to you because no fee is being charged for your order. Please note the following:

- Permission is granted for your request in both print and electronic formats, and translations.
- If figures and/or tables were requested, they may be adapted or used in part.
- Please print this page for your records and send a copy of it to your publisher/graduate school.
- Appropriate credit for the requested material should be given as follows: "Reprinted (adapted) with permission from (COMPLETE REFERENCE CITATION). Copyright (YEAR) American Chemical Society." Insert appropriate information in place of the capitalized words.
- One-time permission is granted only for the use specified in your request. No additional uses are granted (such as derivative works or other editions). For any other uses, please submit a new request.

If credit is given to another source for the material you requested, permission must be obtained from that source.

[BACK](#)
[CLOSE WINDOW](#)

Copyright © 2019 [Copyright Clearance Center, Inc.](#) All Rights Reserved. [Privacy statement](#). [Terms and Conditions](#). Comments? We would like to hear from you. E-mail us at [customercare@copyright.com](mailto:customercare@copyright.com)